T H E U N I V E R S I T Y O F T U L S A

THE GRADUATE SCHOOL

THREE DIMENSIONAL RESERVOIR DESCRIPTION BY INVERSE PROBLEM THEORY USING WELL-TEST PRESSURE AND GEOSTATISTICAL DATA

by

Nanqun He

A dissertation submitted in partial fulfillment of

the requirements for the degree of Doctor of Philosophy

in the Discipline of Petroleum Engineering

The Graduate School

The University of Tulsa

1997

T H E U N I V E R S I T Y O F T U L S A

THE GRADUATE SCHOOL

THREE DIMENSIONAL RESERVOIR DESCRIPTION BY INVERSE PROBLEM THEORY USING WELL-TEST PRESSURE AND GEOSTATISTICAL DATA

by

Nanqun He

A DISSERTATION

APPROVED FOR THE DISCIPLINE OF

PETROLEUM ENGINEERING

By Dissertation Committee

_____, Co-Chairperson

_____, Co-Chairperson

_____

_____

ABSTRACT

Nanqun He (Doctor of Philosophy in Petroleum Engineering)

Three Dimensional Reservoir Description by Inverse Problem Theory Using Well-Test Pressure and Geostastistical Data (208 pp. - Chapter VI)

Co-Directed by Dr. Albert C. Reynolds, Jr. and Dr. Dean S. Oliver

(309 words)

In this work, we developed techniques based on inverse problem theory to generate realizations of reservoir rock property fields (porosity and permeability) and well skin factors conditioned to hard data, geostatistical information and well-test pressure data obtained under single-phase conditions. The probability density function (pdf) for the prior model (reservoir parameters) is constructed based on static information and geostatistics. The uncertainty in the prior means of the model parameters is incorporated using a partially doubly stochastic model. The a posteriori probability density function (pdf) of the model is obtained using Bayes's Theorem. The Gauss-Newton method is applied to minimize the objective function and obtain the maximum a posteriori estimate (most probable model). We developed a procedure to estimate sensitivity coefficients for three dimensional problems. These are required for applying the Gauss-Newton method. Realizations of reservoir rock property fields are obtained by procedures for sampling of the a posteriori pdf. Reparameterization techniques based on spectral decomposition and subspace method are implemented to save computational time and memory storage.

The methodology is applied to synthetic cases and a field example using 10,000 gridblocks. We show how the uncertainty in model parameters is reduced by conditioning

realizations to multiwell pressure data. Although pressure data do not resolve individual gridblock permeabilities very well, pressure data significantly reduce the uncertainty in thickness averaged permeability. In the three-dimensional case, well skin factors can be estimated accurately only by conditioning to both wellbore pressure and layer flow rates. The porosity field is not resolved as well as the permeability field by pressure data; however, if pseudosteady state flow pressure data are used as conditioning data, the uncertainty in the average reservoir porosity is very small.

Procedures to generate realizations by sampling the a posteriori pdf are presented. By making performance predictions using such a set of realizations, we can quantify the uncertainty in predicted reservoir performance.

ACKNOWLEDGMENTS

I wish to express my sincere appreciation and gratitude to Dr. Albert C. Reynolds, Jr., Professor of Petroleum Engineering and Mathematical Sciences, and Dr. Dean S. Oliver of Chevron Petroleum Technology Company for their invaluable assistance and guidance as co-directors of this study. I also thank Dr. Leslie G. Thompson, Associate Professor of Petroleum Engineering, and Dr. Duryodhan Eplili, Assistant Professor of Geosciences for participating in my dissertation committee and for their comments and suggestions.

I would like to extend my thanks and appreciation to all the other faculty members and to my graduate student colleagues in the Petroleum Engineering Department, who contributed to my study as a TU graduate student.

I gratefully acknowledge the financial support from TUPREP (Tulsa University Petroleum Reservoir Exploitation Projects) and Chevron Petroleum Technology Company during my study.

I am especially grateful to my wife, Feng Wang, for her love, understanding and encouragement, and to my beloved daughter, Xinyi. I dedicate this work to all my family members living in China and to the revered memory of my brother, Nanhua He, for their love and support in all my life.

TABLE OF CONTENTS

Page

LIST OF FIGURES

CHAPTER I

INTRODUCTION

Scientists from different disciplines view reservoir description somewhat differently. Geologists may mainly consider reservoir description from the viewpoint of geological setting and architecture. Geophysicists mainly focus on the reservoir shape and structure, including fault locations, but may also consider the estimation of porosity. Engineers have been interested in rock and fluid properties, well conditions and production data. However, the overall goal of all disciplines is the same, i.e., to reduce the uncertainty in reservoir parameters and make correct reservoir performance predictions. The appropriate way to reach the goal is to integrate all the available data: geological, petrophysical, geophysical, and production data. However, how to effectively integrate these data is a challenge to the person or team working in this area. Reservoir characterization is a multistage and cross-disciplinary work process.

The overall objective of this work is to generate realizations of reservoir rock property fields that represent an approximately correct sampling of the a posteriori probability density function for the rock property fields. In order to do this correctly, it is important that one formulates an a posteriori probability density function which is conditioned to all available information and data. Our standard approach for doing this is to estimate a most probable model (maximum a posteriori estimate) and then to generate

realizations using information obtained in generating the maximum a posteriori estimate. However, it is important to recognize that the most important task is to sample the a posteriori probability density function, not to generate the most probable model.

In our work, the rock property fields generated actually represent reservoir simulator gridblock values of permeability and porosity. If one generates a set of N realizations that represents a proper sampling of the a posteriori probability distribution, then one can characterize the uncertainty in performance predictions. To do this, we simply use each reservoir description (each realization) as input data for a reservoir simulation and generate the resulting reservoir performance. From these N flow simulations, one can compute the statistics for each parameter or variable predicted by the flow simulations and estimate the mean and variance for each of the predicted parameters to provide a measure of the uncertainty in predicted performance. Having characterized the uncertainty in predicted performance, one can make reservoir management decisions that account for our lack of complete knowledge of the true reservoir.

It is important to realize that, contrary to popular opinion, the objective is not to construct equiprobable realizations, but to construct a set of realizations which represents a correct sampling of the a posteriori probability distribution for the rock property fields. By simulating reservoir performance with each such realization, one can accurately evaluate the uncertainty in reservoir performance and develop optimum reservoir management strategies. Similar to standard procedures for making reservoir management decisions, our methodology is data driven. However, unlike standard technology, our techniques allow one to directly incorporate the uncertainty in data, to evaluate the uncertainty in estimates of rock property fields and to evaluate the value of data, i.e., to

determine how much given data reduce the uncertainty in reservoir descriptions and performance predictions.

1.1 Integrating Dynamic Data into Reservoir Characterization

Geostatistics provides a tool to generate realizations of rock property fields from static data (logging, core, seismic, geological knowledge). However, due to lack of closely spaced lateral data there is great uncertainty in geostatistical simulation or description. Generally, realizations generated from static data can not match the dynamic performance. To reduce the uncertainty in reservoir characterization and make reliable future performance predictions, we need to effectively couple static information with dynamic data.

For the last several years, much work has been done to generate reservoir descriptions conditioned to both static (non-production) and dynamic (production) data. However, most attempts have not incorporated production data into reservoir description directly, but instead have used the production data to estimate some other parameters which are then used as a constraint when generating reservoir descriptions using prior information. For example, Deutsch[1], Sagar et al.[2] and Holden et al.[3] used pressure data to compute an average permeability within a radius of investigation and then used this average permeability as a constraint when constructing a permeability field which matches the variogram. (Alabert[4] has made an extensive study of the how this average permeability and radius of investigation should be computed.) Since Refs. 1 and 2 use simulated annealing to construct reservoir descriptions, it would not be computationally feasible to incorporate pressure data directly into the objective function because this would require

one run of the reservoir simulator at each iteration of the simulated annealing algorithm, and the simulated annealing algorithm may require several thousand iterations to obtain convergence. While this provides a motivation for incorporating an average permeability instead of pressure into the objective function, it does not mean the procedure is rigorously correct. In fact, since any permeability averaging technique used is only approximate, the permeability field obtained from simulated annealing may not predict the observed pressure data with a high degree of accuracy and the derivatives of these predicted and observed pressures may be radically different[2]. Moreover, it is difficult to interpret what the generated permeability fields represent in a probabilistic sense and it appears that any attempt to quantify the uncertainty in reservoir description from a set of descriptions obtained from simulated annealing as typically applied[1,2] will be difficult. The descriptions obtained more or less honor the data, but it is difficult to argue that a set of such descriptions represents a proper sampling of the correct probability density function.

Huang[5] proposed a method to integrate static data with dynamic data. In his work, porosity is estimated from logging and seismic inversion, then permeability is perturbed within the correlation scatter-cloud relation between porosity and permeability, to match the production data. However, the correlation scatter cloud from core measurement normally does not represent the correct probability density function for rock property fields. Even though the permeability field generated by this method honors dynamic data, it is not feasible to predict reservoir performance from this permeability field.

Datta-Gupta et al.[6] and Vasco et al.[7] also used simulated annealing method to integrate transient pressure data and production data into reservoir characterization. They used a fast streamline simulator rather than traditional numerical simulator for their

forward calculation in order to greatly improve the computational efficiency. But, for a three-dimensional full reservoir model, in which tens or hundreds of thousands of simulations is required to reach convergence by simulated annealing, this method is still extremely computationally demanding and probably impractical. Moreover, their approach represents a regularized history matching procedure oriented towards generating a rock property field which honors the production data rather than a stochastic simulation procedure for generating a suite of realizations which adequately represents the uncertainty in rock property fields.

1.2 History Matching

History matching is a procedure in which grid block values of permeability, porosity and well skin factors are modified to obtain a reservoir description that matches observed production performance. However, classic history matching yields nonunique results and often leads to unreliable predictions of future reservoir performance, especially when future predictions are based on a different producing mechanism than was used in the history matching process. For example, if history matching was done using production data during a water flooding operation, reliable predictions of performance for a planned CO_2 flood can not be expected to be highly accurate.

Mathematically, the nonuniqueness in the classical history matching procedure arises because, in practice, we never have a sufficient number of independent observed data to determine all reservoir parameters uniquely. Nonuniqueness may arise either because the production data are completely insensitive to some of the reservoir parameters

(for example, the gridblock values of porosity and permeability in certain parts of the reservoir) or because production data may be sufficient only to estimate certain linear combinations or regional averages of parameters. The latter case is natural and occurs routinely in pressure transient analysis. For example, single-phase pseudosteady-state flow pressure data can be used to estimate average porosity, but can not be used to estimate gridblock values of porosity or porosity values at specific locations. Standard analysis of radial flow transient pressure data obtained at a completely-penetrating well in a layered reservoir, where each layer is homogeneous, yields a good estimate of thickness-averaged permeability but does not provide a means to estimate the individual layer permeabilities.

If one casts the classical history matching problem in a natural mathematical formulation (see, for example Tang et al.[8]), one arrives an ill-conditioned matrix problem. While one can regularize the problem[8] (for example, by Tikhonov[9] regularization) to obtain a matrix problem with a nonsingular coefficient matrix, the solution or history-match obtained is then determined by the specific form of the regularization procedure. Different regularizations yield different solutions, i.e., different history matches. Moreover in such a procedure, one can not easily characterize the uncertainty in the resulting reservoir description. Perhaps even more importantly, when one obtains a reservoir description by history matching only production data, the resulting description will often violate other information, for example, log data, core data, seismic data, or geologic interpretation. The current practice of reservoir characterization may be thought of as generating reservoir descriptions that honor all available data. Returning to the problem of history matching, intuitively one believes that if history matching of production data is done using other data as constraints, then the nonuniqueness problem should somehow be

reduced. By reduction of the nonuniqueness problem, we do not mean there will be a unique solution; there will still exist an infinite variety of reservoir descriptions which honor all data. Reduction of the nonuniqueness in the history matching process means reduction of the variation or variability in the set of solutions, i.e., a reduction in the uncertainty in the reservoir description. In some cases, we may be able to resolve a few parameters almost perfectly. It is important to note that a reservoir description obtained by such a constrained history matching method will honor all the data, not just the production data.

Gavalas et al.[10] in 1976 recognized that the proper incorporation of prior data stabilizes the history matching problem and also reduces the variability in the set of reservoir descriptions that provide an acceptable match of production data. They used Gaussian type expressions for the co-variance functions of porosity and permeability, the cross covariance between them, and the prior estimates of the means of porosity and permeability to incorporate prior information in the objective function when history matching multiwell pressure data obtained in a synthetic one-dimensional reservoir under single-phase flow conditions. They showed that incorporating the prior information reduced the errors in the estimates of permeability and porosity and also improved the convergence properties of the minimization algorithms considered. Moreover they showed that the Bayesian estimation approach gave better estimates of the true permeability and porosity fields than were obtained by zonation[11,12]. In a later paper[13] the same authors considered the same one-dimensional single-phase flow problem and compared results obtained by reparameterization using zonation, reparameterization using vectors of sensitivity coefficients (derivatives of pressures at observation points with respect to model

parameters) and Bayesian estimation. Their comparisons were based on computing the traces of the a posteriori covariance matrices (i.e., the sum of all a posteriori variances) obtained by assuming the objective function could be linearized around the true model. The trace of the a posteriori covariance matrix gives a measure of the total uncertainty in the parameter estimates. They found that the smallest total uncertainty was obtained with Bayesian estimation. They did not, however, use reparameterization when considering Bayesian estimation, and did not consider estimating well skin factors or generating multiple realizations of the rock property fields.

1.3 **Geostatistics Based Automatic History Matching**

Inverse problem theory[14] provides a methodology to incorporate prior information when history matching production data. The standard application of inverse problem theory rests on the fact that prior information on the model (set of reservoir parameters to be estimated) satisfies a multinormal distribution and that measurement errors in production data can be considered as Gaussian random variables with zero mean and known variance. Under these assumptions, the most probable model (the maximum a posteriori estimate) conditioned to both prior information and production data can be obtained by minimizing an objective function derived directly from the a posteriori probability density function. Since the a posteriori probability density function is derived from Bayes's theorem, this approach is often referred to as Baysian estimation. It is convenient to minimize the objective function by a gradient method to obtain an approximation to the maximum a posteriori estimate. Important aspects of inverse problem theory[15] are that an

estimation of the uncertainty in reservoir description can be obtained from the a posteriori covariance matrix and approximate realizations of the reservoir description can be constructed from the a posteriori covariance matrix. It is important to recognize that from the viewpoint of inverse problem theory[14] the solution of the inverse problem is represented by the probability density function for the model (reservoir description). This probability density function is not arbitrary in that it must properly account for all data and information and must account for the uncertainties in the data and information itself.

The specific objective of this work is to construct realizations of the model (reservoir simulator gridblock values of log-permeability, porosity and well skin factors) that are conditioned to prior means (averages) for these variables, variograms, and multiwell pressure data. For the approach followed here, this is largely a two step process. First, we estimate a most probable model by minimizing an objective function arising naturally from the a posteriori probability density function. Secondly, we generate other realizations of the model. In many cases, we simply generate this set of realizations from a Cholesky decomposition of the a posteriori covariance matrix and this set of realizations can only represent an approximate sampling of the a posteriori probability density function. As discussed later, however, a more computationally efficient approach has recently been presented for generating realizations.

We note that many of the basic ideas we use have been around for some time both in general theoretical form[14,15] and in the language of specific disciplines. For example, in a sequence of excellent papers, Carrera and Neuman[16-18] presented a similar method for the estimation of hydraulic conductivities and storativities from head data and prior informa-

tion by using a maximum likelihood method, where the liklihood function incorporates both head data and prior information.

In a important paper, Oliver[19] re-initialized the research path of Refs. 10 and 13 and introduced the fundamental philosophy of Tarantola[14] to the reservoir characterization field. His approach follows the general procedure outlined above, i.e., estimate the most probable model by minimizing the proper objective function and then construct realizations from the Cholesky decomposition of the prior covariance matrix. Oliver considered the problem of constructing realizations of one-dimensional permeability and porosity fields and two-dimensional permeability fields (assuming porosity is known) conditioned to prior means and covariances, hard data and multiwell pressure data.

In this work, we have followed the basic philosophy and methodology of Tarantola[14] as introduced to the petroleum engineering field by Oliver[19,20]. More specifically, we generate a most probable model by applying the Gauss-Newton method with restricted step[21,22]. For this method to be computationally feasible, the Gauss-Newton method must converge rapidly and an efficient method for generating the sensitivity coefficients must be available. For the problems considered here, the sensitivity coefficients represent the derivatives of wellbore pressures with respect to the model parameters (well skin factors and gridblock values of log-permeability and porosity). For three-dimensional problems, however, individual layer skin factors can not be resolved only by pressure data and individual layer flow rate is also required to resolve skin factors. Chu et al.[23, 24] assumed porosity was known and considered only the problem of constructing realizations of the permeability field and active well skin factors. They derived and implemented a modified generalized pulse spectrum technique (MGPST) to estimate the sensitivity coefficients

using basic results of Tang et al.[8]. Although we later[25] used the same approach to generate sensitivity coefficients related to the porosity field, we eventually discovered that this procedure does not yield good estimates of the sensitivity coefficients related to the porosity field. Thus, in this work and in Refs. 26, 27, 28, we have extended a procedure introduced by Carter et al.[29] to generate sensitivity coefficients related to the permeability and porosity fields. The results of Ref. 29 reproduce the results of Jacquard[30] and Jacquard and Jain[11] who used an electric-circuit analogue to construct formulas for sensitivity coefficients. However, the elegant mathematical derivation of Carter et al. is markedly different than the derivation of Refs. 11 and 30, and is conveniently cast in the language of reservoir engineering.

As we will show, there are computational nuances involved in the implementation of the Carter et al. method that, to the best of our knowledge, have not been recognized prior to our work. In the two-dimensional setting, if conditioning pressure data are observed at N_w wells, then the Carter et al. procedure requires $N_w + 1$ simulation runs to estimate sensitivity coefficients. As presented, the Carter et al. procedure actually computes the sensitivity of simulator gridblock pressures with respect to gridblock values of permeability and porosity. In three dimensions, if each well is vertical and is completed in N_z vertical gridblocks, then there are $N_z N_w$ gridblocks associated with the set of wells. To compute sensitivity coefficients related to this total set of gridblock pressures would require $N_z N_w + 1$ simulation runs. However, in practice, we measure wellbore pressures, not gridblock pressures; i.e., we only need to compute the sensitivity of wellbore pressures to the rock property fields. For three-dimensional problems, we have derived a way to estimate these sensitivity coefficients with only $N_w + 1$ simulation runs.

While our modification of the Carter et al. procedure provides an accurate and relatively efficient method to estimate sensitivity coefficients, it is applicable only for single-phase flow problems. The MGPST[23] has approximately the same computational efficiency as the Carter et al.[29] method and can be extended to multiphase flow problems, but is not sufficiently accurate unless it is restricted to estimation of only sensitivity coefficients related to the permeability field. The direct and gradient simulator methods[31] are accurate and applicable to multiphase flow problems, but are too computationally intensive to be used routinely in practical applications where we may wish to consider thousands or tens of thousands of simulator gridblocks. If we wish to generate values of three permeability values (k_x, k_y and k_z) and one porosity value at each of M grid-blocks, the direct method will require 4M+1 simulation runs. The time required by the gradient simulator method is very roughly comparable to the time required by the direct method, but some reduction in computational costs are achieved by computing all sensitivity coefficients during one simulation run. This requires the solution of an additional 4M linear systems at each time step of the simulation run, but all of these linear systems involve the same coefficient matrix; see Refs. 31 and 32 for additional details.

1.4 Reservoir Performance Prediction

As we mentioned, the ultimate goal of reservoir characterization is to predict future reservoir performance and assess the uncertainty in production predictions. Multiple realizations which represent a correct sampling of the pdf (probability density function) for the rock property fields are required to obtain a reliable prediction. In Refs. 25, 26 and 27,

we generated a set of realizations of the rock property fields that approximate a correct sampling of the a posteriori probability density function using the Cholesky decomposition of the a posteriori covariance matrix, C_{MP}. However, this procedure assumes that the a posteriori probability density function is multivariate Gaussian with covariance matrix C_{MP} and mean given by the maximum a posteriori estimate. At best, this is only approximate since the assumption is strictly valid if and only if the functional relationship between the vector of pressure data and the model (gridblock values of porosity and log-permeability) can be accurately linearized about the maximum a posteriori estimate. As this is not true in general, generating a set of realizations using the Cholesky decomposition of C_{MP} can only generate an approximate sampling of the a posteriori probability density function.

Cunha[33], Cunha et al.[34] and Oliver et al.[35] investigated the possibility of using Markov chain Monte Carlo methods and hybrid Markov chain Monte Carlo methods to sample the a posteriori probability density function. These procedures have been implemented only for two-dimensional problems and only for the case where we wish to sample the a posteriori distribution for the log-permeability field. This assumes that the porosity field can be accurately resolved from other information, for example, from log and seismic data. In the limit, the Markov chain Monte Carlo (MCMC) methods are guaranteed to yield a correct sampling of the a posteriori probability density function. Unfortunately, there is no way to determine how long a chain must be to ensure that the samples at the end of the chain are correct. At best, they can provide only heuristic practical guidelines for making this determination. The implementation of the hybrid Markov chain Monte Carlo Method is superior to a more conventional MCMC procedure

in that the hybrid method provides a more efficient exploration of the set of possible realizations and does not suffer from high rejection rates. However, the hybrid method is computationally expensive. In viewing simulated annealing in the context of Markov chain theory, it can be shown that standard implementations of simulated annealing do not sample the a posteriori probability density function correctly and, contrary to conventional wisdom, when implemented in the standard way, do not generate equally probable realizations. However, as shown in Refs. 33 and 34, with a proper implementation of simulated annealing, one can estimate the maximum a posteriori estimate. It is also possible to use simulated annealing for stochastic simulation. However, the computational time required by simulated annealing is two orders of magnitude greater than is required by the Gauss-Newton method. These aforementioned results on simulated annealing were reported in Refs. 33, 34 and 35.

In this work, we also use an efficient two-step procedure of Oliver et al.[27] (also see, Oliver[36]) to generate multiple realizations conditioned to prior information and well-testing pressure data. The first step is to propose a set of unconditional realizations from a known probability distribution, the prior model. This step could be carried out using any unconditional simulation technique. In Refs. 26 and 27, we used the Cholesky decomposition method to generate unconditional realizations, while in Ref. 28 we applied sequential Gaussian cosimulation[37]. As part of the first step, we also generate unconditional simulations of the pressure data. The second step involves history matching of the unconditional realizations to the simulated well-testing pressure data. By simulation from the set of realizations obtained by history matching, we can predict the future performance and also quantify the uncertainty in predicted performance. Here and Ref. 28, we

incorporate uncertainty in prior means of the rock property fields by using a partially doubly stochastic model[38], because in reality, the true means of the rock properties may be difficult to obtain. This is specially true for the permeability field where means estimated from core or logging are generally not consistent with average value obtained by analysis of well-test data. We show that we can generate the maximum a posteriori estimate of rock property fields and means by Gauss-Newton procedure.

CHAPTER II

INVERSE PROBLEM THEORY

The inverse problem or inversion is widely encountered in variety of science and engineering disciplining. In “solving” an inverse problem, we wish to infer the values of model parameters from observations of some model parameters and/or model performance, while in the forward problem, we predict the response or model performance given the values of all model parameters. In some cases, the inverse problem is “exact” or over-determined, in which the number of observed data are the same as, or more than, the number of model parameters to be determined. If the number of data are greater than the number of model parameters, model parameters are typically estimated by a least-square procedure. Nonlinear regression used in pressure transient analysis provides a typical example of an over-determined problem.

In many cases, however, the number of observed data are less, often far less, than the parameters to be determined, in which case the inverse problem is underdetermined or ‘ill-posed’. To solve an ‘ill-posed’ problem is difficult and generally we need to introduce prior assumptions for the model space (parameters). For the problem considered in this work, the observed data are well-testing pressure data or production data observed at wells and the model parameters are the gridblock values of porosity and permeability and well skin factors. In this work, we assume that reservoir geological model and fluid

properties are known. As the observed independent (not redundant) pressure data are far less than the number of parameters, we need to introduce prior statistics assumptions or constraints on the model space in order to formulate our inverse problem in a way that allows us to generate solutions (realizations of model parameters) that are consistent with the observed data. We do this in a probabilistic way by formulating a prior model characterized by a prior probability density function (pdf). The prior model can be obtained from static data (core, logging, seismic) measurement and analysis (geological interpretation and geostatistics).

2.1 The Prior Model

We assume that permeabilities in three directions (k_x, k_y and k_z) have log-normal distributions with known means and variances given by $\sigma^2_{k_x}$, $\sigma^2_{k_y}$ and $\sigma^2_{k_z}$. Porosity is assumed to be normal with known mean and variance given by σ^2_ϕ. Each rock property attribute ($\ln(k_x)$, $\ln(k_y)$, $\ln(k_z)$) and ϕ) is modeled as a stationary Gaussian random function so that the covariance functions are directly related to the variograms. The correlation coefficients between the various attributes are assumed to be known, but may be zero. If the permeability tensor is isotropic, we use a three-dimensional variogram for log-permeability which can be either isotropic or anisotropic. Both anisotropic log-permeability fields and anisotropic variograms can be considered. In the anisotropic permeability case, we either specify $k_z = a\sqrt{k_x k_y}$ for some constant *a*, or assume k_z is uncorrelated with k_x and k_y and thus has its own mean and variogram. The well skin

factors are modeled as uncorrelated Gaussian random variables with estimates of the means and variances available. The reservoir can also be modeled as a layered system where we may specify different two-dimensional variograms for each layer.

The number of simulator gridblocks is M. Our objective is to determine realizations of the well skin factors and the gridblock values of porosity and permeability. Since permeability is assumed to be log-normal, we actually determine gridblock values of ln(k). For an isotropic reservoir, the complete model to be estimated is represented by the $2M + N_s$ dimensional vector

$$m = \begin{bmatrix} m_\phi \\ m_k \\ m_s \end{bmatrix}, \tag{2.1}$$

where m_ϕ is the M-dimensional column vector of gridblock porosities, m_k is the M-dimensional column vector of gridblock values of ln(k) and m_s is the N_s-dimensional column vector of well skin factors to be estimated. In the most general three-dimensional anisotropic case, Eq. 2.1 is replaced by

$$m = \begin{bmatrix} m_\phi \\ m_{k_x} \\ m_{k_y} \\ m_{k_z} \\ m_s \end{bmatrix}, \tag{2.2}$$

where the notation is obvious. Thus, the number of model parameters to be estimated (denoted by N_p) is equal to $2M + N_s$ for the case of an isotropic permeability field, and $4M + N_s$ in the most general anisotropic case.

Based on our assumption of a multinormal distribution, the prior distribution has a probability density function statisfying the following proportionality relation:

$$\rho(m) \propto \exp\left(-\frac{1}{2}(m-m_{prior})^T C_M^{-1}(m-m_{prior}\right), \tag{2.3}$$

where m_{prior} is the vector containing the estimates of the prior means of the rock properties and well skin factors, C_M is the prior covariance matrix obtained from the variogram model.

A critical assumption is that the prior model has a Gaussian probability density function with prior covariance matrix, C_M, given by

$$C_M = \begin{bmatrix} C_\phi & C_{\phi k} & O \\ C_{k\phi} & C_k & O \\ O & O & C_S \end{bmatrix}. \tag{2.4}$$

In Eq. 2.4, C_ϕ is the covariance matrix for gridblock porosities derived from the porosity variogram, C_k is the covariance matrix for gridblock ln(k)'s, C_S is the covariance matrix for well skin factors, $C_{\phi k}$ is the cross covariance matrix between porosity and ln(k) at the set of gridblocks, $C_{k\phi}$ is equal to the transpose of $C_{\phi k}$ and throughout O's denote null matrices, i.e. matrices with all entries equal to zero. The matrix C_S is diagonal since we assume no correlation between skin factors of different wells and between skin factors of different layers at same well. We avoid specific modeling of the cross covariance matrices by using the "screening hypothesis" of Xu et al.[39] As shown in Ref. 24, this assumption implies that the variograms for porosity and ln(k) are of the same type, and have identical ranges, but different sills, where the ratio of their sills is equal to the corresponding ratios of their variances. Also as shown in Refs. 39 and 24, the screening hypothesis implies that

$$C_{\phi k} = C_{k\phi} = \frac{\rho_{\phi,k}(0)\sigma_\phi}{\sigma_k} C_\phi \ , \tag{2.5}$$

where $\rho_{\phi,k}(0)$ is the correlation coefficient between porosity and permeability at a common location. Detailed expressions for generating the covariance matrices are given in Ref. 24.

In the anisotropic permeability case, the prior covariance matrix, C_M, is given by

$$C_M = \begin{bmatrix} C_\phi & C_{\phi k_x} & C_{\phi k_y} & C_{\phi k_z} & O \\ C_{k_x \phi} & C_{k_x} & C_{k_x k_y} & C_{k_x k_z} & O \\ C_{k_y \phi} & C_{k_y k_x} & C_{k_y} & C_{k_y k_z} & O \\ C_{k_z \phi} & C_{k_z k_x} & C_{k_z k_y} & C_{k_z} & O \\ O & O & O & O & C_s \end{bmatrix}. \tag{2.5a}$$

In Eq. 2.5a, C_{k_x} is the covariance matrix for gridblock x-direction log-permeability $\ln(k_x)$ derived from the variogram for x-direction log-permeability, C_{k_y} is the covariance matrix for gridblock y-direction log-permeabilities $\ln(k_y)$ derived from the variogram for $\ln(k_y)$, C_{k_z} is the covariance matrix for gridblock z-direction log-permeabilities $\ln(k_z)$ derived from the variogram for $\ln(k_z)$, C_s is the $N_s \times N_s$ covariance matrix for well skin factors and is diagonal. $C_{p_1 p_2}$ represents the cross covariance matrix between pair of reservoir property attributes p_1 and p_2, for example $C_{\phi k_x}$ represents the cross covariance matrix between porosity ($p_1 = \phi$) and x-direction log-permeability ($p_2 = \ln(k_x)$). From the definition of covariance, we know that $C_{p_1 p_2}$ equals the transpose of $C_{p_2 p_1}$. So, the overall covariance matrix C_M is symmetric. Throughout *O*'s denote null matrices, i.e., matrices with all entries equal to zero.

Similar to Eq. 2.5, the screening hypothesis is applied to determine the cross-variances $C_{p_1p_2}$ given the correlation coefficients between attributes p_1 and p_2.

It is important to note that the adoption of the screening hypothesis is not a requirement of the procedures presented in this work. This hypothesis simply eliminates the need to develop models for the cross-variograms between pairs of rock property attributes.

2.2 Inverse Solution

2.2.1 Bayes Estimation Theory

In the problem considered here, d_{obs} refers to the vector of observed or measured wellbore pressures data, and contains all N_d pressure measurements that are used as conditioning data. As in Ref. 23-28, measurement errors are modeled as independent identically distributed Gaussian random variables with zero mean and variance σ_d^2. Thus, the covariance matrix for these errors is a diagonal matrix C_D with all diagonal entries equal to σ_d^2. We assume that vector d contains the calculated wellbore pressure data corresponding to d_{obs} and is related to the model by

$$d = g(m). \tag{2.6}$$

The functional relationship of Eq. 2.6 represents the effect of generating d from our reservoir simulator from model m. The reservoir simulator is discussed in more detail in next chapter. For given data, the likelihood function for the model is given by the following relation:

$$L(m|d_{obs}) \propto \exp\left(-\frac{1}{2}(g(m)-d_{obs})^T C_D^{-1}(g(m)-d_{obs})\right). \tag{2.7}$$

From Bayes's theorm, it follows that the a posteriori probability density function for our model, denoted $f_M(m|d_{obs})$, satisfies the following relation

$$f_M(m|d_{obs}) \propto L(d_{obs}|m)\rho(m). \tag{2.8}$$

Using Eqs. 2.3 and 2.7 in Eq. 2.8, we obtain

$$\begin{aligned} f_M(m|d_{obs}) \propto \exp\Bigg[-\frac{1}{2}\Big((m-m_{prior})^T C_M^{-1}(m-m_{prior}) + \\ (g(m)-d_{obs})^T C_D^{-1}(g(m)-d_{obs})\Big)\Bigg]. \end{aligned} \tag{2.9}$$

The most probable model (the maximum a posteriori estimate) which honors prior information and pressure data is obtained by maximizing $f_M(m|d_{obs})$, or equivalently, minimizing the objective function $S(m)$ where

$$\begin{aligned} S(m) = \frac{1}{2}\Big[(m-m_{prior})^T C_M^{-1}(m-m_{prior}) + \\ (g(m)-d_{obs})^T C_D^{-1}(g(m)-d_{obs})\Big]. \end{aligned} \tag{2.10}$$

2.2.2 Gauss-Newton Method

To obtain the most probable model (the maximum a posteriori estimate), we minimize $S(m)$ by applying a restricted-step Gauss-Newton procedure. Thus, we must compute the gradient and the approximate Hessian of S(m). The sensitivity coefficients represent the derivatives of wellbore pressure with respect to model parameters, i.e., $\frac{\partial g_i(m)}{\partial m_j}$ for $1 \le i \le N_d$ and $1 \le j \le N_p$. A sensitivity coefficient gives a measure of how

strongly the data $g_i(m)$ are affected by a change in model parameter m_j. The sensitivity coefficient matrix is given by

$$G = \begin{bmatrix} \frac{\partial g_1(m)}{\partial m_1} & \frac{\partial g_1(m)}{\partial m_2} & \cdots & \frac{\partial g_1(m)}{\partial m_{N_P}} \\ \frac{\partial g_2(m)}{\partial m_1} & \frac{\partial g_2(m)}{\partial m_2} & \cdots & \frac{\partial g_2(m)}{\partial m_{N_P}} \\ \vdots & \vdots & \ddots & \vdots \\ \frac{\partial g_{N_d}(m)}{\partial m_1} & \frac{\partial g_{N_d}(m)}{\partial m_2} & \cdots & \frac{\partial g_{N_d}(m)}{\partial m_{N_P}} \end{bmatrix}. \tag{2.11}$$

Note G is a $N_d \times N_p$ matrix. Again, m denotes the vector of model parameters, m_j denotes the jth model parameter and $g_i(m)$ represents the calculated pressure data corresponding to the *i*th wellbore pressure measurement. If we want to condition to layer flow rates, i.e., production logging data, then *g(m)* represents the vector of calculated layer flow rates corresponding to observed layer flow rates. The procedure for calculating the sensitivity coefficients will be presented in Chapter 3.

At the $(l+1)st$ iteration of the Gauss-Newton method, the gradient of $S(m)$ is

$$\nabla S_l = \nabla_m S(m^l) = G_l^T C_D^{-1}(g(m^l) - d_{obs}) + C_M^{-1}(m^l - m_{prior}), \tag{2.12}$$

and Hessian matrix is given by:

$$H_l = H(m^l) = \nabla\left(\nabla S(m^l)\right)^T = G_l^T C_D^{-1} G_l + C_M^{-1}. \tag{2.13}$$

The Gauss-Newton method is then given by

$$m^{l+1} = m^l - H_l^{-1}\nabla S_l, \tag{2.14}$$

where l denotes the iteration index. Throughout, m^l represents the estimate of the minimum of *S(m)* obtained at the *lth* Gauss-Newton iteration and G_l denotes the sensitivity coefficient matrix G (Eq. 2.11) evaluated at m^l, ∇S_l denotes the gradient

evaluated at the old iterate (lth iterate) and H_l denotes the approximate Hessian evaluated at the old iteration. In applying the Gauss-Newton method, we do not invert H_l directly, but instead solve

$$H_l \delta m^{l+1} = -\nabla S_l , \tag{2.15}$$

for δm^{l+1}. The vector δm^{l+1} gives the search direction at the $(l+1)st$ iteration, and an efficient algorithm would need a line search technique (or similar technique) to determine how far to step in that direction, i.e., the iterative method would actually modify Eq. 2.14 to

$$m^{l+1} = m^l - \mu_l H_l^{-1} \nabla S_l = m^l - \mu_l \delta m^{l+1}, \tag{2.16}$$

where μ_l gives the size of the step in the direction δm^{l+1}. We use a restricted-step method instead of a line search to determine μ_l [21,22].

Using Eqs 2.12 and 2.13, Eq. 2.16 can be written as

$$\begin{aligned} m^{l+1} = m^l - \mu_l \left[G_l^T C_D^{-1} G_l + C_M^{-1} \right]^{-1} \times \\ \left[G_l^T C_D^{-1} (g(m^l) - d_{obs}) + C_M^{-1} (m^l - m_{prior}) \right], \end{aligned} \tag{2.17}$$

Tarantola[14] refers to μ_l as a damping factor.

From the matrix inverse lemma[40], we have

$$\left[G_l^T C_D^{-1} G_l + C_M^{-1} \right]^{-1} C_M^{-1} = I - C_M G_l^T \left[C_D + G_l C_M G_l^T \right] G_l . \tag{2.18}$$

From basic matrix algebra, the following matrix identity can be established.

$$\left[G_l^T C_D^{-1} G_l + C_M^{-1} \right]^{-1} G_l^T C_D^{-1} = C_M G_l^T \left[C_D + G_l C_M G_l^T \right]. \tag{2.19}$$

Using Eqs 2.18 and 2.19 in Eq. 2.17 and rearranging the resulting equation, one obtains the following form of the Gauss-Newton method:

$$m^{l+1} = \mu_l m_{prior} + (1-\mu_l)m^l - \mu_l\Big[C_M G_l^T \left(C_D + G_l C_M G_l^T\right)^{-1} \times \left(g(m^l) - d_{obs} + G_l(m^l - m_{prior})\right)\Big], \tag{2.20}$$

Although Eqs. 2.20 and 2.17 are mathematically equivalent, the computational time for the two schemes may be radically different. The inverse matrix on the right side of Eq. 2.17 is $N_p \times N_p$ where N_p is the number of parameters to be determined. The inverse matrix on the right side of Eq. 2.20 is a $N_d \times N_d$ matrix, where N_d is the total number of observed data. If $N_d << N_p$, which will often be the case, Eq. 2.20 should be applied. In Chapter IV, we will discuss reparameterization techniques which can reduce computational time and memory requirements.

In applying either form of the Gauss-Newton method, we set the convergence criterion as follows:

$$\frac{1}{N_d}\left(g(m^l) - d_{obs}\right)^T \left(g(m^l) - d_{obs}\right) < \sigma_d^2 . \tag{2.21}$$

This means if Eq. 2.21 is satisfied, we accept m^l as the maximum a posteriori estimate.

2.2.3 A Posteriori Covariance

If we assume $d = g(m)$ can be linearized around the maximum a posteriori estimate, m_∞, then

$$g(m) = g(m_\infty) + G_\infty (m - m_\infty) + \varepsilon(m), \tag{2.22}$$

where $\varepsilon(m)$ is the error introduced by linearization and G_∞ represents the sensitivity coefficient matrix evaluated at m_∞.

Using Eq. 2.22 into Eq. 2.10 gives

$$S(m)=\frac{1}{2}\Big[(m-m_{prior})^T C_M^{-1}(m-m_{prior})+\big(g(m_\infty)+G_\infty(m-m_\infty)+\varepsilon(m)-d_{obs}\big)^T \times C_D^{-1}\big(g(m_\infty)+G_\infty(m-m_\infty)+\varepsilon(m)-d_{obs}\big)\Big]. \tag{2.23}$$

We define d_∞ by

$$d_\infty = d_{obs} - g(m_\infty) + G_\infty m_\infty . \tag{2.24}$$

Then Eq. 2.23 becomes

$$\begin{aligned} S(m) &= \frac{1}{2}\Big[(m-m_{prior})^T C_M^{-1}(m-m_{prior})+\big(G_\infty m+\varepsilon(m)-d_\infty\big)^T C_D^{-1}\big(G_\infty m+\varepsilon(m)-d_\infty\big)\Big] \\ &= \frac{1}{2}\Big[(m-m_{prior})^T C_M^{-1}(m-m_{prior})+\big(G_\infty m-d_\infty\big)^T C_D^{-1}\big(G_\infty m-d_\infty\big)\Big] \\ &\quad +\big(G_\infty m-d_\infty\big)^T C_D^{-1}\varepsilon(m)+\frac{1}{2}\varepsilon(m)^T C_D^{-1}\varepsilon(m) \\ &= \hat{S}(m)+\big(G_\infty m-d_\infty\big)^T C_D^{-1}\varepsilon(m)+\frac{1}{2}\varepsilon(m)^T C_D^{-1}\varepsilon(m), \end{aligned} \tag{2.25}$$

where

$$\hat{S}(m)=\frac{1}{2}\Big[(m-m_{prior})^T C_M^{-1}(m-m_{prior})+\big(G_\infty m-d_\infty\big)^T C_D^{-1}\big(G_\infty m-d_\infty\big)\Big]. \tag{2.26}$$

Since $\hat{S}(m)$ is quadratic, any 2nd order Taylor series expansion of $\hat{S}(m)$ is exact, so use a Taylor expansion about m_∞ (most probable model) to obtain

$$\begin{aligned} \hat{S}(m) &= \hat{S}(m_\infty)+\big(\nabla\hat{S}(m_\infty)\big)^T(m-m_\infty)+\frac{1}{2}(m-m_\infty)^T\nabla\big(\nabla\hat{S}(m_\infty)\big)(m-m_\infty) \\ &= \hat{S}(m_\infty)+\big(\nabla\hat{S}(m_\infty)\big)^T(m-m_\infty)+\frac{1}{2}(m-m_\infty)^T\Big[C_M^{-1}+G_\infty^T C_D^{-1}G_\infty\Big](m-m_\infty). \end{aligned} \tag{2.27}$$

From Eq. 2.26,

$$\nabla\hat{S}(m_\infty)=C_M^{-1}(m_\infty-m_{prior})+G_\infty^T C_D^{-1}(G_\infty m_\infty-d_\infty). \tag{2.28}$$

From Eq. 2.24, $G_\infty m_\infty - d_\infty = g(m_\infty) - d_{obs}$, so we can rewrite Eq. 2.28 as

$$\nabla \hat{S}(m_\infty) = C_M^{-1}(m_\infty - m_{prior}) + G_\infty^T C_D^{-1}(g(m_\infty) - d_{obs}). \tag{2.29}$$

Comparing Eq. 2.29 with Eq. 2.12 with m^l replaced by m_∞, we see that

$$\nabla \hat{S}(m_\infty) = \nabla S(m_\infty) = 0, \tag{2.30}$$

where the last equality in Eq. 2.30 follows from the fact that m_∞ minimizes S(m). From Eq. 2.30, it follows that Eq. 2.27 can be reduced to

$$\begin{aligned} \hat{S}(m) &= \hat{S}(m_\infty) + \frac{1}{2}(m - m_\infty)^T \left[C_M^{-1} + G_\infty^T C_D^{-1} G_\infty\right](m - m_\infty) \\ &= \hat{S}(m_\infty) + \frac{1}{2}(m - m_\infty)^T C_{MP}^{-1}(m - m_\infty), \end{aligned} \tag{2.31}$$

where

$$C_{MP} = \left[C_M^{-1} + G_\infty^T C_D^{-1} G_\infty\right]^{-1}. \tag{2.32}$$

Using Eq. 2.31 in Eq. 2.25 gives

$$\begin{aligned} S(m) = \hat{S}(m_\infty) &+ \frac{1}{2}(m - m_\infty)^T C_{MP}^{-1}(m - m_\infty) \\ &+ \left(G_\infty m - d_\infty\right)^T C_D^{-1}\varepsilon(m) + \frac{1}{2}\varepsilon(m)^T C_D^{-1}\varepsilon(m). \end{aligned} \tag{2.33}$$

Thus, our a posteriori pdf can be written as

$$\begin{aligned} f_M(m|d_{obs}) &\propto \exp\left(-\frac{1}{2}S(m)\right) \\ &= \exp\left(-\frac{1}{2}\hat{S}(m_\infty)\right)\exp\left(-\frac{1}{2}\left((m - m_\infty)^T C_{MP}^{-1}(m - m_\infty)\right)\right)\times \\ &\quad \exp\left[\left(G_\infty m - d_\infty\right)^T C_D^{-1}\varepsilon(m) + \frac{1}{2}\varepsilon(m)^T C_D^{-1}\varepsilon(m)\right]. \end{aligned} \tag{2.34}$$

If we assume $\varepsilon(m) = 0$, or equivalently that g(m) are linearly related to the model m (see Eq. 2.22), then Eq. 2.34 gives

$$f_M(m|d_{obs}) \propto \exp\left(-\frac{1}{2}\left((m-m_\infty)^T C_{MP}^{-1}(m-m_\infty)\right)\right). \tag{2.35}$$

Eq. 2.35 shows that when the data are linearly related to the model, the a posteriori probability density function is Gaussian, and the a posteriori covariance matrix is

$$\begin{aligned} C_{MP} &= \left[C_M^{-1} + G_\infty^T C_D^{-1} G_\infty\right]^{-1} \\ &= C_M - C_M G_\infty^T (G_\infty C_D^{-1} G_\infty^T + C_D)^{-1} G_\infty C_M \,. \end{aligned} \tag{2.36}$$

The preceding results were included for completeness but are not novel. The basic result, Eq. 2.35, can be found in Tarantola[13]. Also Eq. 2.34 was used by Oliver et al.[35] as a basis for generating more efficient Markov Chain Monte Carlo method for sampling the a posteriori pdf.

2.2.4 Realizations

In previous subsections, we discussed how to generate the maximum a posteriori estimate and posteriori covariance matrix by the Gauss-Newton procedure. Here, we present a method to generate realizations by sampling the posteriori probability density function of our model after conditioning to all available data. Again, the basic results are known, see for example, Tarantola[14] and Refs. 19, 23 and 24.

If hard data are used as conditioning data, we propose a two-step procedure[23-27] to generate realizations. In the first step, we obtain the most probable model ($m_{h,\infty}$) and posteriori covariance (C_{Mh}) conditioned to hard data and prior information. In subsection (2.3) , we will show how to incorporate hard data into our model. In the second step, we condition to pressure data by minimizing S(m) where S(m) is given by the right side of Eq.

2.10 with m_{prior} replaced by $m_{h,\infty}$ and C_M replaced by C_{Mh}. The a posteriori covariance matrix after conditioning to both hard data and pressure data is given by

$$C_{MP} = C_{Mh} - C_{Mh} G_\infty^T (G_\infty C_{Mh} G_\infty^T + C_D)^{-1} G_\infty C_{Mh}, \tag{2.37}$$

where G_∞ is the sensitivity coefficient matrix evaluated at m_∞ which denotes the maximum a posteriori estimate obtained from the Gauss-Newton procedure. If no hard data are used as conditioning data, then in Eq. 3.37, C_{Mh} is replaced by C_M , i.e., Eq. 2.37 is the same as Eq. 2.36.

As shown in Ref. 23-25, realizations of the porosity and log-permeability fields can be generated from

$$m_r = m_\infty + LZ_r, \tag{2.38}$$

where Z_r is a vector of independent standard random normal deviates, and LL^T represents the Cholesky decomposition of the a posteriori covariance matrix. At best, this procedure only generates an approximate sampling of the a posteriori pdf since it assumes that Eq. 2.6 is linear, i.e., pressure data are linearly related to the model.

The diagonal elements of C_{MP} give the a posteriori variances of model parameters after conditioning to pressure data. If the variance of a particular model parameter m_j is significantly less than the corresponding variance before incorporating pressure data, then pressure data have been of significant value in reducing the level of uncertainty in this model parameter. An approximate 95 percent confidence interval for the *j*th model parameter after conditioning to pressure data is given by $[m_{\infty,j} - 2\sigma_j^2, m_{\infty,j} + 2\sigma_j^2]$ where σ_j^2 is the a posteriori variance for this model parameter, i.e., the *j*th diagonal element of C_{MP}. Reducing the variance reduces the size of the confidence interval and reduces the

variability in realizations of the model parameters obtained by applying Eq. 2.38 to generate realizations. Similarly, the diagonal elements of C_{Mh} give the a posteriori variances for the model parameters after conditioning to hard data. The ratio of these posteriori variances to the corresponding prior variances gives a measure of the reduction in the uncertainty in model parameters achieved by incorporating hard data, i.e., a measure of the value of hard data in terms of the resulting reduction in variability of realizations of the rock property fields. If we condition only to pressure data and all diagonal elements of C_{MP} are equal to the corresponding diagonal elements of C_M, then we say that the incorporation of the pressure data is of no value for reducing the uncertainty in the individual model parameters (gridblock log-permeabilities and porosities). However, even if the uncertainty in individual model parameters is not reduced, it is still possible that pressure data can be of value for reducing the uncertainty in linear combinations of model parameters, e.g., average reservoir porosity and thickness-averaged permeability. As will be seen in the layered reservoir example considered later, conditioning the rock property fields to pressure data reduces the uncertainty in thickness-averaged permeability much more than it reduces the uncertainty in individual gridblock log-permeabilities. This occurs primarily because the variance of a linear combination of model parameters involves the covariance between pairs of individual parameters and these covariances may be negative. Thus, we see that by computing and comparing variances, one can obtain a measure of the value of collecting a particular type of data, where high value means a significant reduction in the uncertainty as measured by the variances.

2.3 **Conditioning to Hard Data**

In this work, hard data refer to "measurements" of gridblock values of porosity and permeability (converted to "measurements" of log-permeability) at the location of wells. This obviously assumes that any measurements of rock properties at the well locations have been properly scaled up to gridblock size. Hard data measurements errors are modeled as independent Gaussian random variables with zero mean and prescribed variances. For hard porosity data, the standard deviation for measurement errors is denoted by $\sigma_{\phi d}^2$ and the standard deviation for the measurement errors in hard log-permeability data is assumed denoted by σ_{kd}^2.

We let $d_{h,obs}$ represent observed data (hard data) for porosity and log-permeability (we assume that there is no hard data for skin factors) and let d_h represent the hard data function which is related to the model by a linear operator G_h so that

$$d_h = G_h m. \tag{2.39}$$

We assume the dimension of d_h and $d_{h,obs}$ is N_h and let $d_{h,i}$ and $d_{h,obs,i}$ respectively represent the components of d_h and $d_{h,obs}$, $i = 1,2,...,N_h$, so that G_h is a $N_h \times N_p$ matrix. Moreover, we let the $d_{h,obs,i}$ represent the measured value of $m_{r_i}, 1 \le i \le N_h$. Then Eq. 2.39 can be written as

$$\begin{bmatrix} d_{h,1} \\ d_{h,2} \\ \vdots \\ d_{h,N_h} \end{bmatrix} = \begin{bmatrix} g_{h,1}^1 & g_{h,2}^1 & \cdots & g_{h,N_p}^1 \\ g_{h,1}^2 & g_{h,2}^2 & \cdots & g_{h,N_p}^2 \\ \vdots & \vdots & \ddots & \vdots \\ g_{h,1}^{N_h} & g_{h,2}^{N_h} & \cdots & g_{h,N_p}^{N_h} \end{bmatrix} \begin{bmatrix} m_1 \\ m_2 \\ \vdots \\ m_{N_p} \end{bmatrix}, \tag{2.40}$$

where $g_{h,j}^i = \begin{cases} 1, \text{ if } j = r_i; \\ 0, \text{ if } j \ne r_i. \end{cases}$, for $i = 1,2,...,N_h$, $j = 1,2,...,N_p$.

Similarly to section 2.2.1, by a standard application of Bayes's theorm, it follows that the most probable model which honors hard data and the prior information is one that minimizes the following objective function

$$S_h(m) = \frac{1}{2}\Big[(m - m_{prior})^T C_M^{-1}(m - m_{prior}) + (G_h m - d_{h,obs})^T C_h^{-1}(G_h m - d_{h,obs})\Big], \tag{2.41}$$

which C_h is the diagonal covariance matrix of hard data measurement error, i.e., errors in porosity and log-permeability measurements.

Setting the gradient of $S_h(m)$ with respect to m equal to zero, we have

$$\nabla_m S_h(m) = C_M^{-1}(m - m_{prior}) + G_h^T C_h^{-1}(G_h m - d_{h,obs}) = 0. \tag{2.42}$$

or

$$C_M^{-1}(m - m_{prior}) = -G_h^T C_h^{-1}(G_h m - d_{h,obs}). \tag{2.43}$$

Adding $G_h^T C_h^{-1} G_h (m - m_{prior})$ to both sides of Eq. 2.43, we obtain

$$(G_h^T C_h^{-1} G_h + C_M^{-1})(m - m_{prior}) = -G_h^T C_h^{-1}(G_h m - d_{h,obs} - G_h(m - m_{prior})), \tag{2.44}$$

or

$$(G_h^T C_h^{-1} G_h + C_M^{-1})(m - m_{prior}) = -G_h^T C_h^{-1}(G_h m_{prior} - d_{h,obs}). \tag{2.45}$$

So, our solution (maximum a posteriori estimate) is

$$m = m_{prior} - (G_h^T C_h^{-1} G_h + C_M^{-1})^{-1} G_h^T C_h^{-1}(G_h m_{prior} - d_{h,obs}). \tag{2.46}$$

The maximum a posteriori estimation conditioned to hard data and prior information can be obtained analytically using Eq. 2.45 and is denoted by $m_{h,\infty}$, i.e., from Eq. 2.46,

$$m_{h,\infty} = m_{prior} - (G_h^T C_h^{-1} G_h + C_M^{-1})^{-1} G_h^T C_h^{-1}(G_h m_{prior} - d_{h,obs}). \tag{2.47}$$

Using the basis given in subsection 2.2.3, the a posteriori covariance matrix after conditioning to hard data and prior information is given by

$$C_{Mh} = C_M - C_M G_h^T (G_h C_M G_h^T + C_{Dh})^{-1} G_h C_M . \tag{2.48}$$

2.4 **Conditioning to Layer Flow Rates**

As shown in Refs. 41 and 42, for three-dimensional problems, measured wellbore pressures can not resolve individual layer properties (permeability, porosity and skin factor). More specifically, even though wellbore pressures resolve thickness averaged permeability reasonably well (i.e., reduce the uncertainty in thickness averaged horizontal permeability), they can not resolve individual layer permeabilities and skin factors. To obtain the estimation of layer properties, we need other information, i.e., individual layer flow rate data. Production logging can provide us with layer flow rate information. Using this information together with wellbore pressure, we can obtain more reliable estimate of layer permeabilities and layer skin factors.

The methodology for conditioning to both wellbore pressure and layer flow rate is theoretically the same as conditioning to wellbore pressure. We can just follow the derivation described in previous sections for conditioning to wellbore pressure. The difference is that now we have more observed data.

As indicated previously, we assume the total number of observed wellbore pressure data is N_d, the number of model parameters is N_p. We assume that the total number of observed layer flow rate data is N_q and assume that measurement errors for layer flow

rates can be modeled as independent Gaussian random variables with zero mean and variance σ_q^2.

The total covariance matrix for measurement errors is now

$$C_D = \begin{bmatrix} C_{D,p} & 0 \\ 0 & C_{D,q} \end{bmatrix}, \tag{2.49}$$

where

$$C_{D,p} = \begin{bmatrix} \sigma_d^2 & 0 & \cdots & 0 \\ 0 & \sigma_d^2 & \cdots & 0 \\ \vdots & \vdots & \ddots & \vdots \\ 0 & 0 & \cdots & \sigma_d^2 \end{bmatrix}, \tag{2.50}$$

is the $N_d \times N_d$ covariance matrix related to wellbore pressure measurement errors and

$$C_{D,q} = \begin{bmatrix} \sigma_q^2 & 0 & \cdots & 0 \\ 0 & \sigma_q^2 & \cdots & 0 \\ \vdots & \vdots & \ddots & \vdots \\ 0 & 0 & \cdots & \sigma_q^2 \end{bmatrix}, \tag{2.51}$$

is the $N_q \times N_q$ covariance matrix for layer flow rate measurement errors. Now C_D is an $(N_d + N_q) \times (N_d + N_q)$ matrix.

The sensitivity coefficient matrix is now given by

$$G = \begin{bmatrix} G_p \\ G_q \end{bmatrix}, \tag{2.52}$$

where G_p is the sensitivity coefficient matrix related to wellbore pressure and is a $N_d \times N_p$ matrix; G_q is the sensitivity coefficient matrix related to layer flow rates and is a $N_q \times N_p$ matrix. The procedure for the calculation of G_q will also be presented in the next chapter. The size of G is $(N_d + N_q) \times N_p$.

The data mismatch includes the mismatch between observed wellbore pressure and calculated wellbore pressure, and also the mismatch between observed layer flow rate and calculated layer flow rate, i.e.,

$$g(m) - d_{obs} = \begin{bmatrix} p(m) - d_{obs}^{p} \\ q(m) - d_{obs}^{q} \end{bmatrix}, \tag{2.53}$$

where $p(m) - d_{obs}^{p}$ is the vector of wellbore pressure mismatches and $q(m) - d_{obs}^{q}$ is the vector of layer flow rate mismatches. Here, d_{obs}^{p} represents the vector of all observed pressure data used as conditioning data, d_{obs}^{q} represents the vector of all observed flow rate data used as conditioning data and our vector of the total observed data is

$$d_{obs} = \begin{bmatrix} d_{obs}^{p} \\ d_{obs}^{q} \end{bmatrix}. \tag{2.53a}$$

Similarly, for a given m, $d^{p} = p(m)$ represents calculated pressure data corresponding to d_{obs}^{p} and $d^{q} = q(m)$ represents calculated flow rate data corresponding to d_{obs}^{q} and

$$d = \begin{bmatrix} d^{p} \\ d^{q} \end{bmatrix} = \begin{bmatrix} p(m) \\ q(m) \end{bmatrix}. \tag{2.53b}$$

With the preceding definitions of d, d_{obs}, C_D and G, all equations presented previously still apply.

With these modifications, we can apply the Gauss-Newton method to obtain the maximum a posteriori estimate and posteriori covariance matrix conditioned to both observed wellbore pressures and observed layer flow rates.

2.5 Computational Examples

2.5.1 True Reservoir Model

A true three-layer reservoir is considered with $k_x = k_y = k$ and $k_z = 0$, i.e., there is no cross-flow between layers. However, layers communicate through the wellbore so cross-flow between layers can occur through the wells. Fig. 2.1 shows the areal grid used, well locations and well numbers for the problem considered. An 11×11 areal grid is used with 100×100 ft^2 gridblocks and three gridblocks in the vertical direction with a uniform vertical grid. Each layer is ten feet thick. The example pertains to a five-well problem. The center well (well A) is located in areal gridblock (6,6) and is produced at a

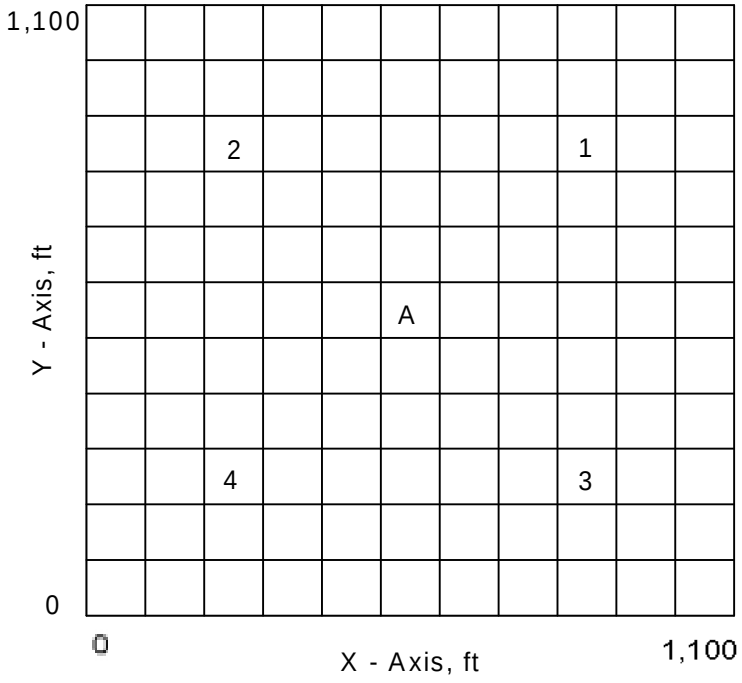

Fig. 2.1 - Areal grids, well locations and well numbers.

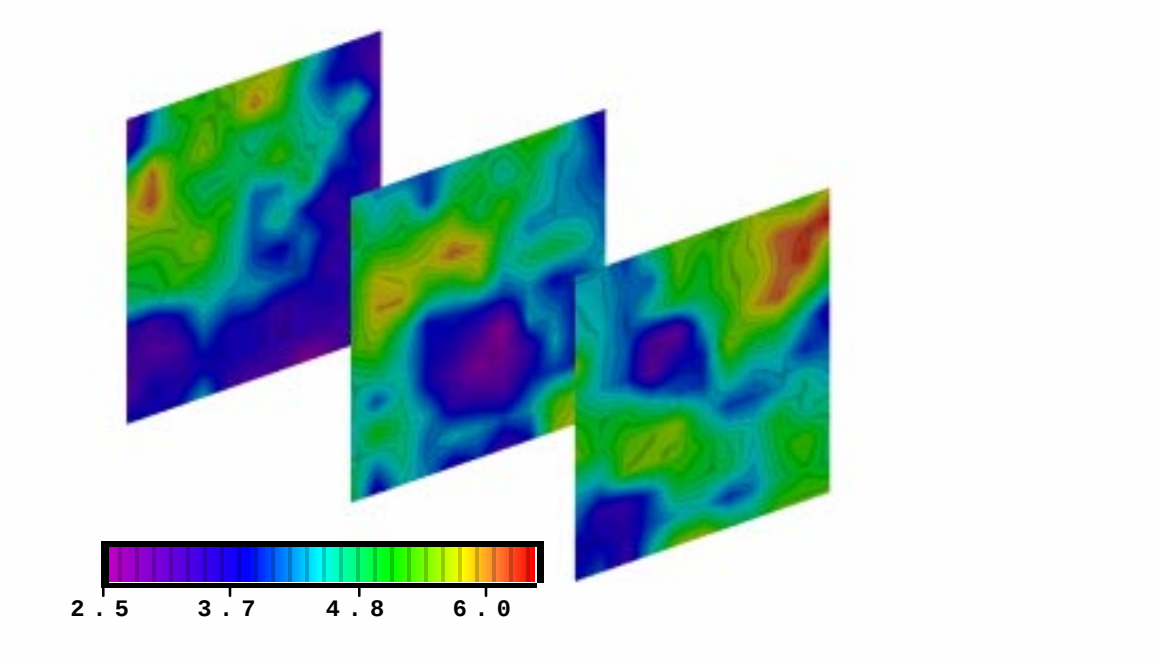

Fig. 2.2 - True log-permeability fields.

constant rate of 500 RB/D. This active well is surrounded by four observation wells located at areal gridblocks (9,9) for observation well 1, (3,9) for observation well 2, (9,3) for observation well 3 and (3,3) for observation well 4.

Each layer has its own two-dimensional isotropic spherical variogram model for the log-permeability field. For layer 1 (top layer), the range of the variogram for log-permeability is 450 ft. The prior mean for $ln(k)$ is 4.0 with variance equal to 0.6. For layer 2, the range of the variogram for log-permeability is 500 ft, the prior variance is equal to 0.5 and the prior mean for $ln(k)$ is 4.5. For layer 3, the range of the variogram for log-permeability is 400 ft, the prior mean is 5.0 and the prior variance is 0.6. In layer 1, the prior mean of the porosity was set equal to 0.15 and the prior variance was 0.0025. In layer 2, the prior mean of the porosity was set equal to 0.20 and the prior variance was 0.0025. In layer 3, the prior mean of the porosity was set equal to 0.25 and the prior variance was 0.0025. A prior correlation coefficient of 0.6 was assumed between the

porosity and log-permeability fields. In each layer, the porosity variogram is obtained from the log-permeability variogram by multiplying the latter variogram by $\sigma_\phi^2 / \sigma_k^2$; see Refs. 3 and 18.

In this problem, the average well skin factor is 4.0. Well skin factors vary significantly from well to well and from layer to layer, and if estimation of well skin factors are not known, we normally assign high variances to the skin factors. However, wellbore pressure can not accurately resolve individual layer skin factors; thus in this example, we use a reasonably small variance ($\sigma_s^2 = 4.0$) on well skin factors.

The "true" permeability and porosity distributions were obtained as an unconditional simulation generated from a Cholesky decomposition of the prior covariance matrix. The true log-permeability field is shown in Fig. 2.2 with the true porosity field shown in Fig. 2.3. Note that the left slice on the figure is the top layer (layer 1) and the right slice is the bottom layer (layer 3). The pressure data were obtained by running the simulator using the true gridblock values of permeability and porosity. The duration of the synthetic multiwell test was 1.7 days. During the test, significant crossflow occurs through observation wells with flows rates on the order of 20 RB/D at the end of the test. The observation well pressure drops are shown in Fig. 2.4.

We use the exact value of log-permeability and porosity at well locations (one active well and four observation wells) as hard data. We assume the variance on log-permeability measurement error is $\sigma_{h,k}^2 = 0.0016$ and variance for porosity measurement error is $\sigma_{h,\phi}^2 = 0.00009$.

2.5.2 Maximum a Posteriori Estimate (Most Probable Model)

The maximum a posteriori estimate of log-permeability obtained by conditioning only to hard data is shown in Fig. 2.5. Comparing Fig. 2.5 with Fig. 2.2, we see that as expected, the maximum a posteriori estimate matches the true field only at regions near the wells. The maximum a posteriori estimate obtained by conditioning to only pressure data is shown in Fig. 2.6. Comparing with the true case, the layer log-permeability maximum a posteriori estimate is quite different. However, we show later that pressure

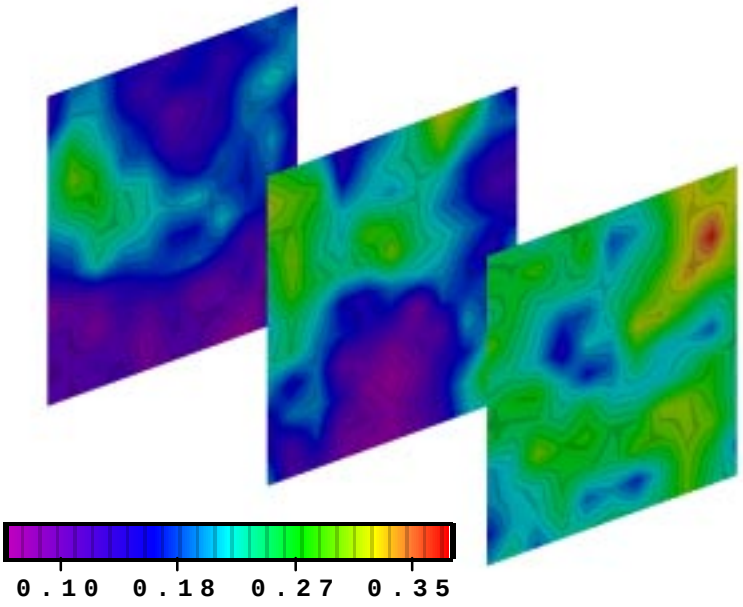

Fig. 2.3 - True Porosity fields.

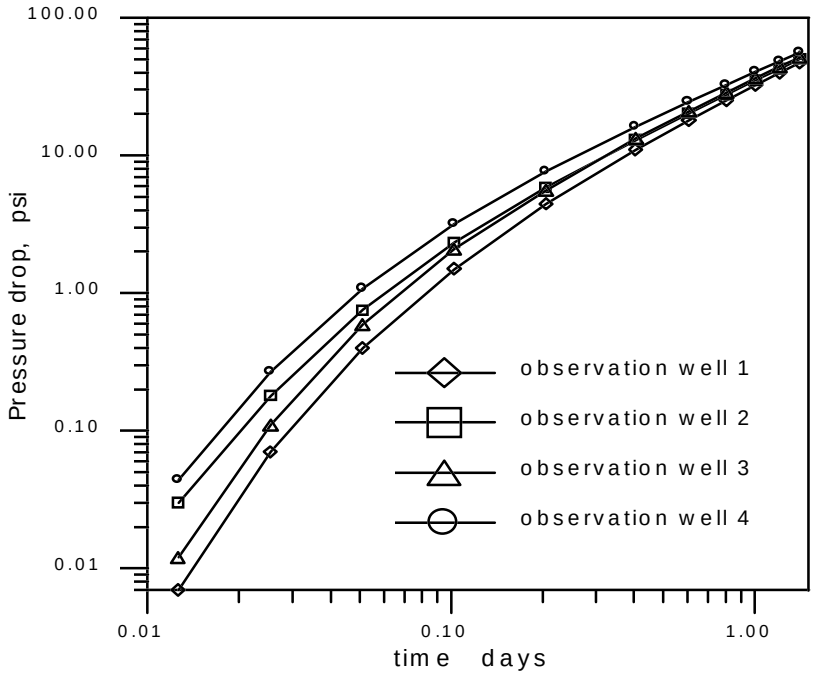

Fig. 2.4 - Pressure drop at four observation wells.

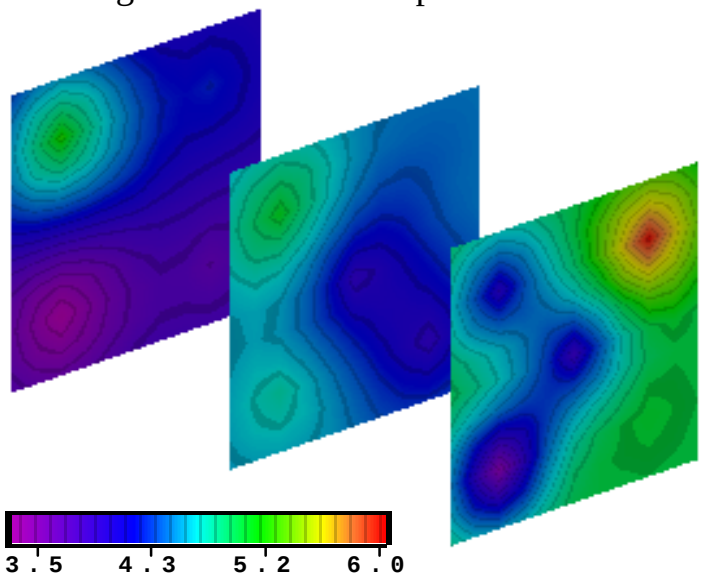

Fig. 2.5 - Maximum a posteriori estimate of log-permeability fields conditioned only to hard data.

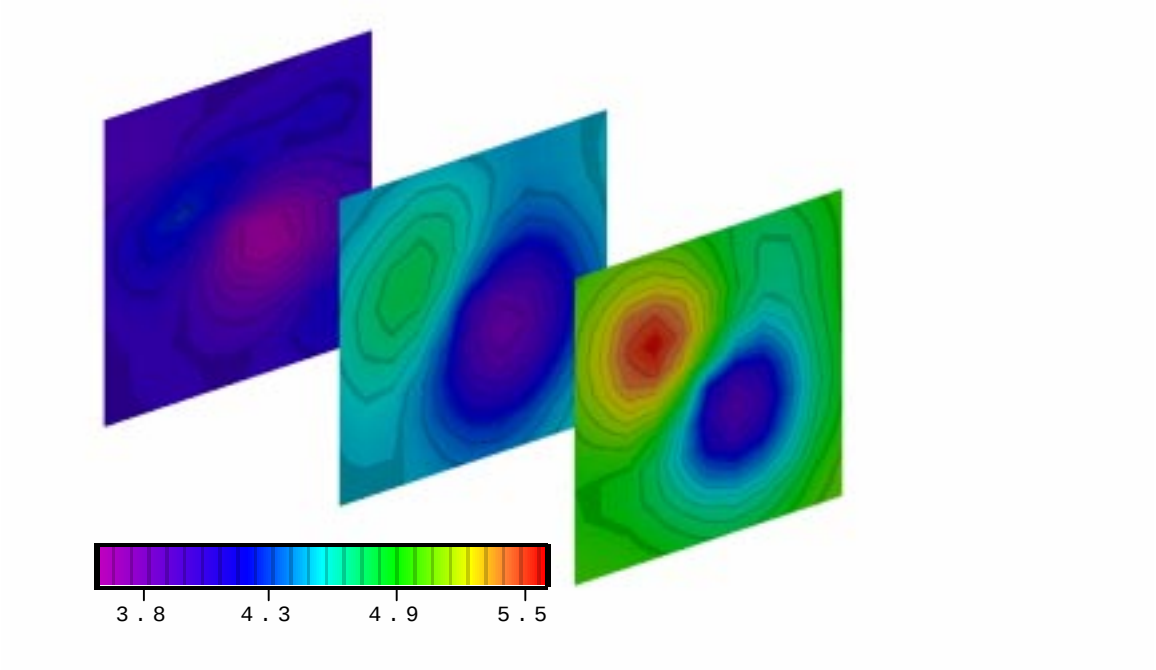

Fig. 2.6 - Maximum a posteriori estimate of log-permeability fields, conditioned only to pressure data.

can resolve the thickness averaged permeability reasonably well. The maximum a posteriori estimate after conditioning to both hard data and pressure data is shown in Fig. 2.7. It is clear that the maximum a posteriori estimate conditioned both to hard data and pressure data is “better” (more closely captures the features of the true case) than the maximum a posteriori estimate obtained by conditioning only to hard data (Fig. 2.5) or only to pressure data (Fig. 2.6). Note that in layer 3, the maximum a posteriori estimate conditioned to both hard data and pressure data gives low permeabilities in the interwell region between the active well and observation well 4. Except for this difference, the maximum a posteriori is qualitatively similar to the true log-permeability field shown in Fig. 2.2. The reason that low permeabilities are obtained in region between the active well and observation well 4 in layer 3 is that the true values of log-permeability at the two well

gridblocks are low. Since these two values are fixed essentially exactly by the hard data and the prior model indicates that log-permeability is correlated over a distance of 400 feet, it is difficult for pressure data to resolve these values correctly even though pressures at the two wells are relatively sensitive to the permeabilities in the interwell region.

Fig. 2.8 shows the maximum a posteriori estimate of the porosity field conditioned to both hard data and pressure data. Even though porosity is correlated to log-permeability for the example considered here, pressure data does not resolve the porosity field well. Note this estimate bears only rough similarity to the true porosity field, Fig. 2.3. However, since pseudosteady-state flow exists at the end of the test, we expect to be able to estimate average reservoir porosity from only pressure data. The average reservoir

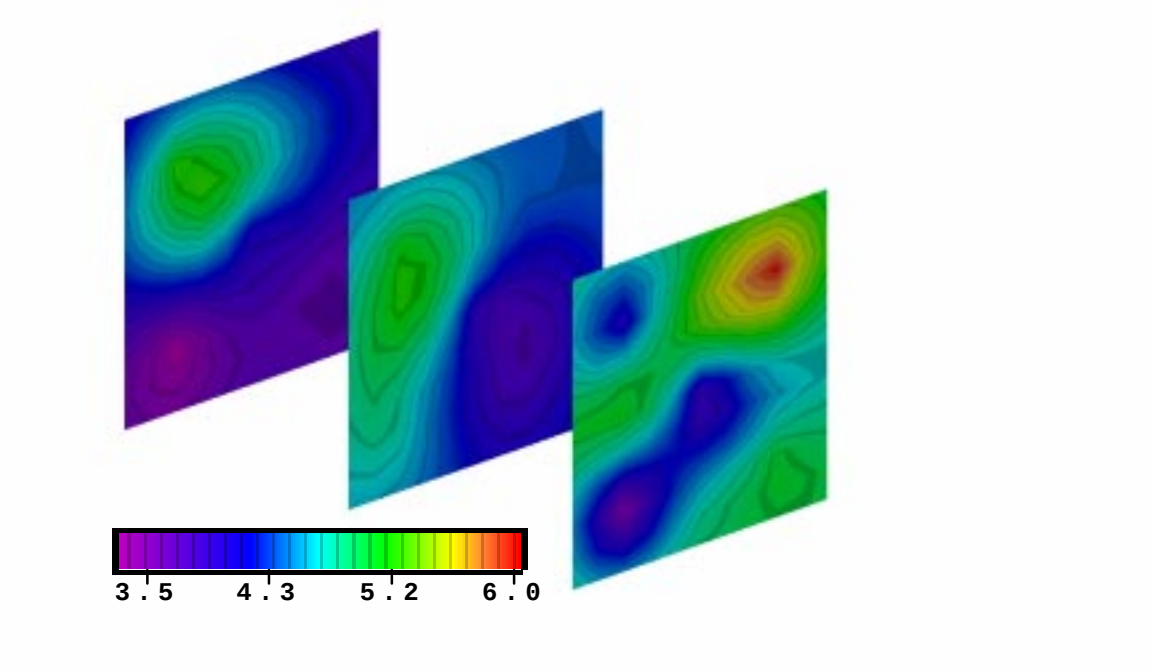

Fig. 2.7 - Maximum a posteriori estimate of log-permeability fields, conditioned to hard data and pressure data.

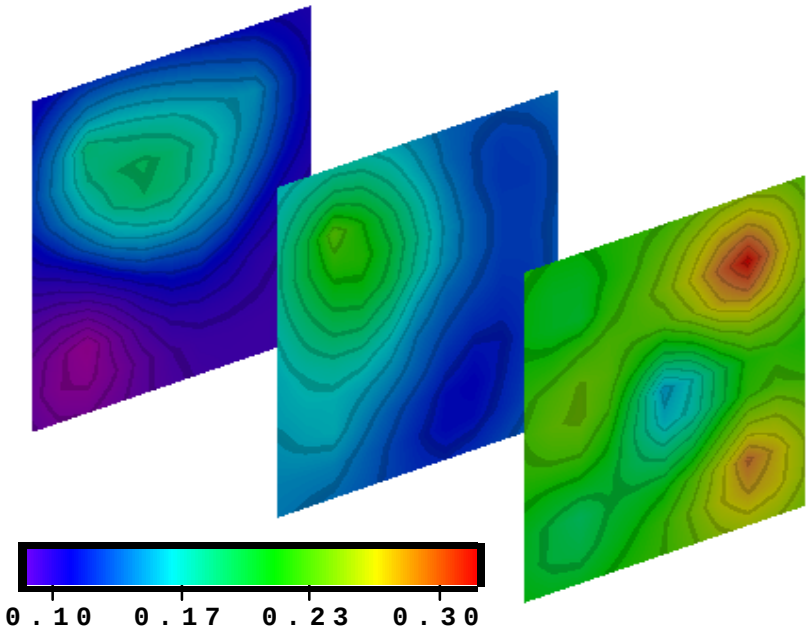

Fig. 2.8 - Maximum a posteriori estimate of porosity fields, condition to hard data and pressure data.

porosity for the truth case was $\bar{\phi} = 0.202$. The average reservoir porosity computed from the maximum a posteriori estimate obtained by conditioning only to pressure data was $\bar{\phi} = 0.192$. The average reservoir porosity computed from the maximum a posteriori estimate obtained by conditioning to both hard data and pressure data was $\bar{\phi} = 0.203$. Thus, we see that pseudosteady-state pressure data by themselves are sufficient to give a good estimate of average reservoir porosity.

2.5.3 Posteriori Covariance

To consider the reduction in uncertainty in the log-permeability field obtained by conditioning to hard data and/or pressure data, normalized variances are plotted i.e., for each layer the normalized a posteriori variances represent the a posteriori variances for the layer divided by the prior variance of log-permeability for the layer. Thus, if adding

conditioning data has no value in reducing the uncertainty for a gridblock value of log-permeability, the normalized variance will be equal to unity and a normalized variance on the order of 0.1 represents a ten fold reduction in the level of uncertainty. We also sum these normalized variances over the gridblocks and divide by the number of gridblocks to obtain a quantitative measure in the overall reduction in uncertainty for the whole log-permeability field. We refer to this last term as the global uncertainty index, $I_G(k)$, or more specifically, the global uncertainty index for the log-permeability field. Similar ideas can be applied to evaluate the uncertainty in the porosity field. So we have

$$I_G(k) = \frac{1}{M}\sum_{i=1}^{M}\frac{Var(\ln(k_{\infty,i}))}{Var((\ln(k_{prior,i}))}, \tag{2.54}$$

$$I_G(\phi) = \frac{1}{M}\sum_{i=1}^{M}\frac{Var(\phi_{\infty,i})}{Var(\phi_{prior,i})}. \tag{2.55}$$

This concept is a slight modification of an idea of Shah et al.[13] who evaluated the accuracy of the maximum a posteriori estimate by considering the magnitude of the trace of the a posteriori covariance matrix.

The normalized a posteriori variances of log-permeability after conditioning only to hard data is shown in Fig. 2.9 and in this case, the global uncertainty index was equal to 0.812. The a posteriori variances after conditioning to only pressure data are shown in Fig. 2.10 and in this case $I_G(k)$ = 0.836. Although the global uncertainty indices are almost the same for these two results, the reduction in uncertainty of individual gridblock values of *ln* (*k*) are quite different for the two cases. Hard data reduce the variance to almost zero at gridblocks containing wells (Fig. 2.9), but results in only a very small reduction in variances at distances far from the wells. When the maximum a posteriori

estimate is conditioned only to pressure data, the variances at gridblocks containing wells are not necessarily small, but the overall reduction in uncertainty as measured by the global uncertainty index is essentially equal to the one obtained after conditioning only to hard data.

The a posteriori variances after conditioning to both hard data and pressure data are shown in Fig. 2.11. In this case, $I_G(k)$ = 0.641. Note the combination of hard data plus pressure data results in a significant decrease in the overall uncertainty in the log-permeability field as well as a reduction in the uncertainty at gridblocks near wells. The reduction in uncertainty is greater than was achieved by using only pressure data or only

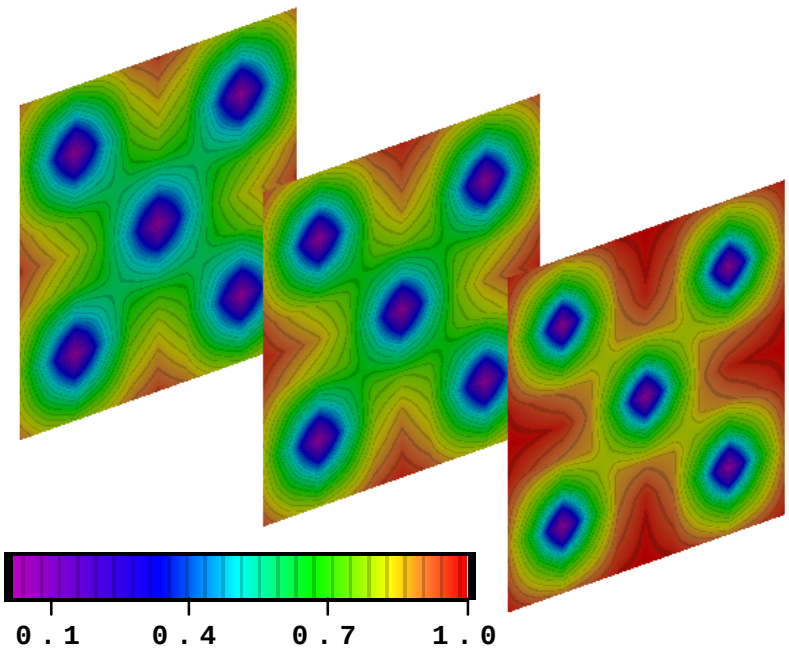

Fig. 2.9 - Normalized a posteriori variances of log-permeability, conditioned only to hard data.

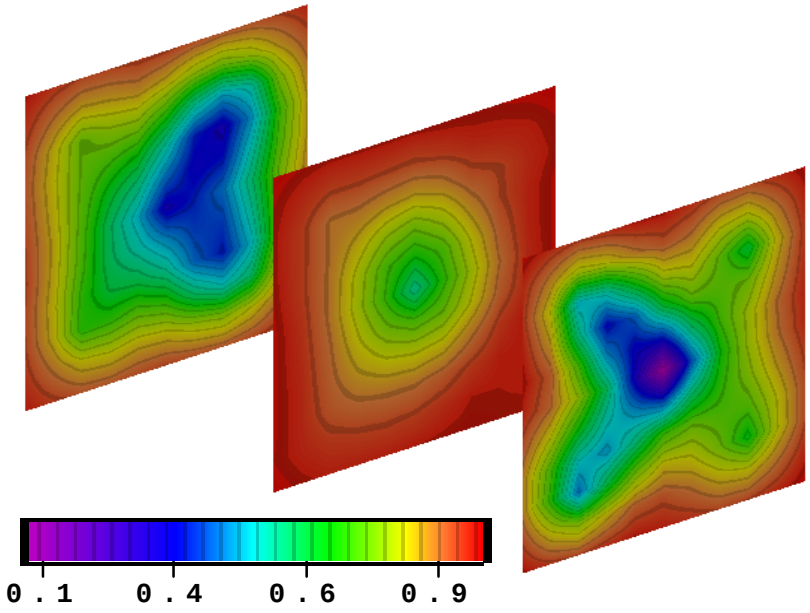

Fig. 2.10 - Normalized a posteriori variances of log-permeability, conditioned only to pressure data.

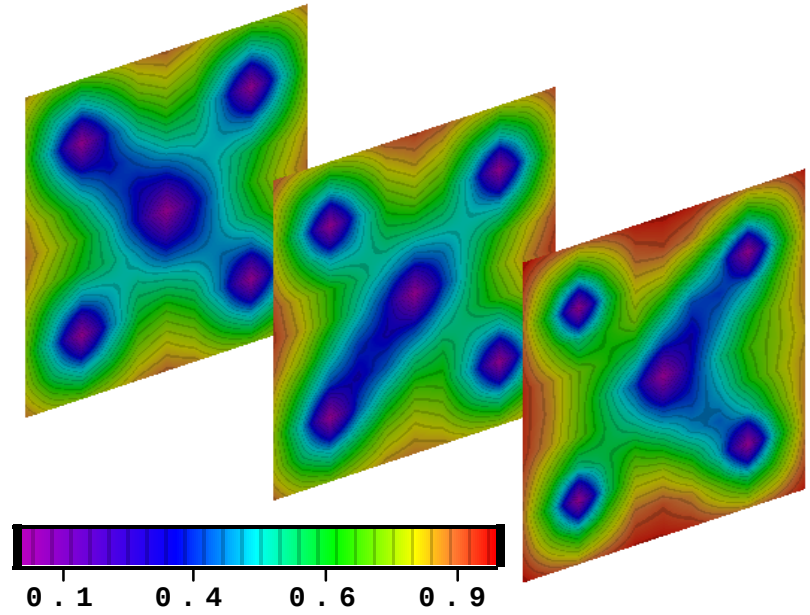

Fig. 2.11 - Normalized a posteriori variances of log-permeability, conditioned to hard data and pressure data.

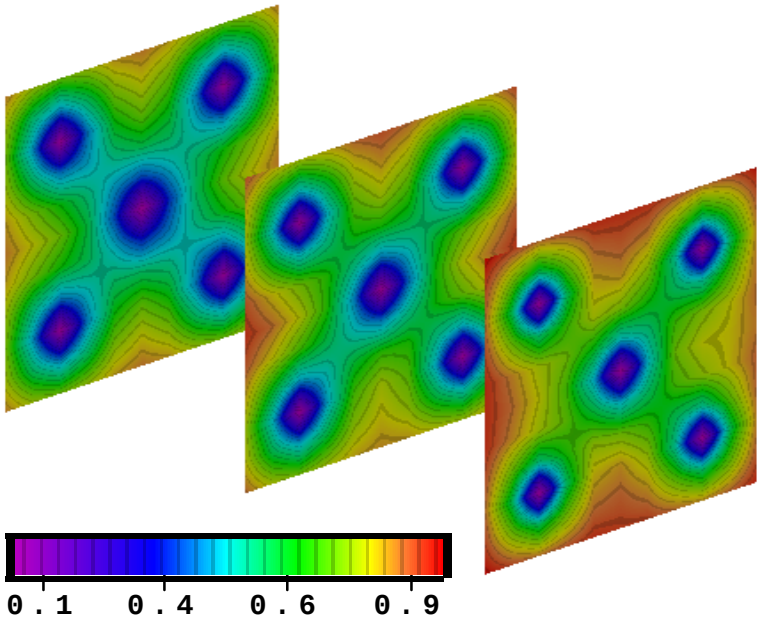

Fig. 2.12 - Normalized a posteriori variances of porosity, conditioned to hard data and pressure data.

hard data as conditioning data. This is the expected result since pressure data often resolve thickness-averaged permeability, but does not resolve individual layer permeabilities. Adding hard data at wells essentially fixes the individual layer permeabilities at the wells, and then by adding pressure data as conditioning data, individual layer permeabilities are much better resolved.

Fig. 2.12 shows the normalized a posteriori variances of porosity after conditioning to both hard data and pressure data. We note that the porosity field is not resolved as well by pressure data as is the log-permeability field. In fact, the normalized a posteriori variances for porosity after conditioning to both hard data and pressure data look very similar qualitatively to the results of Fig. 2.9 (only reduces the variance at near well region). The global uncertainty index for porosity in this case is equal to $I_G(\phi) = 0.745$. The global index only conditioning to hard data is $I_G(\phi) = 0.879$ and the global index only

conditioning to pressure data is $I_G(\phi) = 0.882$. This means that only conditioning to hard data, the overall uncertainty in the porosity field is only reduced a small amount, while by conditioning only to pressure data, the overall uncertainty in porosity field has been reduced much more (about a 30% reduction). By conditioning to both hard data and pressure, the overall uncertainty is reduced slightly more than by conditioning only to pressure data.

2.5.4 Thickness Averaged Permeability

It is well known that for layered systems, classical semilog analysis can only yield an estimate of thickness-averaged permeability. For the example under consideration, there exist three layers of equal thickness so this average permeability is given by

$$\bar{k}(x_i, y_j) = \frac{1}{3}\sum_{l=1}^{3} k_l(x_i, y_j), \tag{2.56}$$

where $k_l(x_i, y_j)$ denotes the horizontal permeability in layer l in the areal gridblock centered (x_i, y_j).

To continue the example, we investigate the resolution of the thickness-averaged permeability. Since the inverse problem is phrased in terms of $\ln(k)$, we must convert variances of $\ln(k)$ to variances for $\bar{k}$. When one converts variances of $\ln(k)$ to variances for *k*, the mean of $\ln(k)$ affects the variance of *k*. Specifically, for a single stochastic

variable $\ln(k)$ having a normal distribution with mean μ and variance σ^2, the mean and variance for *k* are given, respectively, by

$$\alpha = exp(\mu)exp(\sigma^2 / 2), \tag{2.57}$$

and

$$\beta^2 = \alpha^2(exp(\sigma^2) - 1). \tag{2.58}$$

Thus, if *X* and *Y* are log-normal and $\ln(X)$ and $\ln(Y)$ have equal variances, but the mean of $\ln(X)$ is larger than the mean of $\ln(Y)$, the variance for *X* will be larger than the variance of *Y*. This suggests that to compare the uncertainty in *X* to the uncertainty in *Y* on a common scale, each variance should be divided by the mean (expected value) squared, i.e., one can consider dimensionless variances. Thus, in considering thickness-averaged permeability, we divide the variances of $\bar{k}$ by the square of the expected value of $\bar{k}$, to obtain the dimensionless variance. Note this is similar to constructing dimensionless confidence intervals, or confidence intervals in terms of percentages.

For the prior model, Eqs. 2.57 and 2.58 can be applied to compute the expected value and variance for each $k_l(x_i, y_j)$ variable. Permeabilities are uncorrelated in the vertical direction since each layer has its own two-dimensional variogram for log-permeability. Thus, the expected value and variance of the thickness-averaged permeability can be calculated as

$$E\left[\bar{k}(x_i, y_j)\right] = \frac{1}{3}\sum_{l=1}^{3} E\left[k_l(x_i, y_j)\right], \tag{2.59}$$

and

$$Var\left[\bar{k}(x_i, y_j)\right] = \frac{1}{9}\sum_{l=1}^{3} Var\left[k_l(x_i, y_j)\right], \tag{2.60}$$

where *E* denotes expected value and *Var* denotes variance. The corresponding dimensionless variances are given by

$$Var_D\left[\bar{k}(x_i, y_j)\right] = \frac{Var\left[\bar{k}(x_i, y_j)\right]}{E^2\left[\bar{k}(x_i, y_j)\right]}. \tag{2.61}$$

After conditioning to hard data, the maximum a posteriori estimate of each gridblock value of *ln*(*k*) gives the approximate a posteriori mean and the diagonal entries of the a posteriori covariance matrix give the a posteriori variances. Since after conditioning to hard data, log-permeabilities are still uncorrelated in the z-direction, we can use the same procedure used for the prior model to compute the dimensionless variances $Var_{Dh}\left[\bar{k}(x_i, y_j)\right]$, where the subscript *Dh* is used to indicate that these are dimensionless variance after conditioning to hard data.

After conditioning to pressure data, however, permeabilities are correlated in the vertical direction. Thus, converting from variances for $\ln(k)$ at each gridblock to variances for $\bar{k}$ is not straightforward. To estimate expected values and variances for $\bar{k}$, we generate *N* realizations of the rock property fields from Eq. 2.38 and compute $\bar{k}_r(x_i, y_j)$ for each realization *r* at each areal location. (In our case, we used N=50.) We then estimate the expected value and variance at each location from

$$E\left[\bar{k}(x_i, y_j)\right] = \frac{1}{N}\sum_{r=1}^{N}\bar{k}_r(x_i, y_j), \tag{2.62}$$

and

$$Var\left[\bar{k}(x_i, y_j)\right] = \frac{1}{N-1}\sum_{r=1}^{N}\left(\bar{k}_r(x_i, y_j) - E\left[\bar{k}_r(x_i, y_j)\right]\right)^2. \tag{2.63}$$

We let $Var_{Dp}\left[\bar{k}(x_i, y_j)\right]$ denote the corresponding dimensionless variances, where the subscript p is used to denote that these are dimensionless variances after conditioning to pressure data. We use the notation Var_{Dhp} to denote the dimensionless variances after conditioning to both hard data and pressure data. In the following, the terminology normalized variances will refer to ratios of dimensionless variances.

The normalized variance Var_{Dh} / Var_D is plotted in Fig. 2.13. Note this normalized variance represents the dimensionless variance obtained by conditioning to only hard data divided by the prior dimensionless variance. Note the normalized variances are signifi-

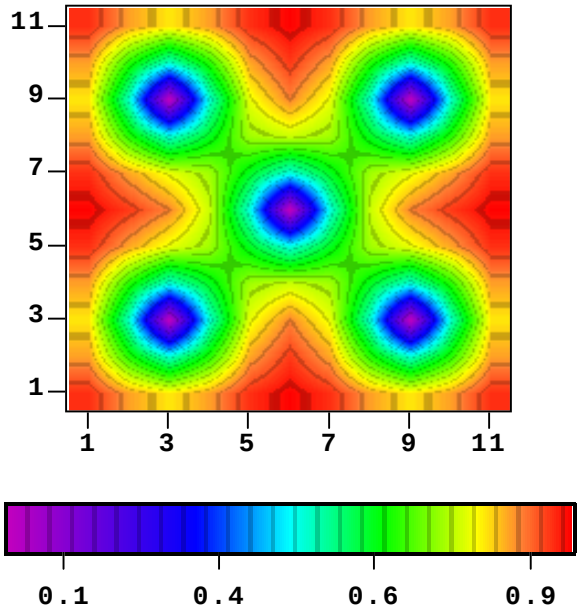

Fig. 2.13 - Average permeability; normalized dimensionless variance conditioned only to hard data.

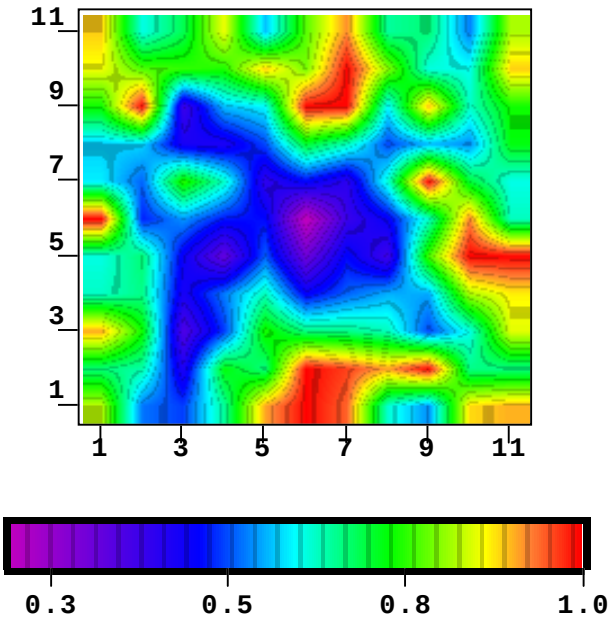

Fig. 2.14 - Average permeability; normalized dimensionless variance conditioned only to pressure data.

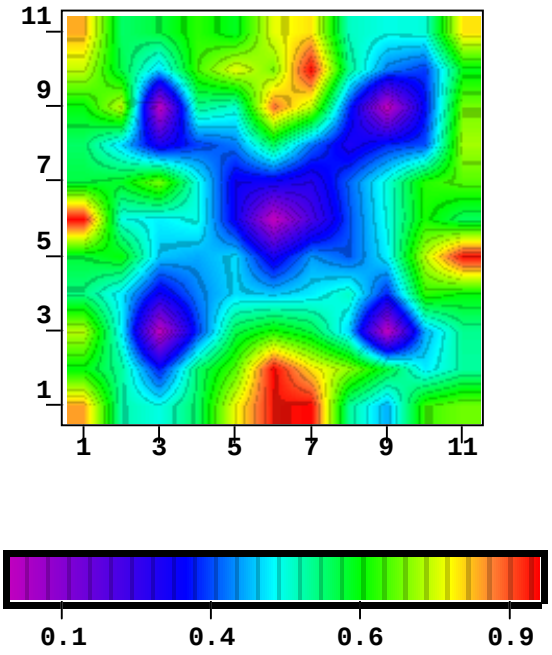

Fig. 2.15 - Average permeability; normalized dimensionless variance conditioned to hard data and pressure data.

cantly less than 1 only at well locations and at the locations within the correlation length (variogram range) from each well. In other locations, the values are still close to or equal to unity; i.e., the variance of the average permeability at those locations has not been reduced by hard data.

Fig. 2.14 shows the normalized dimensionless variance Var_{Dp} / Var_D. Note the normalized variances are significantly less than unity near the active well and in the interwell region between the active well and the two observation wells near the "left" of the reservoir. Comparing these results with those of Fig. 2.10, it is apparent that incorporating pressure data as conditioning reduces the uncertainty in average permeability much more than it reduces the uncertainty in individual layer values of permeability.

Fig. 2.15 shows a plot of Var_{Dhp} / Var_D. Note we have reduced these normalized variances significantly below unity near the wells and the overall reduction in uncertainty is greater than is achieved by conditioning to only pressure data. However, considering the results of Figs. 2.10, 2.14, 2.11 and 2.15 together, it is clear that hard data is of significantly more value for reducing the uncertainty in individual layer values of permeability than it is in reducing the uncertainty in the thickness-averaged permeability.

Fig. 2.16 represents a plot of the "true" thickness averaged permeabilities. Fig. 2.17 shows a plot of average permeabilities computed from the maximum a posteriori estimate obtained by conditioning only to hard data. Fig. 2.18 depicts the thickness-averaged permeabilities computed from the maximum a posteriori estimate obtained by conditioning only to pressure data. Fig. 2.19 shows the corresponding average permeabil-

ities obtained from the maximum a posteriori estimate conditioned to hard data and pressure data. Average permeabilities obtained using only pressure data capture the main trends of the true average permeability better than the corresponding average computed by conditioning only to hard data. In terms of capturing the main features of the true average permeability distribution (Fig. 2.16), the results obtained by conditioning to both hard data and pressure data (Fig. 2.19) are slightly better than those obtained by conditioning to only pressure data (Fig. 2.18).

2.5.5 Realizations

Up to now, we have focused on generating maximum a posteriori estimates of the permeability and porosity fields. However, our final objective is to generate a set of

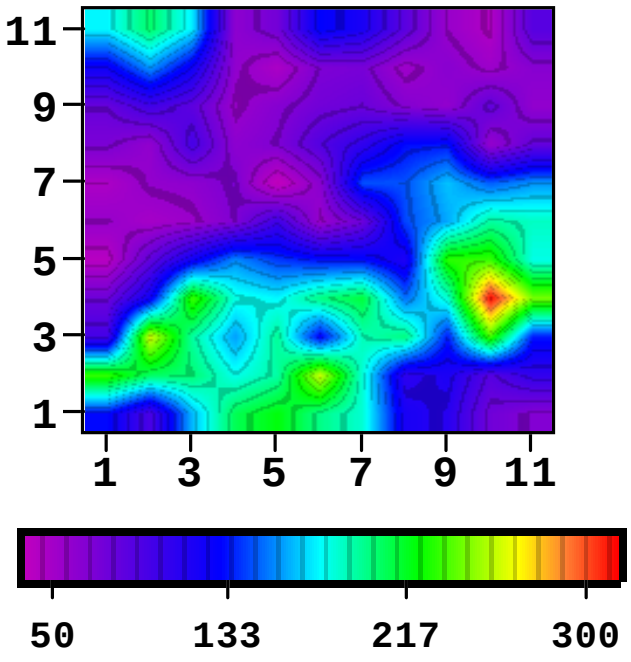

Fig. 2.16 - Average permeability for true case.

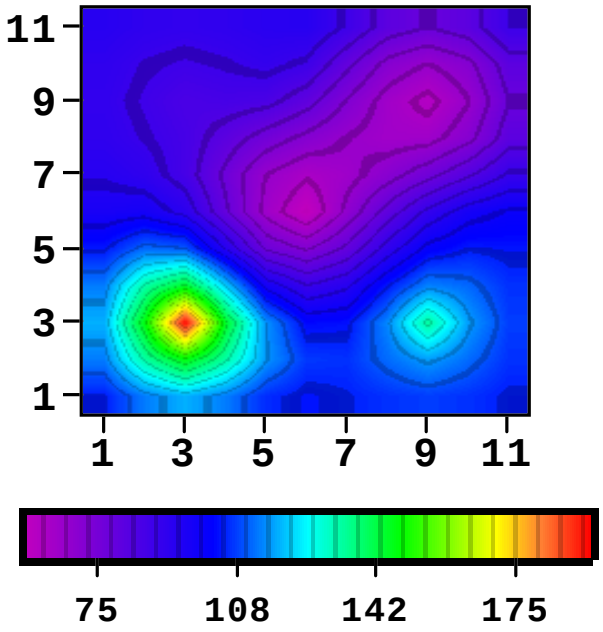

Fig. 2.17 - Average permeability from maximum a posteriori estimate, conditioned to only hard data.

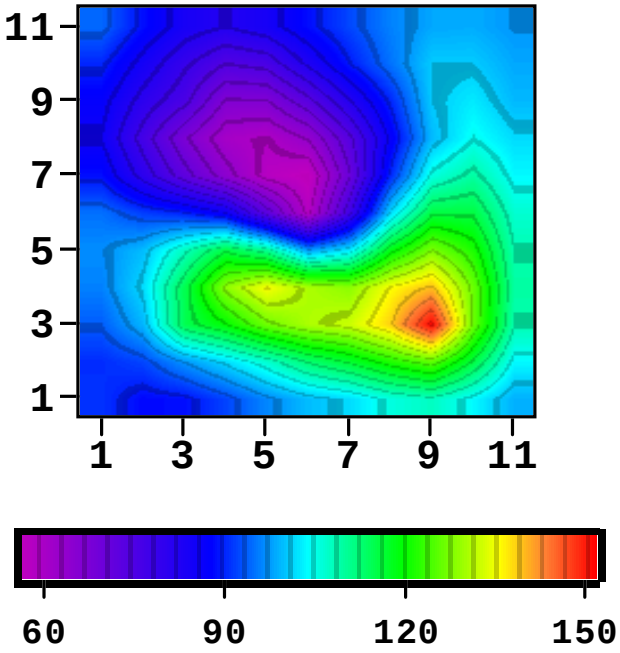

Fig. 2.18 - Average permeability from maximum a posteriori estimate, conditioned to only pressure data.

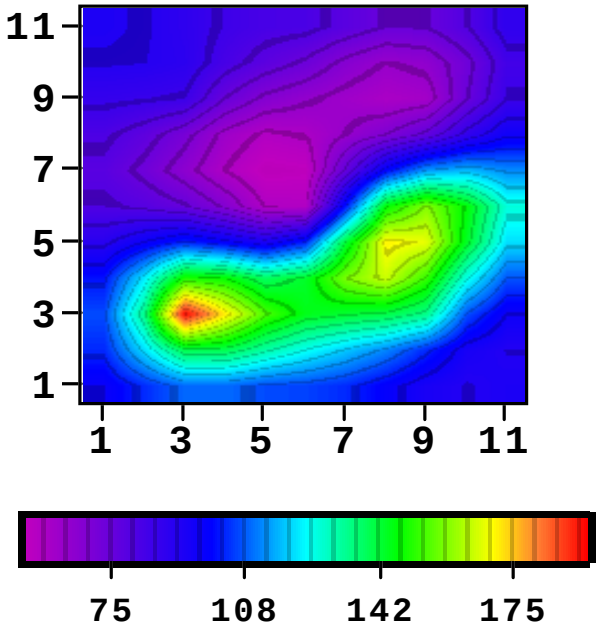

Fig. 2.19 - Average permeability from maximum a posteriori estimate, conditioned to hard data and pressure data.

realizations of the rock property fields which represent a proper sampling of the a posteriori probability density function. As shown in Eq. 2.38, we can generate realizations from the maximum a posteriori estimate and Cholesky decomposition of the a posteriori covariance matrix. However, the set of realizations generated in this way will only represent an approximate sampling of the approximate pdf. Fig. 2.20 and 2.21 show one realization of the log-permeability and porosity fields generated by this procedure after conditioning to both hard data and pressure data. Comparing the realizations with the true case (Fig. 2.2 and Fig. 2.3), we see that realizations exhibit some similar to the true case in some locations. But, they also exhibit differences with the true case, because even through the variance is reduced by conditioning to hard data and pressure data, the variance is still high is some places.

Fig. 2.22 and 2.23 respectively show the log-permeability and porosity values from 50 realizations at specified gridblock. We select three gridblocks ((9, 9, 2), (8, 8, 2) and

(6, 1, 2)) to show that how much variability there is in the realizations. As we can see from Fig. 2.1, gridblock (9,9,2) pertains to the middle gridblock penetrated by observation well 4, gridblock (8, 8, 2) is located between the active well (6,6) and observation well 4, while gridblock (6,1,2) is at an areal location adjacent to x-axis. We can see that the log-permeability and porosity values of gridblock (9,9,2) are quite stable because after conditioning to hard data, the posteriori variance is reduced to almost zero at the observation well. The log-permeability and porosity values at gridblock (6,1,2) vary significantly, because neither pressure data nor hard data at wells is very sensitive to

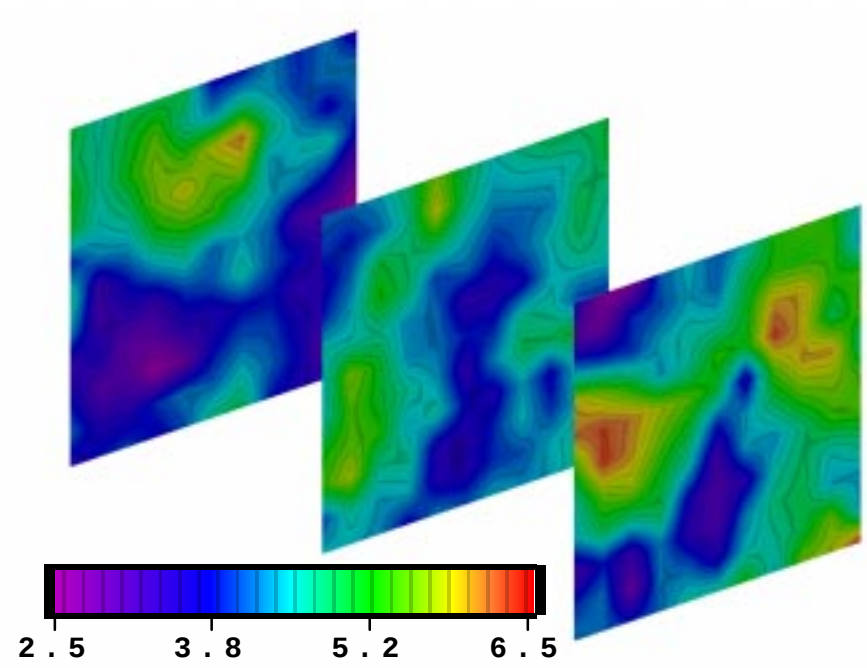

Fig. 2.20 - Realization of log-permeability field.

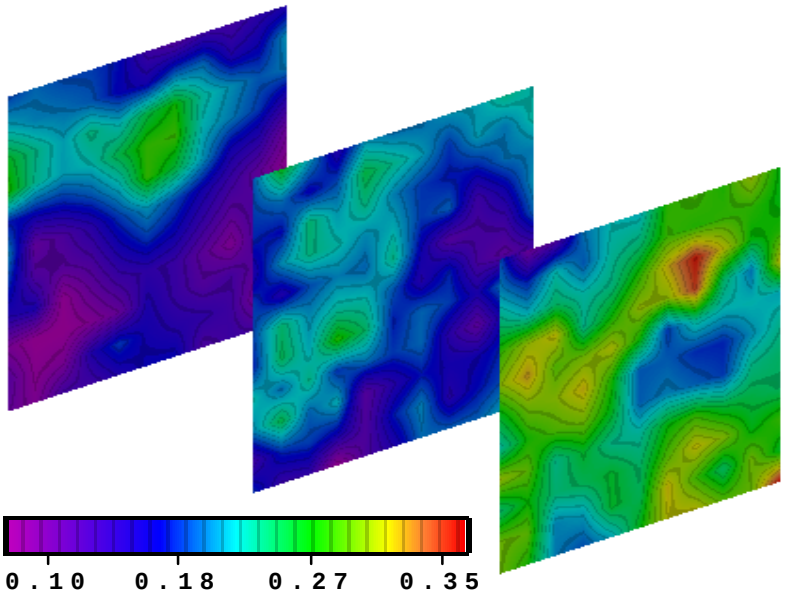

Fig. 2.21 - Realization of porosity field.

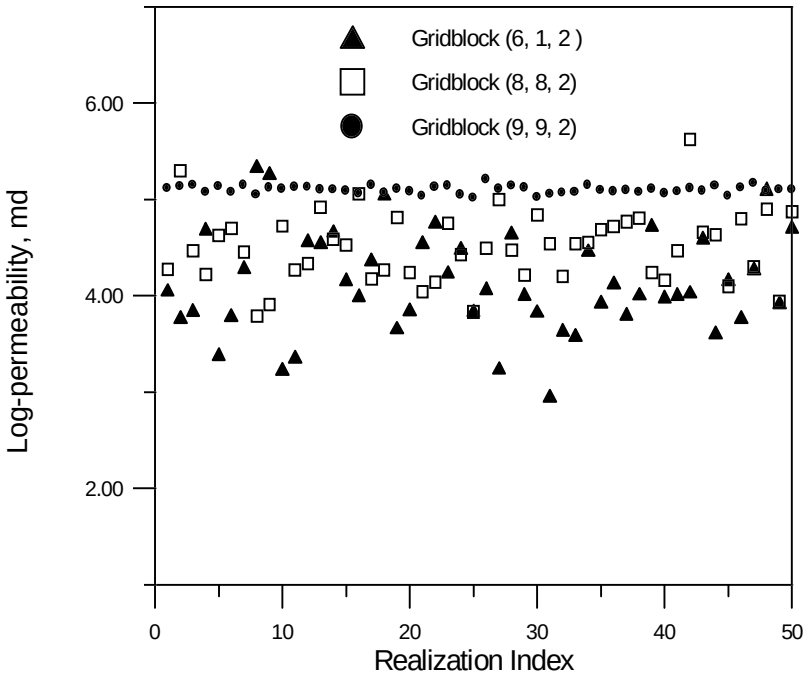

Fig. 2.22 - Gridblock value of log-permeability in realizations.

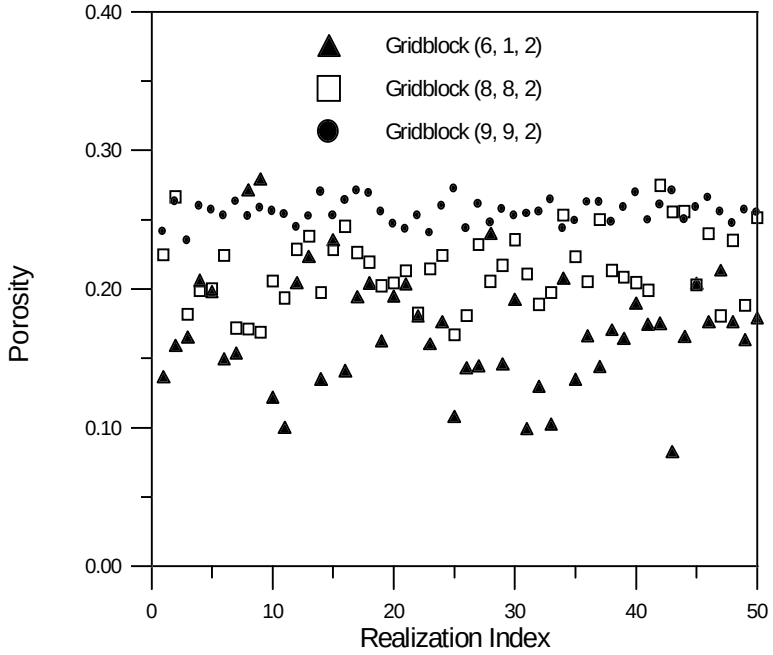

Fig. 2.23 - Gridblock value of porosity in realizations.

permeabilities at gridblocks near the model boundaries, so conditioning to hard data and pressure will not significantly reduce the variance. The log-permeability and porosity values of gridblock (8,8,2) also vary significantly, however compared with the values at gridblock (6,1,2), the variability is less, i.e., conditioning to hard data and pressure data will reduce the uncertainty in the rock property field in the inter-well regions.

2.5.6 Conditioning to Layer Flow Rates

As we have shown, wellbore pressures resolve the thickness averaged permeability (see Fig. 2.16) much better than individual layer permeabilities (see Fig. 2.6). Similarly, pressure data do not resolve gridblock porosity well and we can not determine individual layer skin factors from pressure data. However, if the individual layer flow rate data are available, we can also use this information to obtain reasonable resolution of individual

layer properties. We assume that the variance of the layer flow rates measurement error is $\sigma_q^2 = 1.0$.

Fig. 2.24 shows the maximum a posteriori estimate after conditioning to both wellbore pressure and layer flow rates. No hard data were used as conditioning data. We see that the layer log-permeability field represented by the maximum a posteriori estimate is qualitatively similar to the true log-permeability field, Fig. 2.2. Fig. 2.25 shows the average permeability from the maximum a posteriori estimate after conditioning to both wellbore pressure and layer flow rates. We see that this average permeability qualitatively matches that of the true case (Fig. 2.16), and is better than the average permeability field obtained by conditioning only to pressure data (see Fig. 2.18).

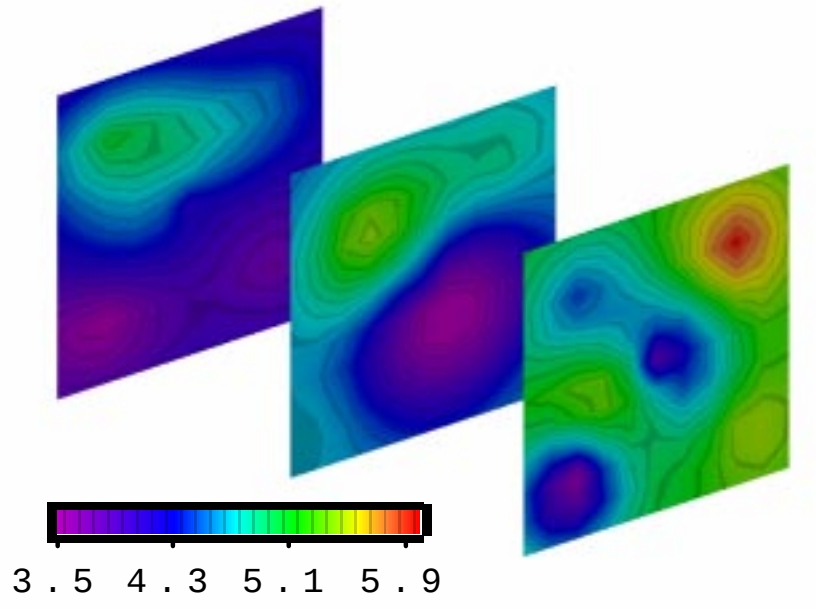

Fig. 2.24 - Maximum a posteriori estimate of log-permeability fields, conditioned to wellbore pressure and layer flow rates.

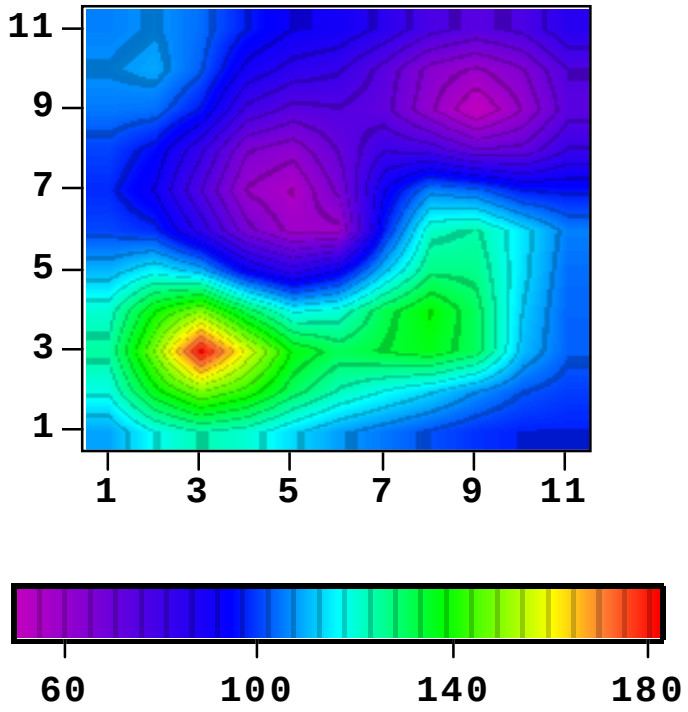

Fig. 2.25 - Average permeability from maximum a posteriori estimate, conditioned to wellbore pressure and layer flow rates.

The following table compares the true skin factors with the maximum a posteriori estimate obtained at the active well.

layer no.	true skin factor	skin factor, conditioned only to wellbore pressure	skin factor, conditioned to pressure and layer flow rates
layer 1	3.35	3.97	3.99
layer 2	-0.04	3.78	-1.37
layer 3	6.34	2.01	8.15

From the table, we see that by conditioning only to wellbore pressure, we can not estimate skin factors very accurately. However, if the maximum a posteriori estimate is conditioned

to both wellbore pressure and layer flow rates, the skin factors at the active well can be estimated with reasonable accuracy. Theoretically, if we have recorded the wellbore pressure and layer flow rates at observation wells, we can estimate the observation well skin factors. However, in this example, we found the skin factors at observation wells can not be accurately estimated. More research is needed on this aspect.

CHAPTER III

FLOW SIMULATION AND SENSITIVITY COEFFICIENT CALCULATION

3.1 The Reservoir Model

We consider single-phase flow in a three-dimensional reservoir. We use a x-y-z Cartesian coordinate system. In some cases, we restrict our attention to two dimensional flow in the x and y directions. Reservoir boundaries are assumed to be no-flow boundaries or constant pressure boundaries. The reservoir can contain any number of complete-penetration or restricted-entry wells. Each well is produced at a specified rate or specified bottom-hole pressure. Pressure buildup tests are simulated by changing the rate to zero after producing for a specified time. Interference or observation wells are simulated by setting the rate to zero at all times. In the three-dimensional case, even though the surface rate at an observation well is zero, crossflow between reservoir layers may occur through the observation well. Fluid properties are assumed to be known. We assume a slightly compressible fluid of constant compressibility and viscosity. The permeability and porosity fields are assumed to be heterogeneous. Permeability may be either isotropic or aniso-tropic, but we assume a diagonal permeability tensor; i.e., the principal permeabilities are aligned with the coordinate axes. Except in special cases, e.g., vertical interference tests,

pressure data can not be expected to yield good estimates of vertical permeability. Thus in our case, we always require that $k_z = a\sqrt{k_x k_y}$, for the anisotropic case, where a is a constant. This means the vertical permeability field is determined directly from the k_x and k_y permeability fields. Normally, we set $a = 0.1$. For the isotropic case, $k_x = k_y = k_z = k$, i.e., there is only one permeability value to estimate at each grid block. Skin factors vary from well to well, and may even vary from gridblock to gridblock in the vertical direction.

Pressure responses are obtained by a finite-difference simulator, i.e., a simulator is used to generate synthetic multiwell pressure data, where wellbore pressure is related to the well gridblock pressure by Peaceman's method[43]. At each well, the pressure at each gridblock penetrated by the well is related to the wellbore pressure by formally applying the two-dimensional Peaceman equation at each vertical gridblock. Since the rate of production from each of these vertical gridblocks (referred to here as gridblock or "model layer" rates) is unknown, the individual Peaceman equations can not be directly used. However, by summing the set of Peaceman's equations, one obtains a relation between the pressures in gridblocks penetrated by the well, the wellbore pressure and total well flow rate. Then the matrix equations relating well gridblock pressures to wellbore pressures can be constructed. These equations are solved for gridblock pressures and wellbore pressures simultaneously and then Peaceman's equation can be applied to calculate individual layer flow rates. Fundamentally, our procedure assumes that at any depth, flow in the neighbor-hood of the wellbore should be primarily radial. Details regarding the simulator are given below.

3.2 Three Dimensional Simulation

3.2.1 Flow Equation for 3-D Problem

For the three-dimensional single-phase flow problem considered here we neglect gravity effects, so the governing flow equation can be written in oil-field units as follows:

$$\frac{c_1}{\mu}\left[\frac{\partial}{\partial x}\left[k_x\frac{\partial p}{\partial x}\right]+\frac{\partial}{\partial y}\left[k_y\frac{\partial p}{\partial y}\right]+\frac{\partial}{\partial z}\left[k_z\frac{\partial p}{\partial z}\right]\right]-$$
$$\sum_{m=1}^{N_w}\sum_{l_m}\hat{q}_m(x_{i_m},y_{j_m},z_{l_m})\delta(x-x_{i_m})\delta(y-y_{j_m})\delta(z-z_{l_m})=\frac{\phi c_t}{c_2}\frac{\partial p}{\partial t},$$

(3.1)

for $0<x<L_x$, $0<y<L_y$, $0<z<L_z$ and $t>0$, where L_x, L_y and L_z are the dimensions of the reservoir. Throughout, $c_1 = 1.127\times10^{-3}$ and $c_2 = 5.615\ ft^3/RB$ and N_w denotes the number of wells. The inner sum in Eq. 3.1 is over the number of gridblocks penetrated by well *m*. In Eq. 3.1, *p* is the pressure at (x, y, z) and time *t*, $p = p(x,y,z,t)$, k_x is x-directional permeability, $k_x = k_x(x,y,z)$, similarly for k_y and k_z. The terms $\delta(x-x_{i_m})$, $\delta(y-y_{j_m})$ and $\delta(z-z_{l_m})$ denote Dirac delta functions in units of ft^{-1}. All wells are assumed to be vertical. The areal location of well *m* is specified by (x_{i_m},y_{j_m}) and may be completed over any interval (or set of intervals) in the vertical direction. The term $\hat{q}_m(x_{i_m},y_{j_m},z_{l_m},t)$ is the source or sink term at time *t* at well *m* at the vertical location $z=z_{l_m}$ in units of RB/D. If well *m* is completed over the interval $h_b \le z \le h_t$, then integrating $\hat{q}_m(x_{i_m},y_{j_m},z_{l_m},t)\delta(z-z_{l_m})$ over this interval gives $q_m(x_{i_m},y_{j_m},t)$ which is the total flow rate of well *m* in units of reservoir barrels per day. The rates are sandface

flow rates; however, we assume that wellbore storage effects are negligible so sandface and surface flow rates are equal. It is important to note that if well *m* is an observation well, i.e., shut-in at the surface at all times, then $q_m(x_{i_m}, y_{j_m}, t) = 0$ but $\hat{q}_m(x_{i_m}, y_{j_m}, z_{l_m}, t)$ may not be zero at any vertical location since crossflow can occur through the observation well. For production at well *m*, q_m is positive, while for injection, q_m is negative.

We let

$$R = \left\{(x, y, z) | 0 < x < L_x, 0 < y < L_y, 0 < z < L_z\right\}, \tag{3.2}$$

i.e., R is the region in three-dimensional space occupied by the reservoir. We let ∂R denotes the boundary of R. Assuming an uniform initial pressure, p_i, the initial boundary condition is then specified by

$$p(x, y, z, 0) = p_i \ , \tag{3.3}$$

for (*x*, *y*, *z*) in R.

For no-flow boundary conditions, we have

$$\frac{\partial p(x, y, z, t)}{\partial n} = 0 \, , \tag{3.4}$$

for (*x*, *y*, *z*) at ∂R and $t > 0$. Eq. 3.4 simply specifies that the normal derivative is zero on all boundaries, i.e., all boundaries are assumed to be no flow boundaries.

In case of constant pressure boundary, the boundary condition equation is

$$p(x, y, z, t) = p_b \, , \tag{3.5}$$

for (*x*, *y*, *z*) at ∂R and $t > 0$, where p_b is pressure at the boundary.

3.2.2 Finite Difference Equations

In the following, we present the difference equations for the initial-boundary-value problem (IBVP) specified by Eqs. 3.1 to 3.5. A purely implicit seven-point difference scheme is used[44, 45].

Differencing Eq. 3.1 at (x_i, y_j, z_k) and multiplying by $\Delta x_i \Delta y_j \Delta z_k$, where $\Delta x_i, \Delta y_j$ and Δz_k are the dimensions of the gridblock centered at (x_i, y_j, z_k) gives

$$\begin{aligned}
&\frac{c_1}{\mu}\Bigg[\Delta y_j \Delta z_k k_{x,i+1/2,j,k}\left[\frac{p^n_{i+1,j,k}-p^n_{i,j,k}}{x_{i+1}-x_i}\right]-\Delta y_j \Delta z_k k_{x,i-1/2,j,k}\left[\frac{p^n_{i,j,k}-p^n_{i-1,j,k}}{x_i-x_{i-1}}\right]\\
&+\Delta x_i \Delta z_k k_{y,i,j+1/2,k}\left[\frac{p^n_{i,j+1,k}-p^n_{i,j,k}}{y_{j+1}-y_j}\right]-\Delta x_i \Delta z_k k_{y,i,j-1/2,k}\left[\frac{p^n_{i,j,k}-p^n_{i,j-1,k}}{y_j-y_{j-1}}\right]\\
&+\Delta x_i \Delta y_j k_{z,i,j,k+1/2}\left[\frac{p^n_{i,j,k+1}-p^n_{i,j,k}}{z_{k+1}-z_k}\right]-\Delta x_i \Delta y_j k_{z,i,j,k-1/2}\left[\frac{p^n_{i,j,k}-p^n_{i,j,k-1}}{z_k-z_{k-1}}\right]\Bigg]-\hat{q}^n_{i,j,k}\\
&=\frac{\phi_{i,j,k}c_t}{c_2}\left[\frac{p^n_{i,j,k}-p^{n-1}_{i,j,k}}{\Delta t_n}\right]\Delta x_i \Delta y_j \Delta z_k .
\end{aligned} \tag{3.6}$$

There are N_x gridblocks in the x-direction, N_y gridblocks in the y-direction and N_z gridblocks in the z-direction with gridblock centers given by (x_i, y_j, z_k) for $i = 1,2,...,N_x$, $j = 1,2,...,N_y$, and $k = 1,2,...,N_z$, where $x_1 < x_2 <...< x_{N_x}$, $y_1 < y_2 <...< y_{N_y}$, and $z_1 < z_2 <...< z_{N_z}$.

We let $x_{i+1/2}$ for $i = 0,1,...,N_x$ denote the gridblock boundaries in the x-direction with $x_{1/2} = 0$ and $x_{N_x+1/2} = L_x$ so the x-direction widths of gridblocks are $\Delta x_i = (x_{i+1/2} - x_{i-1/2})/2$ for $i = 1,2,...,N_x$. We let $y_{j+1/2}$ for $j = 0,1,...,N_y$ denote the gridblock boundaries in the y-direction with $y_{1/2} = 0$ and $y_{N_y+1/2} = L_y$ so the lengths of

gridblocks in the y-direction are $\Delta y_j = (y_{j+1/2} - y_{j-1/2})/2$ for $j = 1,2,...,N_y$. Gridblock boundaries in the z-direction and the Δz_k's are defined in a similar way.

We define *x*, *y* and *z* direction transmissibities by

$$Tx_{i+1/2,j,k} = \frac{C_1 k_x(x_{i+1/2}, y_j, z_k)\Delta y_j \Delta z_k}{x_{i+1} - x_i}\ , \tag{3.7}$$

for $i = 1,2,...,N_x - 1$ and all *j* and *k*,

$$Tx_{1/2,j,k} = Ty_{N_x+1/2,j,k} = 0\,, \tag{3.8}$$

for all j and k;

$$Ty_{i,j+1/2,k} = \frac{C_1 k_y(x_i, y_{j+1/2}, z_k)\Delta x_i \Delta z_k}{y_{j+1} - y_j}, \tag{3.9}$$

for all $j = 1,2,...,N_y - 1$ and all *i* and *k*,

$$Ty_{i,1/2,k} = Ty_{i,N_y+1/2,k} = 0\,, \tag{3.10}$$

for all *i* and *k*;

$$Tz_{i,j,k+1/2} = \frac{C_1 k_z(x_i, y_j, z_{k+1/2})\Delta x_i \Delta y_j}{z_{k+1} - z_k}, \tag{3.11}$$

for $j = 1,2,...,N_z - 1$ and all *i* and *j*,

$$Tz_{i,j,1/2} = Tz_{i,j,N_z+1/2} = 0\,, \tag{3.12}$$

for all *i* and *j*. Throughout we use the following notation:

$$k_{x,i,j,k} = k_x(x_i, y_j, z_k)\,, \tag{3.13}$$

and

$$k_{y,i,j,k} = k_y(x_i, y_j, z_k)\,. \tag{3.14}$$

Permeabilities at gridblock interfaces are computed by the standard harmonic average, for example,

$$k_{x,i+1/2,j,k} = \frac{2(x_{i+1} - x_i)k_{x,i+1,j,k}k_{x,i,j,k}}{k_{x,i,j,k}\Delta x_{i+1} + k_{x,i+1,j,k}\Delta x_i}. \tag{3.15}$$

Harmonic average permeabilities in the y and z direction are defined in a similar way.

In finite difference techniques, we generate an approximate solution of the initial-boundary value problem (Eqs. 3.1 to 3.5) at each gridblock at a set of time steps, t_n, $n = 1,2,...$ where by definition, $t_0 = 0$ and $\Delta t_n = t_n - t_{n-1}$ so $t_n = t_{n-1} + \Delta t_n$ for $n = 1,2,....$ We let $p^n_{i,j,k}$ denote the pressure obtained at the gridblock centered at (x_i, y_j, z_k) by solving the system of finite difference equations at time t_n. For all (*i*, *j*, *k*), we let

$$V^n_{i,j,k} = \frac{\phi(x_i, y_j, z_k)c_t \Delta x_i \Delta y_j \Delta z_k}{5.615\Delta t_n}. \tag{3.16}$$

We define

$$T_{i,j,k} = Tx_{i+1/2,j,k} + Tx_{i-1/2,j,k} + Ty_{i,j+1/2,k} + Ty_{i,j-1/2,k} + Tz_{i,j,k+1/2} + Tz_{i,j,k-1/2} + V^n_{i,j,k},$$

(3.17)

for $i = 1,2,...,N_x$, $j = 1,2,...,N_y$ and $k = 1,2,...,N_z$.

With the preceding notation, the implicit finite difference equation at any gridblock can be written as

$$\begin{aligned} &Tz_{i,j,k-1/2}p^n_{i,j,k-1} + Ty_{i,j-1/2,k}p^n_{i,j-1,k} + Tx_{i-1/2,j,k}p^n_{i-1,j,k} - T_{i,j,k}p^n_{i,j,k} \\ &+ Tx_{i+1/2,j,k}p^n_{i+1,j,k} + Ty_{i,j+1/2,k}p^n_{i,j+1,k} + Tz_{i,j,k+1/2}p^n_{i,j,k+1} - q^n_{i,j,k} = -V^n_{i,j,k}p^{n-1}_{i,j,k}. \end{aligned} \tag{3.18}$$

In Eq. 3.18, $q^n_{i,j,k}$ (RB/D) represents the internal sink or source term at time t_n in gridblock (*i*, *j*, *k*) and is nonzero only if the gridblock is penetrated by a well. When the gridblock is penetrated by a well, $q^n_{i,j,k}$ represents the total sandface flow rate into or out of the well over the interval $z_{k-1/2} \le z \le z_{k+1/2}$. At any well, only the total flow rate will be known; thus, the individual gridblock source and skin terms must be obtained as part of the solution procedure. Also, Eq. 3.16 explicitly involves only gridblock pressures, whereas, we wish to work in terms of wellbore pressures. Our procedures for resolving individual gridblock flow rates and computing wellbore pressures are presented immediately below.

3.2.3 Relating Wellbore Pressure and Gridblock Pressures

We consider a well located at a position with (*x*, *y*) coordinates given by (x_i, y_j), with the well completed in associated vertical gridblocks centered at (x_i, y_j, z_k) for $k = l1, l1+1, ..., l2)$. We denote the total sandface flow rate at time t_n by $q^n_{i,j}$ with the individual source or sink terms given by $q^n_{i,j,k}$ for $k = l1, l1+1, ..., l2)$, i.e., $q^n_{i,j,k}$ gives the source or sink term for gridblock (*i*, *j*, *k*). We relate the individual source and sink terms to the wellbore pressure by applying Peaceman's equations[43] at each location, i.e.,

$$q^n_{i,j,k} = (WI)_k (p^n_{i,j,k} - p^n_{wf}), \tag{3.19}$$

where

$$(WI)_k = \left(\frac{2\pi C_1 \Delta z_k \sqrt{k_{x,i,j,k} k_{y,i,j,k}}}{\mu(\ln[r_{ok} / r_w] + s_k)} \right). \tag{3.20}$$

Here, $C_1 = 1.127 \times 10^{-3}$, r_w is the wellbore radius of the well (wellbore radii may vary from well to well) and

$$r_{o,k} = \frac{0.28073 \Delta x_i \sqrt{1 + \frac{k_{x,i,jk}}{k_{y,i,j,k}} \left(\frac{\Delta y_j}{\Delta x_i} \right)^2}}{1 + \sqrt{k_{x,i,j,k} / k_{y,i,j,k}}}. \tag{3.21}$$

In Eq. 3.20, we have assumed the well is perforated throughout the height of each vertical gridblock. If it is perforated over the fraction α of the gridblock associated with z_k, then in Eq. 3.20, Δz_k should be replaced by $\alpha \Delta z_k$. In Eq. 3.20, s_k represents an effective skin for the well gridblock centered at (x_i, y_j, z_k), i.e., s_k is the skin factor for ``layer" k.

The individual gridblock rates must sum to the total rate; i.e, we must have

$$q^n_{i,j} = \sum_{k=l1}^{l2} q^n_{i,j,k} = \sum_{k=l1}^{l2} (WI)_k (p^n_{i,j,k} - p^n_{wf}). \tag{3.22}$$

Using Eq. 3.19 in Eq. 3.18, we have

$$\begin{aligned} &Tz_{i,j,k-1/2} p^n_{i,j,k-1} + Ty_{i,j-1/2,k} p^n_{i,j-1,k} + Tx_{i-1/2,j,k} p^n_{i-1,j,k} - (T_{i,j,k} + WI_{i,j,k}) p^n_{i,j,k} \\ &+ Tx_{i+1/2,j,k} p^n_{i+1,j,k} + Ty_{i,j+1/2,k} p^n_{i,j+1,k} + Tz_{i,j,k+1/2} p^n_{i,j,k+1} + WI_{i,j,k} p^n_{wf,i,j} \\ &= -V^n_{i,j,k} p^{n-1}_{i,j,k}. \end{aligned} \tag{3.23}$$

for $1 \le i \le N_x$, $1 \le j \le N_y$ and $1 \le k \le N_z$. Eq. 3.22 can be written as

$$\sum_{k=l1}^{l2} WI_{i,j,k} p^n_{i,j,k} - \left(\sum_{k=l1}^{l2} WI_{i,j,k} \right) p^n_{wf,i,j} = q^n_{i,j}. \tag{3.24}$$

Combining Eqs. 3.23 and 3.24, we obtain a matrix equation for the flow problem with well rates specified. By solving the equations, we can obtain gridblock pressure $p^n_{i,j,k}$ and wellbore pressure $p^n_{wf,i,j}$. With known wellbore pressure and gridblock pressure, “layer” flow rates can be computed with Eq. 3.19.

For a problem with wellbore pressures specified, we can rewrite Eq. 3.23 as:

$$T_{z,i,j,k-\frac{1}{2}} p^{n+1}_{i,j,k-1} + T_{y,i,j-\frac{1}{2},k} p^{n+1}_{i,j-1,k} + T_{x,i-\frac{1}{2},j,k} p^{n+1}_{i-1,j,k} - (T_{i,j,k} + WI_{i,j,k}) p^{n+1}_{i,j,k} + T_{x,i+\frac{1}{2},j,k} p^{n+1}_{i+1,j,k} + T_{y,i,j+\frac{1}{2},k} p^{n+1}_{i,j+1,k} + T_{z,i,j,k+\frac{1}{2}} p^{n+1}_{i,j,k+1} = -V^{n}_{i,j,k} p^{n}_{i,j,k} - WI_{i,j,k} p^{n+1}_{wf,i,j} . \quad (3.25)$$

Eq. 3.25 can be solved individually for gridblock pressures. Then Eqs. 3.19 and 3.22 can be applied to compute flow rates.

3.3 Theory for Estimating Sensitivity Coefficients

In this section, we present the equations for computing sensitivity coefficients, which are used when applying the Gauss-Newton method to estimate the most probable model. Specifically, we need sensitivity coefficients at all wells where we measure wellbore pressure and use this pressure data as conditioning data. If $p_{wf}(t)$ denotes the pressure response at a well for a given reservoir description, then the relevant sensitivity coefficients at any time *t*, are $\partial p_{wf}(t)/\partial \phi_{l,m,n}$, $\partial p_{wf}(t)/\partial k_{x,l,m,n}$, $\partial p_{wf}(t)/\partial k_{y,l,m,n}$, $\partial p_{wf}(t)/\partial k_{z,l,m,n}$ for all (*l*, *m*, *n*) and $\partial p_{wf}(t)/\partial s_k$. The first three expressions for sensitivity coefficients give a measure of how strongly a change in a rock property in the gridblock centered at (x_l, y_m, z_n) will affect the wellbore pressure at time *t* and the last expression gives a measure of how much the wellbore pressure will change due to a change in one of the well's ``layer'' skin factors.

3.3.1 Extension of Carter et al.[29] Method for Sensitivity Coefficients

3.3.1.1 Leibnitz rule and Green's theorem

The Leibnitz rule can be stated as follows:

if $f(x,y)$ and $\frac{\partial f(x,y)}{\partial x}$ are continuous on $\left[a(x), b(x)\right]$, then

$$\frac{\partial}{\partial x}\int_{a(x)}^{b(x)} f(x,y)dy = f(x,b(x))\frac{db(x)}{dx} - f(x,a(x))\frac{da(x)}{dx} + \int_{a(x)}^{b(x)} \frac{\partial f(x,y)}{\partial x}dy\,. \tag{3.26}$$

Green's theorem (divergence theorem) can be stated as follows:

let f be a vector field defined on domain D with boundary given by S, then

$$\iiint_D \nabla f dxdydz = \iint_S f \cdot \vec{n} ds\,, \tag{3.27}$$

where $\vec{n}$ is the unit vector outward normal to S.

3.3.1.2 Generalized Reciprocity Principle

For completeness, we outline the Carter et al. derivation of a generalized reciprocity principle.

Consider a problem

$$\frac{C_1}{\mu}\nabla\cdot[k]\nabla p_{d_0}(X,s) - V\frac{\partial p_{d_0}(X,s)}{\partial s} = Q_0(X,s), \text{ on R,} \tag{3.28a}$$

$$p_{d_0}(X,\, s=0) = 0\,, \tag{3.28b}$$

$$\nabla p_{d_0}(X,\, s)\cdot\vec{n} = 0\,, \text{ on } \partial R\,, \tag{3.28c}$$

where R is the domain of the problem, ∂R denotes the domain boundary**,** p_{d_0} is the pressure drop solution, $X = (x,y,z) \in R$ and s represents the time variable.

Consider another problem

$$\frac{C_1}{\mu}\nabla\cdot[k]\nabla p_{d_1}(X,u)-V\frac{\partial p_{d_1}(X,u)}{\partial u}=Q_1(X,u)\text{, on }R, \tag{3.29a}$$

$$p_{d_1}(X,\,u=0)=0\,, \tag{3.29b}$$

$$\nabla p_{d_1}(X,\,u)\cdot\vec{n}=0\text{, on }\partial R, \tag{3.29c}$$

where p_{d_1} is the pressure drop solution for this problem and u represents the time variable. Making the change of variable $u=t-s$, we have $p_{d_1}(X,u)=p_{d_1}(X,t-s)$ and

$$\frac{\partial p_{d_1}}{\partial u}=\frac{\partial p_{d_1}}{\partial s}\frac{\partial s}{\partial u}=-\frac{\partial p_{d_1}}{\partial s}\,. \tag{3.29d}$$

Then, Eq. 3.29a-c becomes

$$\frac{C_1}{\mu}\nabla\cdot[k]\nabla p_{d_1}(X,t-s)+V\frac{\partial p_{d_1}(X,t-s)}{\partial u}=Q_1(X,t-s)\,, \tag{3.30a}$$

$$p_{d_1}(X,\,t-s)|_{t-s=0}=0\,, \tag{3.30b}$$

$$\nabla p_{d_1}(X,\,t-s)\cdot\vec{n}=0\,. \tag{3.30c}$$

Multiply Eq. 3.28a by $p_{d_1}(X,\,t-s)$ and (3.30a) by $p_{d_0}(X,\,s)$ to obtain

$$\begin{aligned}&\frac{C_1}{\mu}p_{d_1}(X,t-s)\nabla\cdot[k]\nabla p_{d_0}(X,s)-p_{d_1}(X,t-s)V\frac{\partial p_{d_0}(X,s)}{\partial s}\\&=p_{d_1}(X,t-s)Q_0(X,s),\end{aligned} \tag{3.31}$$

$$\begin{aligned}&\frac{C_1}{\mu}p_{d_0}(X,s)\nabla\cdot[k]\nabla p_{d_1}(X,t-s)+p_{d_0}(X,s)V\frac{\partial p_{d_1}(X,t-s)}{\partial s}\\&=p_{d_0}(X,s)Q_1(X,t-s).\end{aligned} \tag{3.32}$$

Subtracting Eq. 3.31 from Eq. 3.32 and integrating over time and space, we have

$$\iiint_R\int_0^t\Big(p_{d_0}(X,s)Q_1(X,t-s)-p_{d_1}(X,t-s)Q_0(X,s)\Big)dsdX=S_1+S_2\,, \tag{3.33}$$

where

$$S_1 = \frac{C_1}{\mu}\iiint_R \int_0^t \left[p_{d_0}(X,s)\nabla\cdot[k]\nabla p_{d_1}(X,t-s) - p_{d_1}(X,t-s)\nabla\cdot[k]\nabla p_{d_0}(X,s)\right] ds dX$$

$$= \frac{C_1}{\mu}\iiint_R ds \int_0^t \left[p_{d_0}(X,s)\nabla\cdot[k]\nabla p_{d_1}(X,t-s) - p_{d_1}(X,t-s)\nabla\cdot[k]\nabla p_{d_0}(X,s)\right] dX\,, \qquad (3.34)$$

$$S_2 = \iiint_R \int_0^t \left[p_{d_0}(X,s)V\frac{\partial p_{d_1}(X,t-s)}{\partial s} + p_{d_1}(X,t-s)V\frac{\partial p_{d_0}(X,s)}{\partial s}\right] ds dX\,. \qquad (3.35)$$

We can show that

$$\begin{aligned}
&\int_0^t p_{d_1}(X,t-s)\frac{\partial p_{d_0}(X,s)}{\partial s} ds \\
&= p_{d_1}(X,t-s)p_{d_0}(X,s)\Big|_0^t - \int_0^t p_{d_0}(X,s)\frac{\partial p_{d_1}(X,t-s)}{\partial s} ds \qquad (3.36)\\
&= 0 - \int_0^t p_{d_0}(X,s)\frac{\partial p_{d_1}(X,t-s)}{\partial s} ds.
\end{aligned}$$

Using Eq. 3.36 in Eq. 3.35 gives $S_2 = 0$.

We have the following vector calculus identity:

$$b\nabla\cdot(a\nabla c) = \nabla\cdot(ab\nabla c) - a\nabla c\cdot\nabla b\,. \qquad (3.36a)$$

Using Eq. 3.36a in Eq. 3.34, we obtain

$$\begin{aligned}
S_1 = \frac{C_1}{\mu}\int_0^t ds \iiint_R \Big[&\nabla\cdot\Big([k]p_{d_0}(X,s)\nabla p_{d_1}(X,t-s)\Big) - [k]\nabla p_{d_1}(X,t-s)\cdot\nabla p_{d_0}(X,s) \\
&- \nabla\cdot\Big([k]p_{d_1}(X,t-s)\nabla p_{d_0}(X,s)\Big) - [k]\nabla p_{d_0}(X,s)\cdot\nabla p_{d_1}(X,t-s)\Big] dX \\
= \frac{C_1}{\mu}\int_0^t ds \iiint_R &\nabla\cdot\Big[[k]p_{d_0}(X,s)\nabla p_{d_1}(X,t-s) - [k]p_{d_1}(X,t-s)\nabla p_{d_0}(X,s)\Big] dX\,. \qquad (3.37)
\end{aligned}$$

Applying Green's Theorem (Eq. 3.27), Eq. 3.37 becomes

$$S_1 = \frac{C_1}{\mu}\int_0^t ds \iint_{\partial R}\Big[[k]p_{d_0}(X,s)\nabla p_{d_1}(X,t-s)\cdot\vec{n} - [k]p_{d_1}(X,t-s)\nabla p_{d_0}(X,s)\cdot\vec{n}\Big] d\partial R\,. \qquad (3.38)$$

Applying boundary conditions (3.28c) and (3.30c) in Eq. 3.38, we obtain $S_1 = 0$. Recalling that we also have $S_2 = 0$, Eq. 3.33 becomes

$$\iiint_R \int_0^t \left(p_{d_0}(X,s) Q_1(X,t-s) - p_{d_1}(X,t-s) Q_0(X,s) \right) ds dX = 0, \tag{3.39}$$

or

$$\iiint_R \int_0^t p_{d_0}(X,s) Q_1(X,t-s) ds dX = \iiint_R \int_0^t p_{d_1}(X,t-s) Q_0(X,s) ds dX . \tag{3.40}$$

Eq. 3.40 is the generalized reciprocity theorem.

3.3.1.3 Sensitivity to Permeability Field

The fluid flow in the reservoir is described by the following IBVP (initial boundary value problem)

$$\frac{C_1}{\mu} \nabla \cdot [k] \nabla p - V \frac{\partial p}{\partial s} = Q, \qquad \text{on } R, \tag{3.41a}$$

$$p|_{s=0} = p_i, \tag{3.41b}$$

$$\nabla p \cdot \vec{n} = 0, \qquad \text{on } \partial R, \tag{3.41c}$$

where $p = p(x, y, z, s)$ is the pressure at (x, y, z) and time s, p_i is the initial reservoir pressure and Q includes all well sources and sinks term in the reservoir.

Let $p_d = p_i - p$ be the pressure drop solution, then the above problem can be written as

$$\frac{C_1}{\mu} \nabla \cdot [k] \nabla p_d - V \frac{\partial p_d}{\partial s} = -Q, \text{ on } R, \tag{3.42a}$$

$$p_d|_{s=0} = 0, \tag{3.42b}$$

$$\nabla p_d \cdot \vec{n} = 0, \quad \text{on } \partial R. \tag{3.42c}$$

Consider the same problem with a small perturbation in the permeability field

$$\frac{C_1}{\mu}\nabla \cdot [k+\delta k]\nabla \bar{p}_d - V\frac{\partial \bar{p}_d}{\partial s} = -\bar{Q}, \quad \text{on } R, \tag{3.43a}$$

$$\bar{p}_d|_{s=0} = 0, \tag{3.43b}$$

$$\nabla \bar{p}_d \cdot \vec{n} = 0, \quad \text{on } \partial R, \tag{3.43c}$$

where

$$[\delta k] = \begin{bmatrix} \delta k_x & & \\ & \delta k_y & \\ & & \delta k_z \end{bmatrix}, \tag{3.44a}$$

represents a small perturbation of the permeability tensor $[k]$,

$$[k] = \begin{bmatrix} k_x & & \\ & k_y & \\ & & k_z \end{bmatrix}, \tag{3.44b}$$

$\bar{p}_d$ and $\bar{Q}$, respectively, represent the resulting pressure drop solution and distribution of sources and sinks due to the small perturbation in the permeability field. Note that even through the total flow rate at each well does not change when the permeability field is perturbed, the vertical distribution of fluxes along the well may change.

The total pressure differential due to the perturbation is given by

$$dp_d = \bar{p}_d - p_d. \tag{3.44}$$

We expand Eq. 3.43a as

$$\frac{C_1}{\mu}\nabla \cdot [k]\nabla \bar{p}_d + \frac{C_1}{\mu}\nabla \cdot [\delta k]\nabla \bar{p}_d - V\frac{\partial \bar{p}_d}{\partial s} = -\bar{Q}. \tag{3.45}$$

Subtracting 3.42a from Eq. 3.45 and using Eq. 3.44, we obtain

$$\frac{C_1}{\mu}\nabla\cdot[k]\nabla dp_d - V\frac{\partial dp_d}{\partial s} = -\frac{C_1}{\mu}\nabla\cdot[\delta k]\nabla\overline{p}_d - (\overline{Q}-Q), \tag{3.46a}$$

$$dp_d|_{s=0} = 0, \tag{3.46b}$$

$$\nabla dp_d\cdot\vec{n} = 0, \quad \text{on } \partial R. \tag{3.46c}$$

Define a functional F by

$$F(k) = \iiint_{T_n} G_n(x,y,z)dp_d(x,y,z,t)dxdydz, \tag{3.47}$$

where T_n is a subregion of the reservoir, $T_n \in R$, and define G_n on R so that $G_n(x,y,z) = 0,$ for (*x*, *y*, *z*) not contained in T_n and $\iiint_{T_n} G_n(x,y,z)dxdydz = 1.0$. For our problem, it is convenient to let T_n be any gridblock even through we are now considering the continuous problem. Eq. 3.47 actually gives an average value of $p_d(x,y,z,t)$ on T_n. If we let T_n be the gridblock centered at (x_i, y_j, z_k) and choose $G_n(x,y,z) = \delta(x-x_i)\delta(y-y_j)\delta(z-z_k)$, then $F(k) = dp_d(x_i, y_j, z_k, t)$. Carter et al. actually work in terms of the Frechet derivative and thus need to define this functional. In our work, we will derive formulas for sensitivity coefficients using basic calculus principles.

Consider another pressure drop problem represented by

$$\frac{C_1}{\mu}\nabla\cdot[k]\nabla p_{nd} - V\frac{\partial p_{nd}}{\partial s} = -H(t)G_n(x,y,z), \text{ on } R, \tag{3.48a}$$

$$dp_{nd}|_{s=0} = 0, \tag{3.48b}$$

$$\nabla p_{nd}\cdot\vec{n} = 0, \quad \text{on } \partial R, \tag{3.48c}$$

where $H(t)$ is the Heaviside function

$$H(t)=\begin{cases}0, & t<0;\\ 1, & t>0.\end{cases} \tag{3.49}$$

Note if $G_n(x,y,z)=\delta(x-x_i)\delta(y-y_j)\delta(z-z_k)$, then the sink term for this problem corresponds to the removal of 1 bbl/day of fluid from gridblock T_n. If $H(t)$ is replaced by $\delta(t)$, this would be a Green's function problem.

Applying the generalized reciprocity theorem Eq. 3.40 to problems Eq. 3.46 and Eq. 3.48, we obtain

$$\begin{aligned}&\iiint_R\int_0^t -G_n(x,y,z)H(t-s)dp_d(x,y,z,t)dsdxdydz\\ &=-\frac{C_1}{\mu}\iiint_R\int_0^t \nabla\cdot[\delta k]\nabla\bar{p}_d(x,y,z,s)p_{nd}(x,y,z,t-s)dsdxdydz\\ &\quad-\iiint_R\int_0^t\left(\bar{Q}(x,y,z,s)-Q(x,y,z,s)\right)p_{nd}(x,y,z,t-s)dsdxdydz\,.\end{aligned} \tag{3.50}$$

Since $s<t$, in the first integral, $H(t-s)=1$. Differentiating Eq. 3.50 with respect to time using Leibnitz rule (Eq. 3.26) gives

$$\begin{aligned}&\iiint_R G_n(x,y,z)dp_d(x,y,z,t)dxdydz\\ &=\frac{C_1}{\mu}\iiint_R\left[\int_0^t \nabla\cdot[\delta k]\nabla\bar{p}_d(x,y,z,s)\frac{\partial}{\partial t}p_{nd}(x,y,z,t-s)ds\right.\\ &\quad\left.+\nabla\cdot[\delta k]\nabla\bar{p}_d(x,y,z,s)p_{nd}(x,y,z,t-s)|_{s=t}\right]dxdydz\\ &\quad+\iiint_R\left[\int_0^t\left(\bar{Q}(x,y,z,s)-Q(x,y,z,s)\right)\frac{\partial}{\partial t}p_{nd}(x,y,z,t-s)ds\right.\\ &\quad\left.+\left(\bar{Q}(x,y,z,s)-Q(x,y,z,s)\right)p_{nd}(x,y,z,t-s)|_{s=t}\right]dxdydz\,.\end{aligned} \tag{3.51}$$

But, $p_{nd}(x,y,z,t-s)|_{s=t} = p_{nd}(x,y,z,0) = 0$ and $G_n(x,y,z) = 0$ for (*x*, *y*, *z*) not in T_n, so Eq. 3.51 reduces to

$$\begin{aligned}
&\iiint_{T_n} G_n(x,y,z)\,dp_d(x,y,z,t)\,dxdydz \\
&= \frac{C_1}{\mu}\iiint_R \int_0^t \nabla\cdot[\delta k]\nabla\bar{p}_d(x,y,z,s)\frac{\partial}{\partial t}p_{nd}(x,y,z,t-s)\,dsdxdydz \\
&\quad + \iiint_R \int_0^t \left(\bar{Q}(x,y,z,s) - Q(x,y,z,s)\right)\frac{\partial}{\partial t}p_{nd}(x,y,z,t-s)\,dsdxdydz\,. \qquad (3.52)
\end{aligned}$$

Adding and subtracting term $\frac{C_1}{\mu}\iiint_{T_n}\int_0^t \nabla\cdot[\delta k]\nabla p_d(x,y,z,s)\frac{\partial}{\partial t}p_{nd}(x,y,z,t-s)\,dsdxdydz$ to the right-hand side of Eq. 3.52. We have

$$\begin{aligned}
&\iiint_{T_n} G_n(x,y,z)\,dp_d(x,y,z,t)\,dxdydz \\
&= \frac{C_1}{\mu}\iiint_R \int_0^t \nabla\cdot[\delta k]\nabla\left(\bar{p}_d(x,y,z,s) - p_d(x,y,z,s)\right)\frac{\partial}{\partial t}p_{nd}(x,y,z,t-s)\,dsdxdydz \\
&\quad + \frac{C_1}{\mu}\iiint_R \int_0^t \nabla\cdot[\delta k]\nabla p_d(x,y,z,s)\frac{\partial}{\partial t}p_{nd}(x,y,z,t-s)\,dsdxdydz \\
&\quad + \iiint_R \int_0^t \left(\bar{Q}(x,y,z,s) - Q(x,y,z,s)\right)\frac{\partial}{\partial t}p_{nd}(x,y,z,t-s)\,dsdxdydz\,. \qquad (3.53)
\end{aligned}$$

As $\|\delta k\| \to 0, \left(\bar{p}_d - p_d\right) \to 0$, i.e. $\left|\bar{p}_d - p_d\right| = \mathrm{O}(\|\delta k\|)$, Thus, following Carter et al., by ignoring the second order perturbations, Eq. 3.53 can be written as

$$\begin{aligned}
&\iiint_{T_n} G_n(x,y,z)\,dp_d(x,y,z,t)\,dxdydz \\
&= \frac{C_1}{\mu}\iiint_R \int_0^t \nabla\cdot[\delta k]\left(\nabla p_d(x,y,z,s)\frac{\partial}{\partial t}p_{nd}(x,y,z,t-s)\right)dsdxdydz \\
&\quad + \iiint_R \int_0^t \left(\bar{Q}(x,y,z,s) - Q(x,y,z,s)\right)\frac{\partial}{\partial t}p_{nd}(x,y,z,t-s)\,dsdxdydz\,, \qquad (3.53a)
\end{aligned}$$

Using the vector identity, Eq. 3.36a, with $b = \frac{\partial}{\partial t} p_{nd}(x, y, z, t-s)$, $a = [\delta k]$ and $c = p_d$, we can rewrite Eq. 3.53a as

$$\begin{aligned}
&\iiint_{T_n} G_n(x,y,z)\,dp_d(x,y,z,t)\,dxdydz \\
&= \frac{C_1}{\mu}\left[\int_0^t \iiint_R \nabla\cdot[\delta k]\left(\frac{\partial}{\partial t} p_{nd}(x,y,z,t-s)\nabla p_d(x,y,z,s)\right)dsdxdydz\right. \\
&\quad -\int_0^t \iiint_R \left([\delta k]\nabla\frac{\partial}{\partial t} p_{nd}(x,y,z,t-s)\right)\cdot\nabla p_d(x,y,z,s)\,dsdxdydz\Big] \\
&\quad +\int_0^t \iiint_R \left(\overline{Q}(x,y,z,s)-Q(x,y,z,s)\right)\frac{\partial}{\partial t} p_{nd}(x,y,z,t-s)\,dsdxdydz\,. \qquad (3.53b)
\end{aligned}$$

Applying Green's Theorem (Eq. 3.27) to the first term on the right-hand side of Eq. 3.53b yields

$$\begin{aligned}
&\iiint_R \nabla\cdot\left([\delta k]\frac{\partial}{\partial t} p_{nd}(x,y,z,t-s)\nabla p_d(x,y,z,s)\right)dxdydz \\
&= \iint_{\partial R}\left([\delta k]\frac{\partial}{\partial t} p_{nd}(x,y,z,t-s)\nabla p_d(x,y,z,s)\right)\cdot\vec{n}\,dr \qquad (3.54) \\
&= 0,
\end{aligned}$$

where the last equality follows from the boundary condition, Eq. 3.42c. Thus, Eq. 3.53b reduces to

$$\begin{aligned}
&\iiint_{T_n} G_n(x,y,z)\,dp_d(x,y,z,t)\,dxdydz \\
&= -\frac{C_1}{\mu}\int_0^t \iiint_R \left([\delta k]\nabla\frac{\partial}{\partial t} p_{nd}(x,y,z,t-s)\right)\cdot\nabla p_d(x,y,z,s)\,dsdxdydz \\
&\quad +\int_0^t \iiint_R \left(\overline{Q}(x,y,z,s)-Q(x,y,z,s)\right)\frac{\partial}{\partial t} p_{nd}(x,y,z,t-s)\,dsdxdydz \\
&= -\frac{C_1}{\mu}\int_0^t \iiint_R \left([\delta k]\nabla\frac{\partial}{\partial t} p_{nd}(x,y,z,t-s)\right)\cdot\nabla p_d(x,y,z,s)\,dsdxdydz
\end{aligned}$$

$$+\int_0^t \iiint_R dQ(x,y,z,s)\frac{\partial}{\partial t} p_{nd}(x,y,z,t-s)dsdxdydz\,, \tag{3.55}$$

where we have used $dQ(x,y,z,s) = \overline{Q}(x,y,z,s) - Q(x,y,z,s)$.

If we interpret T_n as gridblock "*n*" centered at (x_i, y_j, z_k) and divide our reservoir into gridblocks $T_m, m = 1,2,...,M$ (M is the total number of gridblocks in reservoir), set G_n equals to the delta function centered at the gridblock, and expand the differential p in terms of the permeability differentials, Eq. 3.55 becomes

$$\begin{aligned}
&dp_d(T_n,t) = \\
&-\frac{C_1}{\mu}\sum_{m=1}^{M}\iiint_{T_m}\int_0^t [\delta k]\nabla\frac{\partial}{\partial t}p_{nd}(x,y,z,t-s)\cdot\nabla p_d(x,y,z,s)dsdxdydz \\
&+\iiint_R\int_0^t\sum_{m=1}^{M}\left[\frac{\partial Q(x,y,z,s)}{\partial k_{x,T_m}}\delta k_{x,T_m}+\frac{\partial Q(x,y,z,s)}{\partial k_{y,T_m}}\delta k_{y,T_m}+\frac{\partial Q(x,y,z,s)}{\partial k_{z,T_m}}\delta k_{z,T_m}\right] \\
&\qquad\frac{\partial}{\partial t}p_{nd}(x,y,z,t-s)dsdxdydz \\
&=-\frac{C_1}{\mu}\sum_{m=1}^{M}\iiint_{T_m}\int_0^t\Bigg[\delta k_{x,T_m}\frac{\partial}{\partial x}\frac{\partial}{\partial t}p_{nd}(x,y,z,t-s)\frac{\partial}{\partial x}p_d(x,y,z,s) \\
&\qquad\qquad+\delta k_{y,T_m}\frac{\partial}{\partial y}\frac{\partial}{\partial t}p_{nd}(x,y,z,t-s)\frac{\partial}{\partial y}p_d(x,y,z,s) \\
&\qquad\qquad+\delta k_{z,T_m}\frac{\partial}{\partial z}\frac{\partial}{\partial t}p_{nd}(x,y,z,t-s)\frac{\partial}{\partial z}p_d(x,y,z,s)\Bigg]dsdxdydz \\
&+\sum_{m=1}^{M}\iiint_R\int_0^t\left[\frac{\partial Q(x,y,z,s)}{\partial k_{x,T_m}}\delta k_{x,T_m}+\frac{\partial Q(x,y,z,s)}{\partial k_{y,T_m}}\delta k_{y,T_m}+\frac{\partial Q(x,y,z,s)}{\partial k_{z,T_m}}\delta k_{z,T_m}\right] \\
&\qquad\frac{\partial}{\partial t}p_{nd}(x,y,z,t-s)dsdxdydz\,.
\end{aligned} \tag{3.55a}$$

By definition, if we discretize the reservoir into gridblocks, the total differential of p_d is given by

$$dp_d = \sum_{m=1}^{M}\left[\frac{\partial p_d}{\partial k_{x,T_m}}\delta k_{x,T_m}+\frac{\partial p_d}{\partial k_{y,T_m}}\delta k_{y,T_m}+\frac{\partial p_d}{\partial k_{z,T_m}}\delta k_{z,T_m}\right]. \tag{3.55b}$$

Comparing Eq. 3.55a with 3.55b, we see that

$$\frac{\partial p_d(T_n,t)}{dk_{x,T_m}} = -\frac{C_1}{\mu}\iiiint_{T_m}\int_0^t \frac{\partial}{\partial x}\frac{\partial}{\partial t} p_{nd}(x,y,z,t-s)\frac{\partial}{\partial x} p_d(x,y,z,s)dsdxdydz + \iiiint_R \int_0^t \frac{\partial Q(x,y,z,s)}{\partial k_{k_{x,T_m}}}\frac{\partial}{\partial t} p_{nd}(x,y,z,t-s)dsdxdydz\,, \tag{3.56a}$$

$$\frac{\partial p_d(T_n,t)}{dk_{y,T_m}} = -\frac{C_1}{\mu}\iiiint_{T_m}\int_0^t \frac{\partial}{\partial y}\frac{\partial}{\partial t} p_{nd}(x,y,z,t-s)\frac{\partial}{\partial y} p_d(x,y,z,s)dsdxdydz + \iiiint_R \int_0^t \frac{\partial Q(x,y,z,s)}{\partial k_{k_{y,T_m}}}\frac{\partial}{\partial t} p_{nd}(x,y,z,t-s)dsdxdydz\,, \tag{3.56b}$$

$$\frac{\partial p_d(T_n,t)}{dk_{z,T_m}} = -\frac{C_1}{\mu}\iiiint_{T_m}\int_0^t \frac{\partial}{\partial z}\frac{\partial}{\partial t} p_{nd}(x,y,z,t-s)\frac{\partial}{\partial z} p_d(x,y,z,s)dsdxdydz + \iiiint_R \int_0^t \frac{\partial Q(x,y,z,s)}{\partial k_{k_{z,T_m}}}\frac{\partial}{\partial t} p_{nd}(x,y,z,t-s)dsdxdydz\,, \tag{3.56c}$$

for $m = 1,2,...,M$, where M is the total number of gridblocks in the reservoir.

Let us examine the second term in Eqs. 3.56a-3.56c. We can see the second term is related to the flow rate change due to the permeability perturbation. We define

$$I(T_n,\alpha_{T_m}) = \iiiint_R \int_0^t \frac{\partial Q(x,y,z,s)}{\partial \alpha_{T_m}}\frac{\partial}{\partial t} p_{nd}(x,y,z,t-s)dsdxdydz\,, \tag{3.57}$$

where α represents k_x, k_y or k_z. As we presented at beginning of this subsection, Q contains the all source/sink terms used in the actual problem, i.e.,

$$Q(x,y,z,s) = \sum_w \sum_{l_w} \hat{q}(x_{i_w}, y_{j_w}, z_{l_w}, s)\delta(x - x_{i_w})\delta(y - y_{j_w})\delta(z - z_{l_w})\,. \tag{3.57a}$$

Using Eq. 3.57a in Eq. 3.57, we obtain

$$I(T_n,\alpha_{T_m}) = \int_0^t \iiint_R \sum_w \sum_{l_w} \frac{\partial}{\partial \alpha_{T_m}} \hat{q}(x_{i_w}, y_{j_w}, z_{l_w}, s)\delta(x - x_{i_w})\delta(y - y_{j_w})\delta(z - z_{l_w}) \times \frac{\partial}{\partial t} p_{nd}(x, y, z, t - s)dsdxdydz$$

$$= \int_0^t \sum_w \sum_{l_w} \frac{\partial}{\partial \alpha_{T_m}} \hat{q}(x_{i_w}, y_{j_w}, z_{l_w}, s) \frac{\partial}{\partial t} p_{nd}(x_{i_w}, y_{j_w}, z_{l_w}, t - s)ds . \quad (3.58)$$

We can evaluate this flow change related term, $I(T_n,\alpha_{T_m})$, in different cases.

Two-dimensional case

In a two-dimensional reservoirs, the flow rate at each well is fixed and there is no any change in flow rate due to parameter perturbation, i.e., $\frac{\partial}{\partial \alpha_{T_m}} \hat{q}(x_{i_w}, y_{j_w}, z_{l_w}) = 0$. Thus, $I(T_n,\alpha_{T_m}) = 0$ and Eqs 3.56a -3.56c reduce to following equations:

$$\frac{\partial p_d(T_n,t)}{dk_{x,T_m}} = -\frac{C_1}{\mu} \iiint_{T_m} \int_0^t \frac{\partial}{\partial x} \frac{\partial}{\partial t} p_{nd}(x, y, z, t - s) \frac{\partial}{\partial x} p_d(x, y, z, s)dsdxdydz , \quad (3.59a)$$

$$\frac{\partial p_d(T_n,t)}{dk_{y,T_m}} = -\frac{C_1}{\mu} \iiint_{T_m} \int_0^t \frac{\partial}{\partial y} \frac{\partial}{\partial t} p_{nd}(x, y, z, t - s) \frac{\partial}{\partial y} p_d(x, y, z, s)dsdxdydz , \quad (3.59b)$$

$$\frac{\partial p_d(T_n,t)}{dk_{z,T_m}} = -\frac{C_1}{\mu} \iiint_{T_m} \int_0^t \frac{\partial}{\partial z} \frac{\partial}{\partial t} p_{nd}(x, y, z, t - s) \frac{\partial}{\partial z} p_d(x, y, z, s)dsdxdydz , \quad (3.59c)$$

Three-dimensional case

For three dimensional reservoirs, if there is sufficient vertical communication (k_z is large enough), so that $\frac{\partial}{\partial t} p_{nd}(x_{i_w}, y_{j_w}, z_{l_w}, t - s)$ does not vary with depth, then

$$\frac{\partial}{\partial t} p_{nd}(x_{i_w}, y_{j_w}, z_{l_w}, t-s) = \frac{\partial}{\partial t} p_{nd}(x_{i_w}, y_{j_w}, z_w, t-s), \tag{3.60a}$$

for $l_w = l1, l1+1, \ldots l2$, where z_w denotes an arbitrarily fixed datum. (Recall that p_{nd} is the solution to a single well problem).

Then, Eq. 3.58 can be written as

$$\begin{aligned} I(T_n, \alpha_{T_m}) &\approx \int_0^t \sum_w \frac{\partial}{\partial t} p_{nd}(x_{i_w}, y_{j_w}, z_w, t-s) \sum_{l_w} \frac{\partial}{\partial \alpha_{T_m}} \hat{q}(x_{i_w}, y_{j_w}, z_{l_w}, s) ds \\ &= \int_0^t \sum_w \frac{\partial}{\partial t} p_{nd}(x_{i_w}, y_{j_w}, z_w, t-s) \frac{\partial}{\partial \alpha_{T_m}} \sum_{l_w} \hat{q}(x_{i_w}, y_{j_w}, z_{l_w}, s) ds \\ &= \int_0^t \sum_w \frac{\partial}{\partial t} p_{nd}(x_{i_w}, y_{j_w}, z_w, t-s) \frac{\partial}{\partial \alpha_{T_m}} q(x_{i_w}, y_{j_w}) ds \\ &= 0. \end{aligned} \tag{3.60b}$$

Note in Eq. 3.60b $q(x_{i_w}, y_{j_w})$ is the flow rate of well w and is fixed, so $\frac{\partial}{\partial \alpha_{T_m}} q(x_{i_w}, y_{j_w}) = 0$. Thus, for a three-dimensional reservoir with good vertical communication, the sensitivity coefficient to permeability field can be computed from Eqs. 3.56a-3.56c.

Layered reservoir case

In a layered reservoir case, with no communication between layers, we expect the correction terms, $I(T_n, \alpha_{T_m})$, to be more important. However, if the reservoir properties of different layers are quite close, then we may still have $I(T_n, \alpha_{T_m}) \approx 0$, so Eqs. 3.56a-3.56c apply.

If the reservoir properties vary widely from layer to layer with no vertical communication between layers within the reservoir, the pressure in different layers will be quite

different. In this case, if there exists an observation well, then there will be a strong cross flow through the wellbore at observation well. Ignoring $I(T_n, \alpha_{T_m})$, in this case, will underestimate the sensitivity coefficients. However, we have no easy way to estimate this term other than using the direct method to compute the sensitivity of layer flow rates to the permeability field. However, computations indicate that ignoring the term $I(T_n, \alpha_{T_m})$ when estimating sensitivity coefficients only has a significant effect when computing the sensitivity of an observation well pressure to the permeability in a gridblock penetrated by an active well. In this case, the active well rates, and hence the observation well rates, are quite sensitive to the permeabilities in active well gridblocks.

3.3.1.4 Sensitivity to Porosity Field

Similar to the last subsection, we can derive the sensitivity coefficient of gridblock pressure with respective to porosity.

We consider the same problem described in Eq. (3.42) , i. e.,

$$\frac{C_1}{\mu}\nabla\cdot[k]\nabla p_d - V\frac{\partial p_d}{\partial s} = -Q \quad \text{on } R, \tag{3.61a}$$

$$p_d|_{s=0} = 0, \tag{3.61b}$$

$$\nabla p_d \cdot \vec{n} = 0, \quad \text{on } \partial R. \tag{3.61c}$$

In Eq. 3.61a, V is defined as $V = \frac{\phi c_t}{5.615}$.

Consider the related problem with a small perturbation on V , i.e.,

$$\frac{C_1}{\mu}\nabla\cdot[k]\nabla\bar{p}_d-(V+dV)\frac{\partial\bar{p}_d}{\partial s}=-\bar{Q}\,,\ \text{on}\ R\,, \tag{3.62a}$$

$$\bar{p}_d|_{s=0}=0\,, \tag{3.62b}$$

$$\nabla\bar{p}_d\cdot\vec{n}=0,\quad \text{on}\ \partial R\,. \tag{3.62c}$$

Here, $\bar{p}_d$ and $\bar{Q}$, respectively, represent the resulting pressure drop solution and distribution of sources and sinks due to a small perturbation in V.

The total pressure differential due to the perturbation is given by

$$dp_d=\bar{p}_d-p_d\,. \tag{3.63}$$

We rewrite Eq. 3.62a as

$$\frac{C_1}{\mu}\nabla\cdot[k]\nabla\bar{p}_d-V\frac{\partial\bar{p}_d}{\partial s}=-\bar{Q}+dV\frac{\partial\bar{p}_d}{\partial s}\,. \tag{3.64}$$

Subtracting Eq. 3.61a from Eq. 3.64 and use Eq. 3.63, we have

$$\frac{C_1}{\mu}\nabla\cdot[k]\nabla dp_d-V\frac{\partial dp_d}{\partial s}=dV\frac{\partial dp_d}{\partial s}-(\bar{Q}-Q)\,, \tag{3.65a}$$

$$dp_d|_{s=0}=0\,, \tag{3.65b}$$

$$\nabla dp_d\cdot\vec{n}=0,\quad \text{on}\ \partial R\,. \tag{3.65c}$$

Define a functional F by

$$F(\phi)=\iiint_{T_n}G_n(x,y,z)dp_d(x,y,z,t)dxdydz\ , \tag{3.66}$$

where T_n is a subregion of reservoir, $T_n\in R$, and define G_n on R so that $G_n(x,y,z)=0$, for (x, y, z) not contained in T_n and $\iiint_{T_n}G_n(x,y,z)dxdydz=1.0$. For our problem, we let T_n represent one of the gridblocks. Eq. 3.66 may be thought of giving an average value of

$p_d(x,y,z,t)$ on T_n. If we let T_n be the gridblock centered at (x_i, y_j, z_k) and choose $G_n(x,y,z) = \delta(x-x_i)\delta(y-y_j)\delta(z-z_k)$, then $F(\phi) = dp_d(x_i, y_j, z_k, t)$.

Consider the problem

$$\frac{C_1}{\mu}\nabla\cdot[k]\nabla p_{nd} - V\frac{\partial p_{nd}}{\partial s} = -H(t)G_n(x,y,z), \text{ on } R, \tag{3.67a}$$

$$p_{nd}|_{s=0} = 0, \tag{3.67b}$$

$$\nabla p_{nd}\cdot\vec{n} = 0, \quad \text{on } \partial R, \tag{3.67c}$$

where $H(t)$ is the Heaviside function

$$H(t) = \begin{cases} 0, & t < 0; \\ 1, & t > 0. \end{cases} \tag{3.68}$$

Note if $G_n(x,y,z) = \delta(x-x_i)\delta(y-y_j)\delta(z-z_k)$, then the sink term for this problem represents the removal of 1 bbl/day of fluid from T_n. If $H(t)$ is replaced by $\delta(t)$, this would be a Green's function problem.

Applying the generalized reciprocity theorem (Eq. 3.40) to problems (3.65) and (3.67) gives

$$\begin{aligned}
&\iiint_R \int_0^t -G_n(x,y,z)H(t-s)dp_d(x,y,z,t)dsdxdydz \\
&= \iiint_R \int_0^t dV\frac{\partial \bar{p}_d(x,y,z,s)}{\partial s}p_{nd}(x,y,z,t-s)dsdxdydz \\
&- \iiint_R \int_0^t \left(\bar{Q}(x,y,z,t) - Q(x,y,z,s)\right)p_{nd}(x,y,z,t-s)dsdxdydz \\
&= \iiint_R \int_0^t dV\frac{\partial \bar{p}_d(x,y,z,s)}{\partial s}p_{nd}(x,y,z,t-s)dsdxdydz
\end{aligned}$$

$$-\iiint_R \int_0^t dQ(x,y,z,s)p_{nd}(x,y,z,t-s)dsdxdydz\,, \tag{3.69}$$

where we have used $dQ(x,y,z,s) = \overline{Q}(x,y,z,s) - Q(x,y,z,s)$.

Since $s < t$ in the first integral, $H(t-s) = 1$. Differentiating Eq. 3.69 with respect to time using Leibnitz rule gives

$$\begin{aligned}
&\iiint_R G_n(x,y,z)dp_d(x,y,z,t)dxdydz \\
&= -\iiint_R \int_0^t [dV \frac{\partial \overline{p}_d(x,y,z,s)}{\partial s}\frac{\partial}{\partial t} p_{nd}(x,y,z,t-s)ds \\
&\qquad + dV \frac{\partial \overline{p}_d(x,y,z,s)}{\partial s} p_{nd}(x,y,z,t-s)|_{s=t}]dxdydz \\
&\quad + \iiint_R \int_0^t [dQ(x,y,z,s)\frac{\partial}{\partial t} p_{nd}(x,y,z,t-s)ds \\
&\qquad + dQ(x,y,z,s)p_{nd}(x,y,z,t-s)|_{s=t}]dxdydz.
\end{aligned} \tag{3.70}$$

But, $p_{nd}(x,y,z,t-s)|_{s=t} = p_{nd}(x,y,z,0) = 0$ and $G_n(x,y,z) = 0$ for (x, y, z) not in T_n. Thus, Eq. 3.70 reduces to

$$\begin{aligned}
&\iiint_{T_n} G_n(x,y,z)dp_d(x,y,z,t)dxdydz \\
&= -\iiint_R \int_0^t dV \frac{\partial \overline{p}_d(x,y,z,s)}{\partial s}\frac{\partial}{\partial t} p_{nd}(x,y,z,t-s)dsdxdydz \\
&\quad + \iiint_R \int_0^t dQ(x,y,z,s)\frac{\partial}{\partial t} p_{nd}(x,y,z,t-s)dsdxdydz\,.
\end{aligned} \tag{3.71}$$

Adding and subtracting terms $\iiint_R \int_0^t dV \frac{\partial p_d(x,y,z,s)}{\partial s}\frac{\partial}{\partial t} p_{nd}(x,y,z,t-s)dsdxdydz$ to the right-hand side of Eq. 3.71, we obtain

$$\iiint_{T_n} G_n(x,y,z)dp_d(x,y,z,t)dxdydz =$$

$$-\iiint_R \int_0^t dV \frac{\partial}{\partial s}\left(\overline{p}_d(x,y,z,s) - p_d(x,y,z,s)\right)\frac{\partial}{\partial t} p_{nd}(x,y,z,t-s)dsdxdydz$$

$$-\iiint_R \int_0^t dV \frac{\partial}{\partial s} p_d(x,y,z,s)\frac{\partial}{\partial t} p_{nd}(x,y,z,t-s)dsdxdydz$$

$$+\iiint_R \int_0^t dQ(x,y,z,s)\frac{\partial}{\partial t} p_{nd}(x,y,z,t-s)dsdxdydz . \quad (3.72)$$

As $\|dV\| \to 0$, $\left(\overline{p}_d - p_d\right) \to 0$, thus following Carter et al., Eq. 3.72 can be written as

$$\iiint_{T_n} G_n(x,y,z)dp_d(x,y,z,t)dxdydz$$

$$= -\iiint_R \int_0^t dV \frac{\partial}{\partial s} p_d(x,y,z,s)\frac{\partial}{\partial t} p_{nd}(x,y,z,t-s)dsdxdydz$$

$$+\iiint_R \int_0^t dQ(x,y,z,s)\frac{\partial}{\partial t} p_{nd}(x,y,z,t-s)dsdxdydz . \quad (3.73)$$

If we interpret T_n as gridblock "*n*" centered at (x_i, y_j, z_k) and divide our reservoir into gridblocks $T_m, m = 1,2,..., M$ (M is the total number of gridblocks in reservoir), then with G_n equals to the delta function centered at the gridblock, Eq. 3.74 becomes

$$dp_d(x_i,y_j,z_k,t) = -\sum_{m=1}^{M}\iiint_{T_m}\int_0^t \delta V_{T_m}\frac{\partial}{\partial s} p_d(x,y,z,s)\frac{\partial}{\partial t} p_{nd}(x,y,z,t-s)dsdxdydz$$

$$+\iiint_R \int_0^t \sum_{m=1}^{M}\frac{\partial}{\partial V_{T_m}} Q(x,y,z,s)\delta V_{T_m}\frac{\partial}{\partial t} p_{nd}(x,y,z,t-s)dsdxdydz$$

$$= -\sum_{m=1}^{M}\iiint_{T_m}\int_0^t \delta V_{T_m}\frac{\partial}{\partial s} p_d(x,y,z,s)\frac{\partial}{\partial t} p_{nd}(x,y,z,t-s)dsdxdydz$$

$$+\sum_{m=1}^{M}\iiint_R \int_0^t \frac{\partial}{\partial V_{T_m}} Q(x,y,z,s)\delta V_{T_m}\frac{\partial}{\partial t} p_{nd}(x,y,z,t-s)dsdxdydz . \quad (3.75a)$$

By definition, if the region is discretized into m gridblocks, the differential dp_d is given by

$$dp_d = \sum_m \frac{\partial p_d}{\partial V_{T_m}} \delta V_{T_m} . \tag{3.75b}$$

Comparing Eq. 3.75a with 3.75b, we obtain

$$\frac{dp_d(T_n,t)}{dV_{T_m}} = -\iiint_{T_m} \int_0^t \frac{\partial}{\partial s} p_d(x,y,z,s) \frac{\partial}{\partial t} p_{nd}(x,y,z,t-s) dsdxdydz$$
$$+ \iiint_R \int_0^t \frac{\partial}{\partial V_{T_m}} Q(x,y,z,s) \frac{\partial}{\partial t} p_{nd}(x,y,z,t-s) dsdxdydz . \tag{3.76}$$

Since $V_{T_m} = \frac{\phi_{T_m} c_t}{5.615}$, applying the chain rule gives

$$\frac{\partial p_d(T_n,t)}{\partial \phi_{T_m}} = \frac{\partial p_d(T_n,t)}{\partial V_{T_m}} \frac{\partial V_{T_m}}{\partial \phi_{T_m}}$$
$$= -\frac{c_t}{5.615} \iiint_{T_m} \int_0^t \frac{\partial}{\partial s} p_d(x,y,z,s) \frac{\partial}{\partial t} p_{nd}(x,y,z,t-s)$$
$$+ \iiint_R \int_0^t \frac{\partial}{\partial \phi_{T_m}} Q(x,y,z,s) \frac{\partial}{\partial t} p_{nd}(x,y,z,t-s) dsdxdydz . \tag{3.77}$$

Ignoring the second term on right-hand side of Eq. 3.77 gives

$$\frac{\partial p_d(T_n,t)}{\partial \phi_{T_m}} = -\frac{c_t}{5.615} \iiint_{T_m} \int_0^t \frac{\partial}{\partial s} p_d(x,y,z,s) \frac{\partial}{\partial t} p_{nd}(x,y,z,t-s) . \tag{3.78}$$

Computations indicate that ignoring this term of Eq. 3.77 involving the flow rates does not have a significant effect on the accuracy of the sensitivity coefficients related to the perosity field. This result is not surprising since changing the porosity at one gridblock should not have a significant effect on flow rates.

3.3.2 Numerical Calculation of Sensitivity Coefficients

Eqs. 3.59a-3.59c and Eq. 3.78 give the equations for sensitivity coefficient calculations. In this section, we will discuss how to implement these results numerically.

If T_m represents the gridblock centered at (x_l, y_m, z_n), using a midpoint integration rule[46] to perform the *y* and *z* integration, then Eq. 3.59a becomes

$$\frac{\partial p_d(x_i, y_j, z_k, t_n)}{\partial k_x(x_l, y_m, z_n)} = -\frac{C_1}{\mu}\Delta y_m \Delta z_n \times \int_0^{t_n}\int_{x_{l-1/2}}^{x_{l+1/2}} \left(\frac{\partial p_d(x, y_m, z_n, s)}{\partial x} \times \frac{\partial}{\partial x}\frac{\partial p_{nd}(x, y_m, z_n, t_n - s)}{\partial (t_n - s)} \right) dx ds, \tag{3.79}$$

for all (*l*, *m*, *n*) at any time t_n. The integrals in Eq. 3.79 are evaluated by a standard composite trapezoidal rule.[18]

In applying the trapezoidal rule to perform the x-integration in Eq. 3.79, we need to evaluate the derivatives $\partial p_d(x^-_{l+1/2}, y_m, z_n, t)/\partial x$ and $\partial p_d(x^+_{l-1/2}, y_m, z_n, t)/\partial x$ as well as similar spatial derivatives of p_{nd}, where the superscripts - and +, respectively, denote derivatives from the left and the right. In evaluating such derivatives, one must recognize that for a heterogeneous permeability field, fluxes are continuous across gridblock interfaces, but pressure derivatives are not. In following subsection, we will discuss how to accurately compute spatial derivatives.

3.3.2.1 Spatial Derivatives

The following figure shows two adjacent gridblocks in the x direction, centered at x_i and x_{i+1} respectively. Here, the x-direction permeabilities of these two gridblock are simply denoted by k_i and k_{i+1}, gridsizes are Δx_i and Δx_{i+1} respectively. Since we are considering only the x-derivative, we suppress any reference to the *y*, *z* and *t* variable.

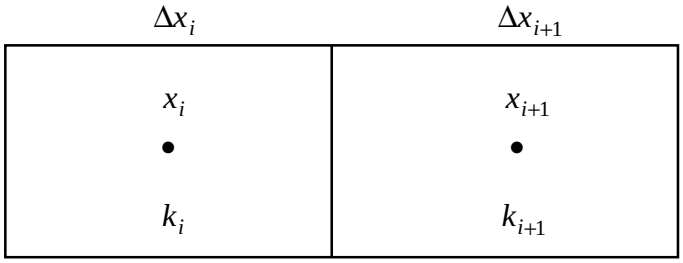

Our simulator incorporates approximation, $\frac{\partial p_d(x_{i+1/2})}{\partial x} = \frac{p_d(x_{i+1}) - p_d(x_i)}{x_{i+1} - x_i}$. But $\frac{\partial p_d(x_{i+1/2})}{\partial x}$ does not make sense, i.e., the x-derivative is discontinuous at $x_{i+1/2}$ unless $k_i = k_{i+1}$. However, one sided derivative exists, e.g., the derivative from the left at $x_{i+1/2}$ is well defined and can be approximated by

$$\frac{\partial p_d(x_{i+1/2}^-)}{\partial x} = \frac{p_{d,i+1/2} - p_{d,i}}{\Delta x_i / 2}. \tag{3.80}$$

At this point, $p_{d,i+1/2}$ is unknown. However continuity of fluxes gives

$$k_i \frac{\partial p_d(x_{i+1/2}^-)}{\partial x} = k_{i+1} \frac{\partial p_d(x_{i+1/2}^+)}{\partial x}, \tag{3.81}$$

or

$$k_i \frac{p_{d,i+1/2} - p_{d,i}}{\Delta x_i / 2} = k_{i+1} \frac{p_{d,i+1} - p_{d,i+1/2}}{\Delta x_{i+1} / 2}. \tag{3.82}$$

Rearranging Eq. 3.82, we have

$$p_{d,i+1/2}\left[\frac{k_i}{\Delta x_i} + \frac{k_{i+1}}{\Delta x_{i+1}}\right] = \frac{k_i}{\Delta x_i} p_{d,i} + \frac{k_{i+1}}{\Delta x_{i+1}} p_{d,i+1}, \tag{3.83}$$

or

$$p_{d,i+1/2} = \left[\frac{k_i}{\Delta x_i} p_{d,i} + \frac{k_{i+1}}{\Delta x_{i+1}} p_{d,i+1}\right] \Bigg/ \left[\frac{k_i}{\Delta x_i} + \frac{k_{i+1}}{\Delta x_{i+1}}\right] = \frac{k_{i+1}\Delta x_i p_{d,i+1} + k_i \Delta x_{i+1} p_{d,i}}{k_i \Delta x_{i+1} + k_{i+1}\Delta x_i}. \tag{3.84}$$

Using Eq. 3.84 in Eq. 3.80

$$\begin{aligned} \frac{\partial p_d(x^-_{i+1/2})}{\partial x} &= \frac{p_{d,i+1/2} - p_{d,i}}{\Delta x_i / 2} \\ &= \frac{2}{\Delta x_i}\left[\frac{k_{i+1}\Delta x_i p_{d,i+1} + k_i \Delta x_{i+1} p_{d,i}}{k_i \Delta x_{i+1} + k_{i+1}\Delta x_i} - p_{d,i}\right] \\ &= \frac{2k_{i+1}}{k_i \Delta x_{i+1} + k_{i+1}\Delta x_i}\left[p_{d,i+1} - p_{d,i}\right]. \end{aligned} \tag{3.85}$$

Similarly, we can show that

$$\frac{\partial p_d(x^+_{i-1/2})}{\partial x} = \frac{2k_{i-1}}{k_{i-1}\Delta x_i + k_i \Delta x_{i-1}}\left[p_{d,i} - p_{d,i-1}\right]. \tag{3.86}$$

Similar formulas for the other spatial derivatives needed in applying the trapezoidal rule to evaluate specific forms of Eq. 3.79 can be easily derived.

3.3.2.2 Linear Interpolation of Pressure Data

In using Eq. 3.79 to calculate sensitivity coefficients where we perform the time integration by the trapezoidal rule, we need to have the value of $p_{nd}(x_l, y_m, z_n, t_n - s)$, $s = t_1, t_2, ..., t_n$. However, we do not compute pressures at all times $t_n - s$, $s = t_1, t_2, ..., t_n$. Here, $t_1, t_2, ..., t_n$ represent the times at which we have obtained a pressure solution from our simulation. In our application we use linear interpolation to find these pressure values.

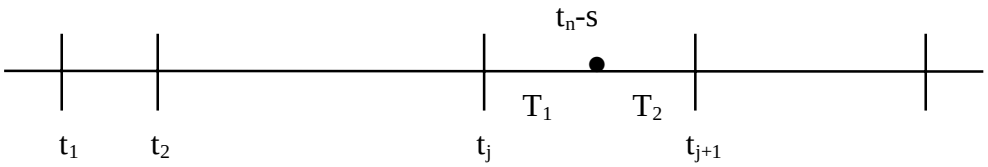

As shown in the above figure, if $t_j < t_n - s < t_{j+1}$, we set $T_1 = (t_n - s) - t_j$ and $T_2 = t_{j+1} - (t_n - s)$. Thus, by linear interpolation, we have

$$p_{nd}(x, y, z, t_n - s) = \frac{p_{nd}(x, y, z, t_j) * T_2 + p_{nd}(x, y, z, t_{j+1}) * T_1}{T_1 + T_2}. \tag{3.87}$$

3.3.2.3 Discrete Form of Sensitivity Coefficients

Using the trapezoidal rule to perform integration, the equation for the sensitivity coefficients related to the x-direction permeability field (Eq. 3.79) can be written as

$$\frac{\partial p_d(x_i, y_j, z_k, t_n)}{\partial k_x}$$

$$= -\frac{C_1}{\mu}\Delta y_m \Delta z_n \int_0^{t_n}\int_{x_{l-1/2}}^{x_{l+1/2}} \left(\frac{\partial p_d(x, y_m, z_n, s)}{\partial x} \times \frac{\partial}{\partial x}\frac{\partial p_{nd}(x, y_m, z_n, t_n - s)}{\partial (t_n - s)} \right) dsdx$$

$$= -\frac{C_1}{\mu}\Delta y_m \Delta z_n \int_{x_{l-1/2}}^{x_{l+1/2}} \sum_{p=1}^{n} \int_{t_{p-1}}^{t_p} \left(\frac{\partial p_d(x, y_m, z_n, s)}{\partial x} \times \frac{\partial}{\partial x}\frac{\partial p_{nd}(x, y_m, z_n, t_n - s)}{\partial (t_n - s)} \right) dsdx$$

$$= -\frac{C_1}{\mu}\Delta y_m \Delta z_n \int_{x_{l-1/2}}^{x_{l+1/2}} \sum_{p=1}^{n} \frac{(t_p - t_{p-1})}{2}$$

$$\left[\frac{\partial p_d(x, y_m, z_n, t_{p-1})}{\partial x}\frac{\partial}{\partial x}\frac{\partial p_{nd}(x, y_m, z_n, t_n - t_{p-1})}{\partial (t_n - s)} + \frac{\partial p_d(x, y_m, z_n, t_p)}{\partial x}\frac{\partial}{\partial x}\frac{\partial p_{nd}(x, y_m, z_n, t_n - t_p)}{\partial (t_n - s)} \right]$$

$$= -\frac{C_1}{2\mu}\Delta x_l \Delta y_m \Delta z_n \sum_{p=1}^{n} \frac{(t_p - t_{p-1})}{2}$$

$$\left\{ \left[\frac{\partial p_d(x_{l-1/2}, y_m, z_n, t_{p-1})}{\partial x}\frac{\partial}{\partial x}\frac{\partial p_{nd}(x_{l-1/2}, y_m, z_n, t_n - t_{p-1})}{\partial (t_n - s)} + \frac{\partial p_d(x_{l-1/2}, y_m, z_n, t_p)}{\partial x}\frac{\partial}{\partial x}\frac{\partial p_{nd}(x_{l-1/2}, y_m, z_n, t_n - t_p)}{\partial (t_n - s)} \right] \right.$$

$$\left. \left[\frac{\partial p_d(x_{l+1/2}, y_m, z_n, t_{p-1})}{\partial x}\frac{\partial}{\partial x}\frac{\partial p_{nd}(x_{l+1/2}, y_m, z_n, t_n - t_{p-1})}{\partial (t_n - s)} + \frac{\partial p_d(x_{l+1/2}, y_m, z_n, t_p)}{\partial x}\frac{\partial}{\partial x}\frac{\partial p_{nd}(x_{l+1/2}, y_m, z_n, t_n - t_p)}{\partial (t_n - s)} \right] \right\}, \quad (3.88a)$$

where the spatial derivative of p_d and p_{nd} can be calculated by Eq. 3.86. Again, p_d is the gridblock pressure drop generated numerically by our simulator, while p_{nd} is the pressure response by using unit source at the gridblock T_n centered at (x_i, y_j, z_k). And $p_{nd}(x_l, y_m, z_n, t_n - t_p),\ p = 1,2,...,n$ is calculated using Eq. 3.87.

According to the convolution rule, the sensitivity coefficients related to the x-direction permeability field (Eq. 3.79) can also be written as

$$\frac{\partial p_d(x_i, y_j, z_k, t_n)}{\partial k_x}$$
$$= -\frac{C_1}{\mu}\Delta y_m \Delta z_n \int_0^{t_n}\int_{x_{l-1/2}}^{x_{l+1/2}} \left(\frac{\partial p_{nd}(x, y_m, z_n, s)}{\partial x} \times \frac{\partial}{\partial x}\frac{\partial p_d(x, y_m, z_n, t_n - s)}{\partial (t_n - s)} \right) dx ds. \tag{3.88b}$$

The integration formula Eq. 3.88b can be obtained by simply interchanging p_d and p_{nd} in Eq. 3.88a. In our application, we averaged the values obtained from Eq. 3.88a and 3.88b and found the average value is more accurate than values from either Eq. 3.88a or Eq. 3.88b.

To compute the sensitivity of gridblock pressure with respect to a gridblock porosity, we can write Eq. 3.78 as

$$\frac{\partial p_d(x_i, y_j, z_k, t_n)}{\partial \phi_{l,m,n}}$$
$$= -\frac{C_1}{\mu}\Delta x_l \Delta y_m \Delta z_n \int_0^{t_n} \frac{\partial p_d(x_l, y_m, z_n, s)}{\partial s}\frac{\partial p_{nd}(x_l, y_m, z_n, t_n - s)}{\partial (t_n - s)} ds$$
$$= -\frac{C_1}{\mu}\Delta x_l \Delta y_m \Delta z_n \sum_{p=1}^{n} \int_{t_{p-1}}^{t_p} \frac{\partial p_d(x_l, y_m, z_n, s)}{\partial s}\frac{\partial p_{nd}(x_l, y_m, z_n, t_n - s)}{\partial (t_n - s)} ds ds$$
$$= -\frac{C_1}{\mu}\Delta x_l \Delta y_m \Delta z_n \sum_{p=1}^{n} \frac{(t_p - t_{p-1})}{2} \times$$
$$\left[\frac{\partial p_d(x_l, y_m, z_n, t_{p-1})}{\partial s}\frac{\partial p_{nd}(x_l, y_m, z_n, t_n - t_{p-1})}{\partial (t_n - s)} + \frac{\partial p_d(x_l, y_m, z_n, t_p)}{\partial s}\frac{\partial p_{nd}(x_l, y_m, z_n, t_n - t_p)}{\partial (t_n - s)} \right]. \tag{3.89a}$$

Again using the convolution rule, the sensitivity coefficient of Eq. 3.78 can also be written as

$$
\begin{aligned}
&\frac{\partial p_d(x_i, y_j, z_k, t_n)}{\partial \phi_{l,m,n}} \\
&= -\frac{C_1}{\mu}\Delta x_l \Delta y_m \Delta z_n \int_0^{t_n} \frac{\partial p_{nd}(x_l, y_m, z_n, s)}{\partial s}\frac{\partial p_d(x_l, y_m, z_n, t_n - s)}{\partial (t_n - s)} ds \\
&= -\frac{C_1}{\mu}\Delta x_l \Delta y_m \Delta z_n \sum_{p=1}^{n} \int_{t_{p-1}}^{t_p} \frac{\partial p_{nd}(x_l, y_m, z_n, s)}{\partial s}\frac{\partial p_d(x_l, y_m, z_n, t_n - s)}{\partial (t_n - s)} ds \\
&= -\frac{C_1}{\mu}\Delta x_l \Delta y_m \Delta z_n \sum_{p=1}^{n} \frac{(t_p - t_{p-1})}{2} \times \\
&\quad \left[\frac{\partial p_{nd}(x_l, y_m, z_n, t_{p-1})}{\partial s}\frac{\partial p_d(x_l, y_m, z_n, t_n - t_{p-1})}{\partial (t_n - s)} \right. \\
&\quad \left. + \frac{\partial p_{nd}(x_l, y_m, z_n, t_p)}{\partial s}\frac{\partial p_d(x_l, y_m, z_n, t_n - t_p)}{\partial (t_n - s)} \right].
\end{aligned}
\tag{3.89b}
$$

We use the average value of Eq. 3.89a and Eq. 3.89b as the sensitivity coefficient related to the porosity field.

Note Eqs. 3.88a, 3.88b, 3.89a and 3.89b require approximations for time derivatives. To show how these approximation are done, we consider Eq. 3.89b. Since t_p corresponds to a time at which pressure is measured, we simply use the approximation

$$
\begin{aligned}
&\frac{\partial p_{nd}(x_l, y_m, z_n, t_p)}{\partial s} = \\
&\quad \frac{1}{t_{p+1} - t_{p-1}} \times \left[\frac{t_{p+1} - t_p}{t_p - t_{p-1}} \left(p_{nd}(x_l, y_m, z_n, t_p) - p_{nd}(x_l, y_m, z_n, t_{p-1}) \right) \right. \\
&\quad \left. + \frac{t_p - t_{p-1}}{t_{p+1} - t_p} \left(p_{nd}(x_l, y_m, z_n, t_{p+1}) - p_{nd}(x_l, y_m, z_n, t_p) \right) \right],
\end{aligned}
\tag{3.89c}
$$

which represents an average of the two one-sided derivatives at t_p. To find the approximation for $\frac{\partial p_d(x_l, y_m, z_n, t_n - t_p)}{\partial (t_n - s)}$, we first find the interval $\left[t_j, t_{j+1}\right]$ such that

$t_j \le t_n - t_p \le t_{j+1}$ and then estimate $p_d(x_l, y_m, z_n, t_n - t_p)$ using Eq. 3.87. Then the approximation for the derivative is

$$\frac{\partial p_{nd}(x_l, y_m, z_n, t_n - t_p)}{\partial (t_n - s)} = \frac{1}{t_{j+1} - t_j} \times \left[\frac{t_{j+1} - (t_n - t_p)}{(t_n - t_p) - t_j} \left(p_d(x_l, y_m, z_n, t_n - t_p) - p_d(x_l, y_m, z_n, t_j) \right) + \frac{(t_n - t_p) - t_j}{t_{j+1} - (t_n - t_p)} \left(p_d(x_l, y_m, z_n, t_{j+1}) - p_d(x_l, y_m, z_n, t_n - t_p) \right) \right], \quad (3.89d)$$

Other time derivatives needed are approximated in a similar way.

3.3.3 Sensitivity of Wellbore Pressure to Reservoir Parameters

In previous sections, we derived the equations for sensitivity coefficients related to gridblock pressures by a straightforward extension of the Carter et al.[28] method. However, the pressure data available are the observed wellbore pressures, not gridblock pressures. In order to condition reservoir properties to wellbore pressure, we need to have sensitivity coefficients related to wellbore pressure. We will show that the wellbore pressure sensitivity coefficients are related directly to the sensitivity coefficients for the gridblock pressures, and can be calculated similar to the calculation of the sensitivity coefficients for gridblock pressures.

As we discussed in section 3.2.3, wellbore pressure is related to gridblock pressure by Peaceman's equation, i.e.,

$$q^n_{i,j,k} = (WI)_k (p^n_{i,j,k} - p^n_{wf}), \quad (3.90)$$

where

$$(WI)_k = \left(\frac{2\pi C_1 \Delta z_k \sqrt{k_{x,i,j,k} k_{y,i,j,k}}}{\mu(\ln[r_{ok} / r_w] + s_k)} \right), \tag{3.91}$$

and

$$r_{0,k} = \frac{0.28073 \Delta x_i \sqrt{1 + \frac{k_{x,i,jk}}{k_{y,i,j,k}} \left(\frac{\Delta y_j}{\Delta x_i} \right)^2}}{1 + \sqrt{k_{x,i,j,k} / k_{y,i,j,k}}}. \tag{3.92}$$

The individual gridblock rates must sum to the total sandface flow rate, $q^n_{i,j}$, i.e,

$$q^n_{i,j} = \sum_{k=l1}^{l2} q^n_{i,j,k} = \sum_{k=l1}^{l2} (WI)_k (p^n_{i,j,k} - p^n_{wf}). \tag{3.93}$$

In our applications, the total flow rate at each well is specified and maintained as a constraint throughout the Gauss-Newton iteration process used to generate the maximum a posteriori estimate of the rock property fields; i.e., total flow rates are not sensitive to the rock property fields so the derivative of $q^n_{i,j}$ with respect to any model parameter is zero. Thus, letting α denote any gridblock value of k_x, k_y, k_z or ϕ, differentiating Eq. 3.93 with respect to α, we obtain

$$\frac{\partial q^n_{i,j}}{\partial \alpha} = 0 = \frac{\partial}{\partial \alpha} \sum_{k=l1}^{l2} (WI)_k (p^n_{i,j,k} - p^n_{wf}), \tag{3.94}$$

or

$$\sum_{k=l1}^{l2} (p^n_{i,j,k} - p^n_{wf}) \frac{\partial}{\partial \alpha} (WI)_k + \sum_{k=l1}^{l2} (WI)_k \left(\frac{\partial p^n_{i,j,k}}{\partial \alpha} - \frac{\partial p^n_{wf}}{\partial \alpha} \right) = 0. \tag{3.94a}$$

Finally, we can obtain

$$\frac{\partial p_{wf}^n}{\partial \alpha} = \frac{\sum_{k=l1}^{l2} (WI)_k \frac{\partial p_{i,j,k}^n}{\partial \alpha}}{\sum_{k=l1}^{l2} (WI)_k} + \frac{\sum_{k=l1}^{l2} (p_{i,j,k}^n - p_{wf}^n) \frac{\partial}{\partial \alpha}(WI)_k}{\sum_{k=l1}^{l2} (WI)_k} \tag{3.95}$$

$$= \left(\frac{\partial p_{wf}^n}{\partial \alpha} \right)^1 + \left(\frac{\partial p_{wf}^n}{\partial \alpha} \right)^2,$$

where

$$\left(\frac{\partial p_{wf}^n}{\partial \alpha} \right)^1 = \frac{\sum_{k=l1}^{l2} (WI)_k \frac{\partial p_{i,j,k}^n}{\partial \alpha}}{\sum_{k=l1}^{l2} (WI)_k}, \tag{3.96}$$

is the term related to the derivatives of gridblock pressures, and

$$\left(\frac{\partial p_{wf}^n}{\partial \alpha} \right)^2 = \frac{\sum_{k=l1}^{l2} (p_{i,j,k}^n - p_{wf}^n) \frac{\partial}{\partial \alpha}(WI)_k}{\sum_{k=l1}^{l2} (WI)_k}, \tag{3.97}$$

is the term related to the derivatives of well indices.

3.3.3.1 Term Related to Gridblock Pressure

Let us first consider $\left(\frac{\partial p_{wf}^n}{\partial \alpha} \right)^1$, and take k_x, i.e., $\alpha = k_{x,l,m,n}$ for concentration.

Then Eq. 3.96 becomes

$$\left(\frac{\partial p_{wf}^n}{\partial k_{x,l,m,n}} \right)^1 = \frac{\sum_{k=l1}^{l2} (WI)_k \frac{\partial p_{i,j,k}^n}{\partial k_{x,l,m,n}}}{\sum_{k=l1}^{l2} (WI)_k}. \tag{3.98}$$

Using Eq. 3.79 in Eq. 3.98 and noting that $p_d(x_i, y_j, z_k, t_n) = p_{in} - p(x_i, y_j, z_k, t_n)$, we have

$$\left(\frac{\partial p_{wf}^n}{\partial k_{x,l,m,n}}\right)^1 = \frac{\sum_{k=l1}^{l2} (WI)_k \frac{\partial p_{i,j,k}^n}{\partial k_{x,l,m,n}}}{\sum_{k=l1}^{l2} (WI)_k}$$

$$= \frac{C_1}{\mu} \Delta y_m \Delta z_n \int_0^{t_n} \int_{x_{l-1/2}}^{x_{l+1/2}} \left(\frac{\partial p_d(x, y_m, z_n, s)}{\partial x} \times \frac{\partial}{\partial x} \frac{\partial}{\partial (t_n - s)} \frac{\sum_{k=l1}^{l2} (WI)_k p_{nd}(x, y_m, z_n, t_n - s)}{\sum_{k=l1}^{l2} (WI)_k} \right) dx ds$$

$$= \frac{C_1}{\mu} \Delta y_m \Delta z_n \int_0^{t_n} \int_{x_{l-1/2}}^{x_{l+1/2}} \left(\frac{\partial p_d(x, y_m, z_n, s)}{\partial x} \times \frac{\partial}{\partial x} \frac{\partial \hat{p}_{nd}(x, y_m, z_n, t_n - s)}{\partial (t_n - s)} \right) dx ds, \tag{3.99}$$

where

$$\hat{p}_{nd}(x, y, z, t) = \frac{\sum_{k=l1}^{l2} (WI)_k p_{nd}(x, y, z, t)}{\sum_{k=l1}^{l2} (WI)_k}. \tag{3.100}$$

As we have shown in section 3.3.1.3, p_{nd} is the solution of

$$\frac{C_1}{\mu} \nabla \cdot [k] \nabla p_{nd} - V \frac{\partial p_{nd}}{\partial s} = -\delta(x - x_i)\delta(y - y_j)\delta(z - z_k) \quad \text{on } R, \tag{3.101a}$$

$$p_{nd}|_{s=0} = 0, \tag{3.101b}$$

$$\nabla p_{nd} \cdot \vec{n} = 0, \quad \text{on } \partial R. \tag{3.101c}$$

Multiplying Eq. 3.101 by $(WI)_k$ for $k = l1, l1+1, ..., l2$, summing the resulting equations over k and then dividing the resulting equation by $\sum_{k=l1}^{l2}(WI)_k$, it follows that $\hat{p}_{nd}(x, y, z, t)$ is also the solution of

$$\frac{C_1}{\mu}\nabla\cdot[k]\nabla\hat{p}_{nd} - V\frac{\partial\hat{p}_{nd}}{\partial s} = -\delta(x-x_i)\delta(y-y_j)\frac{\sum_{k=l1}^{k=l2}(WI)_k\,\delta(z-z_k)}{\sum_{k=l1}^{l2}(WI)_k} \quad \text{on } R \qquad (3.102a)$$

$$\hat{p}_{nd}|_{s=0} = 0, \qquad (3.102b)$$

$$\nabla\hat{p}_{nd}\cdot\vec{n} = 0, \quad \text{on } \partial R. \qquad (3.102c)$$

To obtain the solution $\hat{p}_{nd}$ corresponding to a well location at areal location (x_i, y_j), we simply need to use a sink term equal to $s(i,j,z) = \frac{(WI)_k\,\delta(z-z_k)}{\sum_{k=l1}^{l2}(WI)_k}$ in gridblock (x_i, y_j, z_k), for $k = l1, l1+1, ..., l2$, where gridblocks $(x_i, y_j, z_k), k = l1, l1+1, ..., l2$, represent the gridblocks penetrated by the vertical well. Note that the integral of $s(i,j,z)$ over the wellbore is equal to 1.

From the above derivation, we see that $\left(\frac{\partial p_{wf}^n}{\partial k_{x,l,m,n}}\right)^1$ can be obtained from Eq. 3.99 where $\hat{p}_{nd}$ in the solution of the IBVP specified by Eqs. 3.101a-3.101c. Similarly, $\left(\frac{\partial p_{wf}^n}{\partial k_{y,l,m,n}}\right)^1$, $\left(\frac{\partial p_{wf}^n}{\partial k_{z,l,m,n}}\right)^1$, $\left(\frac{\partial p_{wf}^n}{\partial \phi_{l,m,n}}\right)^1$, respectively, can be obtained from similar equations. After these terms are computed, the sensitivity coefficients related to wellbore

pressure can be computed from Eq. 3.95 once we have estimated the terms related to the derivatives of well indices needed in Eq. 3.97; see next subsection.

Note if $\alpha = s_r$ where s_r is a layer skin factor, then

$$\left(\frac{\partial p_{wf}^n}{\partial s_r}\right)^1 = \frac{\sum_{k=l1}^{l2} (WI)_k \frac{\partial p_{i,j,k}^n}{\partial s_r}}{\sum_{k=l1}^{l2} (WI)_k} = 0 \ . \tag{3.103}$$

Eq. 3.103 follows from the fact that we assume infinitesimally small skin zones, so gridblock pressures are independent of skin factors.

3.3.3.2 Term Related to well Indices

As we can see from Eq. 3.97, $\left(\frac{\partial p_{wf}^n}{\partial \alpha}\right)^2$ involves the sensitivity of well indices $(WI)_k$ to reservoir parameters and skin factors. Also from Eq. 3.91 and 3.92, we see that the well index for a particular gridblock penetrated by the vertical well depends only on the x and y direction permeabilities for that gridblock and the associated skin factor. So

$$\frac{\partial (WI)_k}{\partial \phi_{l,m,n}} = 0 \ , \tag{3.104}$$

for all gridblocks. Moreover,

$$\frac{\partial (WI)_k}{\partial k_{x,l,m,n}} = \frac{\partial (WI)_k}{\partial k_{y,l,m,n}} = \frac{\partial (WI)_k}{\partial k_{z,l,m,n}} = 0 \ , \tag{3.105}$$

for all gridblocks unless $(x_l, y_m, z_n) = (x_i, y_j, z_k)$ and

$$\frac{\partial (WI)_k}{\partial s_r} = 0 \ , \tag{3.105a}$$

if $r \neq k$.

Taking the relevant derivatives of Eq. 3.91 and 3.92, and performing considerable algebraic manipulation, we find

$$\frac{\partial (WI)_k}{\partial k_{x,i,j,k}} = \frac{C_1 \Delta z_k}{2\mu\left(\ln(r_{0k}/r_w)+s_k\right)} \times \left[\sqrt{\frac{k_{y,i,j,k}}{k_{x,i,j,k}}} - \frac{1}{\ln(r_{0k}/r_w)+s_k} \times \left(\frac{\sqrt{k_{x,i,j,k}k_{y,i,j,k}}\Delta y_j^2}{k_{y,i,j,k}\Delta x_i^2 + k_{x,i,j,k}\Delta x_i^2} - \frac{\sqrt{k_{y,i,j,k}}}{\sqrt{k_{x,i,j,k}}+\sqrt{k_{y,i,j,k}}} \right) \right]. \tag{3.106}$$

Similarly,

$$\frac{\partial (WI)_k}{\partial k_{y,i,j,k}} = \frac{C_1 \Delta z_k}{2\mu\left(\ln(r_{0k}/r_w)+s_k\right)} \times \left[\sqrt{\frac{k_{x,i,j,k}}{k_{y,i,j,k}}} - \frac{1}{\ln(r_{0k}/r_w)+s_k} \times \left(\frac{k_{x,i,j,k}\sqrt{k_{x,i,j,k}}\Delta y_j^2}{k_{y,i,j,k}\sqrt{k_{y,i,j,k}}\Delta x_i^2 + k_{x,i,j,k}\sqrt{k_{y,i,j,k}}\Delta x_i^2} - \frac{k_{x,i,j,k}}{k_{y,i,j,k}+\sqrt{k_{x,i,j,k}k_{y,i.j.k}}} \right) \right]. \tag{3.107}$$

Also

$$\frac{\partial (WI)_k}{\partial S_k} = \frac{-(WI)_k}{\ln(r_{0k}/r_w)+s_k}. \tag{3.108}$$

Using the preceding formula for the derivatives of the well index terms in Eq. 3.97, we can compute $\left(\frac{\partial p_{wf}^n}{\partial \alpha}\right)^2$. Summing $\left(\frac{\partial p_{wf}^n}{\partial \alpha}\right)^1$ and $\left(\frac{\partial p_{wf}^n}{\partial \alpha}\right)^2$, we obtain the sensitivity coefficient of wellbore pressure with respect to skin factors, porosity and permeability, see Eq. 3.95.

3.3.3.3 Isotropic Permeability Case

If the permeability field is isotropic ($k_x = k_y = k_z = k$), k controls flow in all three (x, y and z) directions and to compute $\partial p_{wf} / \partial k$, we simply add the three formulas (see Eqs. 3.59a-c) for $\partial p_{wf} / \partial k_x$, $\partial p_{wf} / \partial k_y$ and $\partial p_{wf} / \partial k_z$ to obtain

$$\frac{\partial p_{wf}(x_i, y_j, t)}{\partial k(x_l, y_m, z_n)} = \frac{\partial p_{wf}(x_i, y_j, t)}{\partial k_x(x_l, y_m, z_n)} + \frac{\partial p_{wf}(x_i, y_j, t)}{\partial k_y(x_l, y_m, z_n)} + \frac{\partial p_{wf}(x_i, y_j, t)}{\partial k_z(x_l, y_m, z_n)}. \tag{3.109}$$

If $k_x = k_y = k$ and $k_z = 0$ or k_z is fixed, then k_z is not estimated (or perturbed) during the Gauss-Newton iterations and we use

$$\frac{\partial p_{wf}(x_i, y_j, t)}{\partial k(x_l, y_m, z_n)} = \frac{\partial p_{wf}(x_i, y_j, t)}{\partial k_x(x_l, y_m, z_n)} + \frac{\partial p_{wf}(x_i, y_j, t)}{\partial k_y(x_l, y_m, z_n)}. \tag{3.110a}$$

If $k_x = k_y = k$ and $k_z = \alpha k$, for some constant α, then and change in k_z is directly related to the change in k and

$$\frac{\partial p_{wf}(x_i, y_j, t)}{\partial k(x_l, y_m, z_n)} = \frac{\partial p_{wf}(x_i, y_j, t)}{\partial k_x(x_l, y_m, z_n)} + \frac{\partial p_{wf}(x_i, y_j, t)}{\partial k_y(x_l, y_m, z_n)} + \alpha \frac{\partial p_{wf}(x_i, y_j, t)}{\partial k_z(x_l, y_m, z_n)}. \tag{3.110b}$$

3.3.3.4 Sensitivity to Log-permeability

In our work, we use log-permeabilities instead of permeabilities as model parameters. Thus, we need to know the derivative of wellbore pressure with respect to ln(k). However, by the chain rule

$$\frac{\partial p_{wf}}{\partial k} = \frac{\partial lp_{wf}}{\partial \ln(k)} \frac{\partial \ln(k)}{\partial k} = \frac{1}{k} \frac{\partial lp_{wf}}{\partial \ln(k)}, \tag{3.111}$$

so

$$\frac{\partial p_{wf}}{\partial \ln(k)} = k \frac{\partial p_{wf}}{\partial k}. \tag{3.112}$$

Thus once $\frac{\partial p_{wf}}{\partial k}$ has been calculated, $\frac{\partial p_{wf}}{\partial \ln(k)}$ can be obtained easily with Eq. 3.112.

3.3.4 Sensitivity of Layer Flow Rates

If we have observed (measured) layer flow rates in a multilayered reservoir, we can also condition reservoir properties to them. To apply the Gauss-Newton method, we need the sensitivity of each layer flow rate with respect to reservoir properties (permeability, porosity and skin factor).

As indicated by Eq. 3.90, the layer flow rate $q^n_{i,j,k}$, gridblock pressure $p^n_{i,j,k}$ and wellbore pressure p^n_{wf} are related by following equation:

$$q^n_{i,j,k} = (WI)_k (p^n_{i,j,k} - p^n_{wf}), \tag{3.113}$$

where $(WI)_k$ are the well indices defined by Eq. 3.91. Taking the derivative with respect to reservoir parameters, we obtain

$$\frac{\partial q^n_{i,j,k}}{\partial \alpha} = (p^n_{i,j,k} - p^n_{wf}) \frac{\partial (WI)_k}{\partial \alpha} + (WI)_k \left(\frac{\partial p^n_{i,j,k}}{\partial \alpha} - \frac{\partial p^n_{wf}}{\partial \alpha} \right), \tag{3.114}$$

where $\frac{\partial p^n_{i,j,k}}{\partial \alpha}$ and $\frac{\partial p^n_{wf}}{\partial \alpha}$, respectively, represent sensitivity coefficients related to gridblock pressure and wellbore pressure.

The procedure to calculate $\frac{\partial q^n_{i,j,k}}{\partial \alpha}$ is:

1. Calculate sensitivity of gridblock pressure with respect to reservoir parameters, $\frac{\partial p^n_{i,j,k}}{\partial \alpha}$, using the Carter et al. method.

2. Calculate the sensitivity of wellbore pressure with respect to reservoir parameters, $\frac{\partial p^n_{wf}}{\partial \alpha}$, using Eq. 3.95.

3. Calculate $\frac{\partial q^n_{i,j,k}}{\partial \alpha}$ using Eq. 3.114.

3.4 Computational Examples

In this section, estimates of sensitivity coefficients computed from our three-dimensional extension of the Carter et al. method[29] are compared with those obtained by the direct method which is based on individual parameter perturbations; see, for example, Ref. 23. The direct method yields accurate answers within the limits of the accuracy of the simulator, but is extremely inefficient. Although we only present results for an isotropic permeability case, accurate results were also obtained when the permeability field was anisotropic. Both permeability sensitivity coefficients, $\partial p_{wf}(t)/\partial k_{l,m,n}$, and porosity sensitivity coefficients, $\partial p_{wf}(t)/\partial \phi_{l,m,n}$ are presented. In generating the maximum a posteriori estimate, we actually use derivatives with respect to the log-permeabilities. A simple application of the chain rule (Eq. 3.112) can be used to convert from permeability sensitivity coefficients to log-permeability sensitivity coefficients.

In all results, the values of the following parameters are fixed: $c_t = 10^{-5}\,\text{psi}^{-1}$, $\mu = 0.5\,\text{cp.}$ and $r_w = 0.3$ ft at all wells.

3.4.1 2D Homogeneous Case

We first consider a two-dimensional case where the permeability and porosity fields are homogeneous and consider a 15×15 grid. For this problem, an active well located at gridblock (4,8) was produced at a constant rate of $q = 500$ RB/D and an observation well was located at gridblock (12,8).

Figs. 3.1 and 3.2, respectively, present the natural logarithm of permeability sensitivity coefficients related to the active well computed with the direct method and the Carter et al. method at t = 0.03 days. Figs. 3.3 and 3.4, respectively, present a similar comparison at t = 0.25 days. We see that the results from Carter et al. method are in excellent agreement with those obtained by the direct method. We can also see that as time increases, the wellbore pressure becomes sensitive to permeabilities at a greater distance from the well. However, the wellbore pressure is much more sensitive to permeabilities very near the well than to permeabilities a few gridblocks away from the well.

Figs. 3.5 and 3.6, respectively, present permeability sensitivity coefficients related to the observation well pressure computed with the direct method and the Carter et al. method at t = 0.25 days. We see the two sets of results are in excellent agreement. Fig. 3.7 shows a plot of these sensitivity coefficients at gridblocks on the line through the two wells at four different values of time. Again, we see that the two sets of sensitivity coefficients are in excellent agreement. Note the observation well pressure is insensitive

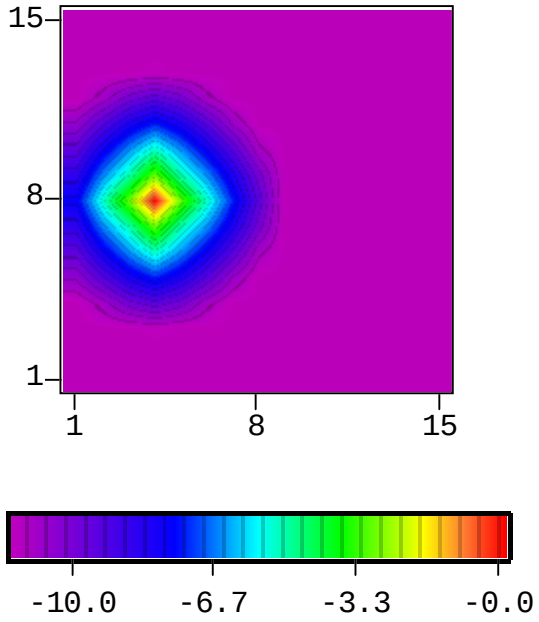

Fig. 3.1 - Log sensitivity of active well pressure to a homogenous log-permeability field at early time, direct method.

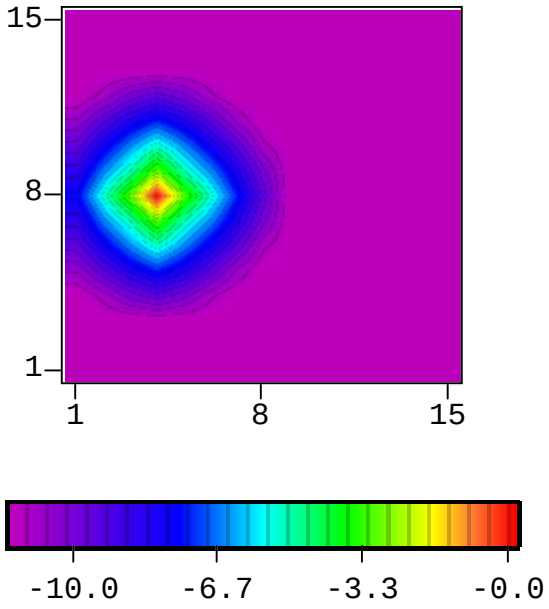

Fig. 3.2 - Log sensitivity of active well pressure to a homogenous log-permeability field at early time, Carter et al. method.

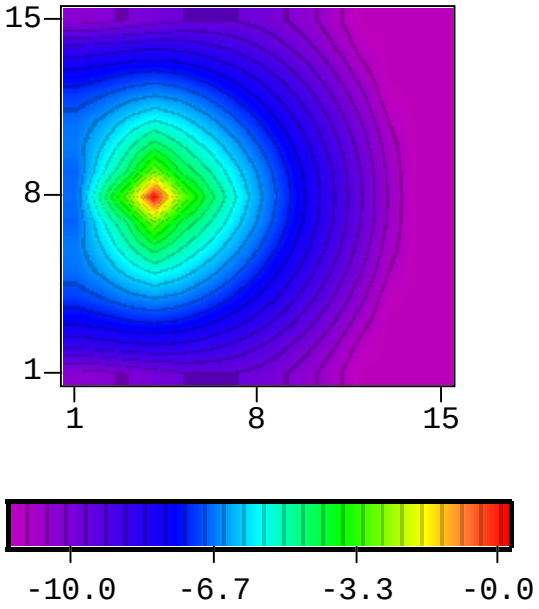

Fig. 3.3 - Log sensitivity of active well pressure to a homogenous log-permeability field at late time, direct method.

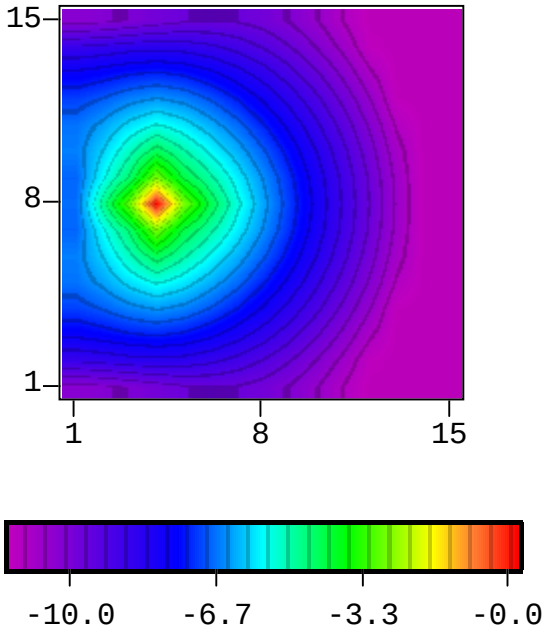

Fig. 3.4 - Log sensitivity of active well pressure to a homogenous log-permeability field at late time, Carter et al. method.

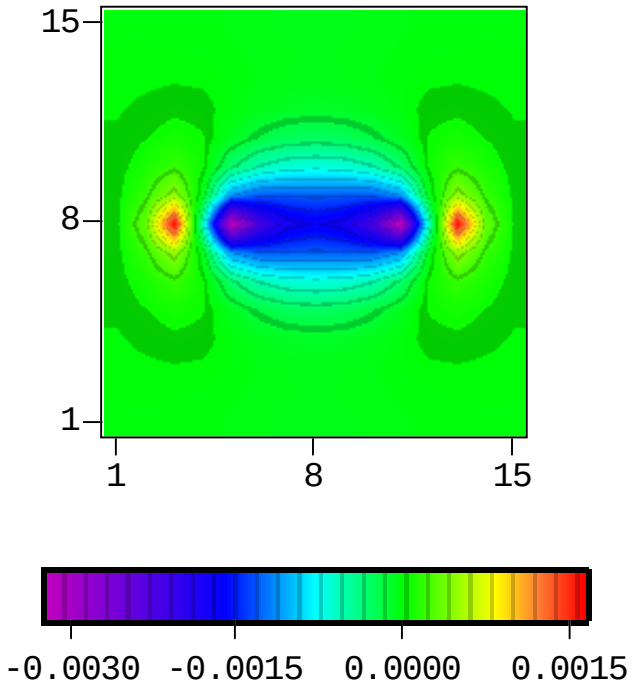

Fig. 3.5 - Sensitivity of observation well pressure to a homogenous log-permeability field, direct method

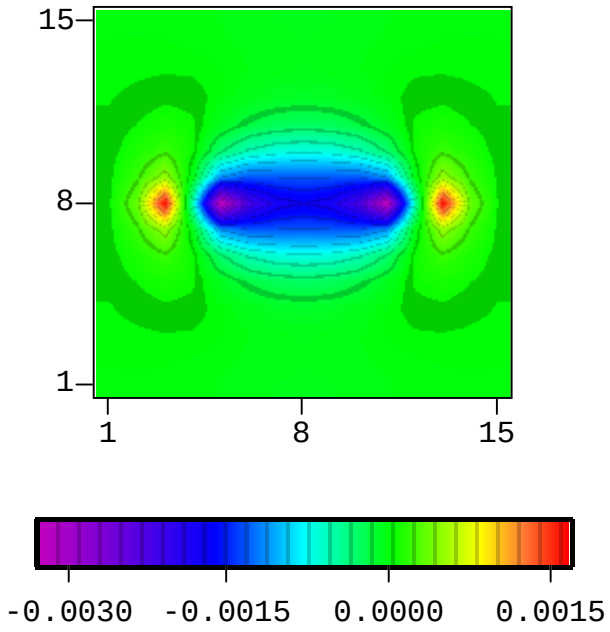

Fig. 3.6 - Sensitivity of observation well pressure to a homogenous log-permeability field, Carter et al. method

to the permeability in the gridblock containing the observation well and to the permeability in the gridblock containing the active well.

We also see that the sensitivity coefficients are symmetric around the two wells, i.e., for all j,

$$\frac{\partial p_{wf}}{\partial k_{4+i,j}} = \frac{\partial p_{wf}}{\partial k_{12-i,j}}, \tag{3.115}$$

for i = -3, -2, ..., 0, 1, 2, 3

and for all i

$$\frac{\partial p_{wf}}{\partial k_{i,8+j}} = \frac{\partial p_{wf}}{\partial k_{i,8-j}}, \tag{3.116}$$

for j =1, 2, ..., 7. For this infinite acting case, this symmetry can be established either from the approximate analytical solution of Oliver[59] or using the reciprocity theorem of Carter et al.[29] Once results are influenced by reservoir boundaries, the sensitivity coefficients related to the observation well pressure will not generally be symmetric around the two wells. However, for the case considered here, with the two wells on a line through y_7 and the two wells equidistant from the x-direction boundaries, the reciprocity theorem of Carter et al.[28] can be used to establish the symmetry of the sensitivity coefficients observed in Figs. 3.5 through 3.7. Also note that between the two wells, the sensitivity coefficients are negative. This means an increase in permeability at one of these gridblocks will cause a decrease in the pressure at the observation well. Physically, a higher permeability in the interwell region causes the pressure to begin dropping sooner at the observation well, thus resulting in a lower pressure at a given time.

This provides a physical explanation of why the sensitivity coefficients on the line segment connecting the two wells are negative.

Beyond the observation well $(i > 12, j = 8)$, the sensitivity coefficients are positive indicating that an increase in permeability in one of these gridblocks will cause an increase in the observation well pressure, or a decrease in permeability will cause a decrease in pressure (increase in pressure drop). In the limit, decreasing permeability towards zero is like introducing a partially sealing fault at that gridblock which will result

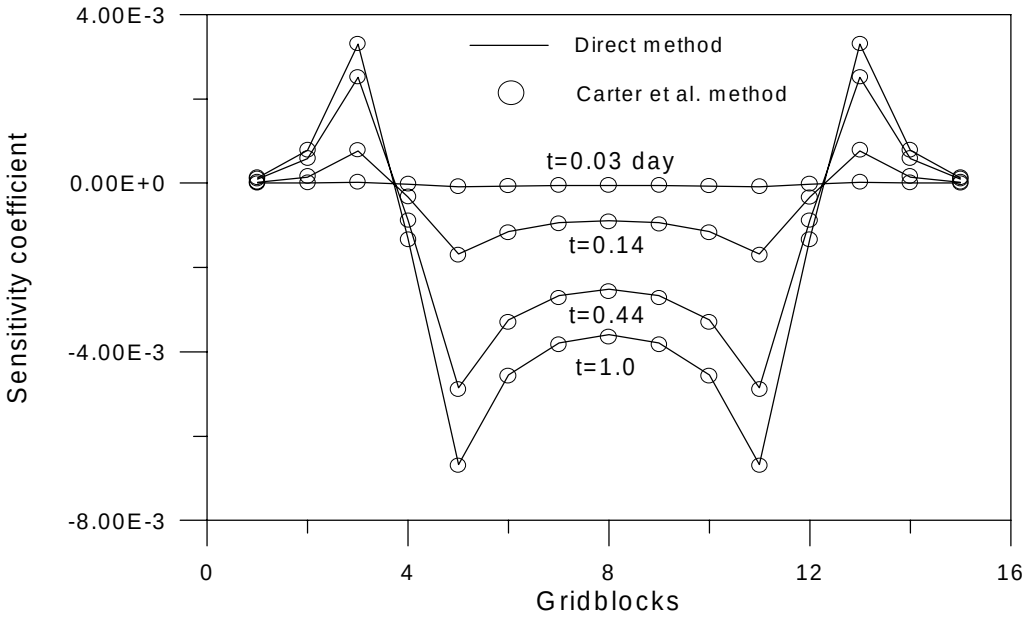

Fig. 3.7 - Sensitivity of observation well pressure to a homogenous log-permeability field, comparison of Carter et al. and direct methods.

in an increase in the pressure drop (decrease in pressure) so again the results are physically reasonable. Similarly, the sensitivity coefficients at j =8, i =1,2,3 are positive. Decreasing permeability at one of these gridblocks results in a greater pressure drop at the active well which results in a greater pressure drop (lower pressure) at the observation well. Also note that the sensitivity coefficients related to permeability at the two well gridblocks are approximately zero. If the size of the gridblocks approaches zero, the sensitivity coefficients should converge to zero. Physically, as the area of the well grids approach the size of the wellbore radii, these gridblock permeabilities act like a skin zone, and skin factors do not affect the observation well pressure for two-dimensional (x-y) problems; three-dimensional problems are different. At an observation well, the net flow into the well is zero so the permeability at the well sandface has no influence on the pressure.

For the same problem, Figs. 3.8 and 3.9, respectively, present the sensitivity of the observation well pressure to the porosity field obtained by the direct and Carter et al. methods at t= 0.25 days. Fig. 3.10 compares the two results along a line through the two wells at four values of time. Again note that the two sets of results are in excellent agreement and results are symmetric around the two wells. Note all porosity sensitivity coefficients are positive. Increasing the porosity at any gridblock increases the fluid in the system for pressure support and hence results in an increase in pressure.

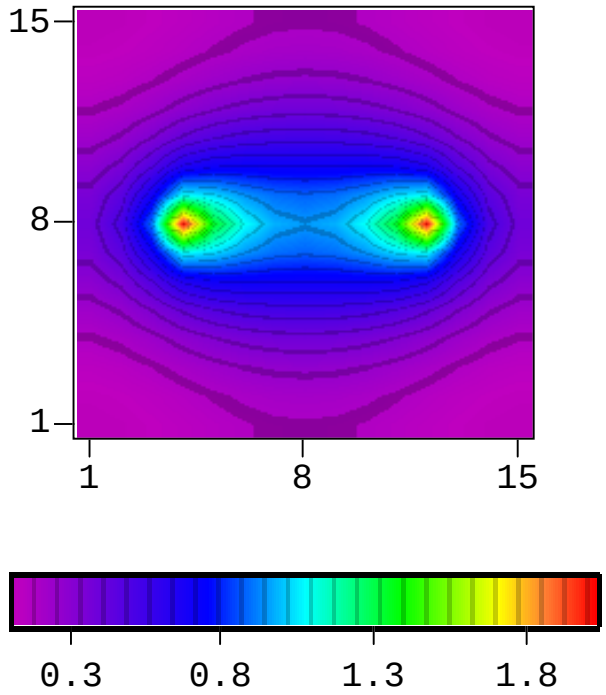

Fig. 3.8 - Sensitivity of observation well pressure to a homogenous porosity field, direct method

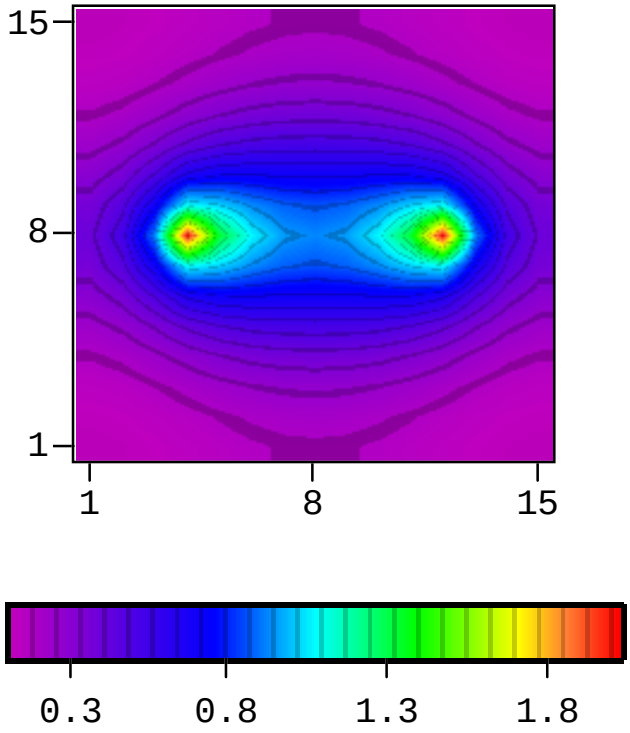

Fig. 3.9 - Sensitivity of observation well pressure to a homogenous porosity field, Carter et al. method.

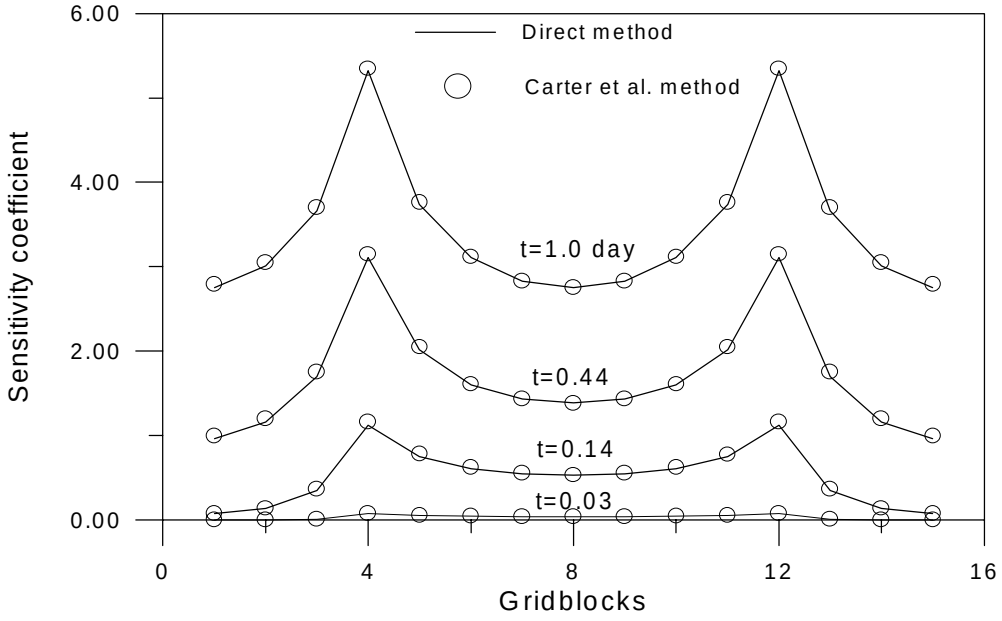

Fig. 3.10 - Sensitivity of observation well pressure to a homogenous porosity field, comparison of Carter et al. and direct methods.

3.4.2 3D Heterogeneous Case

This example pertains to a case with three gridblocks in the z-direction and a 11×11 areal grid with an isotropic heterogeneous permeability field and a heterogeneous porosity field. The active well is located at areal gridblock (3,6) and the observation well at (9,6).

Figs. 3.11 and 3.12, respectively, show the sensitivity of the observation well pressure to the gridblock permeabilities at t = 0.2 days computed by the direct method and our three-dimensional extension of the Carter et al. method. Note that the two sets of results are in excellent agreement. Figs. 3.13 and 3.14, respectively, shows a comparison of the sensitivity of the observation well pressure to permeability and porosity at gridblocks lying on a line through the two wells. Results are presented at four values of time and pertain to the middle "layer." Again the two sets of results are in excellent agreement. Note the results of Figs. 3.12 and 3.13 exhibit no evidence of any errors due to our neglect of the correction involving sensitivities of layer flow rates, see Eqs. 3.57. This is because there is no significant crossflow through the observation wells or in gridblocks containing the wells.

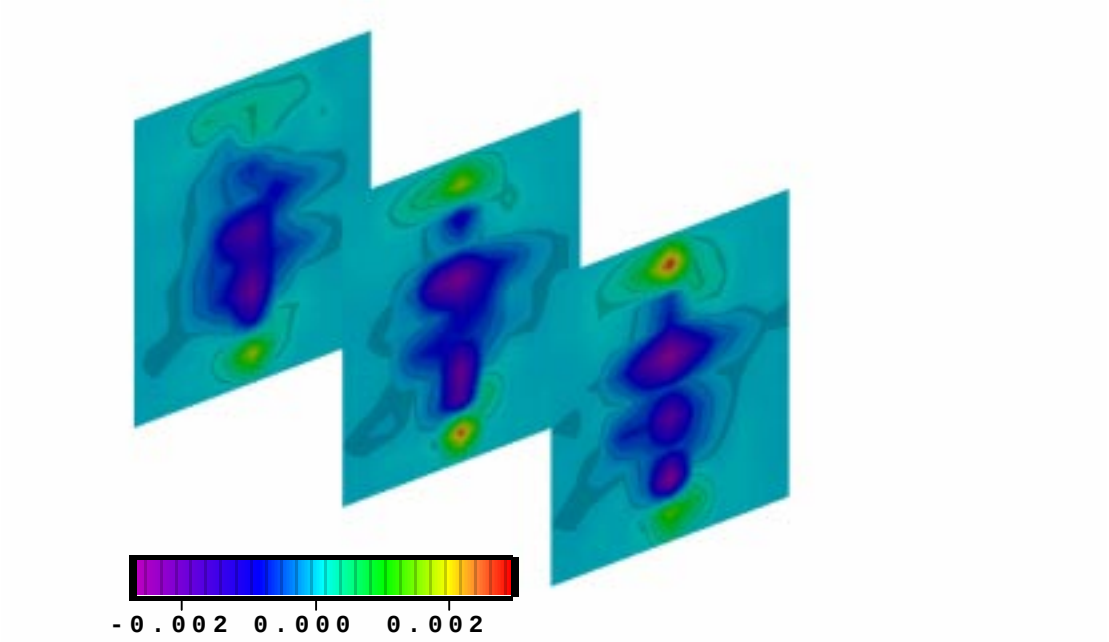

Fig. 3.11 - Sensitivity of observation well pressure to heterogeneous log-permeability field , direct method.

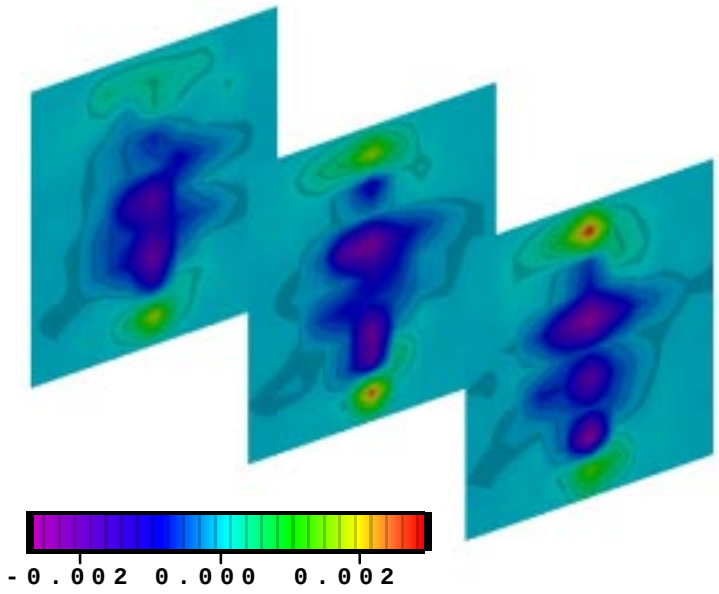

Fig. 3.12 - Sensitivity of observation well pressure to heterogeneous log-permeability field , Carter et al. method.

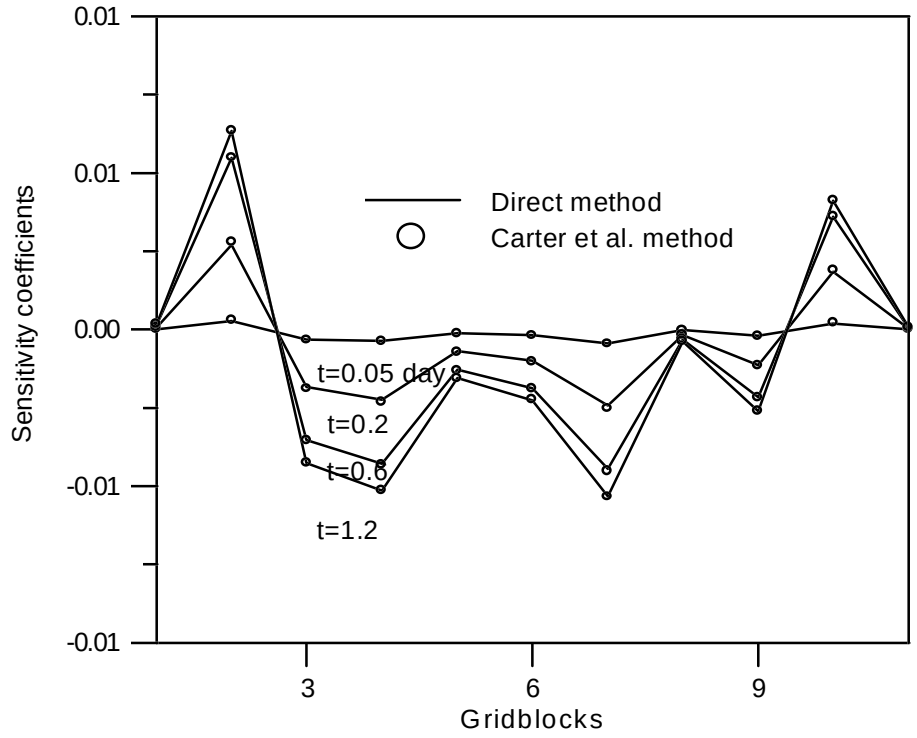

Fig. 3.13 - Sensitivity of observation well pressure to heterogeneous log-permeability field.

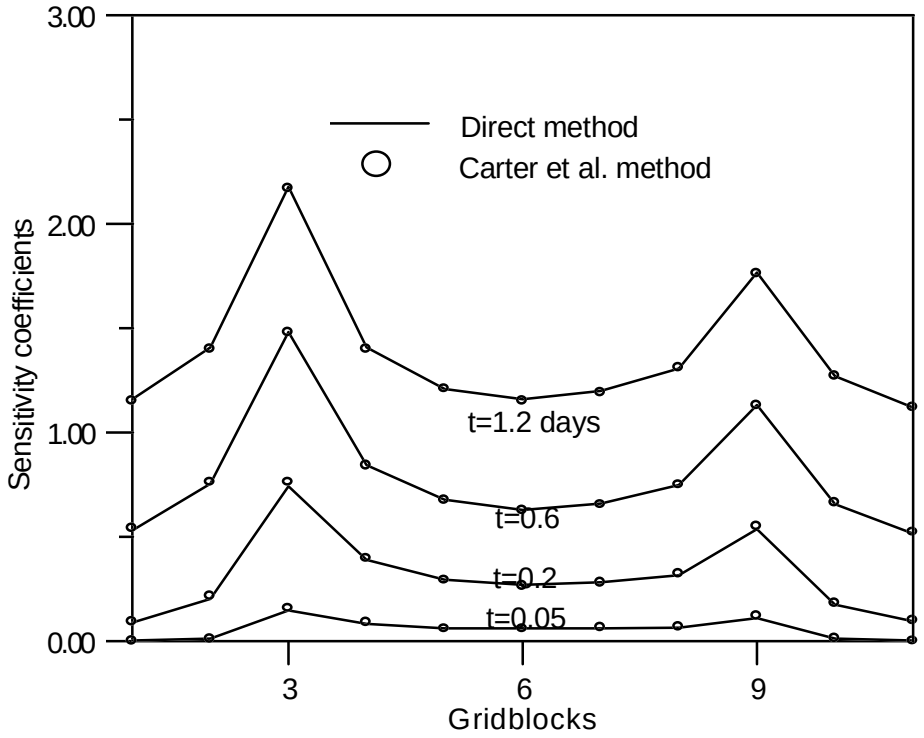

Fig. 3.14 - Sensitivity of observation well pressure to heterogeneous porosity field .

3.4.3 3D Case with Strong Cross-flow

Next, we consider a true commingled three-layer reservoir containing two wells. No crossflow between layers occurs within the reservoir, i.e., $k_z = 0$, but significant crossflow occurs through the observation well. In simulating this system, a 11×11 areal grid was used with one gridblock per layer in the vertical direction. The active and observation wells, respectively, are located at areal gridblocks (6,6) and (3,6). Again the permeability and porosity fields are heterogeneous but the prior means for log-permeability vary from 4.0 in the top layer to 5.0 in the bottom layer. Due to the contrast in layer permeabilities, significant crossflow occurs through the observation well.

Fig. 3.15 shows the sensitivity of the observation well pressure to the gridblock permeabilities of the middle layer lying along a line through the two wells. Note our extension of the Carter et al. method underestimates the sensitivity of the observation well pressure to gridblock permeabilities at the active well. Although not shown, our three-dimensional implementation of the Carter et al. method yields accurate estimates of the sensitivity coefficients related to the active well pressure and accurate estimates of the porosity sensitivity coefficients for this problem. It is important to note that when generating the maximum a posteriori estimate, the active well sensitivity coefficients control the resolution of the gridblock permeabilities penetrated by the active well; thus, the fact that the sensitivity of the observation well pressure to active well gridblock permeabilities is underestimated should not have a great effect on the maximum a posteriori estimate obtained by the Gauss-Newton procedure.

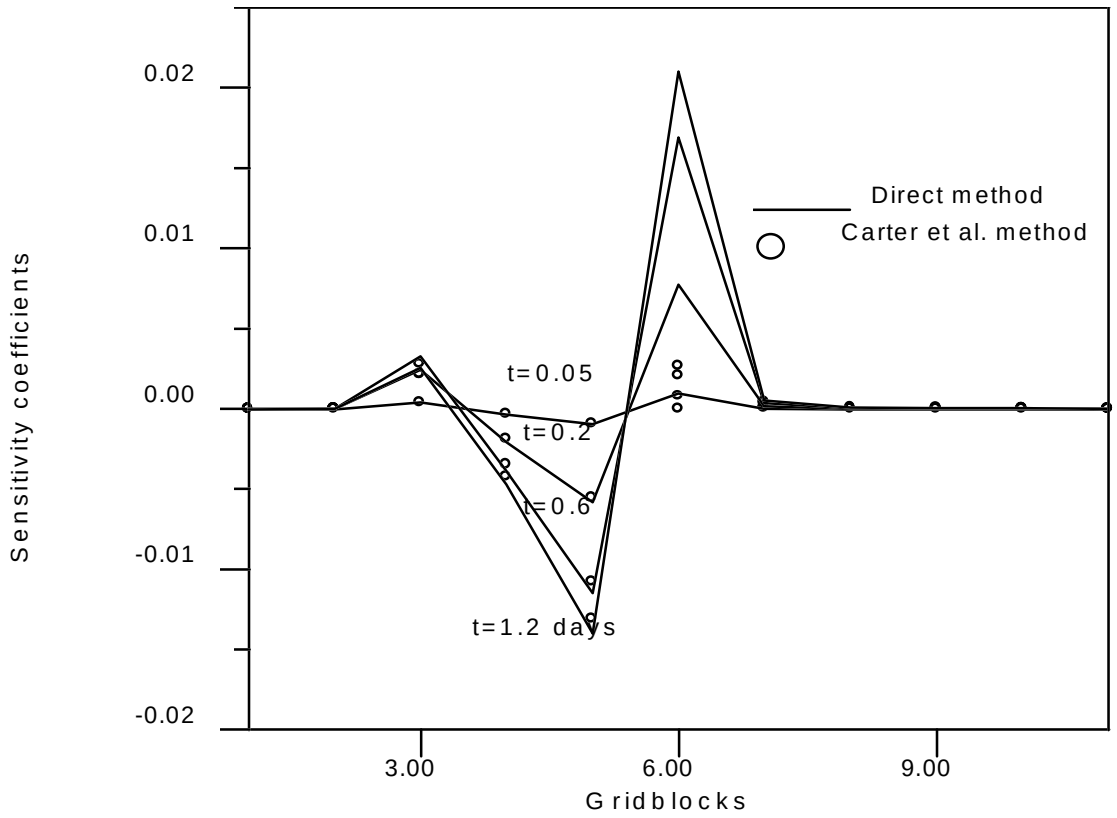

Fig. 3.15 - Sensitivity of observation well pressure to heterogeneous log-permeability field (multiple layer case).

CHAPTER IV

REPARAMETERIZATION TECHNIQUES FOR INVERSE PROBLEM

In Chapter II, we applied the Gauss-Newton method to obtain the maximum a posteriori estimate of the reservoir parameters. If one wishes to determine permeability and porosity values at thousands of gridblocks for use in a reservoir simulator, then inversion of the Hessian matrix at each iteration of the Gauss-Newton procedure becomes computationally expensive. In this work, we present two methods to reparameterize the reservoir model to improve the computational efficiency. The first method uses spectral (eigenvalue/eigenvector) decomposition of the prior covariance matrix. The second method uses a subspace method to reduce the size of the matrix problem that must be solved at each iteration of the Gauss-Newton method. It is shown that proper implementation of the subspace method may significantly reduce the computational time required to generate realizations of the reservoir model, i.e., the porosity and permeability fields and well skin factors, conditioned to prior information on porosity and permeability and multiwell pressure data.

In Ref. 20, Oliver incorporated reparameterization based on the spectral (eigenvalue-eigenvector) decomposition of the prior covariance matrix to determine two-dimensional permeability fields conditioned to well-test pressure data and prior informa-

tion. In one example considered, reparameterization based on spectral decomposition reduced the number of parameters to be obtained by Gauss-Newton iteration from 1089 to 128 without a significant reduction in the quality of the final permeability estimates obtained. The spectral decomposition technique used in Ref. 20 is effectively the same as used in Ref. 10 and also has been considered by Luster[47]. It is important to recognize that the aforementioned results of Oliver[20] were based on the covariance function for a Gaussian variogram with no nugget effect. As discussed later, the number of parameters to be estimated after applying spectral decomposition depends on the rate of decay of the eigenvalues. For the covariance functions associated with common variograms (spherical, exponential and Gaussian), the eigenvalues decay the fastest for the Gaussian covariance[48] and thus the reduction in the number of parameters achieved by spectral decomposition is greatest for this covariance function. Later, we show that adding a nugget effect will decrease the rate of decay of the eigenvalues and thus make spectral decomposition less efficient.

Finally, we note that Oliver[20] considered estimating only the permeability field assuming the porosity field was known. We have found that when the overall prior covariance matrix contains information for both porosity and permeability, spectral decomposition should be applied to the prior correlation matrix in order to obtain meaningful results.

Although reparameterization based on the spectral decomposition may significantly reduce the number of parameters to be estimated by the Gauss-Newton procedure, the size of the resulting Hessian matrix may still be very large. Also, we will see that in case of large reservoir model, the spectral decomposition of the correlation matrix becomes

computationally inefficient. In this work, we show that subspace methods can be applied to significantly reduce the size of the matrix problem solved at each iteration. Subspace methods have recently been applied in the geophysics literature[49-51]. In a subspace method, at each iteration the search direction vector is expanded as a linear combination of basis vectors for a lower dimensional subspace of the model space. The order of the matrix problem to be solved at each iteration of the Gauss-Newton procedure is thereby reduced to the dimension of the subspace.

4.1 Reparameterization Based on Spectral Decomposition

As shown on Chapter II, C_M is the covariance matrix of parameters (permeability, porosity and skin factors). We partition C_M as

$$C_M = \begin{bmatrix} C_B & 0 \\ 0 & C_S \end{bmatrix}, \tag{4.1}$$

where

$$C_B = \begin{bmatrix} C_\phi & C_{\phi k} \\ C_{k\phi} & C_k \end{bmatrix}, \tag{4.2}$$

for the case of an isotropic permeability field.

If the model is reparameterized in terms of the eigenvectors of C_M corresponding to the largest eigenvalues[10,20,47], few of the eigenvectors contain porosity information, thus, one cannot expect to obtain good representations of realizations of the porosity field. More importantly, eigenvalues and eigenvectors of a given matrix C_M are physically meaningful only if all entries of C_M have the same physical dimensions or are dimension-

less[13]. For the preceding reasons, we apply spectral decomposition to the prior correlation matrix.

Let $c_{i,j}$ denote the entry in the *i*th row and *j*th column of C_B, and let D_1 be the $2M \times 2M$ diagonal matrix with *i*th diagonal entry equal to $\sqrt{c_{i,i}}$, i.e.,

$$D_1 = \begin{bmatrix} \sqrt{c_{1,1}} & 0 & \cdots & 0 \\ 0 & \sqrt{c_{2,2}} & \cdots & 0 \\ \vdots & \vdots & \ddots & \vdots \\ 0 & 0 & \cdots & \sqrt{c_{2M,2M}} \end{bmatrix}. \tag{4.3}$$

Note $c_{i,i}$ is simply the variance of the i[th] model parameter.

Then, the correlation matrix is given by

$$\begin{aligned} \tilde{C}_B = D_1^{-1} C_B D_1^{-1} &= \begin{bmatrix} \frac{1}{\sqrt{c_{1,1}}} & 0 & \cdots & 0 \\ 0 & \frac{1}{\sqrt{c_{2,2}}} & \cdots & 0 \\ \vdots & \vdots & \ddots & \vdots \\ 0 & 0 & \cdots & \frac{1}{\sqrt{c_{2M,2M}}} \end{bmatrix} \times \\ &\quad \begin{bmatrix} c_{1,1} & c_{1,2} & \cdots & c_{1,2M} \\ c_{2,1} & c_{2,2} & \cdots & c_{2,2M} \\ \vdots & \vdots & \ddots & \vdots \\ c_{2M,1} & c_{2M,2} & \cdots & c_{2M,2M} \end{bmatrix} \begin{bmatrix} \frac{1}{\sqrt{c_{1,1}}} & 0 & \cdots & 0 \\ 0 & \frac{1}{\sqrt{c_{2,2}}} & \cdots & 0 \\ \vdots & \vdots & \ddots & \vdots \\ 0 & 0 & \cdots & \frac{1}{\sqrt{c_{2M,2M}}} \end{bmatrix} \\ &= \begin{bmatrix} 1 & \frac{c_{1,2}}{\sqrt{c_{1,1}c_{2,2}}} & \cdots & \frac{c_{1,2M}}{\sqrt{c_{1,1}c_{2M,2M}}} \\ \frac{c_{2,1}}{\sqrt{c_{2,2}c_{1,1}}} & 1 & \cdots & \frac{c_{2,2M}}{\sqrt{c_{2,2}c_{2M,2M}}} \\ \vdots & \vdots & \ddots & \vdots \\ \frac{c_{2M,1}}{\sqrt{c_{2M,2M}c_{1,1}}} & \frac{c_{2M,2}}{\sqrt{c_{2M,2M}c_{2,2}}} & \cdots & 1 \end{bmatrix}. \end{aligned} \tag{4.4}$$

Eq. 4.4 shows that the porosity and ln(k) variances have been normalized to unity.

The eigensystem[52] of $\tilde{C}_B$ can be computed by standard techniques[53]. We order the eigenvalues of $\tilde{C}_B$ from largest to smallest, i.e., as $\lambda_1 \geq \lambda_2 \geq \ldots \geq \lambda_{2M}$ and let μ_j denote the $2M$ dimensional eigenvector corresponding to λ_j for $j = 1,2,...,2M$. Throughout, we use this ordering of eigenvalues so the first p eigenvalues, and the pth largest eigenvalues both refer to the set $\{\lambda_j, j = 1,2,..., p\}$. Let U be the $2M \times 2M$ matrix with its jth column equal to μ_j and let Λ_1 be the $2M \times 2M$ diagonal matrix with its jth diagonal element equal to λ_j. It is well known[52] that

$$\tilde{C}_B = U\Lambda_1 U^T, \tag{4.5}$$

and U is an orthogonal matrix, i.e., $UU^T = U^T U = I$.

Throughout I denotes an identity matrix, but the size of I may vary from equation to equation. We refer to Eq. 4.5 as the orthogonal decomposition of $\tilde{C}_B$, the spectral decomposition of $\tilde{C}_B$ or the eigenvalue-eigenvector decomposition of $\tilde{C}_B$.

Now we let p be chosen such that

$$\sum_{j=1}^{p} \lambda_j \geq \theta \sum_{j=1}^{2M} \lambda_j, \tag{4.6}$$

where $0 < \theta \leq 1$. Note Eq. 4.6 indicates that θ is the fraction of the total spectrum (or "energy") contained in the first p eigenvalues. Choosing θ and determining the corresponding value of p effectively determines the reparameterization based on spectral decomposition. Once p has been determined, U and Λ_1 respectively, are partitioned as

$$U = \begin{bmatrix} U_p & U_0 \end{bmatrix}. \tag{4.7}$$

And

$$\Lambda_1 = \begin{bmatrix} \Lambda_p & 0 \\ 0 & \Lambda_0 \end{bmatrix}. \tag{4.8}$$

Here, Λ_p is the diagonal matrix with the first *p* eigenvalues as its diagonal elements and the columns of the $2M \times p$ matrix U_p are given by the first *p* eigenvectors. If the trace of Λ_0 is small compared to the trace of Λ_p, then Eq. 4.5 can be approximated by

$$\tilde{C}_B \approx \begin{bmatrix} U_p & U_0 \end{bmatrix} \begin{bmatrix} \Lambda_p & 0 \\ 0 & 0 \end{bmatrix} \begin{bmatrix} U_p^T \\ U_0^T \end{bmatrix} = U_p \Lambda_p U_p^T = \hat{C}_B, \tag{4.9}$$

where the last equality defines $\hat{C}_B$.

The $(2M + N_S) \times (2M + N_S)$ diagonal matrix *D* is defined by

$$D = \begin{bmatrix} D_1 & 0 \\ 0 & I \end{bmatrix}, \tag{4.10}$$

the $(2M + N_S) \times (p + N_S)$ matrix W_p is defined by

$$W_p = \begin{bmatrix} U_p & 0 \\ 0 & I \end{bmatrix}, \tag{4.11}$$

and the $(p + N_S) \times (p + N_S)$ diagonal matrix Λ is defined by

$$\Lambda = \begin{bmatrix} \Lambda_p & 0 \\ 0 & C_S \end{bmatrix}, \tag{4.12}$$

Using the approximation for $\tilde{C}_B$ (Eq. 4.9), we have the following approximation for C_M:

$$C_M = \begin{bmatrix} C_B & 0 \\ 0 & C_S \end{bmatrix} = \begin{bmatrix} D_1 \tilde{C}_B D_1 & 0 \\ 0 & C_S \end{bmatrix}$$

$$= \begin{bmatrix} D_1 & 0 \\ 0 & I \end{bmatrix} \begin{bmatrix} \tilde{C}_B D_1 & 0 \\ 0 & C_S \end{bmatrix} = \begin{bmatrix} D_1 & 0 \\ 0 & I \end{bmatrix} \begin{bmatrix} \tilde{C}_B & 0 \\ 0 & C_S \end{bmatrix} \begin{bmatrix} D_1 & 0 \\ 0 & I \end{bmatrix}$$

$$\approx \begin{bmatrix} D_1 & 0 \\ 0 & I \end{bmatrix} \begin{bmatrix} U_p \Lambda_p U_p^T & 0 \\ 0 & C_S \end{bmatrix} \begin{bmatrix} D_1 & 0 \\ 0 & I \end{bmatrix}$$

$$= \begin{bmatrix} D_1 & 0 \\ 0 & I \end{bmatrix} \begin{bmatrix} U_p & 0 \\ 0 & I \end{bmatrix} \begin{bmatrix} \Lambda_p & 0 \\ 0 & C_S \end{bmatrix} \begin{bmatrix} U_p^T & 0 \\ 0 & I \end{bmatrix} \begin{bmatrix} D_1 & 0 \\ 0 & I \end{bmatrix} \tag{4.13}$$

$$= D W_p \Lambda W_p^T D.$$

The reparameterized model, m_p, is now defined implicitly by

$$m = D W_p m_p , \tag{4.14}$$

and since $W_p^T W_p = I$, Eq. 4.14 implies

$$m_p = W_p^T D^{-1} m, \tag{4.15}$$

similarly, defining

$$m_{p,prior} = W_p^T D^{-1} m_{prior} \ . \tag{4.16}$$

Note the dimension of m_p is $p + N_S$ which will be much less than the dimension of $(2M + N_S)$ if $p << 2M$, i.e., if spectral decomposition significantly reduces the number of parameters to be directly estimated. Thus, solving for m_p instead of *m* may significantly reduce the computer time required by the inverse procedure.

The Gauss-Newton formulation is given by Eq. 2.20. Multiplying Eq. 2.20 by $W_p^T D^{-1}$, we obtain

$$\begin{aligned} W_p^T D^{-1} m^{l+1} &= \mu_l W_p^T D^{-1} m_{prior} + (1-\mu_l) W_p^T D^{-1} m^l \\ &\quad - \mu_l W_p^T D^{-1} C_M G_l^T \left(C_D + G_l C_M G_l^T \right)^{-1} \left(g(m^l) - d_{obs} + G_l (m^l - m_{prior}) \right). \end{aligned} \tag{4.17}$$

Using Eqs. 4.13, 4.15 and 4.16 in 4.17 gives

$$\begin{aligned} m_p^{l+1} &= \mu_l m_{p,prior} + (1-\mu_l) m_p^l - \mu_l W_p^T D^{-1} (D W_p \Lambda_p W_p^T D) G_l^T \times \\ &\quad \left(C_D + G_l (D W_p \Lambda_p W_p^T D) G_l^T\right)^{-1} \left(g(m^l) - d_{obs} + G_l (m^l - m_{prior})\right) \\ &= \mu_l m_{p,prior} + (1-\mu_l) m_p^l - \mu_l \Lambda_p W_p^T D G_l^T \times \\ &\quad \left(C_D + G_l (D W_p \Lambda_p W_p^T D) G_l^T\right)^{-1} \left(g(m^l) - d_{obs} + G_l (m^l - m_{prior})\right). \end{aligned} \tag{4.18}$$

We define

$$G_{p,l} = G_l D W_p , \tag{4.19}$$

so

$$G_{p,l}^T = W_p^T D G_l^T . \tag{4.20}$$

Using Eqs. 4.19, 4.20, 4.15 and 4.16 in Eq. 4.18,

$$\begin{aligned} m_p^{l+1} &= \mu_l m_{p,prior} + (1-\mu_l) m_p^l - \mu_l \Lambda_p G_{p,l}^T \times \\ &\quad \left(C_D + G_{p,l} \Lambda_p G_{p,l}^T\right)^{-1} \left(g(m^l) - d_{obs} + G_l (m^l - m_{prior})\right) \\ &= \mu_l m_{p,prior} + (1-\mu_l) m_p^l - \mu_l \Lambda_p G_{p,l}^T \times \\ &\quad \left(C_D + G_{p,l} \Lambda_p G_{p,l}^T\right)^{-1} \left(g(m^l) - d_{obs} + G_{p,l} (m_p^l - m_{p,prior})\right). \end{aligned} \tag{4.21}$$

Applying similar matrix algebra used in Eq. 2.17-2.20, we can show

$$\begin{aligned} m_p^{l+1} &= m_p^l - \mu_l (G_{p,l}^T C_D^{-1} G_{p,l} + \Lambda^{-1})^{-1} \times \\ &\quad \left[G_{p,l}^T C_D^{-1} \left(g(m^l) - d_{obs}\right) + \Lambda^{-1} (m_p^l - m_{p,prior})\right]. \end{aligned} \tag{4.22}$$

Throughout G_l denotes the sensitivity coefficient matrix evaluated at m^l where m^l and m_p^l are related by Eqs. 4.14 and 4.15. Note that DW_p can be computed once at the beginning of the process and stored. The advantages of the reparameterized scheme of Eq. 4.22 are two fold. First, the dimension of the model space has been reduced. Secondly, the dense matrix C_M^{-1} of Eq. 2.17 has replaced by the inverse of the diagonal

matrix Λ. The disadvantage is that one must perform a spectral decomposition which may be computationally expensive.

It is important to note that at each iteration, $g(m^l)$ is obtained from the simulator using m^l as input where the conversion between m^l and m_p^l is given by Eqs. 4.14 and 4.15. Thus, even though the Gauss-Newton formula is applied to the reparameterized problem, the simulator run is in terms of the original model parameters.

Throughout, $m_{p,\infty}$ denotes the reparameterized maximum a posteriori estimate obtained by the Gauss-Newton procedure (Eq. 4.22) and m_∞ denotes this maximum a posteriori estimate in terms of the original model parameters.

The a posteriori covariance matrix for the reparameterized model is given by

$$C_{MP,p} = \Lambda - \Lambda G_{p,\infty}^T \left(G_{p,\infty} \Lambda G_{p,\infty}^T + C_D \right)^{-1} G_{p,\infty} \Lambda . \tag{4.23}$$

In Eq. 4.23, $G_{p,\infty} = G_\infty DW_p$, where G_∞ now denotes the sensitivity coefficient matrix evaluated at m_∞. If $L_p L_p^T$ denotes the LU decomposition of $C_{MP,p}$, then realizations of $m_{p,r}$ of the reparameterized model can be obtained from

$$m_{p,r} = m_{p,\infty} + L_p Z_r , \tag{4.24}$$

where Z_r is a vector of independent normal deviates. Corresponding realizations for the original model can then be obtained via Eq. 4.14.

Some remarks on spectral decomposition are in order. For any chosen $\theta < 1$, Eq. 4.6 indicates that the number (p) of eigenvectors used in the reparameterization will depend on the rate of decay of the eigenvalues. A more rapid rate of decay results in a smaller value of p, i.e., a more efficient reparameterization. The rate at which eigenvalues

decrease to zero depends on the specific covariance function or variogram used. For the continuous problem, the eigenvalue problem represents a Fredholm integral equation with the covariance function as its kernel[54] where the covariance function is symmetric positive definite. Assuming that the eigenvalues $(\hat{\lambda}_n, n = 1, 2, \ldots, \infty)$ for the continuous problem are ordered from largest to smallest, Refs. 55 and 56 show that the rate of decay of the eigenvalues depends on the smoothness of the kernel. The spherical and exponential covariance functions are continuous but are not differentiable at the origin. Thus, the results of Ha[56] indicate that $\hat{\lambda}_n = o(1/n)\ as\ n \to \infty$. The Gaussian covariance function, however, has continuous partial derivatives everywhere which is sufficient to guarantee that the associated eigenvalues satisfy $\hat{\lambda}_n = o(1/n^2)$. Thus, the eigenvalues associated with the Gaussian covariance function decay much faster than the eigenvalues associated with the spherical and exponential covariance functions and computations not shown (also see Ababou et al.[48]) here indicate that this is the case. However, if a nugget effect is added to the variogram, the associated covariance function for all variogram models becomes discontinuous at the origin and the eigenvalues asymptotically approach the value of the nugget as $n \to \infty$ instead of decaying to zero. Since the covariance matrix represents a discretized version of the covariance operator, we expect the eigenvalues of the covariance matrix to display a behavior similar to those discussed for the continuous problems (Ababou et al[48]. have verified that this is true for several one-dimensional covariance models). Thus, a Gaussian variogram, as used in Ref. 20, should yield the most efficient reparameterization, i.e., the smallest value of p that satisfies the inequality of Eq. 4.6. As we wish to consider the limitations of spectral decomposition, we consider a

spherical variogram and consequently obtain a less efficient spectral decomposition than was obtained in Ref. 20. Moreover, we illustrate that adding a nugget effect seriously reduces the efficiency of spectral decomposition as is expected based on our theoretical discussion.

4.2 Reparameterization Based on Subspace Methods

4.2.1 Subspace Method

Here, we give a brief description of the subspace method which essentially follows the description given in Refs. 49 through 51. Kennett and Williamson[49] consider a problem of the same form considered here, whereas, Oldenberg et al.[50] and Oldenberg and Li[51] consider a constrained least squares problem.

The basic idea is to choose subspace vectors a_l^j, j= 1,2,..., r and let A_l be the matrix with jth column equal to the column vector a_l^j. The subscript l is used to indicate that the subspace and its basis vectors are recomputed at each iteration of the Gauss-Newton method. The proposed change in the model estimate or search direction vector at the (l + 1)th iteration of Newton's method is then written as

$$\delta m^{l+1} = \sum_{j=1}^{r} \alpha_j^l \, a_l^j = A_l \alpha^l , \tag{4.25}$$

where α is the column vector with jth component equal to α_j^l. Using Eq. 4.25 in Eq. 2.15 of Chapter 2 and multiplying the resulting equation by the transpose of A_l gives

$$(A_l^T H_l A_l)\alpha^l = -A_l^T \nabla S_l . \tag{4.26}$$

Note the coefficient matrix in Eq. 4.26 is an $r \times r$ matrix, whereas the order of H_l is the total number of parameters to be estimated by the Gauss-Newton procedure. Once Eq. 4.26 is solved to obtain α^l, the corresponding δm^{l+1} can be computed directly from Eq. 4.25 and m^{l+1} is obtained from Eq. 2.16.

4.2.2 Choice of Subspace Vectors

Refs. 49-51 consider several procedures for choosing subspace vectors. If one were to use only one subspace vector, an appropriate choice at iteration $l + 1$ would be $a^1 = -\nabla S_l$. With this choice, the subspace method would be equivalent to the steepest descent algorithm which is known to be inefficient.

Refs. 49-51 all suggest partitioning the objective function and its gradient into the part related to the prior model and the part related to the data misfit. Thus, the objective function $S(m)$ is written as $S(m) = f_m(m) + f_d(m)$ where

$$f_m(m) = \frac{1}{2}\left(m - m_{prior}\right)^T C_M^{-1}\left(m - m_{prior}\right), \tag{4.27}$$

and

$$f_d(m) = \frac{1}{2}\left(g(m) - d_{obs}\right)^T C_D^{-1}\left(g(m) - d_{obs}\right). \tag{4.28}$$

If one were to use a two-dimensional subspace, an appropriate choice would be $a^1 = \nabla f_m(m^l)$ and $a^2 = \nabla f_d(m^l)$, but again this choice is too simple to yield a rapidly converging algorithm. Note, however, the negative of these gradients represent the steepest descent vectors for the two sub-objective functions, f_m and f_d. More subspace vectors could be added by multiplying these two gradients by the Hessian[49] to form two

additional descent vectors or by further partitioning of f_d as suggested in Refs. 50 and 51. We follow the later choice but also further partition f_m as suggested by Kennett and Williamson[49]. Oldenberg et al.[50] also suggest that the gradient vectors should be preconditioned by multiplying by C_M. In the two-dimensional subspace case discussed above, this means that the two subspace vectors should actually be modified to $C_M \nabla f_m(m^l)$ and $C_M \nabla f_d(m^l)$. The first of these vectors is actually the steepest descent vector for f_m considered by itself relative to a norm defined in terms of the positive definite matrix C_M. Oldenberg et al.[50] also note that preconditioning by C_M provides appropriate smoothness. It is interesting to note that if we consider minimizing only f_m, $\nabla f_m = C_M^{-1}(m - m_{prior})$ and the Hessian is $\nabla(\nabla f_m)^T = C_M^{-1}$. Thus, the Newton's method is

$$\delta m^{l+1} = -C_M \nabla f_m(m^l), \tag{4.29}$$

or

$$m^{l+1} - m^l = -C_M C_M^{-1}(m^l - m_{prior}) = -m^l + m_{prior}. \tag{4.29a}$$

So $m^{l+1} = m_{prior}$ at all *l*, i.e., Newton's method converges to the minimum, m_{prior}, in one iteration for any initial guess. This provides further motivation for preconditioning gradient vectors by multiplying by C_M. As shown by Oldenberg et al.[50], all gradient vectors should be multiplied by the same preconditioning matrix when forming subspace vectors.

One choice for the subspace vectors which we have found to be efficient for our problem arises by partitioning the data misfit term well by well. Specifically, we partition $g(m) - d_{obs}$ as

$$g(m)-d_{obs}=\begin{bmatrix} g^1(m)-d_{obs}^1 \\ g^2(m)-d_{obs}^2 \\ \vdots \\ g^{N_w}(m)-d_{obs}^{N_w} \end{bmatrix}, \tag{4.30}$$

where d_{obs}^j is the vector of all observed well j pressure data used as conditioning data and $g^j(m)-d_{obs}^j$ is the pressure mismatch vector for well j for $j=1,2,...,N_w$. We also use the same relative partitioning to partition the data covariance matrix as

$$C_D=\begin{bmatrix} C_{D1} & O & \cdots & O \\ O & C_{D2} & \cdots & O \\ \vdots & \ddots & \cdots & \vdots \\ O & \cdots & \cdots & C_{DN_w} \end{bmatrix}, \tag{4.31}$$

where the order of C_{Dj} is the number of observed conditioning pressure data at well j. Finally, we partition the, transpose of the sensitivity coefficient matrix (see Chapter III) as

$$G^T=\left[G_1^T, G_2^T, ..., G_{N_w}^T\right], \tag{4.32}$$

where G_j contains all sensitivity coefficients related to well j. It can then be shown that

$$\nabla f_d(m)=G^T C_D^{-1}(g(m)-d_{obs})=\sum_{j=1}^{nw} G_j^T C_{Dj}^{-1}\left(g^j(m)-d_{obs}^j\right). \tag{4.33}$$

The jth term in the preceding summation gives the part of the gradient related to the total data misfit at well j. Each term in the summation is a candidate for a subspace vector; however, we precondition them by premultiplying by C_M. For now, we simply record these potential subspace vectors as

$$w^j=C_M G_j^T C_{Dj}^{-1}\left(g^j(m)-d_{obs}^j\right), \tag{4.34}$$

for $j=1,2,...,N_w$.

Following a proposal of Kennett and Williamson[49], the gradient of $f_m(m)$ is partitioned into the three parts associated with each of the three attributes; log-permeability, porosity and well skin factors. In our application, we actually precondition the gradient of f_m by premultiplying by C_M and then partition $C_M \nabla f_m$ into parts associated with the three attributes. (This procedure is more computationally efficient, but is equivalent to preconditioning after partitioning the gradient by attributes if and only if there is no correlation between attributes in the prior model.) The resulting three candidate subspace vectors are as follows:

$$w^{N_w+1} = \left[(m_\phi - m_{\phi,prior})^T, 0, 0 \right]^T , \tag{4.35a}$$

$$w^{N_w+2} = \left[0, (m_k - m_{k,prior})^T, 0 \right]^T , \tag{4.35b}$$

and

$$w^{N_w+3} = \left[0, 0, (m_s - m_{s,prior})^T \right]^T . \tag{4.35c}$$

Since the final subspace vectors will be normalized, partitioning the model by attributes removes the dependence on the units of the attributes.

Finally, Oldenberg et al.[50] have noted that convergence of the method is accelerated by adding a constant vector. However, our computational experiments indicate that the results can be further improved by partitioning a constant vector into parts corresponding to each attribute. In our example problem, there is only one skin factor estimated and it is sufficient to add only the two following constant vectors:

$$w^{N_w+4} = \left[1, 1, \cdots, 1, 0, 0, \cdots, 0 \right]^T , \tag{4.36a}$$

and

$$w^{N_w+5} = \left[0, 0, \cdots, 0, 1, 1, \cdots, 1\right]^T . \qquad (4.36b)$$

w^{N_w+4} has its first *m* entries equal to unity and all other entries equal to zero. w^{N_w+5} has its first *m* entries equal to zero and all other entries equal to 1.

In essence, the span of the total set of w^j's represents our subspace. However, if we were unfortunate enough to choose subspace vectors which formed a linearly independent set, then the coefficient matrix of Eq. 4.23 would be singular and the subspace method would fail. Thus, we actually use the Gram-Schmidt[57] procedure to construct an orthonormal set of subspace vectors, a^j, $j = 1,2,...,N_w + 5$, from the w^j's. The resulting set of a^j's represent the subspace basis used in the following example problem. In all cases the w^j are normalized to obtain unit vectors.

4.3 Computational Example

4.3.1 Two-dimensional Case

4.3.1.1 True Reservoir Model

Here, we present results for only one synthetic example, which pertains to two dimensional (*x* - *y*) flow in a rectangular parallelepiped reservoir of thickness *h* = 100 ft and

areal dimensions of of 1,700 ft x 1,700 ft. All reservoir boundaries are no-flow boundaries. Reservoir performance was simulated using a uniform spatial grid with $\Delta x = \Delta y = 100$ ft.

Other relevant reservoir and fluid properties are as follows: system compressibility, $c_t = 10^{-5}$ psi, fluid viscosity, $\mu = 0.5$ cp; all wellbore radii, $r_w = 0.25$ ft; and initial pressure, $p_i = 6{,}000$ psi. The permeability distribution is assumed to be log-normal with log variance of 0.5 and log mean equal to 4.0. We further assume the permeability field is isotropic and spatial continuity can be described by a spherical variogram model with a range equal to 450 ft. It is assumed that porosity has a normal distribution with a mean of 0.25 and a variance of 0.0025. The correlation coefficient between log-permeability and porosity was set equal to $\rho_{\phi,k} = 0.7$. The standard deviation for all pressure measurement errors was assumed to be equal to $\sigma_d = 0.15$ psi.

The areal gridblocks are shown in Fig. 4.1. A number within the gridblock indicates a well in located in the gridblock with the actual number denoting the well number. In the example presented, the center well (well 5) is an active well produced at a constant rate of 500 STB/D and all other wells are observation wells. The skin factor at the active well is equal to 4.0 with the prior mean equal to zero and the prior variance equal to 36.

The "true" distributions of log permeability and porosity, are shown respectively in Figs. 4.2 and 4.3 and represent results from an unconditional simulation generated from the Cholesky decomposition of the prior covariance matrix. In these figures and all subsequent figures, the x-direction and y-direction scales are in feet measured from the "lower left corner" of the reservoir. Note we are only determining the areal distribution

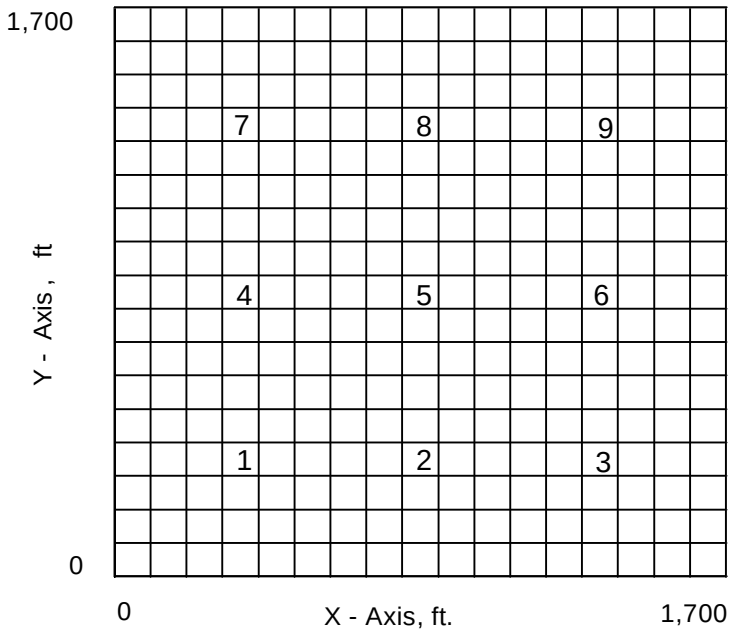

Fig. 4.1—Areal grids, well locations and well numbers.

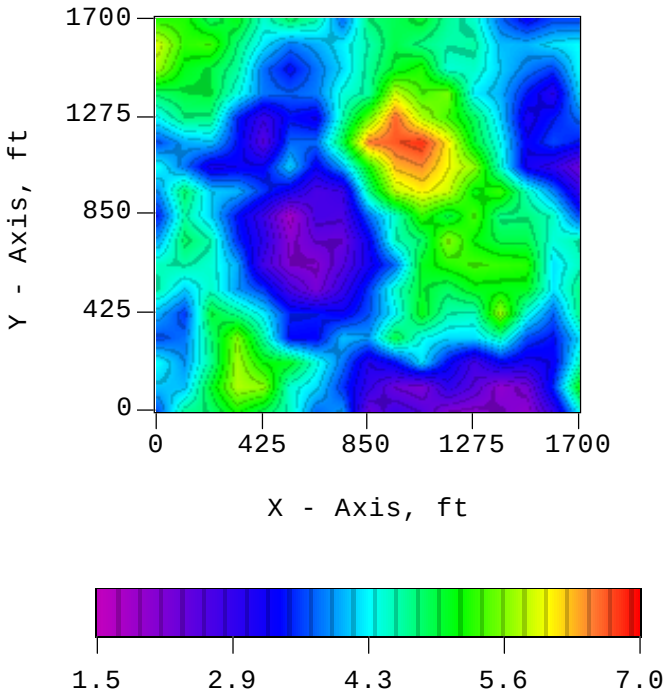

Fig. 4.2 —True log-permeability field.

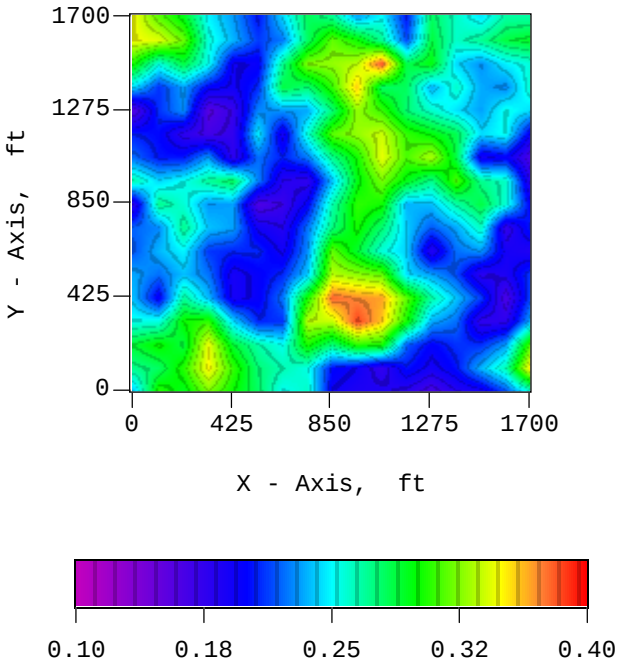

Fig. 4.3—True porosity field.

of rock properties. In terms of ln(k), the scale in Fig. 4.2 ranges from 1.5 to 7.0, i.e., in terms of k, the scale ranges from 4.5 md. to 1,097 md.

In this example, we generate synthetic well test pressure data by running the simulator for a total time of 1.7 days. The maximum pressure drops obtained at the observation wells ranged from 3 psi to 9 psi. In the following, we present realizations of the rock property fields obtained by conditioning to the prior model and the pressure data at the nine wells using the conventional method (Refs. 19, 23 and 24), spectral decomposition, and the subspace method. In the conventional method, Eq. 2.20 in Chapter 2 was applied since this is more computationally efficient formulation of the Gauss-Newton method if no reparameterization is done. In all cases, ten pressure data at each well were used.

4.3.1.2 Spectral Decomposition

Fig. 4.4 and 4.5, respectively, show the maximum a posteriori estimates for ln(k) and porosity obtained using the conventional method of Refs. 19, 23, 24. The corresponding estimate of the skin factor obtained was s = 3.75 as compared to the true value of s = 4.0. Figs. 4.6 and 4.7, respectively, show the maximum a posteriori estimate obtained using spectral decomposition based on retaining ninety per cent of the total spectrum in the reparameterized model, i.e., choosing $\theta = 0.90$ in Eq. 4.6. The associated estimate of the active well skin factor obtained was s = 3.78. Note that qualitatively, the maximum a posteriori estimates obtained with spectral decomposition are almost identical to those obtained by the conventional method, Figs. 4.4 and 4.5. The value

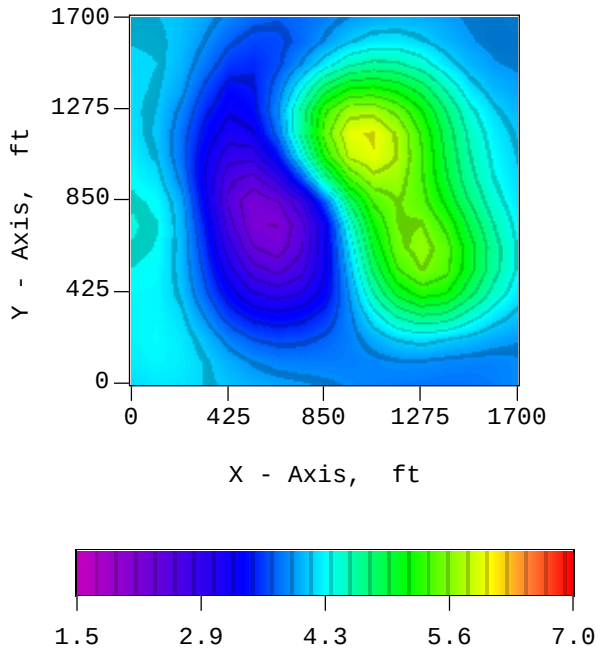

Fig. 4.4—Log-permeability maximum a posteriori estimate; conventional method.

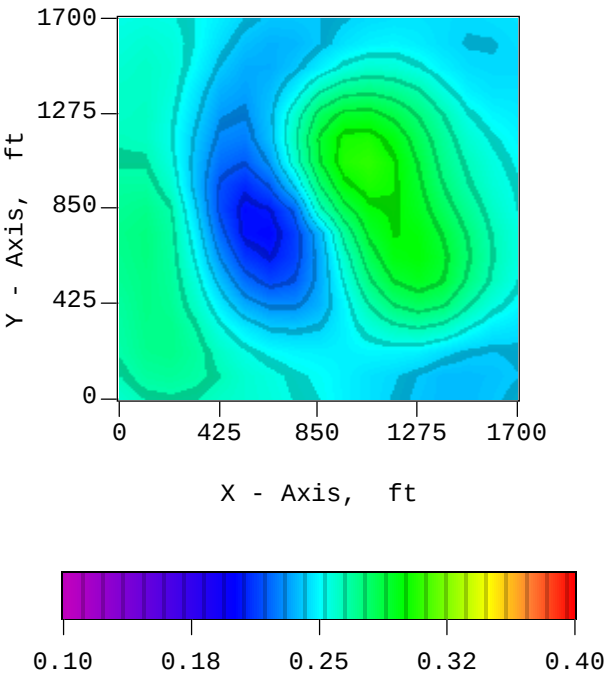

Fig. 4.5 - Porosity maximum a posteriori estimate; conventional method.

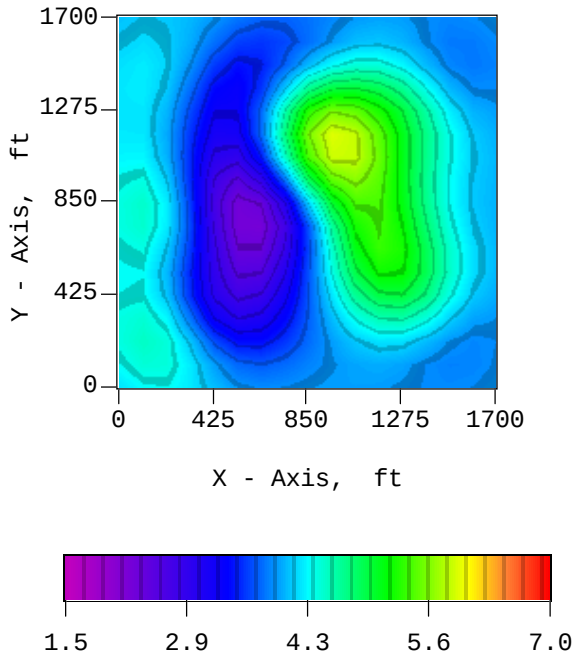

Fig. 4.6 - Log-permeability maximum a posteriori estimate; spectral decomposition.

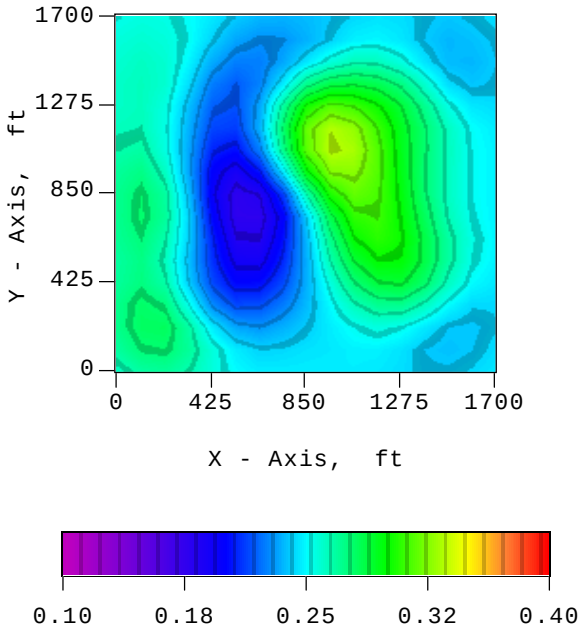

Fig. 4.7 - Porosity maximum a posteriori estimate; spectral decomposition.

of the objective function (see Eq. 2.10) evaluated at the maximum a posteriori estimate was 13.8 for the conventional method and 14.6 for the spectral decomposition method, which further confirms the accuracy of $m_{p,\infty}$. However, the dimension of the reparameterized model m_p is 211 as compared to 579 for the original model *m*. All runs were done on a Pentium-133. The run time for the conventional method was 14.6 minutes as compared to a run time of 7.4 minutes for the spectral decomposition procedure. The Gauss-Newton procedure converged in 5 iterations for the conventional problem, whereas, in the reparameterized case, 6 iterations were required to achieve convergence.

Figs. 4.8 and 4.9 show one realization of the log-permeability and porosity fields obtained from Eqs. 4.24 and 4.14.

In a second example, which only retained 80% of the "energy" ($\theta = 0.8$), maximum a posteriori estimates almost identical to those shown in Figs. 4.6 and 4.7 were obtained, and the corresponding estimate of the active well skin factor was $s = 3.61$. However, for other examples, we have observed a degradation in the accuracy of the maximum a posteriori estimate with $\theta = 0.8$. With $\theta = 0.8$, the dimension of m_p was 98.

Because the eigenvalues of the prior covariance matrix decay fairly rapidly, one might expect spectral decomposition to retain a much smaller percentage of the eigenvalues as the size of the gridblocks decrease without changing the covariance. For example, when we ran a similar case with 625 total gridblocks so that the conventional method estimates 1251 parameters, the dimension of the reparameterized model was 267 for $\theta = 0.90$ in Eq. 4.6. Unfortunately, the computer run time was 107 minutes as compared to

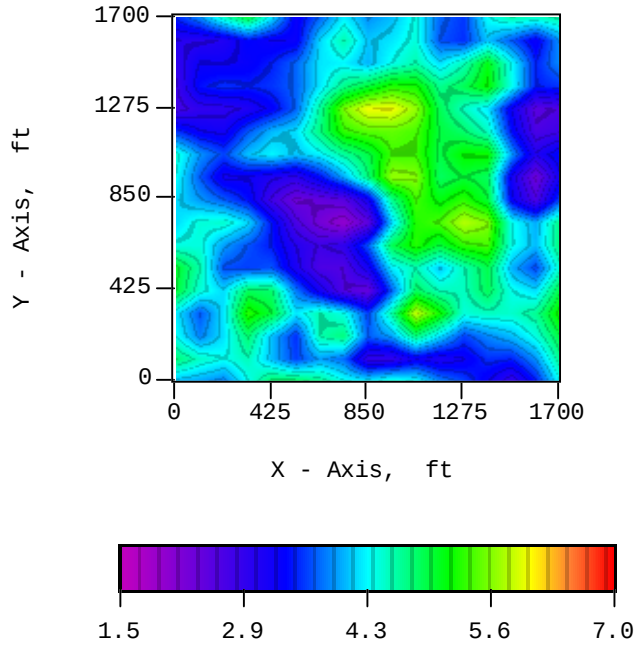

Fig. 4.8 - Realization of log-permeability field; Spectral decomposition method.

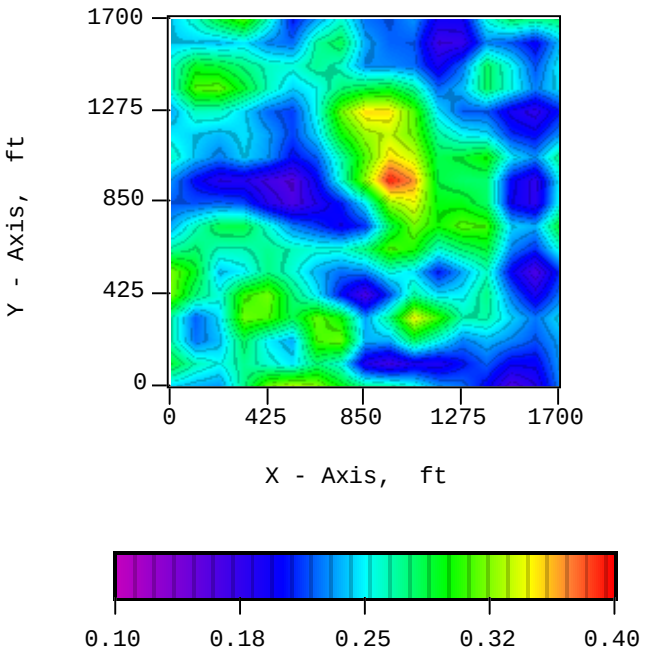

Fig. 4.9 - Realization of porosity field; Spectral decomposition method.

67 minutes for the conventional method. The spectral decomposition alone required over one hour of computer time. The preceding run times refer to the times required to generated the maximum a posteriori estimates.

As mentioned previously, addition of a nugget effect significantly retards the decrease in dimensionality achieved by reparameterization. For example, adding nugget effects of 0.1 to the variogram for ln(k) and 0.0004 to the porosity variogram, resulted in a reparameterized model, m_p of dimension 501 for the 625 gridblock case when reparameterization was based on $\theta = 0.90$.

4.3.1.3 Subspace Method

Figs. 4.10 and 4.11, respectively show the ln(k) and porosity maximum a posteriori estimates obtained by applying the subspace method. The corresponding value of the objective function was 16.6 compared to a value of 13.8 at m_∞. Comparing Fig. 4.10 with Fig. 4.4 and Fig. 4.11 with Fig. 4.5, we see that the estimate of m_∞ obtained with the subspace method is in excellent agreement with m_∞ obtained with the conventional method. The estimate of the active well skin factor obtained from the subspace method was $s = 4.04$. The subspace method required 4.8 minutes of computer time as compared to 14.6 minutes for the conventional method. The subspace method required 7 Gauss-Newton iterations to converge as to compared to 5 iterations for the conventional method.

Fig. 4.12 presents a realization of the log-permeability field obtained from the subspace method. This realization is virtually identical to the corresponding realization

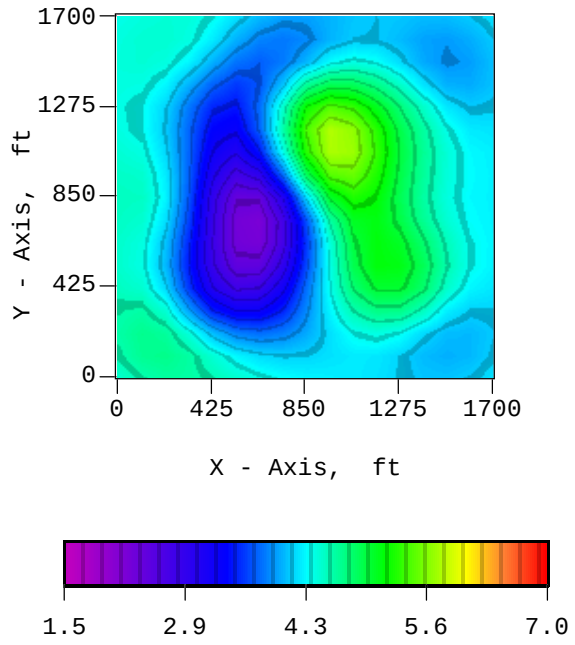

Fig. 4.10 - Log-permeability maximum a posteriori estimate; subspace method.

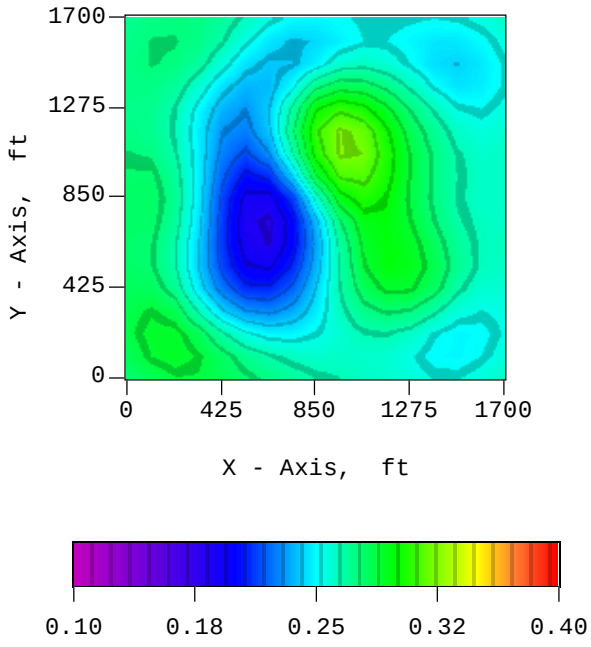

Fig. 4.11—Porosity maximum a posteriori estimate; subspace method.

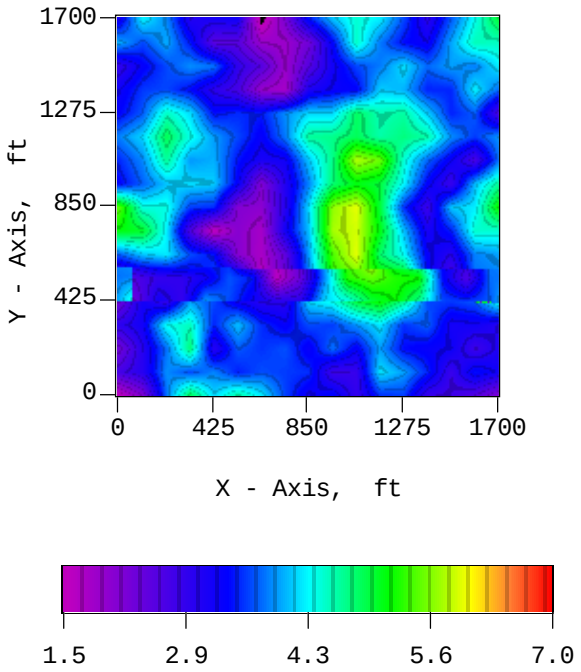

Fig. 4.12—Realization of log-permeability field; Subspace method.

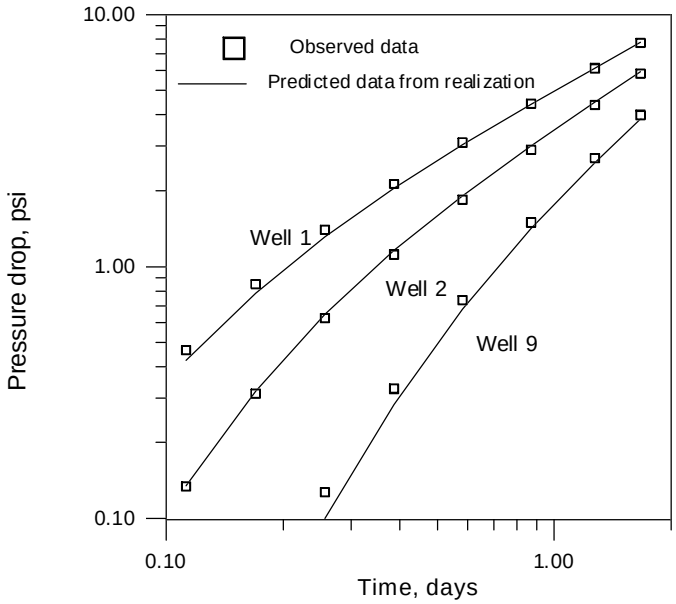

Fig. 4.13—Comparison of true pressure drops with pressure drops predicted from realization at three observation wells.

generated from the conventional method with the same seed and illustrates that the subspace generates realizations of the same quality as obtained with the conventional method.

Fig. 4.13 compares the "true" pressure data at three of the observation wells with the pressure data predicted using the realization of Fig. 12, the associated realization of porosity and the corresponding realization of the active well skin factor as input to the reservoir simulator. Note the realization produces pressure data which are in good agreement with the observed pressure data. Equally good agreement between observed pressure data and pressure data predicted from the realization was obtained at all other wells. Similar to Fig. 5 of Ref. 23, the variograms calculated from the realization of Fig. 12 are in reasonable agreement with the model variograms. However, it is well known that variograms calculated from legitimate realizations of the rock property fields may differ considerably from the model variogram; see Refs. 33 and 35 for additional discussion.

For a similar problem with 625 gridblocks, the subspace method required 30 minutes of computer as compared to 67 minutes for the conventional method. Thus, we see that the subspace method offers the advantage of significant computational savings as the size of the problem becomes large.

4.3.2 Three-dimensional Case

In this subsection, we show a 3D case with same data set as we used in Chapter II. We apply the subspace method to reduce the size of the matrix problem solved at each iteration of the Gauss-Newton method. In selecting subspace vectors, we choose porosity and permeability of each layer as independent subspace vectors, i.e., the vector of Eq.

4.35a was further partitioned into three subspace vectors, and Eq. 4.35b was also replaced by three subspace vectors. Thus, our subspace consists of 3 vectors for porosity, 3 vectors for log-permeability, 2 constant vectors (see Eq. 4.36a and 4.36b); plus 9 vectors arising from Eq. 4.34, i.e., there are 17 subspace vectors.

Fig. 4.14 (same as Fig. 2.7) presents the maximum a posteriori estimate of the log-permeability field obtained by the conventional method by conditioning to both hard data and pressure data, and Fig. 4.15 shows the corresponding maximum a posteriori estimate obtained by the subspace method. Figs. 4.16 (same as Fig. 2.19) and 4.17 show corresponding results for the thickness averaged permeability. Maximum a posteriori estimates of the porosity field obtained by the conventional method and the subspace method are shown in Figs. 4.18 (same as Fig. 2.8) and 4.19 respectively. Note results obtained from the conventional procedure and the subspace method are in good agreement. However, the final value of the objective function obtained by the subspace method was 6.2 as opposed to 4.5 for the conventional method. The conventional method requires 6 Gauss-Newton iterations to converge while the subspace method requires 8 iterations. The subspace estimate required 9.2 minutes of computer time on a Pentium-133 as opposed to 19.5 minutes for the conventional method.

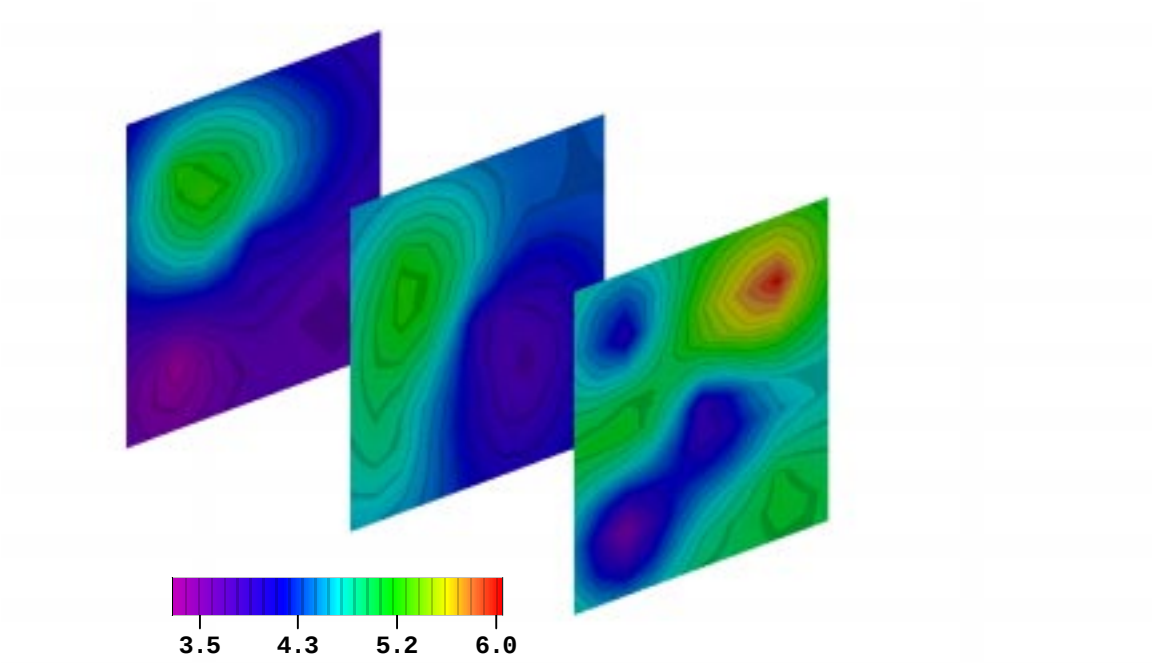

Fig. 4.14 - Max. a posteriori estimate of log-permeability field, conventional method.

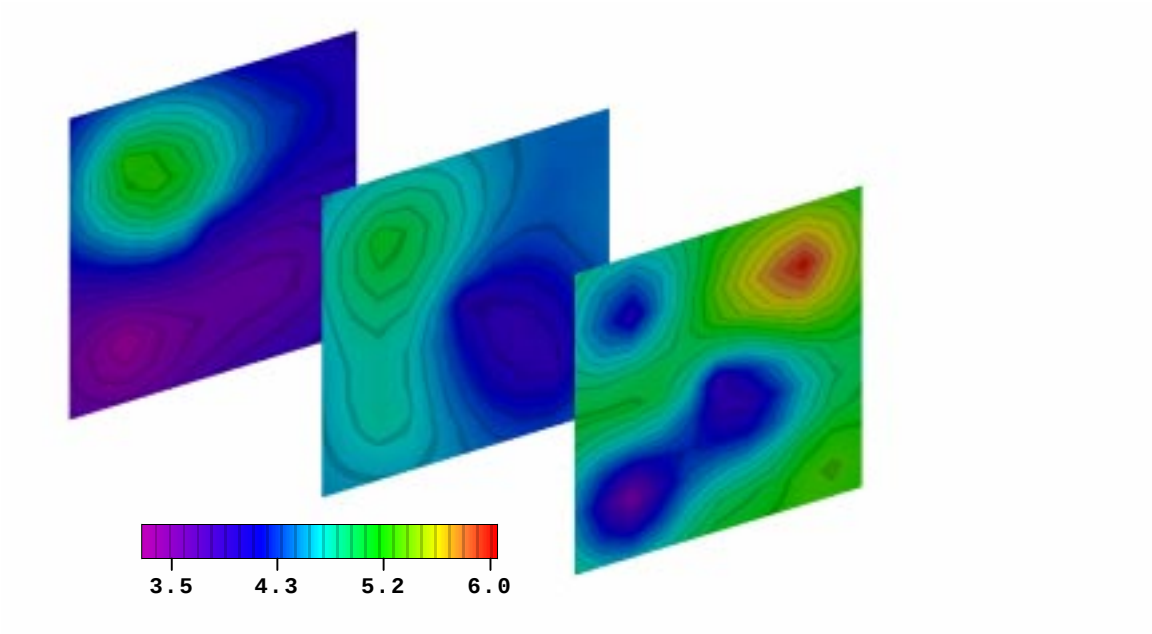

Fig. 4.15 - Max. a posteriori estimate of log-permeability field, subspace method.

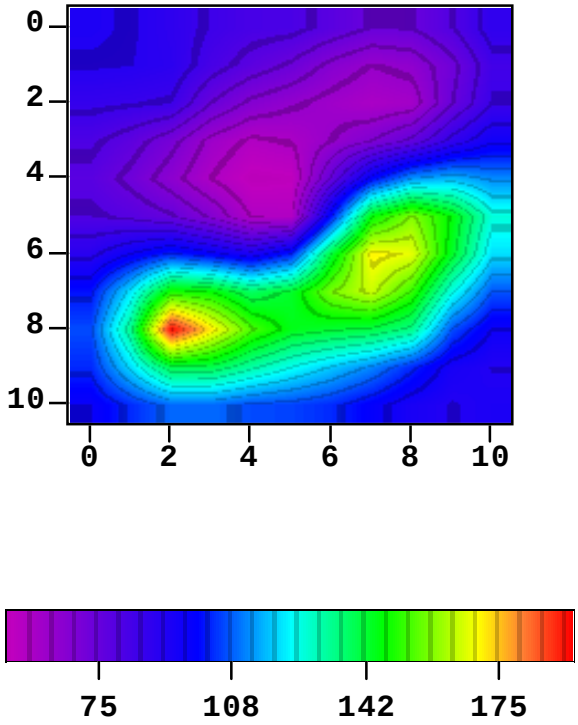

Fig. 4.16 - Thickness averaged permeability field, conventional method.

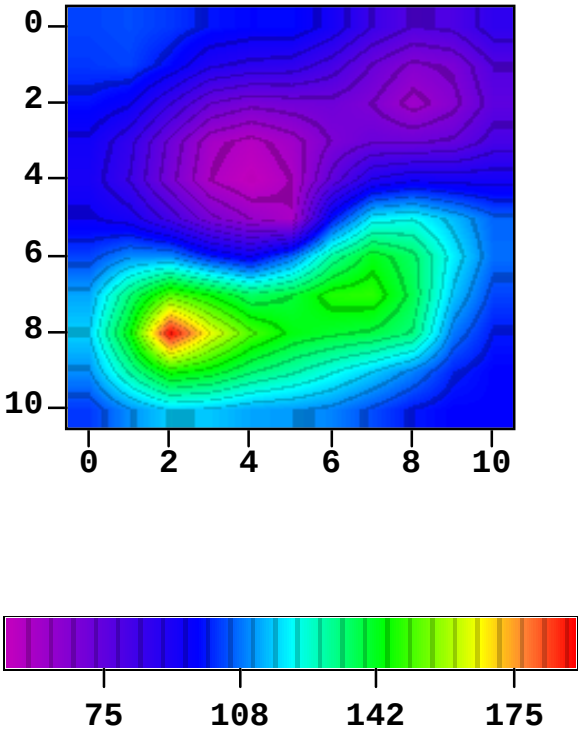

Fig. 4.17 - Thickness averaged permeability field, subspace method.

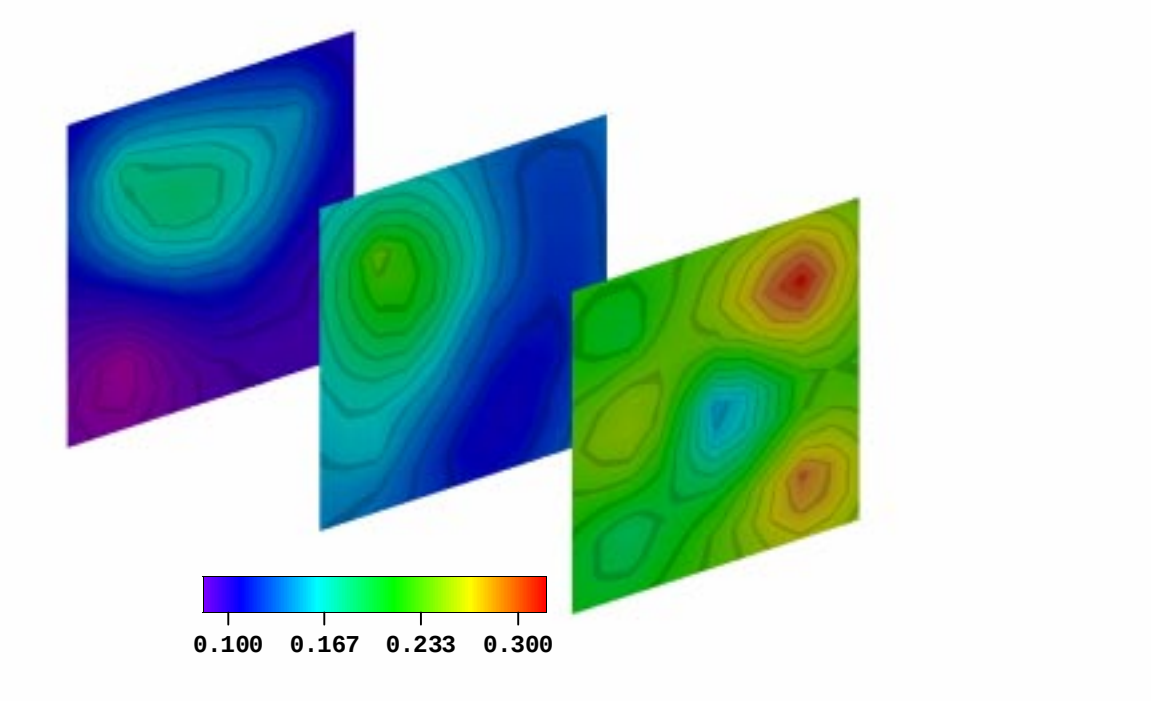

Fig. 4.18 - Max. a posteriori estimation of porosity fields, conventional method

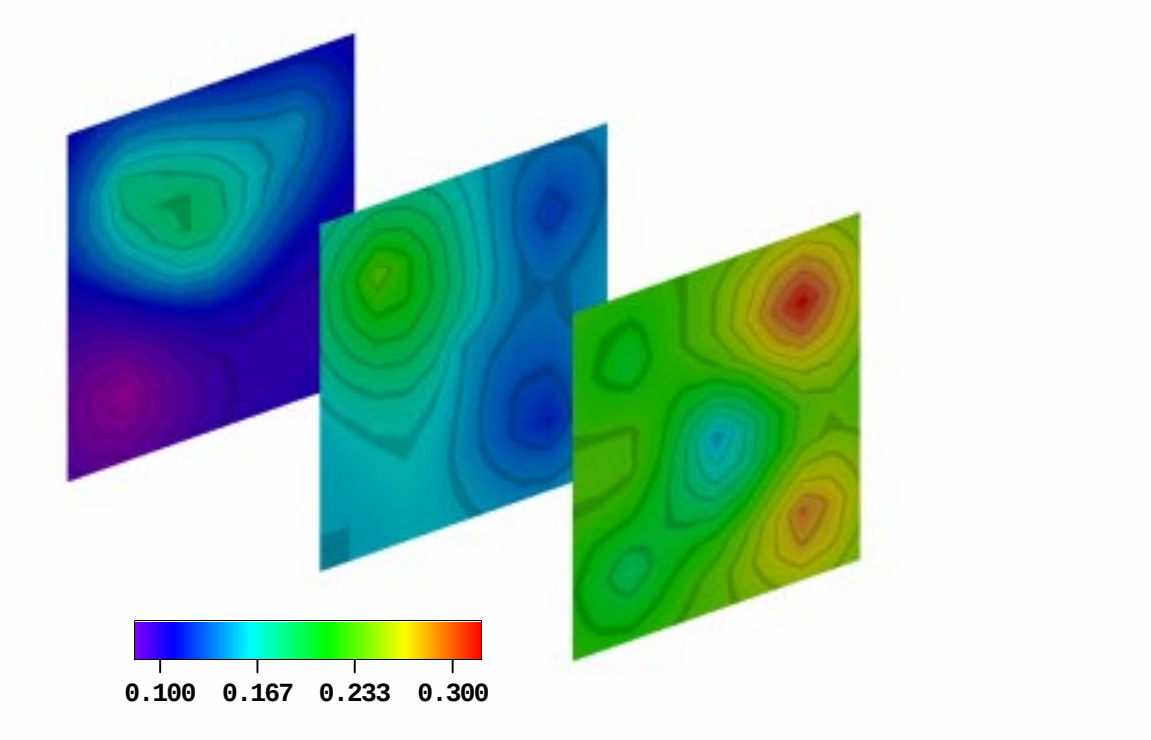

Fig. 4.19 - Max. a posteriori estimation of porosity fields, subspace method.

CHAPTER V

RESERVOIR PERFORMANCE PREDICTION

In previous chapters, we have presented procedures based on inverse problem theory for generating reservoir descriptions (rock property fields) conditioned to pressure data and geostatistical information represented by prior means for log-permeability and porosity and variograms. Although we have shown that the incorporation of pressure data reduces the uncertainty below the level contained in the geostatistical model based only on static information (the prior model), our previous results did not explicitly account for uncertainties in the prior means and the parameters defining the variogram model.

In this chapter, we investigate how pressure data can help detect errors in the prior means. If errors in the prior means are large and are not taken into account, realizations conditioned to pressure data do not properly characterize the uncertainty in the rock property fields, whereas, if the uncertainty in the prior means is incorporated properly into the model, one obtains realistic realizations of the rock property fields.

Our objective is to generate realizations of three-dimensional rock property fields (simulator gridblock values of log-permeability and porosity) conditioned to a prior model and well-test pressure data. The prior model is based on a multivariate Gaussian distribution with known covariance matrix and uncertain prior means. Unlike the past work mentioned in previous chapters, we specifically account for uncertainty in the prior means

by introducing a partially doubly stochastic prior model using basic ideas described in Tjelmeland et al.[38]. Our basic procedure for generating realizations of the rock property fields relies on generating the joint probability density function (pdf) for the rock property fields and the errors in the prior means conditioned to pressure data, and then sampling this pdf to obtain realizations.

An efficient procedure for sampling the pdf is obtained by adapting ideas and techniques presented in Oliver[35] and Oliver et al.[27] to the problem considered here. A procedure for generating the maximum a posteriori estimates of the rock property fields and prior means is also presented. Specific realizations and maximum a posteriori estimates are generated by minimizing an appropriate objective function using the Gauss-Newton method. Sensitivity coefficients are computed using the procedure presented in Chapter III.

It is important to note that our objective in generating realizations of rock property fields is to obtain a set of realizations which represent a correct sampling of the probability density function for the rock property fields. By making a performance prediction with each realization, one can then evaluate the uncertainty in the predicted parameters, e.g., break through time or cumulative oil production. If one simply generates a set of realizations that honor all the data, but the set does not provide a correct sampling of the probability density function, we know of no feasible procedure for evaluating the uncertainty in performance predictions. For simplicity, we give the mathematical details only for the case where the skin factors are known a priori and not estimated. However, in our actual implementation, skin factors can also be estimated.

5.1 Prior and A Posteriori Probability Density Functions

As noted previously, m_{prior} is the vector containing the prior means of the model parameters, i.e., for the case where the permeability field is isotropic and skin factors are known,

$$m_{prior} = \begin{bmatrix} m_{prior,\phi}\, e \\ m_{prior,k}\, e \end{bmatrix}, \tag{5.1}$$

where e is the M-dimensional column vector with all entries equal to unity.

$$e = [1, 1, \ldots, 1]^T. \tag{5.2}$$

Since ln(k) and porosity are modeled as stationary random functions in the prior model, $m_{prior,\phi}$ and $m_{prior,k}$ are treated as scalars, although the general formulation presented allows each entry of m_{prior} to be different.

The random vector Θ represents the error in or correction to m_{prior} with θ denoting specific realizations of Θ. Introduction of Θ allows for the incorporation of uncertainty in the vector of prior means, whereas, in our past work[25-27], we assumed no error in m_{prior}.

The pdf for Θ is assumed to be Gaussian and is given by

$$p_\Theta(\theta) = a \exp\left[-\frac{1}{2}(\theta-\theta_0)^T C_\Theta^{-1}(\theta-\theta_0)\right], \tag{5.3}$$

where θ_0 is the mean or expectation of the random vector Θ and C_Θ is the associated covariance matrix. In this work, we assume that errors in the prior means are independent so C_Θ is a diagonal matrix. Although it is appropriate to choose $\theta_0 = 0$, the derivation is done for any value of θ_0. The conditional distribution (pdf) of M given $\Theta = \theta$ is given by

$$p_{M|\Theta}(m|\theta) = a\exp\left[-\frac{1}{2}(m - m_{prior} - \theta)^T C_M^{-1}(m - m_{prior} - \theta)\right]. \quad (5.4)$$

So the joint pdf for M and Θ is given by

$$p_{\hat{M}}(\hat{m}) = p_{\hat{M}}(m,\theta) = p_{M|\Theta}(m|\theta)p_{\Theta}(\theta)$$
$$= a\exp\left[-\frac{1}{2}(m - m_{prior} - \theta)^T C_M^{-1}(m - m_{prior} - \theta) - \frac{1}{2}(\theta - \theta_0)^T C_{\Theta}^{-1}(\theta - \theta_0)\right], \quad (5.5)$$

where

$$\hat{M} = \begin{bmatrix} M \\ \Theta \end{bmatrix}. \quad (5.6)$$

For simplicity, a realization $\hat{m}$ of $\hat{M}$ is sometimes denoted by (m,θ) instead of $(m^T,\theta^T)^T$. Throughout, the superscript T is used to denote the transpose of a matrix or vector. For convenience, we refer to m_{prior} as the prior mean, however, one should note that Eq. 5.4 indicates that the conditional expectation of M is given by

$$E\left[M|\Theta = \theta\right] = m_{prior} + \theta. \quad (5.7)$$

All measured well-test pressure data that will be used as conditioning data are incorporated in the N_d-dimensional column vector d_{obs}. Note N_d is the total number of observed or measured pressure data used as conditioning data. As is standard, *d* represents the corresponding vector of pressures that will be calculated for a given realization *m* of the rock property fields and the relationship between the data and m is represented by

$$d = g(m). \quad (5.8)$$

Given a specific *m*, Eq. 5.8 represents the operation of calculating wellbore pressures by running the reservoir simulator.

As shown previously, we assume that the random vector ε which represents measurement errors consists of independent identically distributed random variables with zero mean and variance σ_d^2 so that the data covariance matrix C_D is a diagonal matrix with all diagonal entries equal to σ_d^2. Given *m*, the observed pressure data may be regarded as a realization of the random vector $D = g(m) + \varepsilon$. Thus, the a posteriori pdf for $\hat{M}$ conditional to the observed pressure data, d_{obs}, can be derived as in Tjelmeland et al.[32] by a standard applications of Bayes theorem and is given by

$$\pi(m,\theta) = p_{\hat{M}|D}(\hat{m}|d_{obs}) = a\exp\left[-\frac{1}{2}(g(m)-d_{obs})^T C_D^{-1}(g(m)-d_{obs})\right.$$
$$\left.-\frac{1}{2}(m-m_{prior}-\theta)^T C_M^{-1}(m-m_{prior}-\theta)-\frac{1}{2}(\theta-\theta_0)^T C_\Theta^{-1}(\theta-\theta_0)\right], \qquad (5.9)$$

where the first equality of Eq. 5.9 simply defines notation and *a* is a normalizing constant. Eq. 5.9 gives the pdf we wish to sample to generate realizations (m,θ) of $\hat{M}$. To generate the most probable model (maximum a posteriori estimate) for $\hat{M}$, we need to minimize the objective function $O(\hat{m})$ given by

$$O(\hat{m}) = \frac{1}{2}(g(m)-d_{obs})^T C_D^{-1}(g(m)-d_{obs})$$
$$+\frac{1}{2}(m-m_{prior}-\theta)^T C_M^{-1}(m-m_{prior}-\theta)+\frac{1}{2}(\theta-\theta_0)^T C_\Theta^{-1}(\theta-\theta_0). \qquad (5.10)$$

At this point, the dimension of θ is the same as the dimension of m, i.e., N_p.

5.2 Gauss-Newton Method for Partially Doubly Stochastic Model

5.2.1 Iteration Precedure

It is convenient to partition the gradient as

$$\nabla O(\hat{m}) = \begin{bmatrix} \nabla_m O(\hat{m}) \\ \nabla_\theta O(\hat{m}) \end{bmatrix}, \tag{5.11}$$

where ∇_m represents the gradient operator with respect to m and ∇_θ represents the gradient operator with respect to θ. Using basic vector calculus, it follows that

$$\nabla_m O(\hat{m}) = G^T C_D^{-1}(g(m) - d_{obs}) + C_M^{-1}(m - m_{prior} - \theta). \tag{5.12}$$

Similarly,

$$\nabla_\theta O(\hat{m}) = -C_M^{-1}(m - m_{prior} - \theta) + C_\Theta^{-1}(\theta - \theta_0), \tag{5.13}$$

where G^T is the transpose of the $N_d \times N_p$ sensitivity coefficient matrix G which is defined as

$$G = \nabla_m \left[g(m)^T \right]. \tag{5.14}$$

Using Eqs. 5.12 and 5.13 in Eq. 5.11 gives the total gradient of the objective function. Again using basic vector calculus, the Hessian matrix for the Gauss-Newton iteration is given by

$$H = \begin{bmatrix} G^T C_D^{-1} G + C_M^{-1} & -C_M^{-1} \\ -C_M^{-1} & C_M^{-1} + C_\Theta^{-1} \end{bmatrix}. \tag{5.15}$$

The Hessian is guaranteed to be positive semidefinite. It is well known (Fletcher[58]) that if the Hessian is modified, the Gauss-Newton method will still converge to the same maximum a posteriori estimate provided the modified Hessian is positive definite. Thus, in order to obtain a simpler computational scheme, we replace the Hessian H by $\hat{H}$ where

$$\hat{H} = \begin{bmatrix} G^T C_D^{-1} G + C_M^{-1} & O \\ O & C_M^{-1} + C_\Theta^{-1} \end{bmatrix}. \tag{5.16}$$

Since C_D, C_M and C_Θ are all positive definite matrices, it is clear that $\hat{H}$ is positive definite.

When $\hat{H}$ is used as the modified Hessian in the Gauss-Newton iteration procedure, the overall iteration can be decomposed as follows:

$$(G_k^T C_D^{-1} G_k + C_M^{-1}) \delta m^{k+1} = -G_k^T C_D^{-1} (g(m^k) - d_{obs}) - C_M^{-1} (m^k - m_{prior} - \theta^k), \tag{5.17}$$

$$(C_M^{-1} + C_\Theta^{-1}) \delta\theta^{k+1} = C_M^{-1} (m^k - m_{prior} - \theta^k) - C_\Theta^{-1} (\theta^k - \theta_0), \tag{5.18}$$

$$m^{k+1} = m^k + \mu_k \delta m^{k+1}, \tag{5.19}$$

$$\theta^{k+1} = \theta^k + \mu_k \delta\theta^{k+1}, \tag{5.20}$$

where *k* refers to the iteration index and μ_k is the step size determined by the restricted step method (Fletcher[58]). Note in the spirit of the restricted step, it is important to use the same value of μ_k in both Eqs. 5.19 and 5.20, otherwise we effectively change the search direction. Note by replacing H by $\hat{H}$, we avoid inversion of H, i.e., we have decoupled the iteration on the model (*m*) from the iteration on the correction (θ) to the prior mean.

Let *e* represent a column vector of dimension N_e with all components equal to unity, i.e.,

$$e = [1, 1, \ldots, 1]^T, \tag{5.21}$$

Then the prior mean given by Eq. 5.1 can be written as more general form

$$m_{prior} = \begin{bmatrix} m_{prior,1}\, e \\ m_{prior,2}\, e \\ \vdots \\ m_{prior,N_a} e \end{bmatrix}. \tag{5.22}$$

In this case, it is reasonable to require that the correction to the prior mean have the same structure as m_{prior}, i.e., we require that

$$\theta = \begin{bmatrix} \alpha_1 e \\ \alpha_2 e \\ \vdots \\ \alpha_{N_a} e \end{bmatrix} = \begin{bmatrix} \theta_1 e \\ \theta_2 e \\ \vdots \\ \theta_{N_a} e \end{bmatrix}, \tag{5.23}$$

for some constants, $\alpha_j, j = 1,2,...,N_a$. Since m_{prior} and θ are both N_p- dimensional column vectors, $N_a N_e = N_p$. For the case where all attributes are modeled as stationary random functions, N_a is equal to the number of attributes, e.g., $N_a = 2$ if Eq. 5.1 applies. However, if the mean of each attribute varies from gridblock to gridblock, then $N_a = N_p$ (the dimension of the model *m*). In this case, *e* is one dimensional and Eq. 5.23 does not place any restrictions on the components of θ. When Eq. 5.23 applies, C_Θ is defined as a block diagonal matrix with the *j*th diagonal block given by $\sigma^2_{\theta,j} I$ for $j = 1,2,...,N_a$ where I is the $N_e \times N_e$ identity matrix.

The $(N_a N_e) \times N_a = N_p \times N_a$ matrix *E* is defined by

$$E = \begin{bmatrix} e & O & \cdots & O \\ O & e & \cdots & O \\ \vdots & \vdots & \ddots & \vdots \\ O & O & \cdots & e \end{bmatrix}, \tag{5.24}$$

so the transpose of *E* is given by

$$E^T = \begin{bmatrix} e^T & O & \cdots & O \\ O & e^T & \cdots & O \\ \vdots & \vdots & \ddots & \vdots \\ O & O & \cdots & e^T \end{bmatrix}. \tag{5.25}$$

If $N_a = N_p$ ($N_e = 1$), then E is the $N_p \times N_p$ identity matrix. Defining the N_a dimensional column vector α by

$$\alpha = \left[\alpha_1, \alpha_2, ..., \alpha_{N_a}\right]^T \tag{5.26}$$

Eq. 5.23 can be written as $\theta = E\alpha$.

5.2.2 Partial Subspace Procedure

In Chapter IV, we showed that using subspace methods can significantly enhance the computational efficiency of the Gauss-Newton method. Here, we consider only a partial subspace procedure where $\delta\theta^{l+1}$ in Eq. 5.18 is expanded as

$$\delta\theta^{k+1} = E\delta\alpha^{k+1}, \tag{5.27}$$

at all Gauss-Newton iterations. Using Eq. 5.27 in Eq. 5.18 and multiplying the resulting equation by $E^T C_M$ gives

$$E^T(I + C_M C_\Theta^{-1})E\delta\alpha^{k+1} = E^T(m^k - m_{prior} - \theta^k) - E^T C_M C_\Theta^{-1}(\theta^k - \theta_0). \tag{5.28}$$

Eq. 5.27 indicates that $\delta\theta^{l+1}$ is a linear combination of the columns of *E*, i.e., the columns of *E* represent the associated subspace vectors. If the initial guess for θ, $\theta^0 = \theta_0$, is also a linear combination of these subspace vectors, then by mathematical induction, it follows that for all *l*, θ^l is a linear combination of these subspace vectors.

This result is apparent because if θ^l is a linear combination of these subspace vectors, i.e., $\theta^l = E\alpha^l$, it follows from Eqs. 5.20 and 5.27 that

$$\theta^{l+1} = E\alpha^l + \mu_l E\delta\alpha^{l+1} = E(\alpha^l + \mu_l \delta\alpha^{l+1}). \tag{5.29}$$

It now follows that when Eq. 5.18 is replaced by Eq. 5.28, Eq. 5.20 can be replaced by

$$\alpha^{l+1} = \alpha^l + \mu_l \delta\alpha^{l+1}, \tag{5.30}$$

and

$$\theta^{k+1} = E\theta^{k+1}. \tag{5.31}$$

With this modification, the overall computational scheme for estimating the maximum a posteriori estimate (Eqs. 5.17 through 5.20) can now be written as

$$\delta m^{l+1} = m_{prior} + \theta^l - m^l - C_M G_l^T (C_D + G_l C_M G_l^T)^{-1} \times \left[g(m^l) - d_{obs} - G_k (m^l - m_{prior} - \theta^l) \right], \tag{5.32}$$

$$E^T (I + C_M C_\Theta^{-1}) E\delta\alpha^{l+1} = E^T (m^l - m_{prior} - \theta^l) - E^T C_M C_\Theta^{-1} (\theta^l - \theta_0). \tag{5.33}$$

$$m^{l+1} = m^l + \mu_l \delta m^{l+1}, \tag{5.34}$$

and Eqs. 5.30 and 5.31. Eq. 5.32 was obtained from Eq. 5.17 by using basic matrix inversion lemmas (see Eqs. 2.18 and 2.19). The preceding subspace implementation of the Gauss-Newton iteration will converge to the so-called maximum a posteriori estimate $(m_\infty, \theta_\infty)$, which is commonly referred to as the most probable model. However, as noted previously, our objective is not to simply generate the most probable estimate of $\hat{m}$, but to

generate a suite of realizations which represent a correct sampling of the pdf of Eq. 5.9. The sampling procedure we used is presented in the following section.

5.3 SAMPLING THE A POSTERIORI DISTRIBUTION

Markov chain Monte Carlo (MCMC) methods provide theoretical techniques which are guaranteed to produce a correct sampling of a given pdf if a sufficiently large number of states are generated. However, current implementations (Oliver et al.[35], Cunha[33] and Cunha et al.[34]) are too computationally intensive for practical applications when the goal is to generate realizations conditioned to production data and the generation of each state in the Markov chain requires a run of a reservoir simulator. Procedures based on approximating the a posteriori pdf by a Gaussian centered at the maximum a posteriori estimate require computing either the Cholesky decomposition or the square root of the a posteriori covariance matrix and do not always generate a correct sampling of the pdf (Oliver et al.[35], Cunha[33] and Cunha et al.[34]). Thus, we pursue a computationally efficient alternative. For the case where uncertainty in the prior mean is ignored, the basic procedure has been discussed by Oliver et al.[27] and relies on underlying theory developed by Oliver[36]. The basic procedure is technically correct only for the case where the data are linearly related to the model, however, Oliver et al.[27] have presented arguments which suggest that the procedure should give an approximately correct sampling in the nonlinear case.

5.3.1 Linear Case

Here, we extend the results of Oliver[36] and Oliver et al.[27] to the case where we incorporate uncertainty in the prior mean. We consider the case where the data are linearly related to the model, so Eq. 5.8 can be written as

$$d = Gm, \tag{5.35}$$

where G is an $N_d \times N_p$ matrix. For this case, the maximum a posteriori estimate can be obtained by solving the following two equations: $\nabla_\theta O(\hat{m}) = 0$ and $\nabla_m O(\hat{m}) = 0$ (see Eqs. 5.12 and 5.13) to obtain m_∞ and θ_∞. It is easy to show that this solution satisfies

$$\begin{bmatrix} G^T C_D^{-1} G + C_M^{-1} & -C_M^{-1} \\ -C_M^{-1} & C_M^{-1} + C_\theta^{-1} \end{bmatrix} \begin{bmatrix} m_\infty \\ \theta_\infty \end{bmatrix} = \begin{bmatrix} C_M^{-1} m_{prior} + G^T C_D^{-1} d_{obs} \\ -C_M^{-1} m_{prior} + C_\Theta^{-1} \theta_0 \end{bmatrix}. \tag{5.36}$$

Note that the coefficient matrix on the left side of Eq. 5.36 is the Hessian matrix defined in Eq. 5.15. Moreover, when Eq. 5.35 applies it is easy to show that the a posteriori pdf for $\hat{M}$ (Eq. 5.9) is Gaussian with covariance matrix given by H^{-1} and expectation given by $(m_\infty, \theta_\infty)$ (Tarantola[14]).

Next, we present a procedure for sampling $\pi(m,\theta)$ which does not require the generation of the Cholesky or square root decomposition of H^{-1}. To construct a realization, we generate an unconditional simulation of m, which is denoted by m_{uc} and is given by

$$m_{uc} = m_{obs} + C_M^{1/2} Z, \tag{5.37}$$

where the components of the N_p-dimensional column vector Z are independent standard random normal deviates. Similarly, unconditional simulations of the data and the correction to the prior mean, respectively, are generated by

$$d_{uc} = d_{obs} + C_D^{1/2} Z_D, \tag{5.38}$$

and

$$\theta_{uc} = \theta_0 + C_\Theta^{1/2} Z_\Theta \,, \tag{5.39}$$

where again the components of Z_D and Z_θ are independent standard random normal deviates. The 1/2 superscript on the matrices in the preceding three equations represent the square root of the matrix, but the square roots could also be replaced by the lower triangular matrix arising from the LL^T decomposition of the matrix. However, C_D and C_θ are diagonal matrices, thus, it is trivial to compute their square root. Because we wish to avoid explicit factorization of C_M or the generation of its square root, in our computer implementation, we actually use sequential Gaussian cosimulation (e.g., Gomez-Hernandez and Journel[37]) in place of Eq. 5.38 to generate m_{uc}. If we replace, m_{prior} by m_{uc}, d_{obs} by d_{uc} and θ_0 by θ_{uc} in Eqs. 5.12 and 5.13, set both equations to zero and solve to obtain the solution denoted by (m_s, θ_s), then similar to Eq. 5.36, we find that

$$\begin{bmatrix} G^T C_D^{-1} G + C_M^{-1} & -C_M^{-1} \\ -C_M^{-1} & C_M^{-1} + C_\theta^{-1} \end{bmatrix} \begin{bmatrix} m_s \\ \theta_s \end{bmatrix} = \tag{5.40}$$

$$\begin{bmatrix} C_M^{-1}(m_{prior} + C_M^{1/2} Z) + G^T C_D^{-1}(d_{obs} + C_D^{1/2} Z_D) \\ -C_M^{-1}(m_{prior} + C_M^{1/2} Z) + C_\theta^{-1}(\theta_0 + C_\theta^{1/2} Z_\theta) \end{bmatrix}.$$

Subtracting Eq. 5.36 from 5.40, we see that the conditional simulations, m_s and θ_s satisfy

$$\begin{bmatrix} G^T C_D^{-1} G + C_M^{-1} & -C_M^{-1} \\ -C_M^{-1} & C_M^{-1} + C_\theta^{-1} \end{bmatrix} \begin{bmatrix} m_s - m_\infty \\ \theta_s - \theta_\infty \end{bmatrix} = \tag{5.41}$$

$$\begin{bmatrix} C_M^{-1} C_M^{1/2} Z + G^T C_D^{-1} C_D^{1/2} Z_D \\ -C_M^{-1} C_M^{1/2} Z + C_\theta^{-1} C_\theta^{1/2} Z_\theta \end{bmatrix} = B,$$

where the last equality of Eq. 5.41 serves to define *B*. The random vector $\hat{M}_s$ is defined by

$$\hat{M}_s = \left[m_s^T, \quad \theta_s^T \right]^T . \tag{5.42}$$

Since the expected values of Z, Z_D and Z_θ are all zero, it is clear that the expected values of $\hat{M}_s$ is given by

$$E(\hat{M}_s) = \begin{bmatrix} m_\infty \\ \theta_\infty \end{bmatrix}, \tag{5.43}$$

i.e., $E(m_s) = m_\infty$ and $E(\theta_s) = \theta_\infty$. The covariance of the random vector, $\hat{M}_s$, is given by

$$E\left[\left(\hat{M}_s - E\left[\hat{M}_s\right] \right) \left(\hat{M}_s - E\left[\hat{M}_s\right] \right)^T \right] = H^{-1} E\left[BB^T \right] H^{-1}, \tag{5.44}$$

where B is defined by the last equality of Eq. 5.41. Thus,

$$\begin{aligned} E\left[BB^T\right] = & \\ & E\left[\begin{bmatrix} C_M^{-1} C_M^{1/2} Z + G^T C_D^{-1} C_D^{1/2} Z_D \\ -C_M^{-1} C_M^{1/2} Z + C_\theta^{-1} C_\theta^{1/2} Z_\theta \end{bmatrix} \times \right. \\ & \left. \left[\left(C_M^{-1} C_M^{1/2} Z + G^T C_D^{-1} C_D^{1/2} Z_D \right)^T \quad \left(-C_M^{-1} C_M^{1/2} Z + C_\theta^{-1} C_\theta^{1/2} Z_\theta \right)^T \right] \right] \\ = & E\left[\begin{matrix} \left(C_M^{-1} C_M^{1/2} Z + G^T C_D^{-1} C_D^{1/2} Z_D \right)\left(C_M^{-1} C_M^{1/2} Z + G^T C_D^{-1} C_D^{1/2} Z_D \right)^T \\ \left(-C_M^{-1} C_M^{1/2} Z + C_\theta^{-1} C_\theta^{1/2} Z_\theta \right)\left(C_M^{-1} C_M^{1/2} Z + G^T C_D^{-1} C_D^{1/2} Z_D \right)^T \end{matrix} \right. \\ & \qquad \left. \begin{matrix} \left(C_M^{-1} C_M^{1/2} Z + G^T C_D^{-1} C_D^{1/2} Z_D \right)\left(C_M^{-1} C_M^{1/2} Z + G^T C_D^{-1} C_D^{1/2} Z_D \right)^T \\ \left(C_M^{-1} C_M^{1/2} Z + G^T C_D^{-1} C_D^{1/2} Z_D \right)\left(C_M^{-1} C_M^{1/2} Z + G^T C_D^{-1} C_D^{1/2} Z_D \right)^T \end{matrix} \right]. \end{aligned} \tag{5.45}$$

Using the fact that Z, Z_D and Z_θ are independent vectors, with components of each vector representing independent standard random normal deviates, Eq. 5.45 can be reduced to

$$E\left[BB^T\right]=\begin{bmatrix} G^T C_D^{-1} G + C_M^{-1} & -C_M^{-1} \\ -C_M^{-1} & C_M^{-1} + C_\Theta^{-1} \end{bmatrix} = H\,. \tag{5.46}$$

Using Eq. 5.46 in Eq. 5.44 , we obtain

$$E\left[\left(\hat{M}_s - E\left[\hat{M}_s\right]\right)\left(\hat{M}_s - E\left[\hat{M}_s\right]\right)^T\right] = H^{-1}\,. \tag{5.47}$$

Thus, we have shown that the covariance and expectations of $\hat{M}$ and $\hat{M}_s$ are the same. Since both random vectors satisfy Gaussian distributions when Eq. 5.35 applies, we can generate a sampling of $\hat{M}$ by sampling the distribution for $\hat{M}_s$. Samples of $\hat{M}_s$ can be generating by solving Eq. 5.40 for m_s and θ_s for a set of independent unconditional simulations, m_{uc}, d_{uc} and θ_{uc}.

5.3.2 Nonlinear Case

For the nonlinear case of interest, the same type of procedure is applied except we restrict θ by introducing a subspace method, i.e., samples are generated by the computational algorithm of Eqs. 5.32, 5.33, 5.34, 5.30 and 5.31 with m_{prior} replaced by m_{uc}, d_{obs} replaced by d_{uc} and θ_0 replaced by θ_{uc}. Note this simulation procedure represents automatic history matching of the perturbed pressure data , d_{uc}, with prior information used as a regularization term.

In this process, θ_{uc} must be generated so it lies in the appropriate subspace. To do this, recall that C_Θ is a block diagonal matrix where the jth diagonal block is given by $\sigma_{\theta,j}^2 I$ and introduce the associated covariance matrix C_α, which is related to C_Θ by

$$C_\alpha^{-1} = E^T C_\Theta^{-1} E\ . \tag{5.48}$$

C_α is an $N_a \times N_a$ diagonal matrix with *j*th diagonal entry denoted by $\sigma^2_{\alpha,j}$. We compute

$$\alpha_{uc} = \alpha_0 + C_\alpha^{1/2} Z_\alpha , \tag{5.49}$$

where the components of the N_a dimensional column vector are independent standard random normal deviates and set

$$\theta_{uc} = E\alpha_{uc} . \tag{5.50}$$

5.4 COMPUTATIONAL EXAMPLE

5.4.1 Synthetic 3D Case

The example considered pertains to a reservoir containing nine completely-penetrating wells. A simulation grid with 25 gridblocks in the x and y directions and 10 gridblocks in the z direction is used, i.e., 6,250 gridblocks are used. Since we wish to generate realizations of the log-permeability and porosity fields, there are 12,500 model parameters. The areal grid is 400 ft by 400 ft and all gridblocks in the z directions have thickness (height) 10 feet. Fig. 5.1 shows the areal grid and well locations.

The reservoir is areally isotropic $k_x = k_y = k$ and we require that $k_z = k$. Thus, determination of a distribution for *k* automatically determines the vertical permeability at each gridblock. An anisotropic spherical variogram for $\ln(k)$ is used with the range in the x-direction equal to 3,200 ft, the range in the y-direction equal to 1,600 ft and the range in the z-direction equal to 30 feet. The variance of $\ln(k)$ (sill of the variogram) is specified as $\sigma_k^2 = 0.5$. The anisotropic variogram for porosity is identical to the one for ln(k) except the variance for porosity is specified as $\sigma_\phi^2 = 0.002$. The correlation coefficient between log-permeability and porosity is specified as $\rho_{k,\phi} = 0.7$.

The true log-permeability is shown in Fig. 5.2. This truth case was obtained by unconditional simulation (Eq. 5.38) using $m_{prior,k} = 4.0$ and $m_{prior,\phi} = 0.20$. This unconditional simulation also yields the true porosity field. For convenience, we refer to $m_{prior,k} = 4.0$ and $m_{prior,\phi} = 0.20$ as the true prior means.

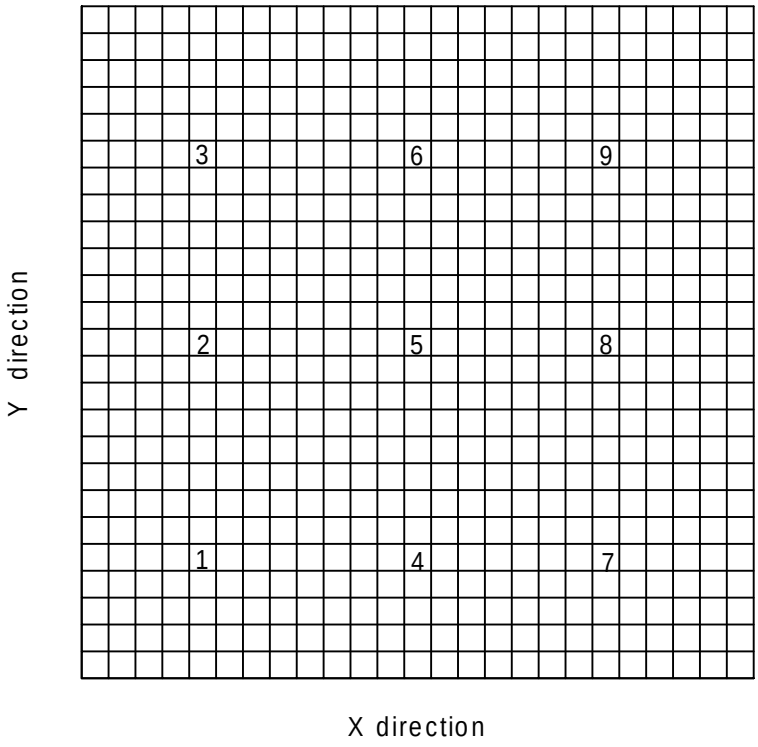

Fig. 5.1 - Areal grid, well locations and well numbers.

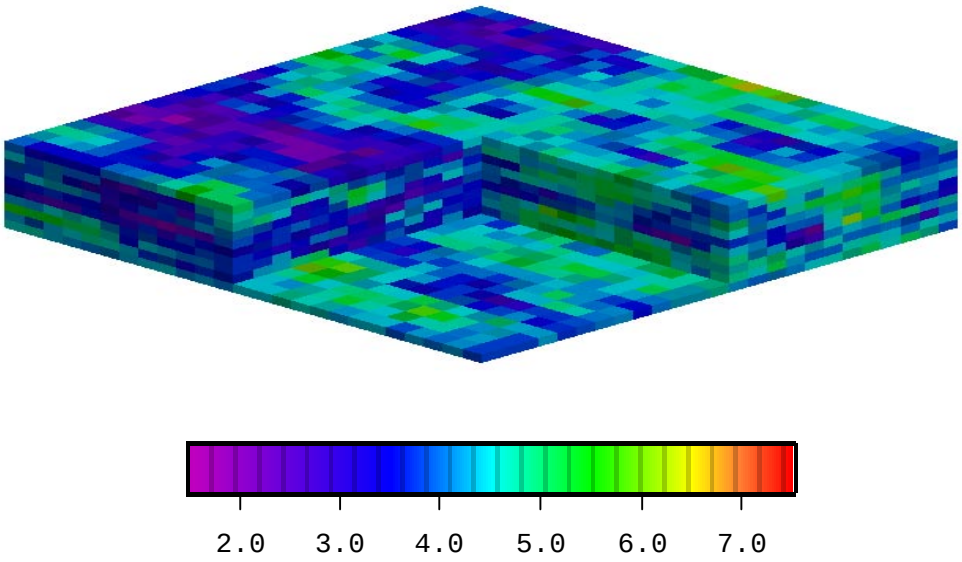

Fig. 5.2 - True log-permeability field.

Other relevant reservoir and fluid properties are as follows: system compressibility, $c_t = 10^{-5}$ psi, fluid viscosity, μ=0.8 cp; all wellbore radii, $r_w = 0.30$ ft; and initial pressure, $p_i = 3{,}230$ psi. The prior mean for skin factors is equal to 5, and the prior variance of skin factors is equal to 1.0. We set a small variance (1.0) on all skin factors because wellbore pressure does not contain sufficient information to correctly estimate the individual "layer" skin factors. Synthetic well-test pressure data were generated by running the simulator using the true permeability, true porosity fields and well skin factors. All nine wells are open to flow simultaneously with the flow rates equal to 700, 820, 450, 630, 430, 740, 590, 780, 910 STB from well one to well nine. Well-test pressure data were collected at wells 2, 4, 5, 6 and 8 (see Fig. 5.1) during a period when the other four wells were produced at a specified rate. At the center well (well 5), a two-day drawdown followed by a one-day buildup test was run. At the other four tested wells (wells 2, 4, 6 and 8) pressure data were measured during three day drawdown tests. These synthetic pressure data are referred to as measured pressure data from this point onward.

In the following, we apply our procedures for sampling the a posteriori pdf (Eq. 5.9). We consider a case where we use $m_{prior,k} = 5.0$ and $m_{prior,\phi} = 0.25$ (referred to as the incorrect prior means) with and without allowing for uncertainty (errors) in the prior means.

Fig. 5.3 shows an unconditional simulation of the log-permeability field generated from Gaussian cosimulation using the true prior mean. Fig. 5.4 shows an unconditional simulation of the log-permeability obtained from Gaussian cosimulation using the incorrect prior means. As expected the gridblock values of log-permeability tend to be much higher

when the incorrect mean is used; compare Figs. 5.3 and 5.4. Similar results were obtained for the porosity field since the incorrect mean for porosity is higher than its true mean.

Fig. 5.5 shows a conditional simulation of the log-permeability field obtained by applying the method of Oliver et al.[26] using true prior means for $\ln(k)$ and porosity. This is equivalent to our basic procedure with θ set equal to zero at all iterations, i.e., we do not incorporate uncertainty in the prior mean. Fig. 5.6 shows a conditional simulation obtained by the same procedure except in this case, the incorrect prior means were used. Note that the log-permeability values obtained in Fig. 5.6 tend to be much higher than those obtained in Fig. 5.5. This is the expected result because the incorrect prior means are much higher than the true values, but we did not apply our procedure to correct the prior means. We can see that the log-permeability field has been reduced significantly at locations near wells 2, 4, 5, 6 and 8, where the property fields have been conditioned to their pressure. At other locations, the log-permeability field has not been changed.

Fig. 5.7 shows a conditional realization obtained by our basic procedure. In this case, we used the incorrect prior means, but accounted for uncertainty in the prior means, where the 2×2 diagonal covariance matrix C_α (see Eq. 5.47) has as its two entries $\sigma^2_{\alpha,1} = 0.001$ and $\sigma^2_{\alpha,1} = 0.2$. Note the realization in Fig. 5.7 is almost identical to the one of Fig. 5.5 which was generated with the true prior means by assuming no errors in the prior means. Although they are not presented here, similar results were obtained for the porosity field.

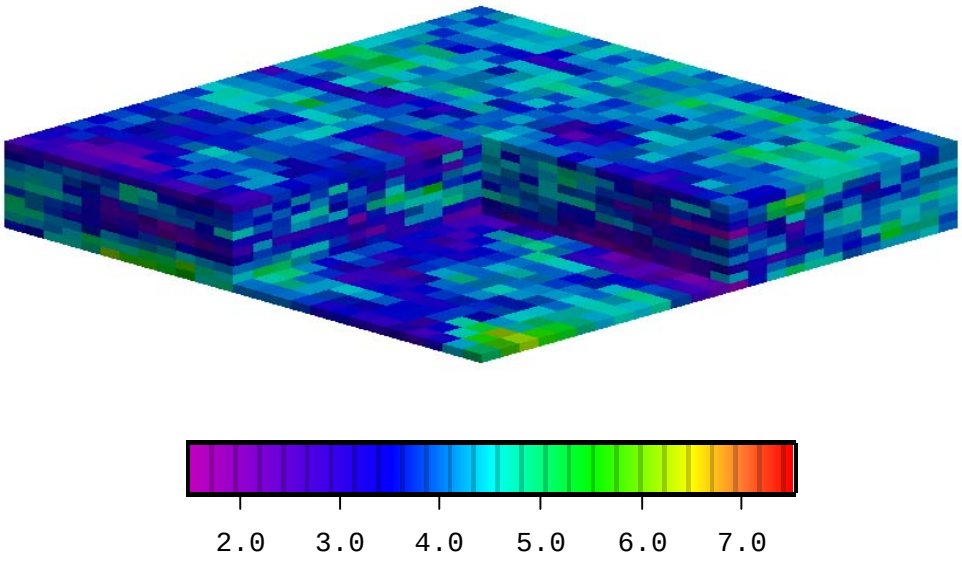

Fig. 5.3 - Unconditional realization of log-permeability field with true prior means.

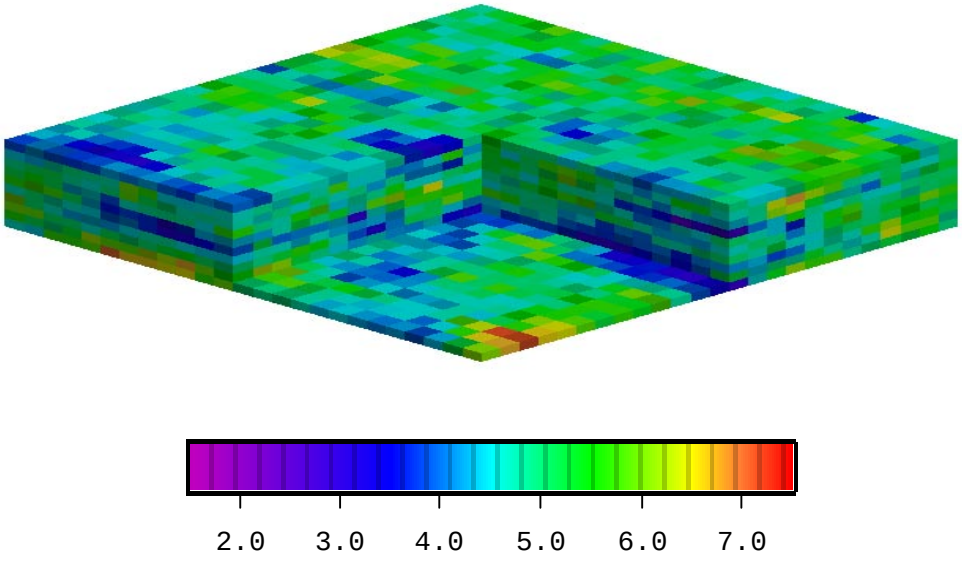

Fig. 5.4 - Unconditional realization of log-permeability field with incorrect prior means.

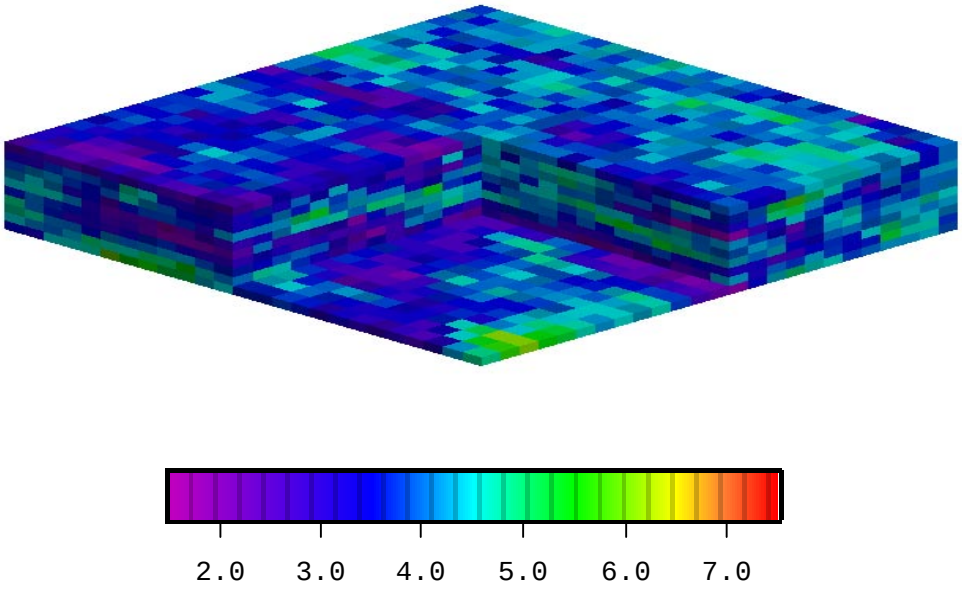

Fig. 5.5 - Realization of log-permeability field conditioned to pressure data using true prior means.

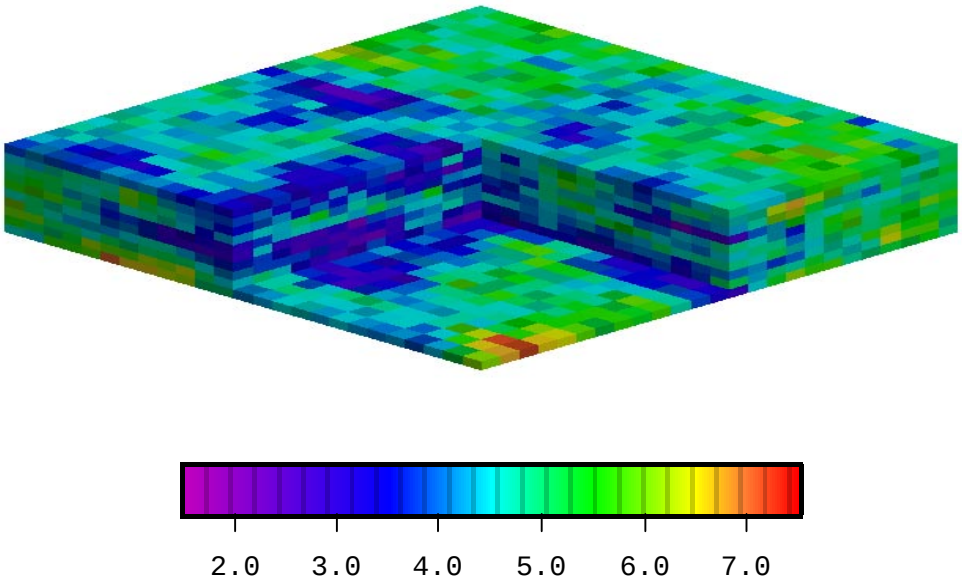

Fig. 5.6 - Realization of log-permeability field conditioned to pressure data using incorrect prior means without correction to prior means.

The results of Figs. 5.5 through 5.7 and the corresponding results for porosity (not shown) illustrate that our procedure for accounting for uncertainty in the prior means is viable and yields reasonable realizations of the rock property fields. The values of θ_s obtained by our basic procedure, which gave the results of Fig. 5.7, indicate that the correction to the prior mean for $\ln(k)$ was -1.041 and the correction to the prior mean for porosity was -0.047. Note these values are very close to the true error in the incorrect prior means.

The permeability values corresponding to the results of Fig. 5.7 and associated porosity values were input to the simulator to predict pressure data at the five wells tested. Fig. 5.8 shows that the pressure data predicted at well 5 from this realization are in good agreement with the measured pressure data. Equally good agreement was obtained at the other tested wells. The dashed curve in Fig. 5.8 represents the pressure data predicted using the corresponding unconditional simulation, m_{uc}, as input to the reservoir simulator. As this m_{uc} was used as the initial guess in the Gauss-Newton method when constructing the conditional simulation by our basic simulation method, the results of Fig. 5.8 give a qualitative measure of how the incorporation of pressure data changes estimates of rock property fields obtained solely from the prior model.

We also generated 50 conditional simulations of the rock property fields using our basic simulation procedure. As discussed previously, this suite of realizations of the rock property fields represents an approximate sampling of the a posteriori pdf of Eq. 5.9. For each realization, we simulated reservoir performance for 1,000 days where all nine wells were produced at a constant bottom-hole pressure of 1500 psi. Reservoir performance

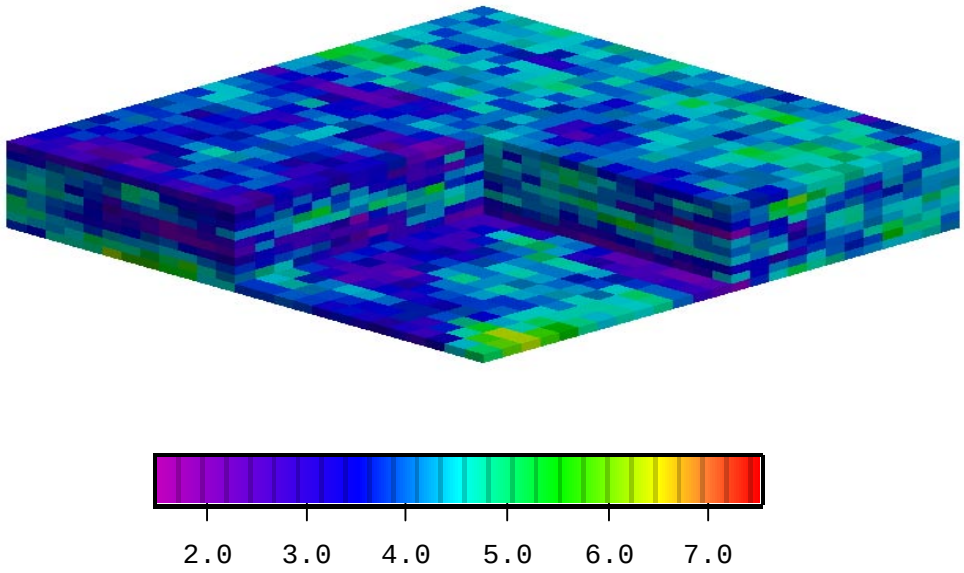

Fig. 5.7 - Realization of log-permeability field conditioned to pressure data with correction to incorrect prior means.

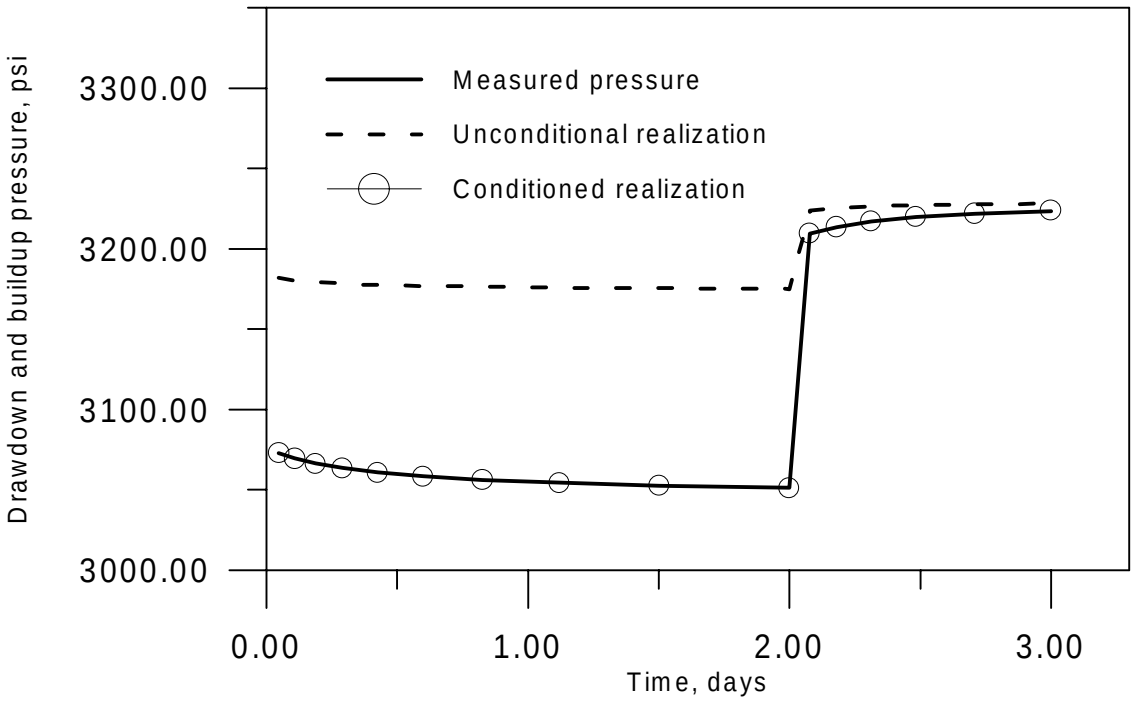

Fig. 5.8 - Pressure data predicted at well 5 from conditional and unconditional simulations of rock property fields compared to measured pressure data.

was also predicted from the set of 50 realizations of *m* generated by sampling the prior pdf for m and θ, Eq. 5.5, using Gaussian cosimulation. Fig. 5.9 represent the predictions of cumulative oil production obtained from this set of 50 realizations. The curve through the solid dots represents the field cumulative oil production generated using the true permeability and porosity fields as simulator input. Note these realizations predict erroneously high values of cumulative oil production since the incorrect prior means are much higher than the true prior means. Since the predictions vary over wide range, there is a large uncertainty in performance predictions. Fig. 5.10 represent the field cumulative oil production predicted from the 50 history-matched realizations. Comparing Fig. 5.10 with Fig. 5.9, we see that the predictions from history matched realizations are much closer to the true case, and the variability in predictions from history matched realizations is much smaller than that from the unconditional realizations.

A histogram of the cumulative oil production at 1,000 days and associated cumulative distribution function are shown in Fig. 5.11. The expected value (mean) is 5.70×10^6 STB, the median is 5.74×10^6 STB, and the standard deviation is 1.68×10^5 STB. Note the bar in the histogram over 5.80×10^6 represents the number of outcomes (15) between 5.70×10^6 STB and 5.80×10^6 STB. The cumulative oil production at 1,000 days predicted using the true rock property fields was 5.68×10^6 STB.

Fig. 5.12 represent the cumulative oil production of well 2 predicted from the 50 history-matched realizations. Note that the line with solid dots represents the cumulative oil production of true case. A histogram of the cumulative oil production at 1,000 days

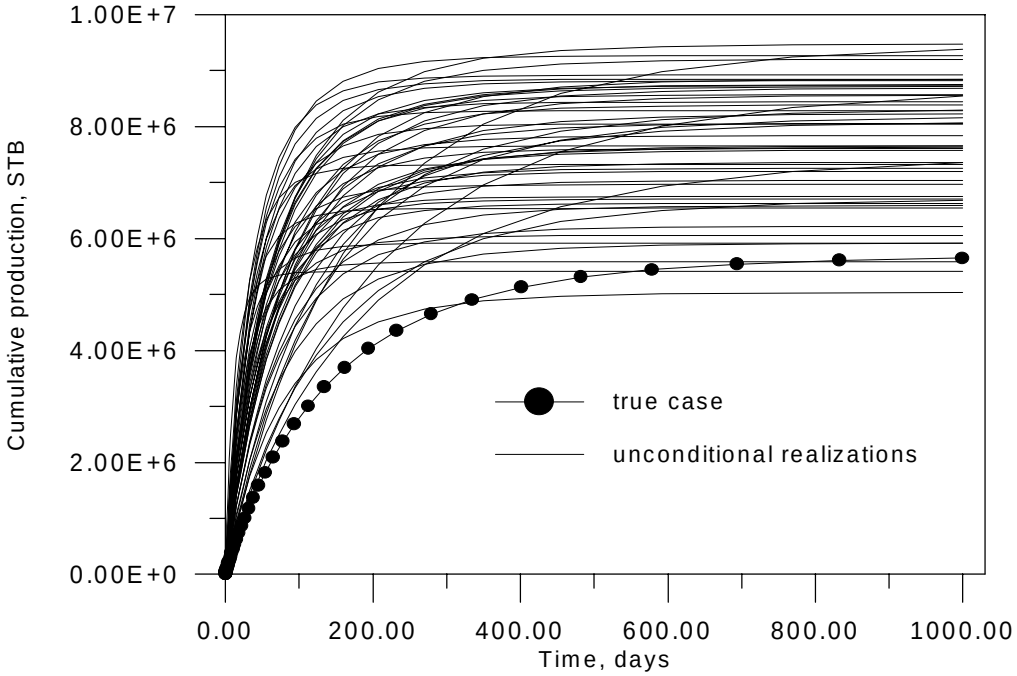

Fig. 5.9 - Reservoir performance predicted from the true case and a suite of unconditional realizations with incorrect prior means.

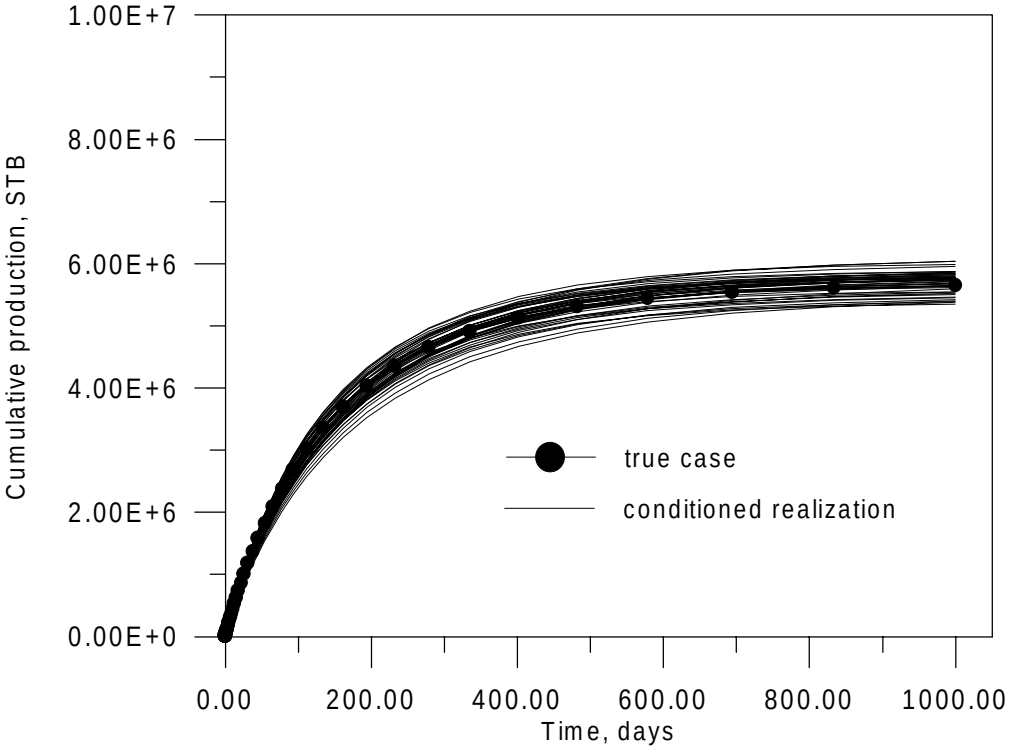

Fig. 5.10 - Reservoir performance predicted from the true case and a suite of realizations conditioned to pressure data with correction of prior means.

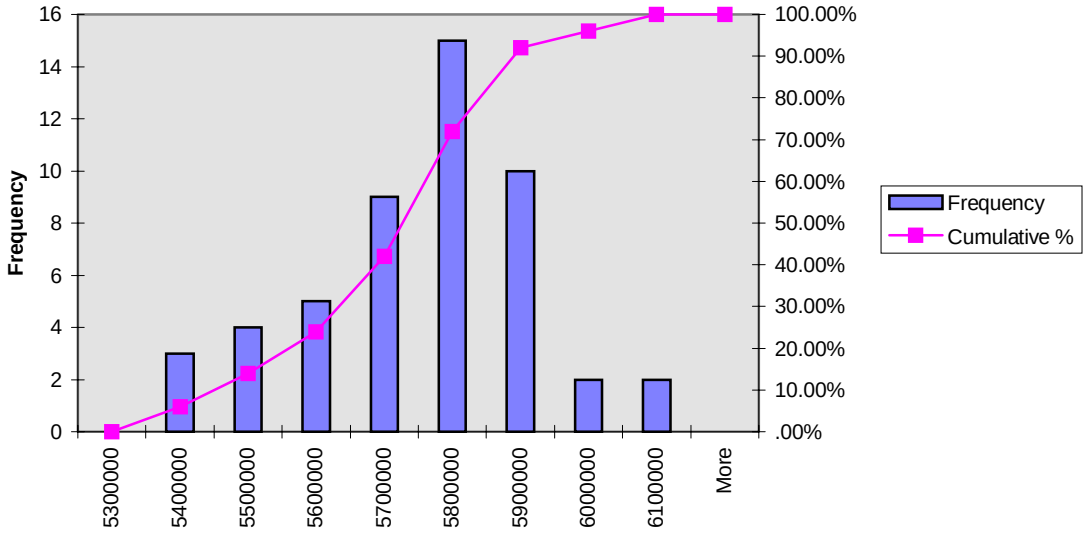

Fig 5.11 - Histogram and cumulative distribution of cumulative oil production at 1,000 days.

and associated cumulative distribution function are shown in Fig. 5.13. The cumulative oil production and the histogram of the cumulative oil production of well 3 from the 50 history-matched realizations are shown in Figs. 5.14 and 5.15. Note that well 2 has been tested and the realizations are conditioned to the pressure data obtained at well 2, while well 3 has not been tested.

For well 2, the expected value (mean) of cumulative oil production at 1,000 days is 5.03×10^5 STB, the median is 5.02×10^5 STB, the standard deviation is 0.78×10^4 STB, and predicted value using the true rock property fields is 5.30×10^5 STB. For well 3, the expected value (mean) of cumulative oil production at 1,000 days is 6.64×10^5 STB, the median is 6.52×10^5 STB, and the standard deviation is 1.95×10^4 STB. The predicted value using the true rock property fields is 7.57×10^5 STB. From these statistical data and also from the comparison between Fig. 5.12 and 5.14, we see that the variance on predicted cumulative oil production in well 2 is smaller that that of well 3. This simply means that after conditioning to well-test pressure, the uncertainty on properties field near the well has been reduced, therefore the performance prediction for well 2 will have less variability than for well 3.

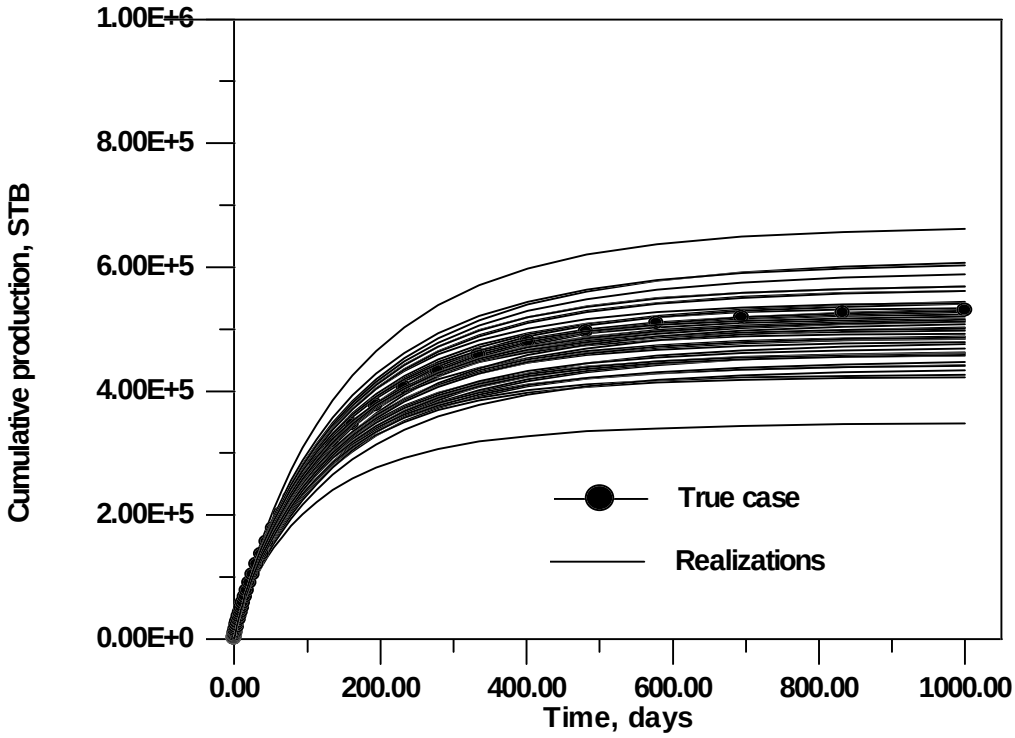

Fig. 5.12 - Well 2 production performance predicted from a suite of conditioned simulations.

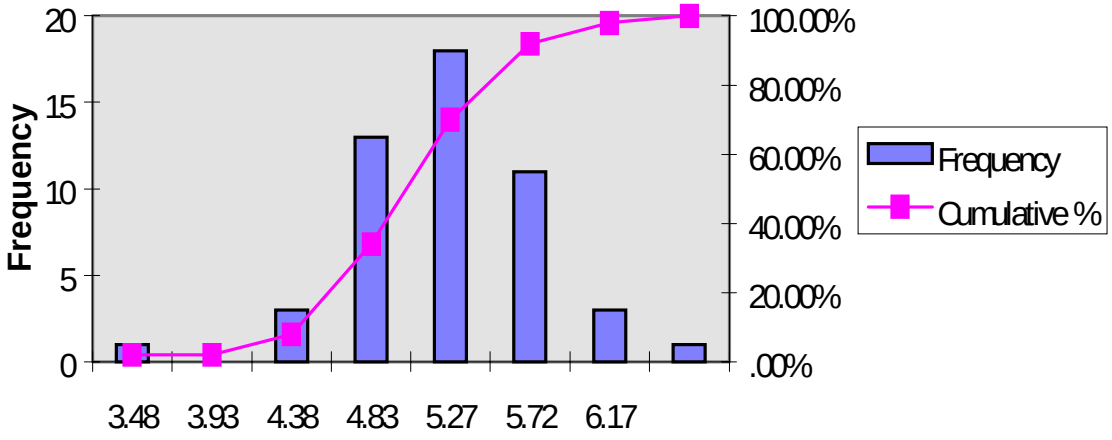

Fig 5.13 - Histogram and cumulative distribution of cumulative oil production from well 2 at 1,000 days.

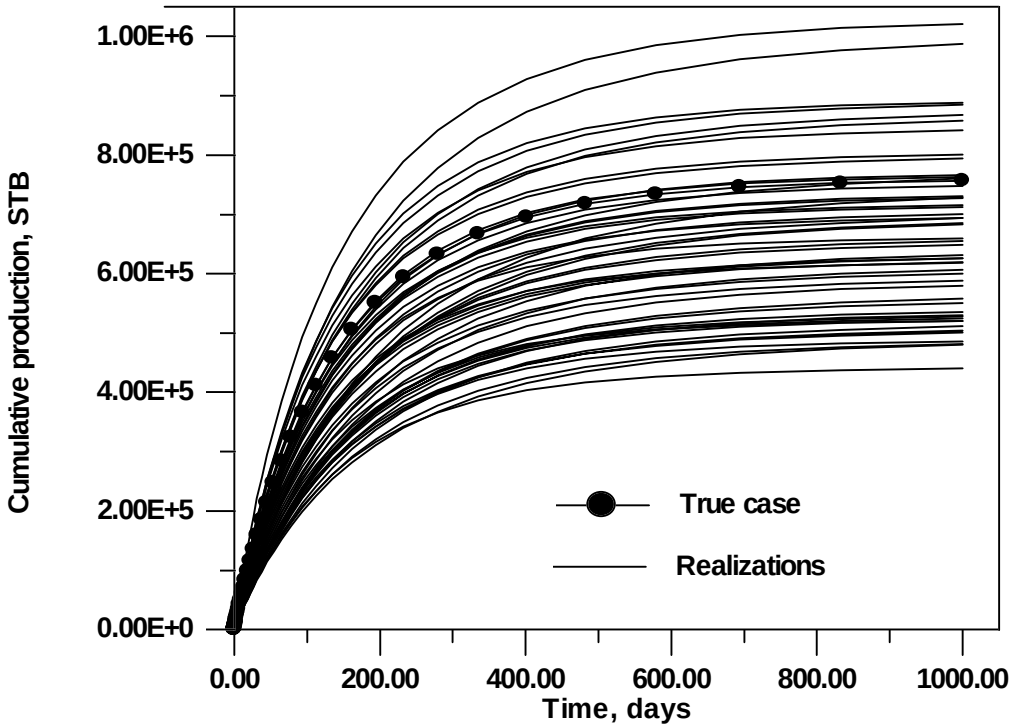

Fig. 5.14 - Well 3 production performance predicted from a suite of conditioned simulations.

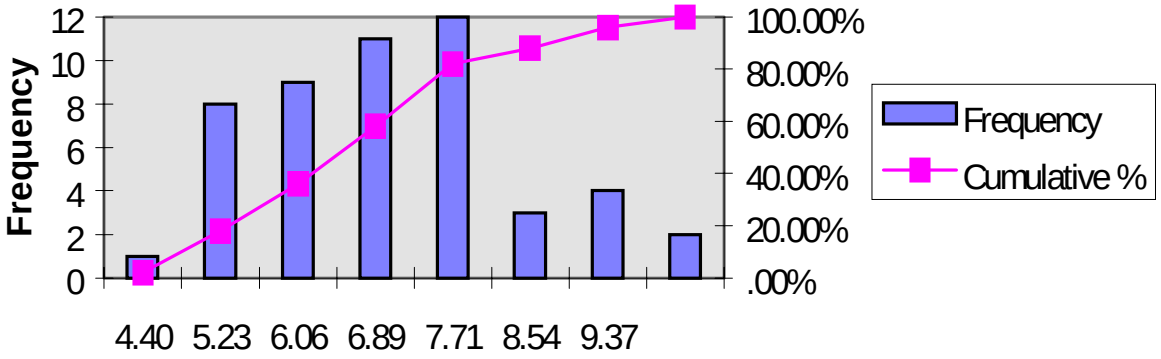

Fig. 5.15 - Histogram and cumulative distribution of cumulative oil production from well 3 at 1,000 days.

5.4.2 Field Case

Finally, we apply our method to a real field case. The production zone contains two sandstone units. On the top is fluvial sandstone and on the bottom is shoreface sandstone. The reservoir is cut by several faults running in the southeast to northwest direction. These were assumed to be impermeable barriers to flow. In the field, 29 wells have been drilled. Logging data are available for all the wells. However, there are few well-testing data and most well-testing data are not of good quality. Wells 21 and 25 are adjacent and both have well-testing data. They both produce only oil. Thus, we try to do history matching on the region around these two wells.

Approximate fluid properties (at reservoir conditions: $p = 2500$ psi, $T = 160$ ^{O}F) in the oil zone are oil viscosity 3.6 cp, gas viscosity 0.01403 cp, oil compressibility 7.4×10^{-6} psi^{-1}.

Fig. 5.16 shows a view of the top of the productive zone. The model is generated using sequential Gaussian simulation with $135 \times 70 \times 70$ cells. The horizontal gridsize is uniform with DX=DY=100 ft. Average reservoir thickness is 60 ft. Wells 21 and 25 are located at the top-right corner of Fig. 5.16.

For history matching, we cut a region with $20 \times 20 \times 70$ cells from the original model. The region was chosen to be large enough that it included the regions of investigation of well tests in both wells. We upscaled the model into the $20 \times 20 \times 23$ coarse grid model which is shown in Fig. 5.17. From a geostatistical analysis of the coarse model, we approximated the variogram by a spherical model with Rx (range in x direction) = 300 ft, Ry = 500 ft, Rz = 17 ft; the variances of porosity and log-

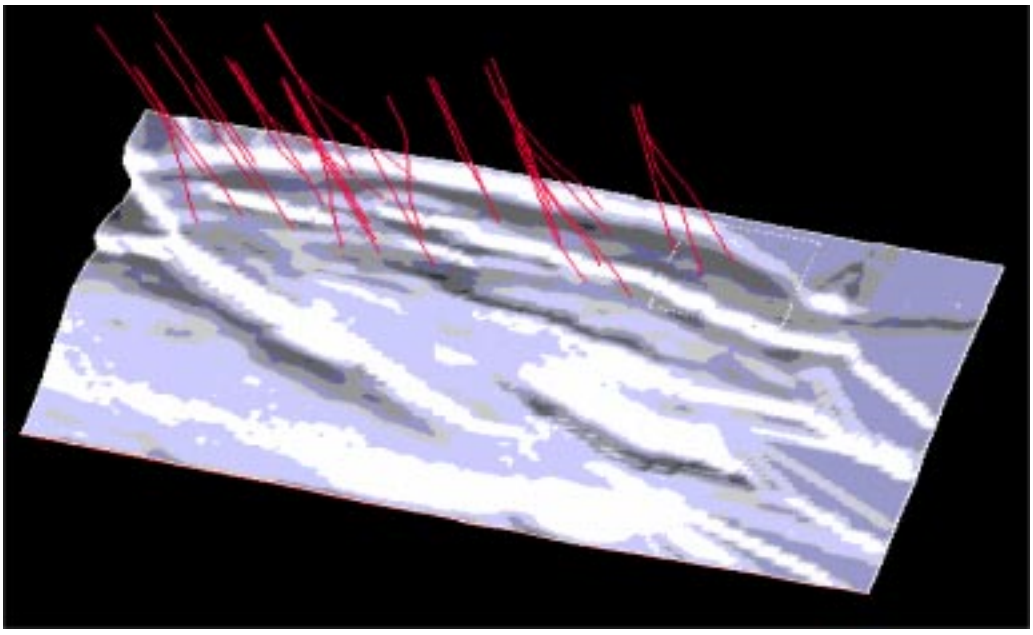

Fig. 5.16 - Top structure map on producing zone and well locations.

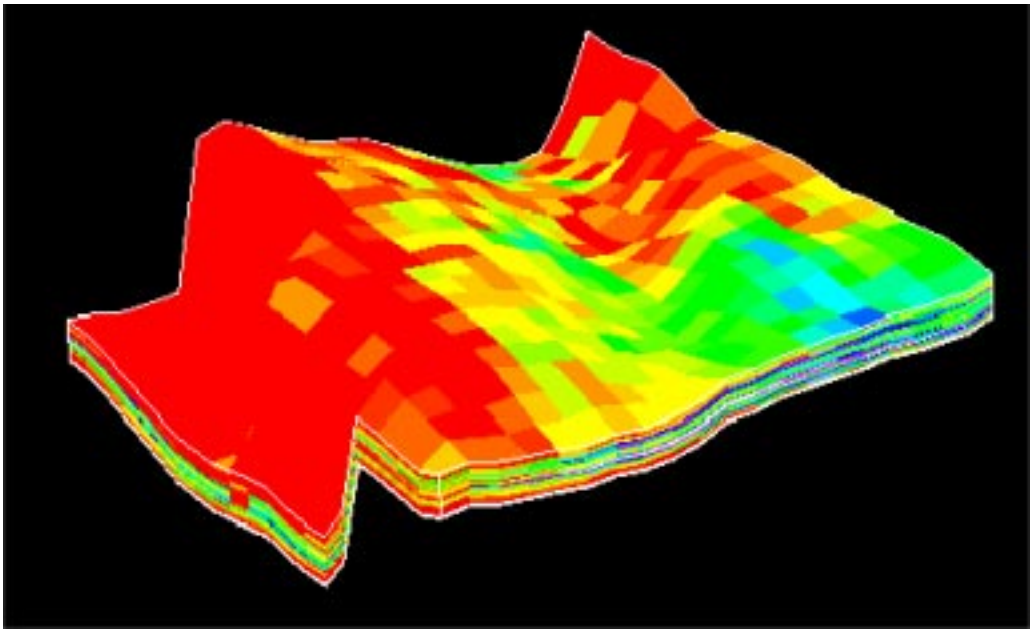

Fig. 5.17 - Log-permeability field cut from full model and scale-up

permeability respectively are 0.006 and 6.0; correlation coefficient between porosity and log-permeability is 0.7. We assumed that $k_x = k_y = k$ and $k_z = 0.1k$.

The porosity field is generated from sequential Gaussian simulation conditioned to core data and logging data. We consider the porosity field to be quite accurate. Thus, in the history matching process, we use a small variance for the porosity field, $\sigma_\phi^2 = 0.001$. From a classical well-test analysis of the data, we estimated that the skin factors are about 10. So, in our work we set the prior mean of the skin factor equal to 10 and set the variance of the skin as $\sigma_s^2 = 2.0$. We assumed that the variance on pressure measurement error is $\sigma_d^2 = 0.1$.

Fig 5.17 shows the original model log-permeability field cut through the location of well 25. Assuming the prior means are correct, we conditioned the log-permeability field to well-test pressure data using our history matching procedure. Fig. 5.19 shows the result after history matching. Comparing Fig. 5.19 with Fig. 5.18, we see that the log-permeability in the region very near well 25 has been reduced tremendously, while the log-permeability in most of the reservoir has not changed. If we assume that the log-permeability field is stationary, then Fig. 5.19 is unrealistic (values near the well are far lower than values at other location). This suggests that the prior means of the property fields may not be correct; i.e., we need to incorporate uncertainty in the prior means, and generate a correction to the prior means during the history matching process. Fig. 5.20 shows the results of history matching where we incorporated uncertainty in the prior means. The variance in the prior mean of the log-permeability field is equal to 0.5

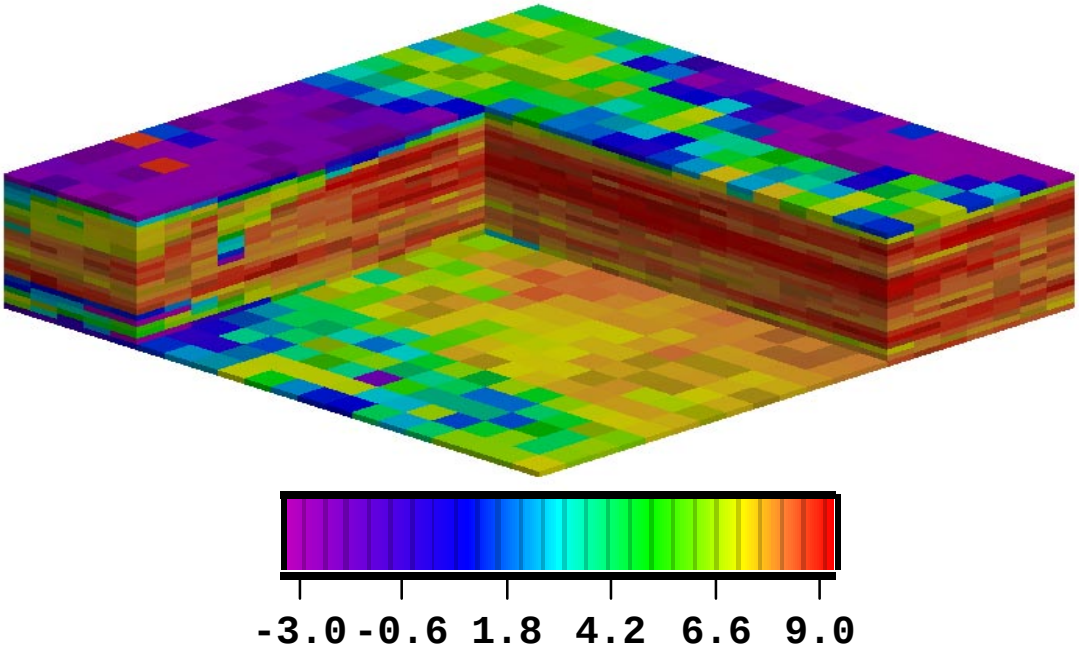

Fig. 5.18 - Original model log-permeability field, cutout at well 25.

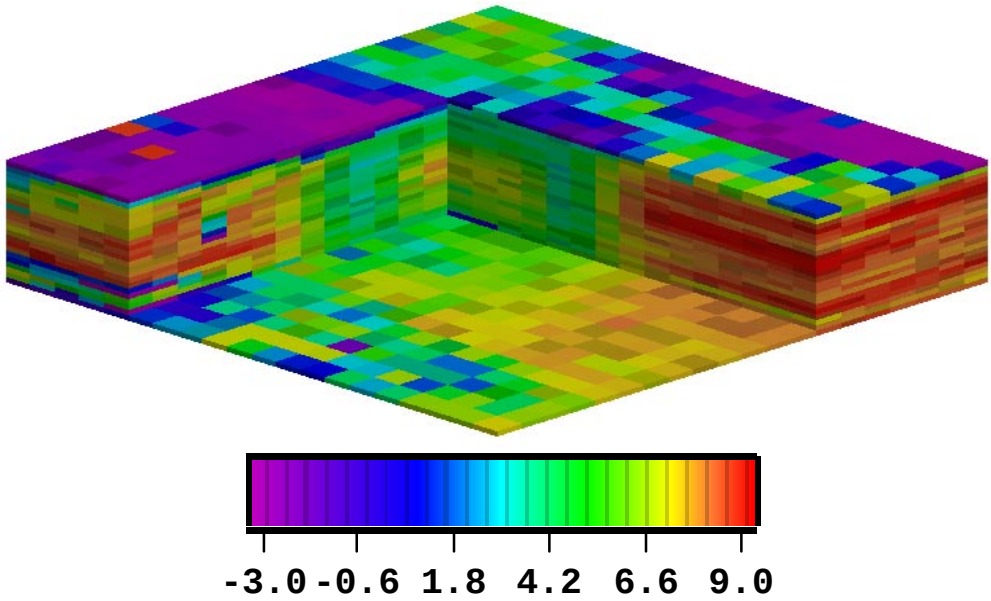

Fig. 5.19 - Log-permeability field conditioned to pressure data without correction to prior mean, cutout at well 25.

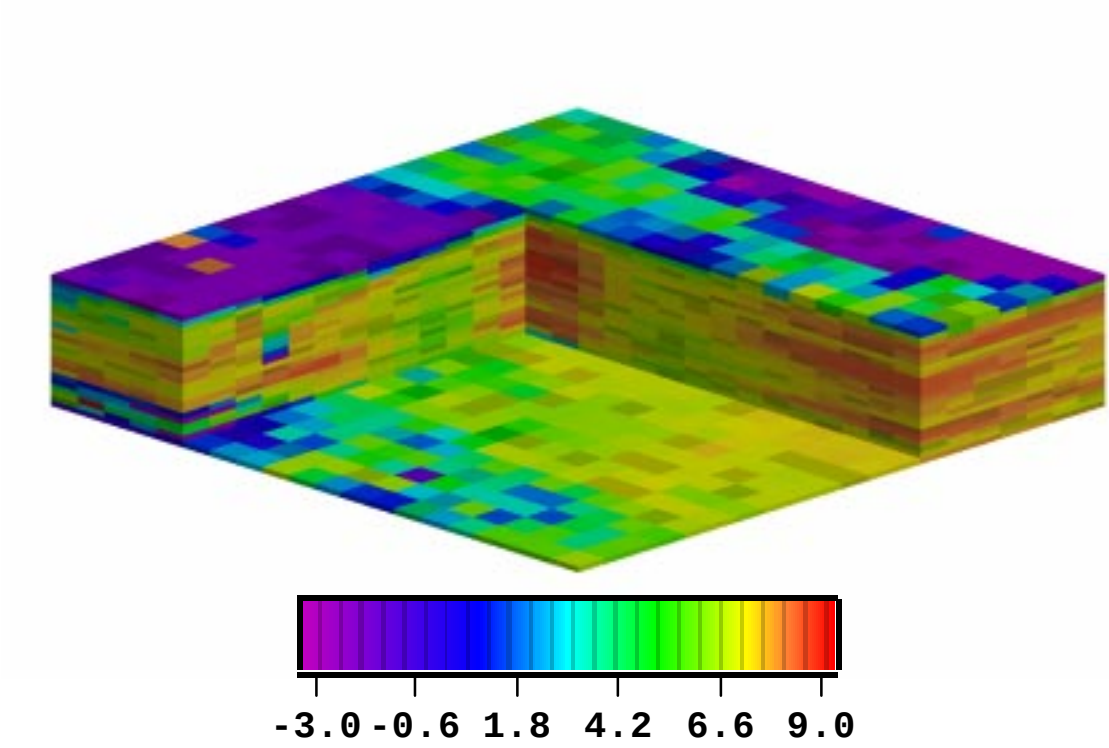

Fig. 5.20 - Log-permeability field conditioned to pressure data with correction to prior mean, cutout at well 25

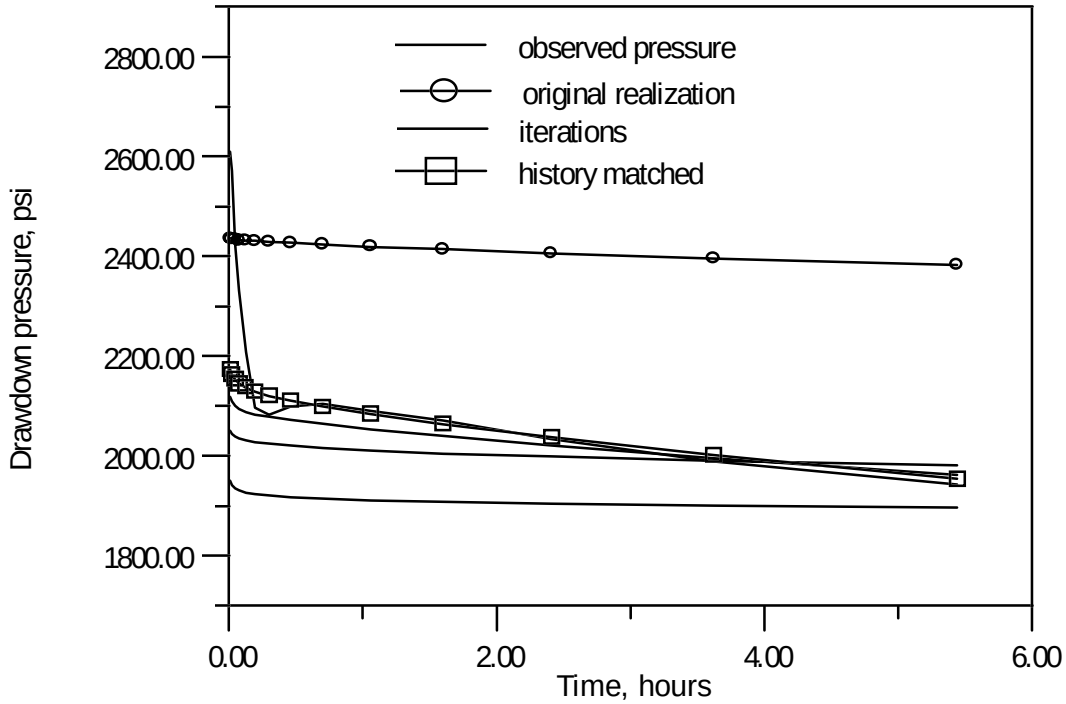

Fig. 5.21 - Pressure data for well 25

and variance in the prior porosity mean is set to be very small (0.0001). Comparing Fig. 5.20 with Fig. 5.18, we see that most of the fine detail is unchanged, but the mean of log-permeability has been reduced from 7.1 to 6.5.

Fig. 5.21 shows the observed drawdown pressure at well 25 and pressures from simulation during the history matching iterations. We see that the pressure simulated from original model is significantly different from observed data (about 400 psi). After history matching, the pressure mismatch is reduced to less than 10 psi.

Fig. 5.22 and Fig. 5.23, respectively, show the original log-permeability field and the result after history matching well 21 pressure data, both figures are cut at the location of well 21. Again note that history matching significantly reduced the mean of log-permeability field. Fig. 5.24 shows the pressure data recorded at well 21. Note that the flow rate is varied during drawdown test of well 21, but we do not have the detailed flow rate information. Thus, we used a constant rate in the history matching procedure and used only the last pressure data in drawdown as conditioning data. Even through the pressure data are not ideal, Fig. 5.24 shows that after history matching the pressure mismatch is significantly reduced.

The log-permeability field in the 10^{th} 'layer' (10^{th} gridblock in vertical direction) of the original model is shown on Fig. 5. 25. The history matching result is shown on Fig. 5.26. Note the mean value has been reduced after history matching. However, the local value of log-permeability close to the two wells have been altered more than values far away in order to match the well-test pressure data.

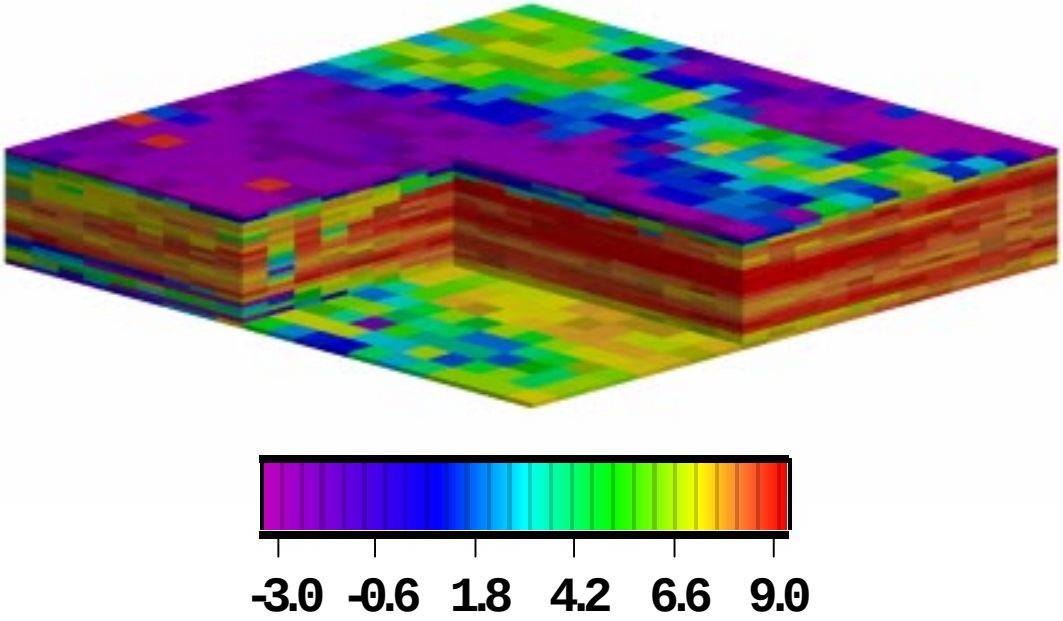

Fig. 5.22 Original log-permeability field, cutout at well 21.

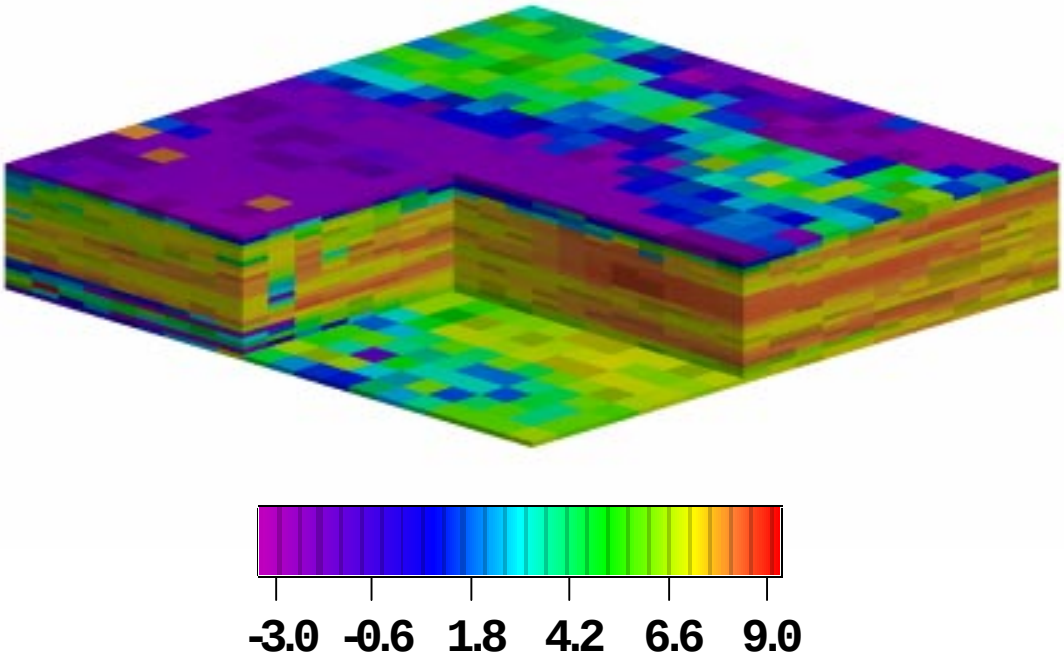

Fig. 5.23 Log-permeability field after history match, cutout at well 21.

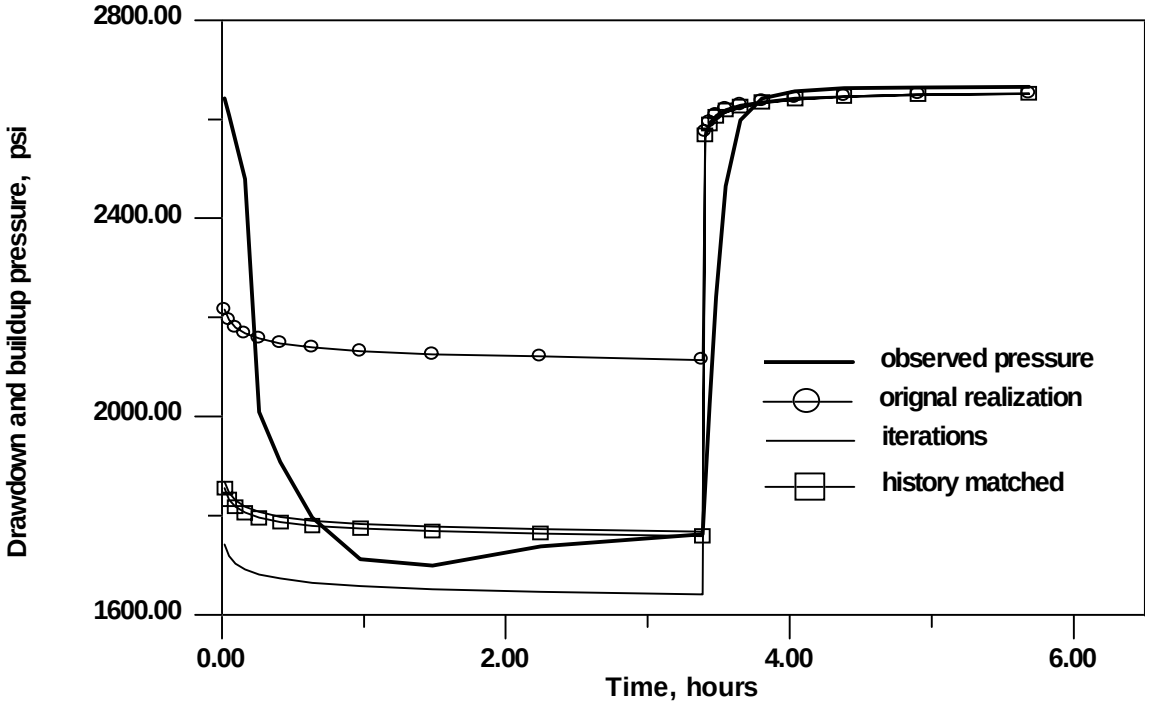

Fig. 5.24 - Pressure data for well 21.

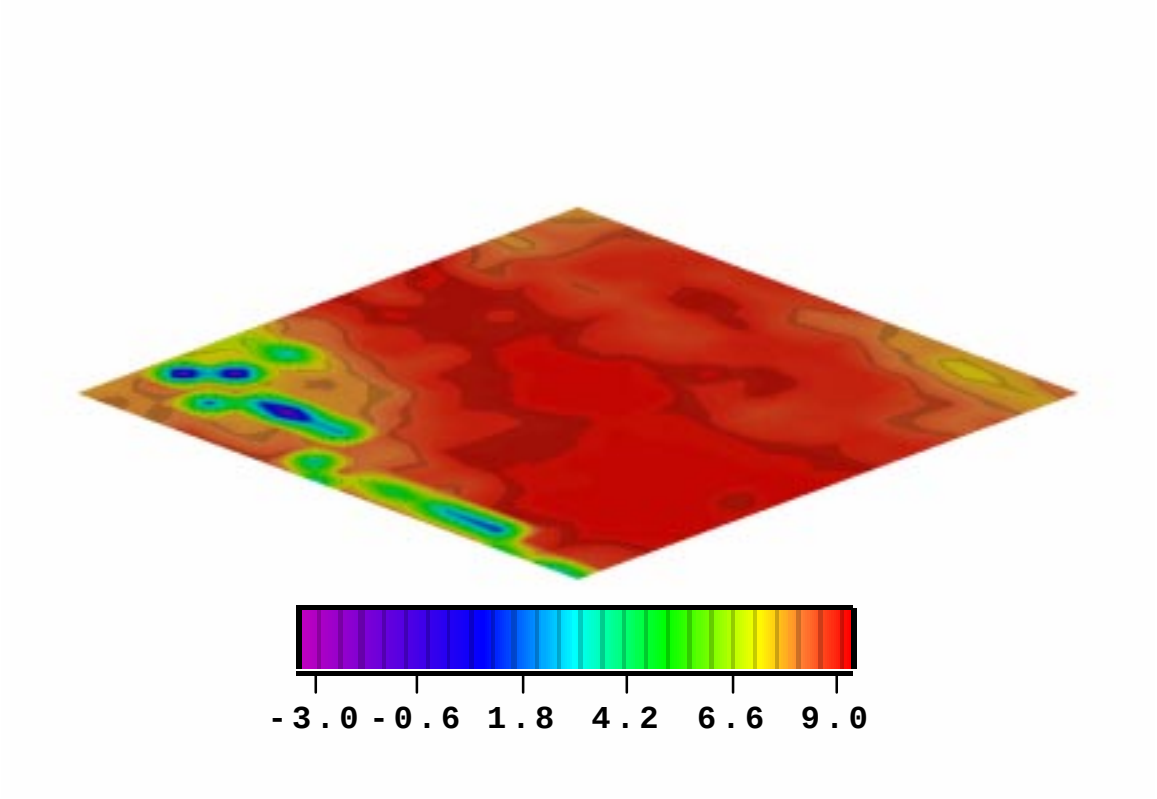

Fig. 5.25 - Original log-permeability field, 10 th layer.

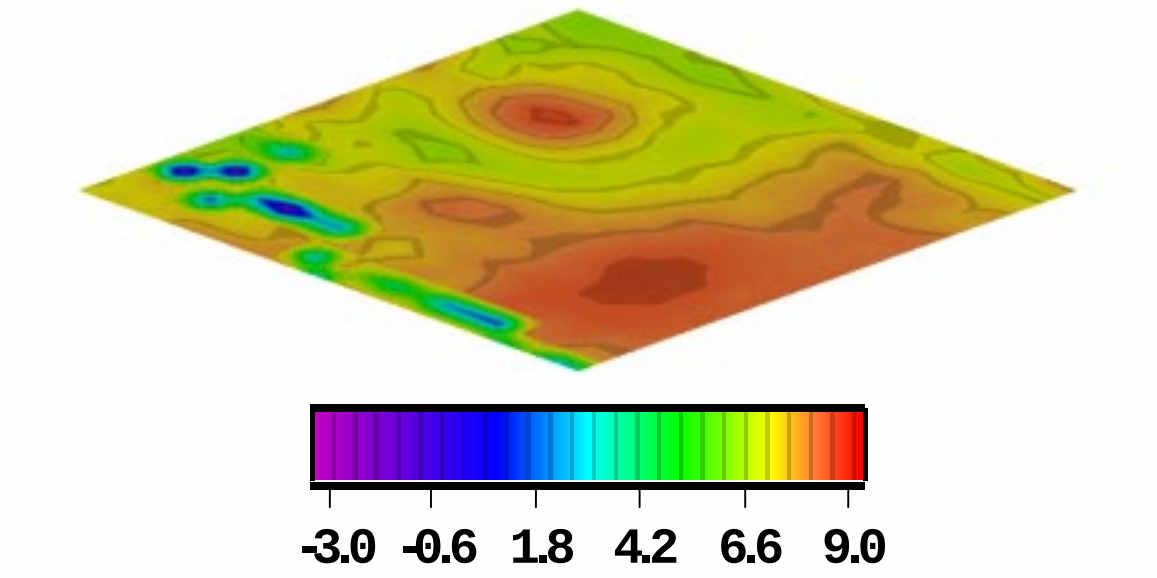

Fig. 5.26 - Log-permeability field conditioned to pressure data, 10th layer.

CHAPTER VI

CONCLUSIONS

We have presented a method to incorporate well test pressure, hard data and geostatical data into reservoir characterization. The ultimate goal of this work was to present procedures to characterize the uncertainty in realizations of rock property fields and reservoir performance predictions. As demonstrated, this objective can be achieved by first generating realizations of rock property fields and well skin factors conditioned to the available data using the techniques presented here. By simulating reservoir performance with each realization, one can construct statistics on the set of outcomes from each predicted parameter of interest, e.g., cumulative oil production. We have shown that success in application of this method will hinge primarily on three factors: (1) construction of the correct prior and a posteriori probability density functions (pdf) of rock property fields; (2) a correct sampling of the a posteriori pdf to generate realizations, (3) an efficient iteration procedure to condition property field to production data (history matching); (3a) an efficient way to generate sensitivity coefficients needed at each iteration of the history matching procedure; and (3b) procedures to reduce the computational time required to perform the numerical linear algebra required at each iteration of the computational scheme.

Regarding factor (1), the prior pdf can be estimated from static data, such as logging data, core measurement and seismic data. The prior pdf assuming the estimated prior means are correct is discussed in Chapter II, while the prior pdf with uncertainty in the prior means is given in Chapter V. In our work, we assume prior information on the model (set of reservoir parameters to be estimated) satisfies a multinormal distribution and that measurement errors in production data can be considered as Gaussian random variables with zero mean and known variance. The correct a posteriori pdf is constructed using Bayes's Theorem (Chapter II and V). We showed in Chapter V that uncertainty in the prior means can be incorporated into reservoir characterization from dynamic data using a partially doubly stochastic model.

Regarding factor (2), we presented two different procedures to generating a set of realizations which represents an approximately correct sampling of the a posteriori pdf;

(1) obtain the maximum a posteriori estimate and posteriori covariance matrix, then generate realizations by Cholesky decomposition or square root decomposition of the a posteriori covariance matrix (Chapter II);

(2) generate unconditional realizations of the model from prior pdf, unconditional realizations of the pressure data and unconditional realizations of the error in the prior means and then perform history matching to generate model parameters and adjust prior means that reproduce the simulated pressure data (Chapter V).

Both procedures for sampling the pdf are correct if measured data are linearly related to the model. Procedure 1 is efficient in the sense that it only requires one history match to obtain the maximum a posteriori estimation. However, realizations require that

we generate the a posteriori covariance matrix and its Cholesky or square root decomposition. Moreover, the set of realizations may not represent a correct sampling of the posteriori pdf, see Refs. 33 and 34. Procedure 2 is more time consuming since the generation of each realization requires a history match; however, based on the work of Oliver et al.[27], it provides a better sampling of the a posteriori pdf.

Regarding factor (3), as discussed in Chapter III, the Gauss-Newton iteration provides an efficient way to do the automatic history matching. In most cases, it only requires 3 to 8 iterations to obtain convergence. Our formulation (based on the assumption that the prior model can be represented by a multivariate Gaussian probability distribution) yields an objective function for which the Gauss-Newton method is ideally suited. At each iteration, the Gauss-Newton method requires one solution of the forward problem, i.e., one simulation run. However, the Hessian and sensitivity coefficients need to be updated at every iteration and the work required to generate the sensitivity coefficients related to each well where we match pressure data is essentially equivalent to one simulation run.

Regarding factor (3a), we have extended the Carter et al. method (Chapter III) for computing sensitivity coefficients to three-dimensional single-phase flow problems in a way that requires only one additional simulation run per well to estimate the sensitivity coefficients. If one is forced to resort to a procedure such as the one based on the gradient simulator method[31] to generate sensitivity coefficients, the computational time required will increase dramatically. We have shown that our three-dimensional extension of the Carter et al. method generally gives extremely accurate estimation of sensitivity coefficients. The only exception is when there is strong cross-flow through the wellbore; in this

case the sensitivity of the pressure at an observation well to the permeability at a gridblock penetrated by an active well is generally underestimated. However, this error should not have a strong effect on resolving the permeability at an active well location, because this permeability is well resolved by the active well pressure data themselves.

Considering factor (3b), we have investigated two reparameterization techniques, spectral decomposition and the subspace method. For spectral decomposition, any reduction is computational costs achieved by this method depends on the type of variogram, the nugget effect and the size of the problem. If the nugget is equal to zero, spectral decomposition may be beneficial, especially if one wishes to generate a set of realizations, but any computational savings decreases dramatically if the nugget is large. When the model is large, decomposition of the covariance matrix requires significant computer time which in most cases eliminates any advantage of this reparameterization. On the other hand, we show that the subspace method represents a procedure that can achieve significant computational savings for large problems. For the problems considered in this work, our choice of subspace vectors yields reliable maximum a posteriori estimates and realizations of similar quality to those obtained with the conventional method and requires roughly one-half the computer time at least for the problems we have considered.

We have applied the computational technique to several synthetic cases and one field case. Our results indicate that for three-dimensional problems, pressure data themselves do not accurately resolve individual values of gridblock log-permeabilities. However, pressure data do significantly reduce the uncertainty in the thickness-averaged horizontal permeability, especially near an active well. Using both hard data at the wells and pressure data significantly reduces the uncertainty in the permeability field. In general,

the porosity field is not as well resolved by pressure data, however, if pseudosteady-state flow pressure data is available, then computing the reservoir average porosity by averaging the porosity values contained in the maximum a posteriori estimate gives a good estimate of average reservoir porosity. Layer skin factors can not be determined accurately using only pressure data. However, if data on layer flow rates are available, by conditioning to both wellbore pressure data and individual layer flow rate data, we can obtain reasonable estimates of layer skin factors.

NOMENCLATURE

c_t	total system compressibility, psi^{-1}.
C_D	covariance matrix for pressure measurement errors.
C_{Dh}	covariance matrix for hard data measurement errors.
C_M	prior covariance matrix.
C_{MP}	a posteriori covariance matrix after incorporating all data.
$C_{MP,P}$	reparameterized a posteriori covariance matrix.
C_Θ	covariance matrix for errors in prior means.
d	vector of pressures calculated from simulator, psi.
d_{obs}	vector of measured wellbore pressure data, psi.
G_l	sensitivity coefficient matrix at lth Gauss- Newton iteration.
$g(m)$	calculated pressure and layer flow rate data from simulation.
h	formation thickness, ft.
H_l	Hessian matrix at lth Gauss-Newton iteration.
k	permeability, md.
k_x	x-direction permeability.
k_y	y-direction permeability.
k_z	z-direction permeability.
m	vector of model parameters.
m_{prior}	vector of prior means of model parameters.
$m_{p,\infty}$	reparameterized maximum a posteriori estimate.

m_∞	maximum a posteriori estimate after conditioning to all data.
M	number of simulator gridblocks.
N_d	number of conditioning pressure data.
N_h	number of hard data.
N_p	number of model parameters estimated.
N_s	number of skin factors estimated.
N_w	number of wells at which pressure is measured.
p_i	initial reservoir pressure, psi.
r_w	wellbore radius, ft.
s	skin factor.
t	time, days.
θ	vector of correction to prior means.
μ	viscosity, cp.
ϕ	porosity, fraction.
σ^2	variance.

Superscripts

T	matrix transpose.

REFERENCES

1. Deutsch, C.: "*Annealing Techniques Applied to Reservoir Modeling and the Integration of Geological and Engineering (Well-Test) Data*," PhD dissertation, Stanford U., 1992.
2. Sagar, R. K., Kelkar, M. G., and Thompson, L. G.: "Reservoir Description by Integrating Well-Test Data and Spatial Statistics," *SPE Formation Evaluation* (Dec. 1995) 267-274.
3. Holden, L. et al.: "Use of Well Test Data in Stochastic Reservoir Modeling" paper SPE 30591, presented at the 1995 SPE Annual Technical Conference and Exhibition, Dallas, Oct. 22-25.
4. Alabert, F. G.: "Constraining Description of Randomly Heterogeneous Reservoirs to Pressure Test Data: A Monte Carlo Study," paper SPE 19600 presented at the 1989 SPE Annual Technical Conference and Exhibition, San Antonio, Oct. 8-11.
5. Huang, Xuri.: "*Data Driven Description of Reservoir Petrophysical properties,"* PhD dissertation, U. of Tulsa, 1995.
6. Datta-Gupta, A., Vasco, D. W. and Long, J. C. S.: "Sensitivity and Spatial Resolution of Transient Pressure and Tracer Data For Heterogeneity Characterization," paper SPE 30589, presented at the 1995 SPE Annual Technical Conference and Exhibition, Dallas, Oct. 22-25.
7. Vasco, D. W , Datta-Gupta, A. and Long, J. C. S.: "Integrating Field Production History in Stochastic Reservoir Characterization," paper SPE 36567, presented at the 1996 SPE Annual Technical Conference and Exhibition, Denver, Oct. 6-9.

8. Tang, Y. N., Chen, Y. M., Chen, W. H. and Wasserman, M. L.: “Generalized Pulse-Spectrum Technique for 2-D and 2-Phase History Matching,” *Applied Numerical Mathematics* (1989) Vol. 5, 529-539.

9. Tikhonov, A. N.: “Regularization of Incorrectly Posed Problems,” *Soviet Math. Dokl.* (1963) Vol. 4, 1624-1627.

10. Gavalas, G. R., Shah, P. C. and Seinfeld, J. H.: “Reservoir History Matching by Bayesian Estimation,” *Soc. Pet. Eng. J.*, (Dec. 1976), Vol. 16, 337-350.

11. Jacquard, P. and Jain, C.: "Permeability Distribution From Field Pressure Data," *Soc. Pet. Eng. J.* (Dec. 1965) Vol. 5, 281-294.

12. Jahns, H. O.: "A Rapid Method for Obtaining a Two-Dimensional Reservoir Description From Well Pressure Response Data," *Soc. Pet. Eng. J.* (Dec. 1966) Vol. 6, 315-327.

13. Shah, P. C., Gavalas, G. R. and Seinfeld, J. H.: "Error Analysis in History Matching: The Optimum Level of Parameterization," *Soc. Pet. Eng. J.*, (June 1978) Vol. 18, 219-228.

14. Tarantola, A.: *Inverse Problem Theory, Methods for Data Fitting and Model Parameter Estimation*, Elsevier Science Publishers (1987) Amsterdam.

15. Tarantola, A. and Valette, B.: “Generalized Nonlinear Inverse Problems Solved Using the Least Squares Criterion,” *Reviews of Geophysics and Space Physics* (May 1982) Vol. 2, 219-232.

16. Carrera J. and Neuman, S. P.: “Estimation of Aquifer Parameters Under Transient and Steady State Conditions: 1. Maximum Likelihood Method Incorporating Prior Information,” *Water Resources Res.* (1986) Vol. 22, 199-210.

17. Carrera J. and Neuman, S. P.: “Estimation of Aquifer Parameters Under Transient and Steady State Conditions: 2. Uniqueness, Stability and Solution Algorithms,” *Water Resources Res.* (1986) Vol. 22, 211-227.

18. Carrera J. and Neuman, S. P.: ``Estimation of Aquifer Parameters Under Transient and Steady State Conditions: 3. Application to Synthetic and Field Data," *Water Resources Res.* (1986) Vol. 22, 228-242.

19. Oliver, D. S.: “Incorporation of Transient Pressure Data into Reservoir Characterization,” *In Situ* (1994) Vol. 18, 243-275.

20. Oliver, D. S.: “Multiple Realizations of the Permeability Field From Well Test Data,” paper SPE 27970, presented at the University of Tulsa Centennial Petroleum Engineering Symposium, Tulsa, August 29-31, *Soc. Pet. Eng. J.* (June 1996), 145-154.

21. Fletcher, R.: *Practical Methods of Optimization*, John Wiley & Sons, Inc. (1987) New York.

22. Carvalho, R. S., Redner, R. A., Thompson, L. G. and Reynolds, A. C.: “Robust Procedures for Parameter Estimation by Automated Type-Curve Matching,” paper SPE 24732, presented at the 1992 SPE Annual Technical Conference and Exhibition, Washington D. C., Oct. 4-7.

23. Chu, L., Reynolds, A. C. and Oliver, D. S.: “Computation of Sensitivity Coefficients For Conditioning the Permeability Field to Well-Test Pressure Data,” *In Situ* (1995) Vol. 19, 179-223.

24. Chu, L., Reynolds, A. C. and Oliver, D. S.: “Reservoir Description From Static and Well-Test Pressure Data Using Efficient Gradient Methods,” paper SPE 29999, pre-

sented at the 1995 SPE International Meeting on Petroleum Engineering, Beijing, Nov. 14-17.

25. Reynolds, A. C., He, N., Chu, L. and Oliver, D. S.: “Reparameterization Techniques for Generating Reservoir Descriptions Conditioned to Variograms and Well-Test Pressure Data,” paper SPE 30588, presented at the 1995 SPE Annual Technical Conference and Exhibition, Dallas, Oct. 22-25. *Soc. Pet. Eng. J.* (December 1996), 145-154.
26. He, Nanqun, Reynolds, A. C. and Oliver, D. S.: “Three-Dimensional Reservoir Description from Multiwell Pressure Data and Prior Information,” paper SPE 36509, presented at the 1996 SPE Annual Technical Conference and Exhibition, Denver, Oct. 6-9.
27. Oliver, D. S., He, Nanqun and Reynolds, A. C.: “Conditioning Permeability Fields to Pressure Data,” 5th European Conference on the Mathematics of Oil Recovery, Leoben, Austria, Sept. 3-6, 1996.
28. Reynolds, A. C., He, Nanqun and Oliver, D. S.: “Reducing Uncertainty in Geostatistical Characterization By Well-Testing Pressure Data,” Fourth International Reservoir Characterization Technical Conference, March 2-4, 1997, Houston, Texas.
29. Carter, R. D, Kemp, L. F., Jr., Pierce, A. C. and Williams, D. L.: “Performance Matching With Constraints,” *Soc. Pet. Eng. J.* (April 1974) 187-196.
30. Jacquard, P.: ``Theorie de l'Interpretation des Mesures de Pression," *Revue de l'Institute du Petrole* (March 1964) Vol. 19, 297-338.
31. Yeh, W.: “Review of Parameter Identification Procedures in Groundwater Hydrology: The Inverse Problem,” *Water Resources Res.* (1986) Vol. 22, 95-108.

32. Anterion, F., Eymard, R. and Karcher, B.: "Use of Parameter Gradients for Reservoir History Matching," paper SPE 18433 presented at the 1989 SPE Symposium on Reservoir Simulation, Houston, Feb. 6-8.

33. Cunha, L. B.: *"Sampling the A Posteriori Density Function for Permeability Fields Conditioned to the Variogram and Well-Test Pressure Data,"* PhD dissertation, U. of Tulsa, 1996.

34. Cunha, L. B., Oliver, D. S., Redner, R. A. and Reynolds, A. C.: "A Hybrid Markov Chain Monte Carlo Method for Generating Permeability Fields Conditioned to Multi-well Pressure Data and Prior Information," paper SPE 36566, presented at the 1996 SPE Annual Technical Conference and Exhibition, Denver, Oct. 6-9.

35. Oliver, D. S., Cunha, L. B. and Reynolds, A. C.: "Markov Chain Monte Carlo Methods for Conditioning a Permeability Field to Pressure Data," *Mathematical Geology*, V. 29, No. 1, P. 61-91 (1997).

36. Oliver, D. S.: "On Conditional Simulation to Inaccurate Data," *Math. Geology*, v. 28, p. 811-817 (1996).

37. Gomez-Hernandez, J. J. and A. G. Journel: "Joint Sequential Simulation of Multi-Gaussian Random Variables," 1993, in Soares, A., editor, Geostatistic Troia 92, Kluwer, p. 133-144.

38. Tjelmeland, H., H. Omre, and B. J. Hegstad: "Sampling from Bayesian Models in Reservoir Characterization," Technical Report Statistics No. 2, University of Trond-heim, 1994.

39. Xu, W., Tran, T. T., Srivastava, R. M., and Journel, A. G.: "Integrating Seismic Data in Reservoir Modeling: The Collocated Cokriging Approach," paper SPE 24742,

presented at the 1992 SPE Annual Technical Conference and Exhibition, Washington D.C., Oct. 4-7.

40. Beck, J. V. and Arnold, K. J.: *Parameter Estimation in Engineering and Science*, John Wiley & Sons, Inc., New York, 1977.
41. Kucuk, F. and Ayestaran, L.: "Well Test Analysis of Commingled Zones without Crossflow," paper SPE 13081, presented at the 1984 SPE Annual Technical Conference and Exhibition, Houston, Texas, September 16-19.
42. Ehlig-Economides, C. A. and Joseph, J. A.: "A New Well Test for Determination of Individual Layer Properties in a Multilayered Reservoir," paper SPE 14167, presented at the 1985 SPE Annual Technical Conference and Exhibition, Las Vegas, NV, September 22-25.
43. Peaceman, D. W.: "Interpretation of Well-Block Pressures in Numerical Reservoir Simulation With Non-Square Grid Blocks and Anisotropic Permeability," Soc. Pet. Eng. J. (June 1983) Vol. 13, 531-54.
44. Peaceman, D. W.: *Fundamental of Reservoir Simulation*, Elsevier Publishing Company, New York, 1977.
45. Thomas, G. W.: *Principle of Hydrocarbon Reservoir Simulation*, International Hydrocarbon Resources Development Corporation, Boston, 1982.
46. Burden, R. L., Faires, J. D. and Reynolds, A. C.: *Numerical Analysis*, Prindle, Weber & Schmidt (1978) Boston.
47. Luster, G. R.: Raw Materials for Portland Cement: *Application of Conditional Simulation of Coregionalization*, PhD dissertation, Stanford U., 1986.

48. Ababou, R., Bagtzoglou, A. C. and Wood, E. F.: “On the Condition Number of Covariance Matrices in Kriging Estimation and Simulation of Random Fields,” *Math. Geol.*, Vol. 26 (1994) 99-133.

49. Kennett B. L. N. and Williamson, P. R.: "Subspace Methods for Large Scale Nonlinear Inversion," in *Mathematical Geophysics: A Survey of Recent Developments In Seismology and Geodynamics*, eds. Vlarr, N. J. et al., D. Reidel Publishing Company, Dordrecht (1988) 139-154.

50. Oldenberg, D. W., McGillivray, P. R. and Ellis, R. G.: "Generalized Subspace Methods for Large-Scale Inverse Problems," *Geophysics J. Int.* (1993) Vol. 10, 12-20.

51. Oldenberg, D. W. and Li, Y.: "Subspace Linear Inverse Method," *Inverse Problems* (1994) Vol. 10, 915-935.

52. Franklin, J. *N.: Matrix Theory*, Prentice-Hall Inc. (1968) Englewood Cliffs, NJ.

53. Press, W. H., Teukolsky, S. A., Vetterling, W. T. and Flannery, B. P.: *Numerical Recipes in Fortran, the Art of Scientific Computing*, Second Edition, Cambridge University Press (1992) New York.

54. Christakos, G.: *Random Field Models in Earth Sciences*, Academic Press (1992) San Diego.

55. Reade, J. B.: "Eigenvalues of Positive Definite Kernels," *SIAM J. Math. Anal.* (1983) Vol. 14, 152-157.

56. Ha, C.: "Eigenvalues of Differentiable Positive Definite Kernels," *SIAM J. Math. Anal.* (1986) Vol. 17, 415-419.

57. Horn, Roger A. and Johnson, Charles A., 1985, *Matrix Analysis*, Cambridge University Press.

58. Fletcher, R., 1987, *Practical Methods of Optimization*, John Wiley & Sons, Inc., New York.

59. Oliver, D. S.: "The Influence of Nonuniform Transmissibility and Storativity on Drawdown," *Water Resource Res.* (1993) Vol. 29, 169-178.